ABSTRACT

Title of Document: DISSOLVED OXYGEN AND NUTRIENT CYCLING IN CHESAPEAKE BAY: AN EXAMINATION OF CONTROLS AND BIOGEOCHEMICAL IMPACTS USING RETROSPECTIVE ANALYSIS AND NUMERICAL MODELS

Jeremy Mark Testa, Doctor of Philosophy, 2013

Directed By: Professor W. Michael Kemp
Marine Estuarine Environmental Sciences

Hypoxia, the condition of low dissolved oxygen, is a topic of interest throughout aquatic ecology. Hypoxia has many realized and potential impacts on biogeochemical cycles and animal populations, many of which are negative. The extent and occurrence of hypoxic conditions has been on the rise globally, despite some reductions due to nutrient management success stories. Long-term increases in the volume of bottom-water hypoxia have been observed in Chesapeake Bay. Although there is evidence for the occurrence of low oxygen conditions historically in Chesapeake Bay, including direct observations of anoxia prior to the mid-20th century large-scale nutrient load increases, hypoxic volume has increased over the last 50 years. Surprisingly, the volume of hypoxia observed for a given nutrient load has doubled since the mid-1980s, suggesting controls beyond nutrient loading.

I conducted retrospective data analyses and numerical modeling studies to understand the controls on and consequences of hypoxia in Chesapeake Bay over multiple time and space scales. The doubling of hypoxia per unit TN load was associated

with an increase in bottom-water inorganic nitrogen and phosphorus concentrations, suggesting the potential for a positive feedback, where hypoxia-induced increases in N and P recycling support higher summer algal production and subsequent O_2 consumption. I applied a sediment biogeochemical model at several stations in Chesapeake Bay, which revealed that hypoxic conditions substantially reduce denitrification and phosphorus sorption to iron oxyhydroxides, leading to the elevated sediment-water N and P fluxes that drive this feedback. An analysis of O_2 dynamics during the winter-spring indicate that the day of hypoxia onset and the rate of March-May water-column O_2 depletion are most strongly correlated to chlorophyll-*a* concentrations in bottom water; this suggests that the spring bloom drives early season O_2 depletion. Metrics of winter-spring O_2 depletion were un-correlated with summer hypoxic volumes, however, suggesting that other controls (including physical forcing and summer algal production) are important. I used a coupled hydrodynamic-biogeochemical model for Chesapeake Bay to discover that summer algal production is necessary to maintain hypoxia throughout the summer, and that nutrient load-induced increases in hypoxia are driven by elevated summer respiration in the water-column of lower-Bay regions.

DISSOLVED OXYGEN AND NUTRIENT CYCLING IN CHESAPEAKE BAY: AN EXAMINATION OF CONTROLS AND BIOGEOCHEMICAL IMPACTS USING RETROSPECITVE ANALYSIS AND NUMERICAL MODELS

By

Jeremy Mark Testa

Dissertation submitted to the Faculty of the Graduate School of the
University of Maryland, College Park, in partial fulfillment
of the requirements for the degree of
Doctor of Philosophy
2013

Advisory Committee:

Professor W. Michael Kemp, Chair
Professor Walter R. Boynton
Professor Jeffrey C. Cornwell
Professor Ming Li
Professor Dominic M. Di Toro, University of Delaware
Professor David R. Tilley, Dean's Representative

© Copyright by
Jeremy Mark Testa
2013

DEDICATION

I would first like to thank my advisor and friend, Michael Kemp, for his support, guidance, and instruction over the past nine years, which includes the duration of both my Masters and Ph.D. studies. It has been an enormous pleasure to be his student, and the opportunities he has provided me have been instrumental in my intellectual development and career advancement. I look forward to much new and exciting collaboration in the future. My committee members were instrumental players in my dissertation development: Walter Boynton made sure I kept my eye on the big picture and the role of my work in the greater understanding and management of coastal ecosystems, Jeff Cornwell helped to ground me in the realities of biogeochemistry while I ventured into the world of numerical models, Dominic Di Toro clearly helped me to "become" a numerical modeler and always challenged me to truly understand the processes I was studying, while Ming Li helped me to better understand hydrodynamics, numerical modeling, and the role of physical forcing on biogeochemical cycling. I am indebted to them for their time and guidance.

As my research is an interdisciplinary venture, I had the pleasure of working with, and learning from, a number of great individuals over the course of my dissertation. Damian Brady convinced me that Matlab would change my life for the better, and his help and collaborations have been as productive as they were fun over the past six years. Yun Li and Younjoo Lee were a pleasure to work with in the adventure of applying a new model of Chesapeake Bay. James Fitzpatrick was incredibly generous with his time and expertise to discuss biogeochemical modeling. Rebecca Murphy was an incredible help with interpolation techniques that played a key role in two of my chapters, while Randall Burns and Eric Pearlman maintained the CBEO testbed that made data acquisition and analysis a breeze.

Several other individuals were always able to lend a helping hand or engage in a lively discussion, including Peter Stæhr, Carl Cerco, Bill Ball, Cassie Gurbisz, Laura Murray, Debbie Hinkle, Maureen Brooks, Jen Bosch, Dong-Yoon Lee, Mike Owens, Roger Newell, Larry Sanford, and many others within the Horn Point Community. I am also indebted to the many state and federal agencies that collect and distribute the data I have used in this effort, including the U.S. Environmental Protection Agency, the National Oceanographic and Atmospheric Administration (NOAA), the Maryland Department of Natural Resources (MD DNR), and the National Atmospheric Deposition Program. I would lastly like to thank the National Science Foundation, NOAA, MD DNR, and Horn Point Laboratory for funding my research.

Finally, I would like to thank the three most important women in my life. I am grateful for my mother, Kendra, who has been a persistent source of love, support, and encouragement since I first started planning my life as a Wall Street money man. My daughter Juniper, although she doesn't realize yet, has been an incredible source of joy and calm during a period of occasional stress and seemingly never-ending work. Finally, my wife Jamie and been an incredibly supportive, optimistic, and loving partner. For no less than four months, Jamie supported and encouraged a sometimes distracted, exhausted, and over-scheduled husband. Undoubtedly, she is an unofficial co-author on my dissertation. We have many happy years ahead of us.

TABLE OF CONTENTS

LIST OF TABLES

LIST OF FIGURES

Chapter 1: INTRODUCTION AND OVERVIEW

Overview

Depletion of dissolved oxygen from coastal waters is a widespread phenomenon that appears to be growing globally (Díaz and Rosenberg, 2008; Gilbert et al., 2010; Rabalais and Gilbert, 2009). There is considerable interest in this phenomenon because low oxygen causes physiological stress for most marine metazoans. Oxygen concentrations below approximately 30% saturation ("hypoxia" = O_2 < 62.5 μM or 2 mg l^{-1}) interrupt normal metabolism and behavior of fish and invertebrates causing reduced growth and increased mortality (Díaz, 2001). Extended periods of hypoxia and relatively brief exposure to anoxia (zero O_2) tend to cause mortality for many marine animals (Vaquer-Sunyer and Duarte, 2008). Hypoxia may also affect predator-prey interactions and food web structures, with low O_2 zones providing more tolerant organisms extended habitat for foraging and/or for refuge from predation (Decker et al., 2004; Nestlerode and Diaz, 1998). In addition, low O_2 levels alter the oxidation-reduction balance in marine sediments and associated biogeochemical processes, including coupled nitrification-denitrification (Kemp et al., 1990) and inorganic phosphorus sorption to metal oxide-hydroxide complexes (Middelburg and Levin, 2009; Slomp and Van Cappellen, 2007).

Oxygen depletion occurs at various time and space scales from an imbalance between biological and physical sources and sinks for O_2. In very shallow (1-5 m) tidal rivers and lagoons with non-stratified water columns that are enriched with inorganic nutrients, hypoxic conditions tend to appear and disappear on short (hours-days; Fig. 1.1) time-scales (D'Avanzo and Kremer, 1994; Tyler et al., 2009). Slightly deeper (3-8 m) microtidal systems typically experience periodic stratification that may allow episodic hypoxia to occur on daily-to-weekly scales (Fig. 1.1), fluctuating with changes in wind-

driven mixing (Park et al., 2007). In deeper (10-50 m) estuaries and shelf systems with stratified water columns, hypoxia often occurs during much of the summer (2-4 mo; Fig. 1.1) season (Kemp et al., 1992; Rabalais and Turner, 2006). In much deeper (>100 m) coastal seas and fjords, strongly stratified water columns result in virtually permanent hypoxia/anoxia, that may change in size and position with decadal-scale variations in circulation (Zillen et al., 2008).

It has been made clear that eutrophication (i.e., anthropogenic nutrient and organic enrichment of waters) is contributing to the expansion of occurrence, intensity, and duration of hypoxic conditions in coastal waters worldwide (Díaz and Rosenberg, 2008). Dissolved inorganic nutrient additions tend to fertilize growth, sinking and decomposition of phytoplankton in bottom waters of estuaries, bays, and inland seas. For many coastal systems in the industrialized regions of the world, there have been major socio-economic commitments to remediate hypoxic zones by reducing nutrient loading from the adjacent catchment and overlying atmosphere (Boesch, 2002; Carstensen et al., 2006). Although substantial socio-economic investments have been made to reduce hypoxia in many regions worldwide (Kronvang et al., 2005), recent analyses of historical data from European and North American coastal systems suggest little evidence for simple and straightforward responses of hypoxia to remediation actions (Conley et al., 2009a; Duarte et al., 2009; Kemp et al., 2009).

One of the complicating factors in understanding eutrophication impacts on dissolved O_2 is the significant contribution of hydrodynamic variability to O_2 dynamics. In many coastal systems, density stratification is sufficient to create a bottom layer isolated from surface waters and impede downward mixing of O_2 from surface waters,

thereby reducing physical replenishment and allowing depletion of bottom water O_2 through aerobic respiration of accumulated organic matter (Kemp et al., 1992). Buoyancy of the upper layer is increased and stratification is strengthened by seasonal inputs of fresh water (Boicourt, 1992) and warming of surface waters (Welsh and Eller, 1991). Relatively weak stratification in systems such as the Neuse River estuary, Long Island Sound, and Mobile Bay can be disrupted by typical summer wind events (O'Donnell et al., 2008; Stanley and Nixon, 1992; Turner et al., 1987). In any given year, stronger stratification, created by larger freshwater input or warmer surface water, is more resistant to disruption by wind events (Lin et al., 2008). Ventilation of bottom-water hypoxia may involve relatively complex mechanisms, where for example wind stress induces the straining of density fields (Scully et al., 2005), lateral tilting of the pycnocline (Malone et al., 1986), alteration of far-field coastal circulation (Wiseman et al., 1997), or interaction with spring-neap tidal cycles (Sharples et al., 1994). In stratified systems with estuarine circulation, bottom-water O_2 pools are also replenished by landward transport of O_2-rich water from downstream or offshore sources (Kemp et al., 1992; Kuo et al., 1991; Wiseman et al., 2004). Because hypoxia in stratified coastal systems is confined to the bottom layer, respiration must be fueled by labile organic matter, typically organic particles sinking from the upper water column (Chen et al., 2007; Hagy et al., 2005).

Long-term trends and decadal-scale cycles in climatic forcing can also exert control over O_2 concentrations in bottom waters via changes in temperature, salinity, freshwater inputs, and wind stress (Rabalais et al., 2009). For example, recent increases in water temperature (Nixon et al., 2004), which are expected to continue with increases in atmospheric CO_2 concentrations, will have direct and indirect consequences for

hypoxia. The direct effects include decreased solubility of O_2 in water and enhanced respiration rates, while indirect effects include changes in food webs resulting from spatial and temporal shifts in species distribution and abundance (Najjar et al., 2010; Nixon et al., 2009). In addition, long-term increases in relative sea level occurring in many coastal regions worldwide (Holgate and Woodworth, 2004) may result in elevated bottom water salinities (Hilton et al., 2008), thus potentially enhancing stratification and reducing ventilation of deep waters. Long-term increases or decreases in freshwater input caused by global climate change will influence hypoxia in many coastal systems by increasing or decreasing (respectively) the stratification strength and nutrient delivery rate (Arnell, 1999; Justíc et al., 2003). Lastly, long-term trends and decadal-scale shifts in atmospheric pressure fields and circulation (Ogi et al., 2003) may alter the magnitude and direction of wind stress, causing changes in vertical mixing and oxygenation of O_2-depleted bottom waters in coastal systems (Scully, 2010a; Wilson et al., 2008).

Although external forcing of physical and biological processes strongly influences coastal ecosystem dynamics and hypoxia development, internal ecosystem structure and associated processes are also important. For example, internal processes regulate key biogeochemical fluxes, including production and consumption of organic carbon and cycling of inorganic nutrients. These processes, which create positive and negative feedbacks within the ecological system, can influence O_2 dynamics in coastal water columns (Kemp et al., 2005). Marine suspension-feeding benthic bivalves can effectively control phytoplankton growth, especially in shallow coastal systems (Dame and Olenin, 2005; Prins et al., 1998), leading to the suggestion that mussels, oysters and other reef-forming benthic bivalves could potentially regulate phytoplankton sufficiently to reduce

hypoxia in eutrophic coastal systems (Newell and Ott, 1999). Although field-scale documentation of benthic grazing impacts mitigating coastal hypoxia is limited, several modeling studies have demonstrated potential effectiveness (Banas et al., 2007; Cerco and Noel, 2007). Bottom water O_2 concentrations can influence the balance between decomposition and preservation of organic matter deposited on the seafloor through a variety of complex interactions (Middelburg and Levin, 2009). Numerous experiments where natural organic matter is allowed to decompose under controlled conditions with and without O_2 have been generally inconclusive (Westrich and Berner, 1984); however, more recent laboratory and field investigations tend to support the idea that decomposition rates are retarded by absence of O_2 due to a range of mechanisms including loss of macrofauna activity and sulfide inhibition of microbial metabolism (Middelburg and Levin, 2009).

Sediment biogeochemical processes, porewater chemistry, and nutrient recycling are clearly influenced by low water column O_2 and associated sediment oxidation-reduction (redox) profiles. For both nitrogen (N) and phosphorus (P), benthic recycling efficiency (the fraction of inputs of organic N and P to sediments that efflux back to overlying water) tends to increase with decreasing bottom water O_2 concentrations (Testa and Kemp, 2012). In the presence of O_2, NH_4^+ tends to be oxidized completely to NO_3^- (or to NO_2^- and N_2O) by chemoautotrophic nitrifying bacteria, where a substantial fraction of the NO_3^- generated in nitrification is generally reduced in surrounding anaerobic zones via denitrification to gaseous N_2 (or N_2O) - forms that are virtually unavailable for assimilation by plants (Seitzinger, 1988). Under conditions with hypoxic overlying water, sediments with low redox levels and high sulfide concentrations favor

dissimilatory reduction of NO_3^- back to NH_4^+ over denitrification (Tiedje, 1987) and strongly inhibit nitrification (Joye and Hollibaugh, 1995). Although anammox (anaerobic oxidation of NH_4^+ to N_2 with NO_2^-) may occur with anoxia, it is limited by availability of NO_2^-, and rates tend to be substantially lower than denitrification in most coastal sediments (Revsbech et al., 2006). Thus, hypoxic and anoxic bottom waters greatly suppress nitrification and denitrification rates, causing a higher % of total nitrogen to be recycled to overlying water as NH_4^+ (Fig. 1.2). Similar dynamics involving hypoxia and PO_4^{3-} recycling are attributable to totally different mechanisms (Fig. 1.3). Under normoxic conditions, dissolved PO_4^{3-} binds to oxides and hydroxides of Fe and Mn, forming amorphous solid-phase substances that are retained in sediments (Froelich et al., 1982). In contrast, hypoxic conditions promote reduction of Fe and Mn to soluble states, thereby releasing bound PO_4^{3-}. The presence of free sulfide, which has a very high affinity for binding sites on Fe and Mn, further promotes rapid release PO_4^{3-} and efflux to overlying waters (Caraco et al., 1989).

Many benthic invertebrate macrofauna (e.g., polychaetes, bivalves, amphipods), which are highly susceptible to physiological stresses or mortality from bottom-water hypoxia and anoxia (Díaz and Rosenberg, 1995) and exert strong influence on N and P cycling in coastal marine sediments. Although direct excretion by these organisms tends to increase nutrient recycling, activities of many species also retard recycling of NH_4^+ and PO_4^{3-} by enhanced O_2 advection into sediment porewater. Macrofauna burrows, tunnels and tubes that penetrate (0.2 – 10 cm) into sediments are ventilated by natural circulation and by active animal pumping of overlying water (Aller, 1982), which stimulates sediment nitrification and strengthens its coupling to denitrification by

increasing the effective area of oxic-anoxic interfaces (Pelegrí and Blackburn, 1995) and retards dissolution of Fe-Mn-oxide-hydroxide complexes, promoting burial of PO_4^{3-} rather than release to overlying waters (Middelburg and Levin, 2009; Welsh, 2003). In summary, hypoxia and anoxia can further stimulate NH_4^+ and PO_4^{3-} recycling to overlying waters by both geochemical and biological processes.

As a result of such complex bio-chemical-physical integrations, a broad range of possible aquatic ecosystem responses to changes in nutrient loading have been defined from theory and observation. There are surprisingly few documented examples of coastal hypoxia response to reduced nutrient loading (Kemp et al., 2009); however, basic ecological theory (Scheffer et al., 2001; Testa and Kemp, 2011) suggests several possible response trajectories (Fig. 1.4, left panels). In the simplest case, responses of hypoxia to loading might be relatively continuous and linear (Murphy et al., 2011), where hypoxia increases and decreases along the same pathway in proportion to changes in nutrient loading (Fig. 1.4). Alternatively, hypoxia might minimally respond to an initial increase or decrease in nutrients until the system approaches a "threshold" (Fig. 1.4), where relatively small changes in nutrient input cause abrupt changes in hypoxia (Cox et al., 2009). Coastal ecosystems may, however, follow complex non-linear trajectories (including hysteresis; Fig. 1.4) in response to nutrient input declines if nutrient-induced eutrophication changed the fundamental ecosystem character, including trophic structure, habitat conditions, and biogeochemical cycles (Duarte et al., 2009). Such altered systems may require larger nutrient reductions to return the system to its original state (Oguz and Gilbert, 2007).

Recent reviews have examined case studies of how coastal ecosystems have responded to changes in nutrient loading and other external variables (Kemp et al., 2009; Rabalais et al., 2007). For example, improved and more widely applied secondary sewage treatment in the 1960s through the 1980s led to major reductions discharge of labile organic matter and reduced inorganic ions to coastal waters in North America and Europe (Patrick, 1988). As a result, O_2 conditions were restored to near-pre-eutrophication levels (e.g., Fig. 1.4, right panel) in many major metropolitan areas (Brosnan and O'Shea, 1996; Jones, 2006; Patrick, 1988; Soetaert et al., 2006). For some heavily enriched coastal systems (Andrews and Rickard, 1980), however, recovery trajectories exhibited threshold responses (Fig. 1.4, right panel). In contrast, many larger estuaries where diffuse inorganic nutrient loads dominate, responses of hypoxia to changes in nutrient loading have been less clear. Although major reductions in nutrient loads have resulted in reduced hypoxia via reduction (Fig. 1.4, right panel) in nutrient-fueled algal biomass (Mallin, 2005; Mee, 2006), many partially stratified coastal ecosystems have reported little change, or even increased hypoxia, in response to reduced nutrient loading (Conley et al., 2009a; Hagy et al., 2004; Testa et al., 2008; Turner et al., 2008).

On such system with apparently non-linear responses of hypoxia to nutrient loading is Chesapeake Bay, a large estuary in the United States that receives freshwater, nutrient, and organic matter inputs from several rivers, the largest of which is the Susquehanna. Dramatic ecological changes have occurred in Chesapeake Bay during the past century as a result of nutrient enrichment driven by human population growth and land-use changes in its watershed (Kemp et al., 2005). Effects of Bay eutrophication have been compounded by extensive loss of key habitats, including tidal marshes, seagrass

beds, and reefs of the filter-feeding eastern oyster, which harbor diverse animal populations and act as sinks for suspended particles and dissolved nutrients. One of the most important ecologically damaging effects of nutrient enrichment in Chesapeake Bay has been a long-term increase in the duration and volume of seasonal bottom-water hypoxia (Hagy et al., 2004; Murphy et al., 2011). Because Chesapeake Bay has a large ratio of watershed–to-estuary area, a deep channel isolated from the atmosphere during summer stratification, and a long water-residence-time, it is particularly susceptible to hypoxia and related effects of eutrophication (Kemp et al., 2005). Although incidents of hypoxia were reported as early as the 1930s (Newcombe and Horne, 1938), direct measurements and geochemical indicators suggest that intense and recurrent hypoxia and anoxia were uncommon before a rapid increase in nutrient loading starting in the 1950s (Hagy et al., 2004; Zimmerman and Canuel, 2000). Extensive efforts to curb nutrient enrichment of Chesapeake Bay are reflected in the stabilization and slight decline in spring nitrogen loading from the Susquehanna River since ~1990, which appears to have been associated with a decline in later summer hypoxic volumes (Murphy et al., 2011). During this period of declining N loading, however, early summer hypoxia volume has continued to rise (Hagy et al., 2004; Murphy et al., 2011), resulting in an abrupt doubling of the hypoxia volume per unit spring N load (see Chapter 2).

Causes for this shift in hypoxia volume per N-loading are uncertain, however, it generally coincided with notable changes in several key factors that may have contributed to the hypoxia increase (Kemp et al., 2009). The rapid increase in surface water temperatures (~0.7^{o}C) that occurred over two decades around 1985 (Kaushal et al., 2010) would be sufficient to reduce O_2 saturation level by ~ 0.20 mg l^{-1} and possibly increase

respiration by ~5-10% (Sampou and Kemp, 1994). The relative abundance and filtering capacity of the eastern oyster (*Crassostera virginica*) in Chesapeake Bay have declined by almost 100-fold over the past 150 years due to over-fishing and two disease outbreaks (Newell, 1988). The drought-induced final decline in oyster harvest during the 10-15 years around 1985 (Kimmel and Newell, 2007) was ~10% of this overall drop between 1900 and the present (Fig. 1.5). Recent modeling (Cerco and Noel, 2007) studies have concluded that 10-fold increases in oyster filtration (equivalent to reversing the decline in the 1980s) would induce a 0.3 mg l^{-1} increase in average mid-Bay bottom water O_2 concentration. The absence of any signal of increased phytoplankton corresponding to the oyster decline, however, raises some doubt about this explanation for the hypoxia shift. Other large changes in the Bay, including losses of marshes and seagrass beds, were important for Bay nutrient budgets (Kemp et al., 2005); however, they are out of phase with this abrupt increase in hypoxia.

On the other hand, abrupt changes in atmospheric forcing or continental shelf circulation might be strong enough to alter vertical or horizontal replenishment of bottom water O_2 in the Bay. For example, recent modeling and data analysis suggest that sea level rise tends to cause increases in salt flux and bottom-layer salinity in Chesapeake Bay (Hilton et al., 2008), which could have increased stratification. Other evidence suggests an increase in the latitude of the north wall of the Gulf Stream since the 1980s (Taylor and Stephens, 1998) that may have reinforced the trend associated with sea level rise by causing an increase in salinity at the Bay mouth (Lee and Lwiza, 2008). A shift from negative to positive values for the winter North Atlantic Oscillation (NAO) index in the late 1970s (http://www.cgd.ucar.edu/cas/jhurrell/indices.html, Fig. 1.5) may be related to the

change in the Gulf Stream position (Taylor and Stephens, 1998). Such a shift in NAO might also lead to changes in the prevailing wind direction and intensity during summer (Ogi et al., 2003; Scully, 2010a), which could affect the strength of stratification and associated ventilation of hypoxic bottom waters in summer. Although many of the ecological and biogeochemical factors discussed here may have contributed to the initiation and resilience of this hypoxia regime shift, it remains unclear what the primary driver of the regime shift may be.

Thus, it is clear that many questions remain regarding long-term changes in Chesapeake Bay hypoxia. It is the aim of this dissertation to address several of these questions using a combination of retrospective data analysis and numerical models. Because the dynamics of dissolved O_2 result from a complex suite of controls over multiple time-scales, tools like numerical models are preferred, if not necessary tools to address these questions.

Synopsis

Chapter 2: Hypoxia-induced shifts in nitrogen and phosphorus cycling in Chesapeake Bay

We investigated interactions between hypoxia and nutrient cycling in Chesapeake Bay using quantitative analysis of long-term monitoring data covering the periods 1965-1980 and 1985-2007. The data included vertical water column profiles of temperature, salinity, NH_4^+, PO_4^{3-}, and O_2, as well as rates of total nitrogen (TN) and total phosphorus (TP) loading to the Bay from the Susquehanna River. We investigated the hypothesis that a doubling of the volume of hypoxic (O_2<62.5 μmol L^{-1}) water generated per unit TN load in the past 25 years is related to enhanced water-column and sediment recycling of NH_4^+ and PO_4^{3-} under low O_2, and that this increased nutrient recycling creates a

feedback that further generates hypoxia. We found that bottom-water in the upper Bay region, where seasonal hypoxia first develops, was enriched in NH_4^+ and PO_4^{3-} relative to other regions. Evidence for the positive feedback effect of low O_2 on nutrient recycling was found in the fact that bottom-water pools of NH_4^+ and PO_4^{3-} per unit TN and TP loading, respectively, were significantly and positively related to hypoxic volume in upper Bay regions during June. Similarly, NH_4^+ pools generated per unit TN load were significantly higher during 1985-2007, when hypoxic volume had been approximately doubled relative to values estimated for 1965-1980. This positive feedback effect on nutrient recycling may help to explain the persistence of extensive hypoxia in June, even during years of reduced N loading.

Chapter 3: ***Spatial and temporal patterns in winter-spring oxygen decline in Chesapeake Bay bottom waters***

Although seasonal hypoxia is a well-studied phenomenon in many coastal systems, most previous studies have focused on variability and controls on low-oxygen water masses during summer when hypoxia is most extensive. Surprisingly little attention has been given to investigations of what controls the development of hypoxic water in the months leading up to seasonal maxima. Thus, we investigated aspects of winter-spring oxygen depletion using a 25-year dataset by computing rates of water-column O_2 depletion and the date of hypoxia onset in Chesapeake Bay. On average, hypoxia (O_2 < 62.5 μM) initiates in the northernmost region of the deep, central channel in early May and extends southward over ensuing months; however, the day of hypoxia onset varies by > 50 days (April 6 to May 31 in the upper Bay). Water-column O_2 depletion rates were consistently highest in the upper Bay, and elevated Susquehanna River flow resulted in more rapid O_2 depletion and earlier hypoxia onset. Winter-spring chlorophyll-*a*

concentration in the bottom water was the primary driver of inter-annual variability in hypoxia onset and water-column O_2 depletion rates in the upper and middle Bay, while stratification strength is a more important driver in the lower Bay. O_2-depletion rates and hypoxia onset were significantly correlated to early summer hypoxic volumes, but were poorly correlated to mid-summer volumes, suggesting that climatic fluctuations and organic matter production during late spring and summer are also important in controlling summer hypoxia. Hypoxia initiated earlier in 2012 (April 6) than recorded previously, which may be related to extraordinary climatic conditions in the winter-spring of 2012 and the carry-over of large organic matter loads associated with a tropical storm in September 2011.

Chapter 4: ***Sediment Flux Modeling in Chesapeake Bay: Simulating nitrogen, phosphorus, and silica cycles***

Sediment-water exchanges of nutrients and oxygen play an important role in the biogeochemistry of shallow coastal environments. Sediments process, store, and release particulate and dissolved forms of carbon and nutrients and sediment-water solute fluxes are significant components of nutrient and oxygen cycles. Consequently, sediment biogeochemical models of varying complexity have been developed to better understand the processes regulating porewater profiles and sediment-water exchange. We have calibrated and validated a sediment biogeochemical model (i.e., two-layers: aerobic and anaerobic) that is suitable for application as a stand-alone tool or coupled to water-column biogeochemical models. We calibrated and tested a stand-alone version of the model against observations of sediment-water flux, porewater concentrations, and process rates at 12 stations in Chesapeake Bay over a 4 - 17 year period.

The model successfully reproduced sediment-water fluxes of ammonium (NH_4^+), nitrate (NO_3^-), phosphate (PO_4^{3-}), and dissolved silica ($Si(OH)_4$ or DSi) across environments with different chemical and physical characteristics. A root mean square error (RMSE)-minimizing optimization routine was used to identify best-fit values for many kinetic parameters. The results of this routine reveal the need for (1) an aerobic-layer denitrification formulation to accommodate NO_3^- reduction at the oxic-anoxic interface, (2) spatial variability in denitrification that depends on oxygen levels in the overlying water, (3) a spatially-dependent term for solid-solute PO_4^{3-} partitioning that accounts for patterns in Fe availability, and (4) the dependence of DSi fluxes on solubility and reduced solid-solute partitioning relative to PO_4^{3-}. This new calibration balances the need for a universal set of parameters that remain true to biogeochemical processes with site-specificity that represents differences in physical processes, external loading, and sediment characteristics. This stand-alone model is rapidly executed on a personal computer and is well-suited to compliment observational studies in a wide range of environments.

Chapter 5: ***Quantifying the effects of nutrient loading and carbon production on dissolved O_2 in Chesapeake Bay using a coupled hydrodynamic-biogeochemical model***

Dissolved oxygen concentrations in Chesapeake Bay are influenced by external climatic, hydrologic, and anthropogenic forcing, internal biogeochemical interactions, and physical transport. Because observations are often inadequate to understand interactions among these varied and complex biological and physical processes over multiple time and space scales, numerical models are needed to simulate these processes towards understanding their effects on dissolved oxygen. Recent modeling efforts have

highlighted many of the important physical processes controlling dissolved oxygen in Chesapeake Bay, but fewer have investigated interactions with biogeochemical controls. Thus, we coupled an implementation of the Regional Ocean Modeling System (ROMS) to a biogeochemical model (RCA) in Chesapeake Bay to understand the controls on organic carbon production and transport and associated oxygen depletion. Model simulations were performed for a 10-year period (1996-2005) and water-column state variables, sediment-water fluxes, and metabolic rates were validated against existing data. A series of nutrient-load experiments were run using the year 2000 to understand model sensitivity to loads of nitrogen and phosphorus and the spatial and temporal nature of Chesapeake Bay's response to nutrient loads. ROMS-RCA represented observed seasonal and regional dynamics of water-column and sediment processes, capturing interannual variability in hypoxic volumes. Nutrient loading experiments revealed a non-linear response of hypoxia to nitrogen load, with hypoxic-volume-days maximizing at nitrogen loads twice that of observed. O_2 levels were more sensitive to nitrogen loads than phosphorus loads, consistent with the preponderance of nitrogen limitation in Chesapeake Bay in late spring and summer months. Expanded hypoxic volumes under higher nitrogen loads were associated with increases in water-column production and respiration in seaward regions of Chesapeake Bay during summer (June to August) months. Analysis of the 10-year model run with realistic hydrodynamics and nutrient loading revealed a similar pattern, emphasizing the role of stimulation of phytoplankton growth in more-nutrient-limited lower-Bay regions during summer as a primary mechanism supporting elevated hypoxic volumes. ROMS-RCA is a useful tool for investigating system processes in Chesapeake Bay and other coastal ecosystems.

Conclusions

The study of dissolved O_2 in coastal ecosystems is a central problem, due to the association of O_2 dynamics with nearly all sub-disciplines of aquatic ecology and the varied and complex suite of interactions that ultimately control aquatic O_2 concentrations. Additionally, the fact that the negative impacts of O_2 on many higher organisms are widespread, O_2 is a major target of water quality management in fresh and marine waters alike. Chesapeake Bay is an estuary plagued by hypoxia and despite a long history of insightful analyses leading to an advanced understanding of controls on O_2, many important questions concerning controls on and effects of hypoxia remain. It is the purpose of this dissertation to further elucidate these mechanisms in Chesapeake Bay.

Figure Legends

Figure 1.1: Temporal distributions of O_2 concentrations in 3 different estuary types: (a) a well-mixed water column of a temperate estuary with diel cycling hypoxia (Corsica River estuary), where winter concentrations are higher than summer due to increased solubility, but also less variable due to reduced biological activity (Maryland Department of Natural Resources; www.eyesonthebay.com), (b) an episodically mixed water column of a temperate estuary (Pamlico River estuary), where surface concentrations always higher than bottom concentrations, but bottom concentrations occasionally are depleted to hypoxia during calm and/or productive periods (Lin et al., 2008), and (c) a temperate, stratified estuary (Chesapeake Bay), where surface and bottom concentrations are comparable during winter, when the water column is well mixed, but bottom water concentrations are nearly zero during summer when O_2 uptake rates are high and physical replenishment is minimal (Chesapeake Bay Program; www.chesapeakebay.net).

Figure 1.2: Conceptual diagram of nitrogen cycling in a coastal ecosystem under oxygenated (left panel) and hypoxic/anoxic conditions (right panel).

Figure 1.3: Conceptual diagram of phosphorus cycling in a coastal ecosystem under oxygenated (left panel) and hypoxic/anoxic conditions (right panel).

Figure 1.4: Hypothetical (left panel) and observed (right panel) relationships between nutrient loading and hypoxia in three estuaries with different responses.
(a) Linear relationship between loading and O_2 conditions in the Scheldt estuary, (b) Threshold relationship between organic matter loading and O_2 conditions in the Thames estuary near London, and (c) Threshold-hysteretic relationship between nutrient loading and hypoxia in the northwestern shelf of the Black Sea. See Kemp et al. (2009) for an expanded collection of potential trajectories.

Figure 1.5: Time-series (1945-2007) of (a) Susquehanna River Flow at Conowingo, MD, (b) January-May NO_3^- loads to Chesapeake Bay, (c) July hypoxic volume in Chesapeake Bay, (d) mean annual water temperature at Solomons, MD, (e) January to March North Atlantic Oscillation, and (f) annual Maryland (MD) and Virginia (VA) oyster harvest. All data are from Kemp et al. (2005), except temperature data (Kaushal et al., 2010) and NAO data (http://www.cgd.ucar.edu/cas/jhurrell/indices.html).

Fig. 1.1

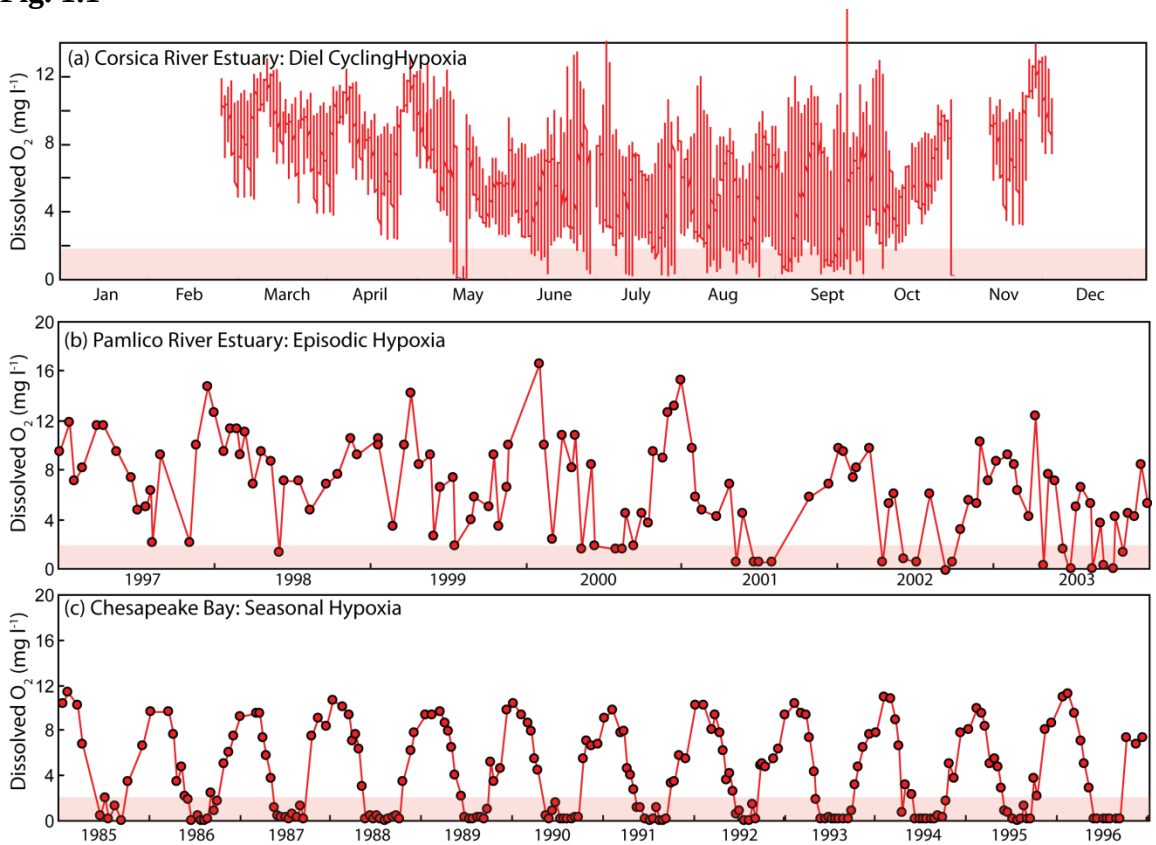
(a) Corsica River Estuary: Diel CyclingHypoxia
Dissolved O2 (mg l-1)
0
4
8
12
Jan
Feb
March
April
May
June
July
Aug
Sept
Oct
Nov
Dec
(b) Pamlico River Estuary: Episodic Hypoxia
Dissolved O2 (mg l-1)
0
4
8
12
16
20
1997
1998
1999
2000
2001
2002
2003
(c) Chesapeake Bay: Seasonal Hypoxia
Dissolved O2 (mg l-1)
0
4
8
12
16
20
1985
1986
1987
1988
1989
1990
1991
1992
1993
1994
1995
1996

Fig. 1.2

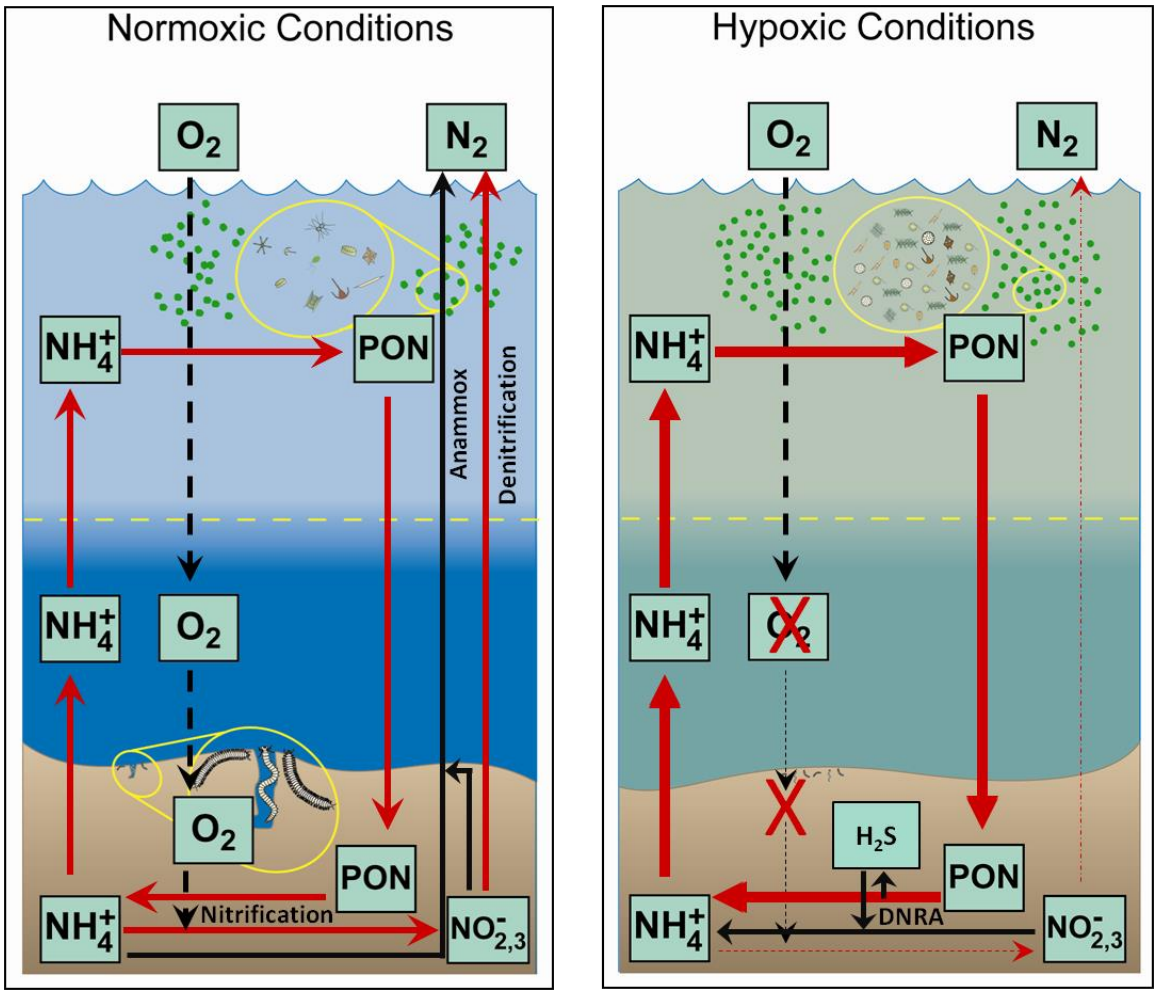
Normoxic Conditions
O2
N2
NH4+
PON
Anammox
Denitrification
NH4+
O2
O2
PON
NH4+
Nitrification
NO2,3-
Hypoxic Conditions
O2
N2
NH4+
PON
NH4+
O2
H2S
PON
NH4+
DNRA
NO2,3-

Fig. 1.3

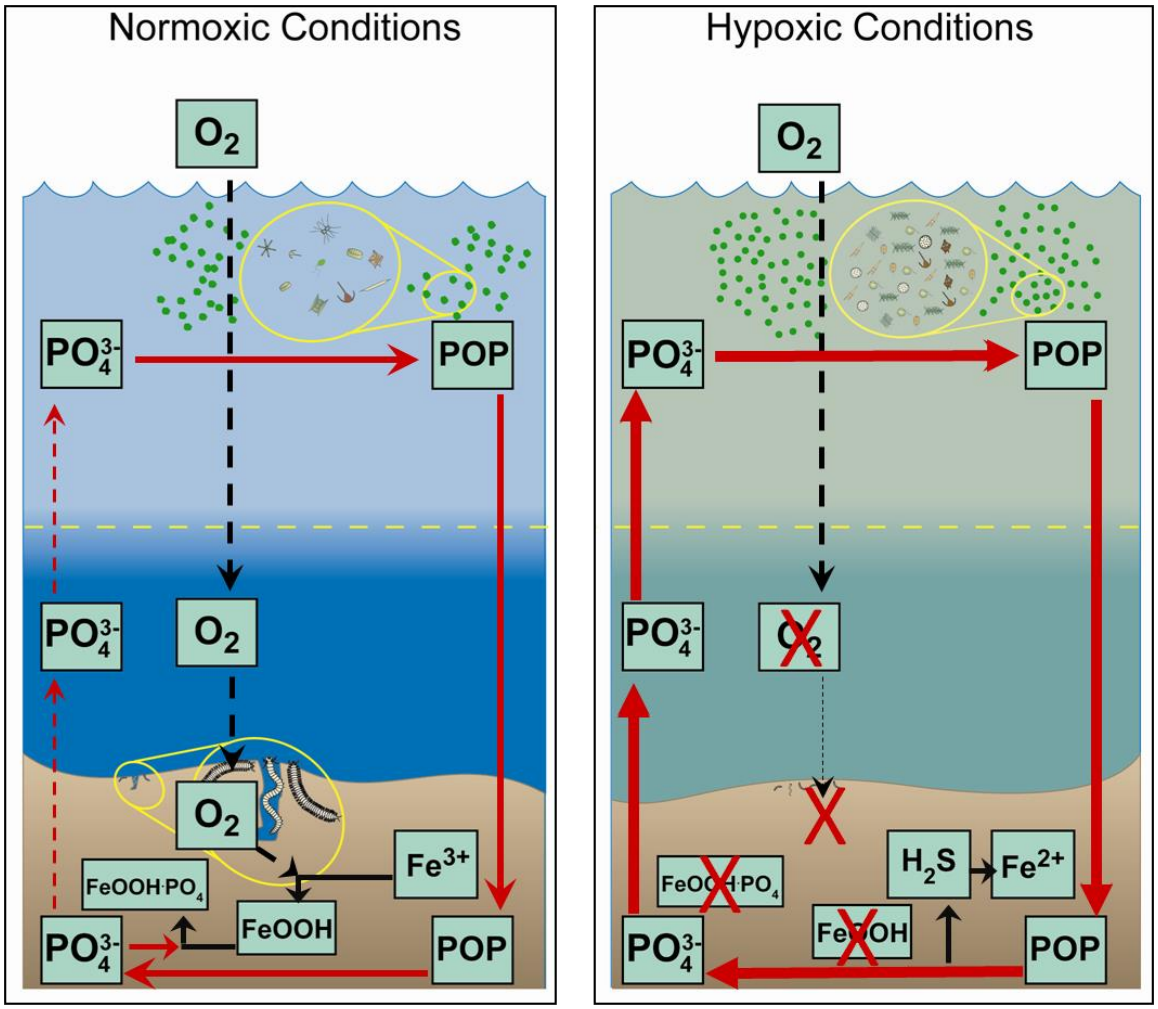
Normoxic Conditions
Hypoxic Conditions
O2
PO4 3-
POP
Fe3+
FeOOH·PO4
FeOOH
H2S
Fe2+

Fig. 1.4

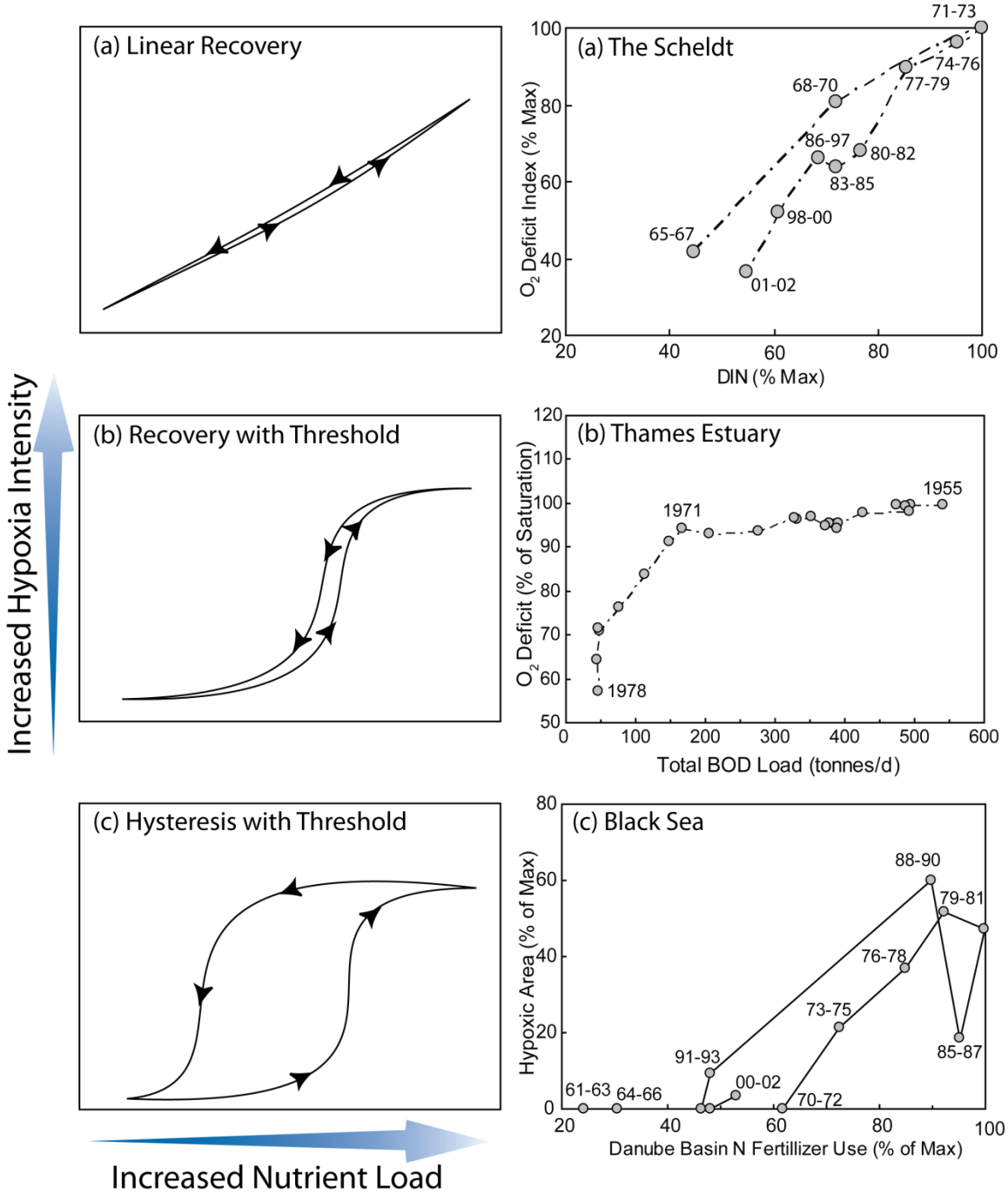
(a) Linear Recovery
(b) Recovery with Threshold
(c) Hysteresis with Threshold
Increased Hypoxia Intensity
Increased Nutrient Load
(a) The Scheldt
O2 Deficit Index (% Max)
DIN (% Max)
71-73
74-76
77-79
68-70
86-97
80-82
83-85
98-00
65-67
01-02
(b) Thames Estuary
O2 Deficit (% of Saturation)
Total BOD Load (tonnes/d)
1955
1971
1978
(c) Black Sea
Hypoxic Area (% of Max)
Danube Basin N Fertillizer Use (% of Max)
88-90
79-81
76-78
73-75
85-87
91-93
00-02
61-63
64-66
70-72

Fig. 1.5

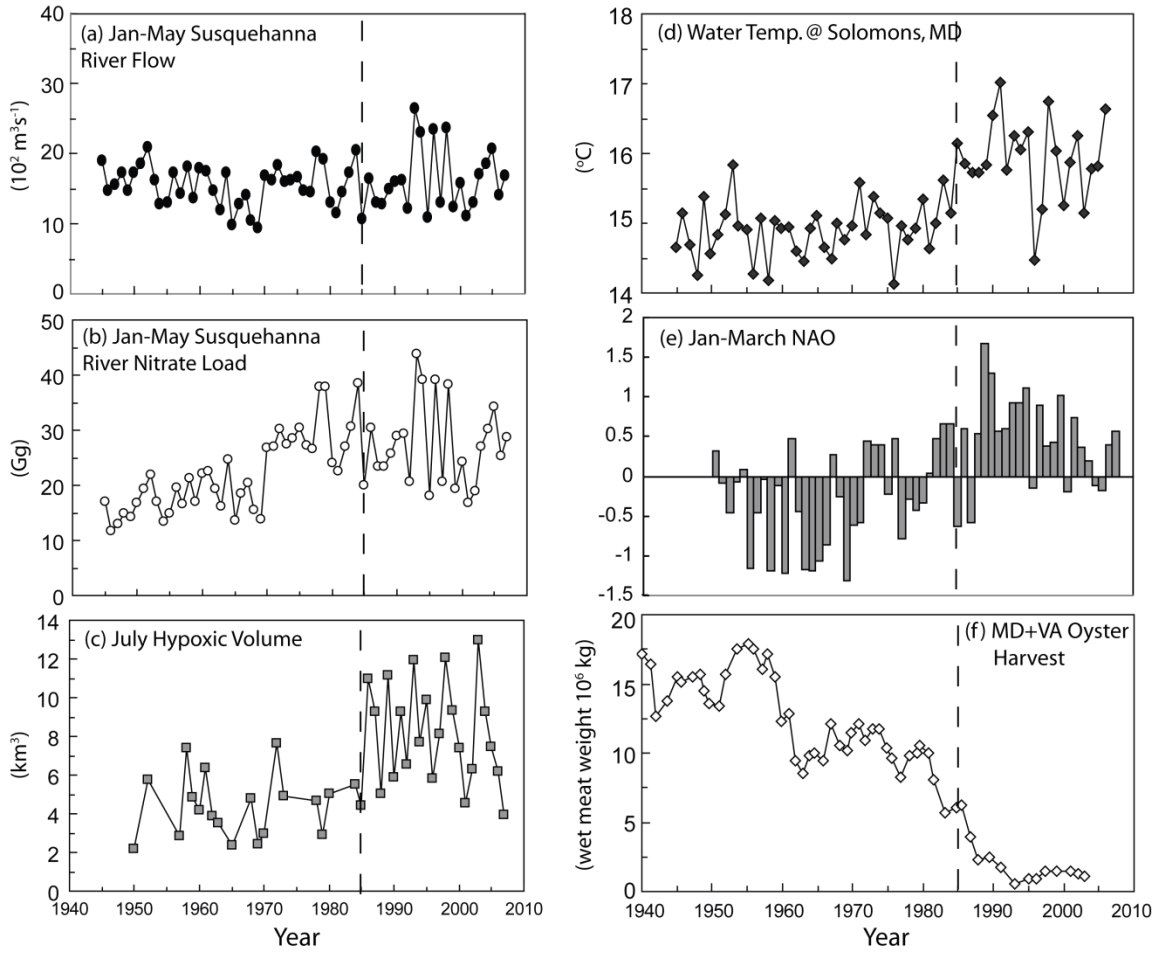
(a) Jan-May Susquehanna River Flow
(10² m³s⁻¹)
(b) Jan-May Susquehanna River Nitrate Load
(Gg)
(c) July Hypoxic Volume
(km³)
Year
(d) Water Temp. @ Solomons, MD
(°C)
(e) Jan-March NAO
(f) MD+VA Oyster Harvest
(wet meat weight 10⁶ kg)
Year

CHAPTER 2: HYPOXIA-INDUCED SHIFTS IN NITROGEN AND PHOSPHORUS CYCLING IN CHESAPEAKE BAY

Abstract

We investigated interactions between hypoxia and nutrient cycling in Chesapeake Bay using quantitative analysis of long-term monitoring data covering the periods 1965-1980 and 1985-2007. The data included vertical water column profiles of temperature, salinity, NH_4^+, PO_4^{3-}, and O_2, as well as rates of total nitrogen (TN) and total phosphorus (TP) loading to the Bay from the Susquehanna River. We investigated the hypothesis that a doubling of the volume of hypoxic (O_2<62.5 μmol L^{-1}) water generated per unit TN load in the past 25 years is related to enhanced water-column and sediment recycling of NH_4^+ and PO_4^{3-} under low O_2, and that this increased nutrient recycling creates a feedback that further generates hypoxia. We found that bottom-water in the upper Bay region, where seasonal hypoxia first develops, was enriched in NH_4^+ and PO_4^{3-} relative to other regions. Evidence of the positive feedback effect of low O_2 on nutrient recycling was found in the fact that bottom-water pools of NH_4^+ and PO_4^{3-} per unit TN and TP loading, respectively, were significantly and positively related to hypoxic volume in upper Bay regions during June. Similarly, NH_4^+ pools generated per unit TN load were significantly higher during 1985-2007, when hypoxic volume had been approximately doubled, relative to 1965-1980. This positive feedback effect on nutrient recycling may help to explain the persistence of extensive hypoxia in June, even during years of reduced N loading.

Introduction

Depletion of dissolved oxygen (O_2) from coastal waters is a widespread phenomenon that appears to be growing globally (Díaz and Rosenberg, 2008). There is considerable interest in this phenomenon because low O_2 causes physiological stress for

most marine metazoans, where O_2 levels below ~30% saturation ('hypoxia' = O_2<62.5 μmol L^{-1} or 2 mg L^{-1}) interrupt normal metabolism and behavior of invertebrates and fish, causing reduced growth and increased mortality (Díaz, 2001). Extended periods of hypoxia and relatively brief exposure to anoxia (O_2=0) can cause mortality for many marine animals (Vaquer-Sunyer and Duarte, 2008) and may also affect predator-prey interactions and food web structures (Decker et al., 2004). Consequently, many large-scale, expensive socio-economic commitments have been made to reduce hypoxia through remediation of eutrophication.

In addition to the negative effects of hypoxia on organism physiology, low O_2 levels and associated conditions (e.g., sulfide accumulation) also influence several key biogeochemical processes within the nitrogen and phosphorus cycles. For nitrogen, reduced O_2 concentrations limit nitrification and restrict coupled nitrification-denitrification (Kemp et al., 1990). Sulfide accumulations under low O_2 further inhibit nitrification and reduce the potential for anammox (Jensen et al., 2008), while also favoring dissimilatory nitrate reduction to ammonium (DNRA) over denitrification (McCarthy et al., 2008). The sum of these effects is reduced removal of inorganic N as N_2 and thus increased NH_4^+ accumulation. For the phosphorus cycle, inorganic phosphorus sorbed to metal oxide-hydroxide complexes is released under reduced O_2 (Sundby et al., 1992), while phosphorus regeneration from organic matter is enhanced (Jilbert et al., 2011). As a result of these processes, many recent reports suggest that an increasing fraction of the nitrogen and phosphorus deposited to sediments will be recycled back to the water column with expanding hypoxic conditions (Conley et al., 2002; Kemp et al., 2005). One possible consequence is that such increased nutrient

regeneration from sediments and bottom water will lead to higher availability of N and P for growth of nutrient-deficient summer phytoplankton (Conley et al., 2007; Ingall and Jahnke, 1994).

There have been few direct tests of this hypothesis at the ecosystem scale based on observations of nutrient loading and concentrations with metrics of hypoxia and anoxia. Previous observational and modeling studies have reported: 1) inverse correlations between O_2 and dissolved inorganic nutrient concentrations (Conley et al., 2002; Savchuk et al., 2008), 2) increased sediment-water nutrient fluxes under higher organic matter loads and reduced O_2 (Enoksson, 1993), 3) reduced sediment-N recycling efficiency (NH_4^+ flux/(NH_4^++NO_{23}^-+N_2) flux) under low O_2 or high respiration (Eyre and Ferguson, 2009; Kemp et al., 2005), and 4) enhanced sediment phosphorus release under O_2 declines (Meier et al., 2011; Reed et al., 2011). Inverse correlations between O_2 and nutrient concentrations may, however, be misleading due to the tendency of both to co-vary with particulate organic matter (POM) loading to sediments (Jensen et al., 1990). Because these interactions form a complete causal loop (nutrients –> phytoplankton –> POM –> hypoxia –> recycling –> nutrients), ecosystem-scale data analyses and/or modeling are needed to elucidate the positive-feedback connections between eutrophication and hypoxia in coastal aquatic ecosystems.

In Chesapeake Bay, the mid-summer volume of hypoxic water has been correlated with total nitrogen (TN) loading (Hagy et al., 2004) and its expansion over the past 60 years has been linked with the overall eutrophication of the estuary (Kemp et al., 2005). It appears that the volume of summer hypoxia generated per unit winter-spring TN load doubled abruptly in the early 1980s (Hagy et al., 2004). Although a clear

explanation for this expansion has been lacking, recent reports have suggested that a suite of biological and climatic shifts in the early 1980s may be involved (Murphy et al., 2011; Scully, 2010a). One hypothesis states that the expanded volume of hypoxic water in Chesapeake Bay and other coastal waters may have increased the fraction of winter-spring nutrient loads that are released back to the water column during summer (Kemp et al., 2005), resulting in elevated nutrient availability, algal growth, POM deposition, and associated summer O_2 consumption. A direct test of this feedback hypothesis is, however, generally lacking for Chesapeake Bay and other hypoxic, aquatic ecosystems.

The purpose of this paper is to quantify how long-term changes and variability in seasonal O_2 depletion may have altered summer accumulations of nutrients in Chesapeake Bay bottom-water. We hypothesize that increased hypoxic extent and intensity enhanced inorganic nutrient recycling rates in sediments and sub-pycnocline water, resulting in elevated bottom-water pools of NH_4^+ and PO_4^{3-} for a given nutrient load. We tested this hypothesis by examining concurrent, long-term time series of nutrient loading, concentration, and recycling rates with metrics of hypoxic volume along the mainstem of Chesapeake Bay.

Methods

We investigated interactions between hypoxia and nutrient cycling in Chesapeake Bay using quantitative analysis of long-term monitoring data covering two specific periods when there were sufficient vertical profile data for NH_4^+, PO_4^{3-}, and O_2. The first period, from 1965-1980, includes NH_4^+ and O_2 data from various research cruises and estimates of total nitrogen loading from Susquehanna River, the Bay's primary source of freshwater. The second period, from 1985-2007, includes routine nutrient and O_2

monitoring data and computations of both total nitrogen and total phosphorus (TP) loading from the Susquehanna River. There were insufficient data in the years 1981-1984 to include in our historical analysis. This study was carried out in the mainstem (tributaries omitted) of Chesapeake Bay, a semi-enclosed estuary in the mid-Atlantic region of the United States (Fig. 2.1). Many of the Bay's ecological and geographic features have been described previously (Hagy et al., 2004; Kemp et al., 2005), including long-term changes in key chemical, biological, and physical conditions.

TN and TP loading

We used TN and TP loading rates from the Susquehanna River in our analysis for the two periods of this study (1965-1980 and 1985-2007). Monthly TN loading rates from 1965 to 1980 were obtained from (Hagy et al., 2004), who reconstructed NO_3^- and TN loads from 1945-2001 from a time series of NO_3^- concentrations and stream flow measurements in the lower Susquehanna River. No TP loading rates were available for this period. Monthly loading rates for the 1985 to 2007 period for TN and TP were acquired from the United States Geological Survey (USGS) website (http://va.water.usgs.gov/chesbay/RIMP/loads.html). USGS nutrient loads were estimated using a multiple linear regression model based on daily mean streamflow and sub-monthly nutrient samples (Langland et al., 2006). Where TN loads computed by USGS and Hagy et al. overlapped in time, the two estimates were highly correlated and quantitatively similar (Hagy et al., 2004).

We focused on Susquehanna River loads because this river contributes 65% of the TN and 42% of the TP that is discharged into Chesapeake Bay on average for the months of January to May (1985-2007; USGS data). In contrast to other tributary rivers of the

Bay, the Susquehanna discharges freshwater and nutrients directly into the main stem of Chesapeake Bay (our study area). Nutrients from other, smaller rivers must pass through tributary estuaries (*see* Fig. 2.1), where a substantial portion is assimilated before entering the main stem Bay (Boynton et al., 1995). In any case, seasonal and long term trends in TN and TP loading from the Bay's next largest tributary rivers (Potomac, James, Rappahannock, and York) are highly correlated with those from the Susquehanna River (Murphy et al., 2011). Thus, inputs from the Susquehanna River represent the largest and most direct source of TN and TP to the main stem Bay, and it provides a consistent index of interannual variation in nutrient loading to our study area.

Water-column concentrations

Vertical profiles of temperature, salinity, NH_4^+, PO_4^{3-}, and O_2 were obtained for the months April-August in the two study periods. For 1965-1980, we collated only NH_4^+ measurements from various monitoring and research cruises in Chesapeake Bay (*see* Table 2.1 for list of data sources). For 1985-2007, we obtained data for all of these water quality variables from the Chesapeake Bay Program Water Quality database (http://www.chesapeakebay.net/data_waterquality.aspx). In the latter dataset, profiles were routinely collected at 20 stations along the Bay's central channel (Fig. 2.1, Table 2.1), where temperature, salinity, and O_2 were generally measured at 1-m depth intervals, while NH_4^+ and PO_4^{3-} were measured at 4-5 depths for each station (2-10 m intervals, Fig. 2.1). NH_4^+ measurements in the recent (1985-2007) and historical (1965-1980) data sets were made by using the spectrophotometric phenolhypochlorite method (EPA, 1997; Solorzano, 1969), a methodological consistency that permits comparisons of data between the two periods. PO_4^{3-} in the recent data set was determined colormetrically

using standard methods (EPA, 1997; Murphy and Riley, 1962). If multiple measurements were made at a particular station and depth within a month (fortnightly sampling was common post-1985), concentrations were averaged to monthly means.

Stratification

We estimated pycnocline depth for particular regions as the vertical position in the water column (depth in m, *z*) where the square of the Brunt-Väisälä frequency was at its maximum value (Pond and Pickard, 1983):

$$N^2(z) = \frac{g}{\sigma_z} \cdot \frac{\partial \sigma}{\partial z}$$

where g = gravitational constant, 9.81 m s^{-2}, σ_z is the water density at depth (kg m^{-3}), and $\frac{\partial \sigma}{\partial z}$ is the density gradient at depth *z*, which was calculated using a 2-m window around *z*. Density was computed (Fofonoff, 1985) from profiles of temperature and salinity data at 1-m depth intervals using the Chesapeake Bay Program Water Quality database.

Interpolations

We interpolated spatial distributions for NH_4^+, PO_4^{3-}, and O_2 concentrations during the summer hypoxic periods (June, July, and August) of 1985 through 2007 and for NH_4^+ observations in 11 years between 1965 and 1980. Observed NH_4^+, PO_4^{3-}, and O_2 vertical profiles along the main channel for a given month (Fig. 2.1) were interpolated to a 2 dimensional length-depth grid using ordinary kriging (Murphy et al., 2010; Murphy et al., 2011). The statistical package R with the geoR package (Ribeiro and Diggle, 2009) was used for all interpolations, as described in (Murphy et al., 2011). The resulting 2D distributions were assumed to be constant laterally at a given depth and organized to correspond to tabulated cross-sectional volumes (Cronin and Pritchard, 1975).

The interpolated concentration data were multiplied by the cross-sectional volumes to compute NH_4^+-N and PO_4^{3-}-P pools along the Bay axis. The vertical dimension of the bottom-water volume for which we computed nutrient pools was defined by the distance from sediment surface to the average pycnocline position. The pycnocline depth was slightly different for the two analyses we performed. In the first analysis, where we compared the bottom-water nutrient pools in different regions over the 1965-1980 and 1985-2007 periods, nutrient pools were summed beneath 10 m depth in water for four Bay regions: between a) 200-250, b) 150-200, c) 100-200, and d) 75-250 km from the Atlantic Ocean. Although the pycnocline depth varies regionally and inter-annually (Murphy et al., 2011), we lacked salinity profiles in some of the historic years, making it impossible to estimate pycnocline depth in each year. We chose 10 m as an approximate average summer position of the pycnocline in this region of the Bay, and this allowed us to compare the nutrient accumulation in the same volume of water in each year. Thus, the accumulated pool of NH_4^+ between two years was attributable to differences in recycling processes but not due to differences the exact pycnocline position. In the second analysis where we investigated the region-specific relationship between bottom-water nutrient pools and hypoxic volumes during 1985-2007, we summed nutrient pools below the region-specific average pycnocline depth (Hagy, 2002) for 8 regions of Chesapeake Bay (Regions II-IX, Fig. 2.1, Table 2.1). Although the mid-summer volume of hypoxic water in Chesapeake Bay has been previously computed over 1950-2001 (Hagy et al., 2004) and 1984-2007 (Murphy et al., 2011), for this analysis we computed monthly hypoxic volumes for the years 1985-2007 by summing

the volume of all interpolated cells in Chesapeake Bay with an O_2 concentration <62.5 μmol L^{-1}.

The sampling frequency and density for NH_4^+ was lower in the years before the modern monitoring program (6-8 stations, 19-35 samples per month pre-1985; 20 stations, 70-130 samples per month for 1985-2007). We tested the potential for bias in the NH_4^+-N pools computed from data sets in the pre-1985 period by comparing computations on the full 1985-2007 data with computations using smaller datasets generated from sub-sampling at the lower observational densities characteristic of the pre-1985 data. Sub-sampling of the modern observations was achieved by using observed sample locations (depth, distance from Atlantic Ocean along the central channel of Chesapeake Bay) from each pre-1985 year to extract stations with similar locations in the modern data set. At each 1.85 kilometer segment along the Bay's central channel where a sample was taken in the pre-1985 year, a routine searched for any observation in the modern data set that was within 3 m depth of each historic sample that section. Once the routine extracted the appropriate stations from the modern data set, this sub-sampled data set was interpolated as described above. This routine was applied for June, July, and August data for the years 1985-2007 for each historic year (11 years total), resulting in 11 new sets of monthly NH_4^+ distributions and NH_4^+-N masses representing the years 1985-2007. We omitted a pre-1985 year from the analysis if the mean NH_4^+-N pools computed from the sub-sampled distributions were significantly different from the fully-sampled distributions (analysis of variance (ANOVA), SAS version 9.2) or where sub-sampled NH_4^+-N masses were consistently more than 20% different than fully-sampled masses.

Statistical analysis

We tested the compiled time-series of hypoxic volume per unit TN load in Chesapeake Bay (Fig. 2.2) for a significant shift using a simple change-point detection routine (http://www.variation.com/cpa/tech/changepoint.html). The method is used to identify a single change in a time-series using cumulative sum charts, or CUMSUM (Pettitt, 1980) with bootstrapping (Hinkley and Schechtman, 1987). This is accomplished by computing the cumulative sum of the difference between the observed value at a given point in a time series and the average of the entire time-series. The change-point occurred at the point in time where the difference between the maximum and minimum CUMSUM (S_{diff}) is greatest. Once the original time-series was tested for the time when a shift in the mean of the data existed, a bootstrapping analysis was run, where the time-series was reordered 1000 different ways and the process repeated. The confidence level (CL) is computed as the percentage of the 1000 iterations where S_{diff} of the randomly reordered data is less than S_{diff} in the original time-series. We considered CL >95% to be significant. We further tested the change-point by summing the squared differences between the data and the mean of the data for the periods before and after the change-point identified by the CUMSUM approach (i.e., the mean square error, MSE). This approach was performed an additional 8 times by assuming the change-point occurred at each of the 4 years before and after the actual change-point. The lowest MSE value represents the last point before the change-point.

We tested for differences in the regional mean pools of NH_4^+-N and PO_4^{3-}-P in bottom-water near the upward shift in hypoxic volume using *t*-tests (SAS 9.2). We selected regions that spanned the seasonally-hypoxic part of the mainstem of Chesapeake

Bay during the months when hypoxia is most extensive and consistent. Thus, data were separated into two groups (1965-1980 and 1985-2007) and mean comparisons were conducted on bottom-water pools in three regions (200-250, 150-200, and 100-200 km) for three summer months (Table 2.3).

Because the conditions that generate extensive hypoxia (i.e., elevated river flow, nutrient load, and phytoplankton biomass) also tend to elevate water column nutrient levels, we sought a measure of nutrient accumulation that might be linked more directly to hypoxia. Thus, we defined 'nutrient recycling indices' as the ratios of summer, bottom-water pools of NH_4^+-N and PO_4^{3-}-P to winter-spring TN and TP load (nitrogen pool per nitrogen load (NP NL^{-1}) and phosphorus pool per phosphorus load (PP PL^{-1}), respectively), which normalizes nutrient accumulation to nutrient input. We also used simple linear regressions (general linear models (GLM) procedure; SAS 9.2) to evaluate relationships between hypoxic volume and nutrient recycling indices in a more spatially-resolved set of 6 regions (II-VII, Fig. 2.1, Table 2.1) than used for nutrient pool comparisons. The comparisons here were evaluated in terms of *r* and *p*-values.

Results

The July volume of hypoxic water in Chesapeake Bay increased over the 1950-2007 period (Hagy et al., 2004), with a concurrent increase in nitrogen and phosphorus loading to Chesapeake Bay. The volume of hypoxia observed for a given winter-spring loading of total nitrogen (TN) from the Susquehanna River, however, nearly doubled in the period from 1986 to 2007, at 0.24 km^3 Gg^{-1} (Gg = gigagram), relative to 1950-1985 (0.14 km^3 Gg^{-1}). Change-point detection analysis indicated that this increase occurred

between 1985 and 1986 (Fig. 2.2), where the change-point CL was >99% over the 1000-iteration bootstrap analysis.

The ratio of NH_4^+ pools in sub-pycnocline Bay water to TN load (hereafter NP NL^{-1}) also increased over the last 5 decades (Fig. 2.3). This long-term increase in NP NL^{-1} corresponds to the increase in hypoxia per unit TN load over the same period, as represented by higher NP NL^{-1} during June in the 1985-2007 period relative to the 1965-1980 period (Figs. 2, 3). Although NP NL^{-1} is on average higher during the 1985-2007 period in three regions of the middle Bay in three summer months, this apparent increase was significant only in June within the most landward region (200-250 km, Region III-IV, $p<0.05$); it is also nearly significant in August in the 200-250 km region (V-VI) in August ($p=0.058$, Table 2.3). Too few years include measurements of both NH_4^+ and O_2 to allow direct comparisons of the effect of hypoxia on these NH_4^+ patterns.

We did not find substantial bias or large discrepancies in the regional NH_4^+-N pools computed in the 1985-2007 period using the full data sets compared sub-sampled spatial densities representative of the pre-1985 data for 8 of the 11 years (73%) in the historic data set. The years 1969, 1971, and 1979 were omitted. In the other 8 cases, NH_4^+-N pools calculated from full and sub-sampled data sets were highly correlated ($0.72<R^2<0.97$) with slopes ranging from 0.88 to 1.15 (Fig. 2.4) and no significant differences in the means for the sub-sampled vs. fully-sampled data. We used data from these 8 years for the rest of the analysis.

Analysis of experimental data collected in recent decades provides evidence for interactions between O_2 and the nitrogen and phosphorus cycles. Sediment-water NH_4^+ and PO_4^{3-} fluxes, as measured at two stations in mesohaline Chesapeake Bay (Fig. 2.1),

were inversely related to O_2 concentrations in overlying water (Fig. 2.5). Enhancement of sediment-water NH_4^+ and PO_4^{3-} fluxes is most evident below 50 μmol O_2 L^{-1} (Fig. 2.5), and multiple means comparisons of the nutrient fluxes in each of the 5 O_2 ranges (GLM procedure, SAS version 9.2, 1-way ANOVA with a Duncan's test) confirmed that NH_4^+ and PO_4^{3-} fluxes at O_2<50 μmol L^{-1} were significantly (p<0.05) higher than the other groupings. However, NH_4^+ fluxes gradually increase with lowered O_2, while PO_4^{3-} fluxes exhibited an abrupt jump at O_2 below 50 μmol L^{-1} (Fig. 2.5). During May to July, bottom-water NH_4^+ and PO_4^{3-} concentrations (at 1-2 m above sediment for the nearby monitoring station) were significantly and positively correlated to sediment-water NH_4^+ (R^2=0.30, p<0.001) and PO_4^{3-} fluxes (R^2=0.40, p<0.001). These sediment-water NH_4^+ and PO_4^{3-} fluxes under hypoxic conditions (<50 μmol L^{-1} in Fig. 2.5) were sufficient to fully replace sub-pycnocline pools of NH_4^+ and PO_4^{3-} in 33 and 14 days, respectively.

Contour plots representing vertical distributions of O_2, NH_4^+ and PO_4^{3-} along the mainstem Bay channel reveal spatial covariance between depleted O_2 and elevated nutrients (Fig. 2.6). NH_4^+ and PO_4^{3-} concentrations were highest in June in the landward channel region between 200 and 250 km from the Atlantic; this is the region where very low O_2 concentrations (<50 μmol L^{-1}) first appear seasonally in Chesapeake Bay (Fig. 2.6). By August, bottom-water with low O_2 and high nutrient concentrations extends seaward to Regions VI and VII. Vertically, these waters with high nutrients and low O_2 generally extend up from the sediment surface to depths of 8-12 m (Fig. 2.6), where the pycnocline develops each summer, reaching maximum strength in June (Murphy et al., 2011).

Vertical NH_4^+, PO_4^{3-}, O_2, and salinity profiles at station CB4.3C (Region V) during July provide a more detailed picture of physical controls on O_2 and nutrient distributions (Fig. 2.7). In comparing profiles from July 1998 (2nd highest winter-spring Susquehanna River flow since 1985) with that of July 1999 (a year with moderate-low river flow), it is evident that elevated spring flow led to larger differences between surface and bottom salinity in 1998 (Fig. 2.7). Computations of stratification revealed that maximum N^2 was 2.3 s^{-2} at 9 m in 1998 and 1.3 s^{-2} at 14 m in 1999 (Fig. 2.7). Stronger stratification and a shallower pycnocline resulted in near anoxia at 10 m in 1998, compared to 16 m in 1999, and hypoxia at 8 m in 1998, compared to 10.5 m in 1999. Profiles of NH_4^+ and PO_4^{3-} exhibited patterns inverse to those of O_2, where nutrient levels were low in surface waters (<10 m), but increased rapidly below 10 m where O_2 was depleted (Fig. 2.7). Bottom-water pools of PO_4^{3-} and NH_4^+ were higher in 1998 than in 1999, associated with stronger stratification and a larger anoxic zone (Fig. 2.7). High NH_4^+ concentrations existed above the pycnocline in 1998, while PO_4^{3-} was only elevated in deeper, anoxic water (Fig. 2.7).

Although NH_4^+ and PO_4^{3-} accumulations and O_2-depleted zones were spatially linked during summer, these spatial relationships varied seasonally along the salinity gradient of Chesapeake Bay (Fig. 2.8). On average, hypoxic water extended from Region III-IV, and NH_4^+ and PO_4^{3-} concentrations reached their Bay-wide peaks in this region (Fig. 2.8). NH_4^+ and PO_4^{3-} concentrations were both significantly lower in April (<12 and 0.3 μmol L^{-1}, respectively) when O_2 was near saturation (Fig. 2.8) than peak values in July and August (ANOVA with Scheffe's test, SAS version 9.2). As moderate hypoxia was established in June, NH_4^+ concentrations reached their seasonal maxima in the mid-

bay, at Regions IV and V, where NH_4^+ was significantly higher than landward and seaward positions (ANOVA with Scheffe's). PO_4^{3-} remained relatively low throughout the Bay during April and June (Fig. 2.8), although PO_4^{3-} was significantly higher in June than April in Region IV-V (ANOVA with Scheffe's). In August, when O_2 was near-anoxic in Region IV-V, PO_4^{3-} reached its seasonal maximum and was significantly higher than April and June in all Bay regions, while elevated NH_4^+ concentrations persisted, albeit below the June peaks (Fig. 2.8).

Plots of monthly mean concentrations of O_2 vs. PO_4^{3-} and NH_4^+ (1985-2007, Fig. 2.9) in the mesohaline Region V, reveal that PO_4^{3-} concentrations did not substantially increase as O_2 declined during April and May. O_2 concentrations became hypoxic and then anoxic from June through August, however, and PO_4^{3-} consequently increased by an order of magnitude (Fig. 2.9). In contrast, NH_4^+ concentrations increased linearly and by a factor of 4 as O_2 declined from normoxic to hypoxic conditions from April to June; however, from July to August, NH_4^+ declined to April levels (Fig. 2.9).

Larger hypoxic volumes generally lead to higher nutrient recycling (NP NL^{-1} and PP PL^{-1}) in June throughout most of Chesapeake Bay. NP NL^{-1} and PP PL^{-1} were significantly correlated with the associated regional volume of hypoxia in Region II (NP NL^{-1}, PP PL^{-1}) and III (NP NL^{-1}) for the month of June (Table 2.4, Fig. 2.10). NP NL^{-1} and PP PL^{-1} in Region IV were also significantly correlated (r=0.65 and 0.57, respectively, p<0.01) to upper Bay hypoxic volume (Region IV) in June. The day of year that hypoxia initiated in Region III was also significantly correlated with NP NL^{-1} and PP PL^{-1} in that region (r=0.44, 0.62, respectively, p<0.05). Bay-wide, correlations between NP NL^{-1}, PP PL^{-1} and hypoxia indices were weak during July and August (Table 2.4).

Discussion

The discovery of a two-fold increase in the Bay's July hypoxic volume per unit winter-spring Susquehanna River TN loading after 1985 (Hagy et al., 2004) has generated considerable analysis and speculations as to controlling factors . Similar shifts in the relationship between nutrient loading and hypoxia have been reported for other coastal ecosystems, where these ecosystems also appeared to be more susceptible to hypoxia at a given nutrient load (Conley et al., 2009a; Turner et al., 2008). Although the ability to analyze such phenomena over large time and space scales is often data-limited, the availability of long-term observational data throughout the mainstem of Chesapeake Bay provided an opportunity to investigate such physical-biological-chemical interactions.

Hypoxia-enhanced nutrient recycling represents a positive feedback that could reinforce hypoxia via several biogeochemical interactions. Specifically, nitrogen and phosphorus entering the Bay each spring and summer are assimilated by phytoplankton to form particulate organic forms of nitrogen (PON) and phosphorus (POP). These particulate nutrients ultimately sink to be decomposed in bottom-water and sediments via hydrolysis reactions involving a sequence of available terminal electron acceptors (Middelburg and Levin, 2009). NH_4^+ and PO_4^{3-} generated by this decomposition and released to interstitial sediment and overlying water are potentially cycled by several O_2-sensitive biological and chemical processes (McCarthy et al., 2008; Middelburg and Levin, 2009; Sundby et al., 1992), whereby reduced bottom-water O_2 can increase (via various mechanisms) the accumulation of both NH_4^+ and PO_4^{3-} in bottom-water pools (Conley et al., 2002; Ingall and Jahnke, 1994; Kemp et al., 1990). In addition to direct

effects on biogeochemical processes, low-O_2 can indirectly elevate N and P recycling by imparting physiological stress or mortality on many benthic invertebrate macrofauna (Levin et al., 2009), which otherwise ventilate the sediments with O_2 (Welsh, 2003). Macrofauna ventilation delivers O_2 to sediments to stimulate coupled nitrification-denitrification (Pelegrí and Blackburn, 1995), restrict preferential phosphorus remineralization under low-O_2 (Jilbert et al., 2011), and retard the dissolution of oxidized Fe and Mn complexes that promote burial or immobilization of metal-sorbed PO_4^{3-} rather than release to overlying waters (Middelburg and Levin, 2009) Increased NH_4^+ and PO_4^{3-} availability then has the potential to fuel increased surface-layer phytoplankton growth and associated organic matter deposition, bottom-water O_2 consumption, and hypoxia.

Measurements of sediment-water NH_4^+ and PO_4^{3-} fluxes in seasonally-hypoxic and anoxic regions of Chesapeake Bay reveal relationships between low O_2 and elevated nutrient recycling. Specifically, as O_2 declines in overlying water, rates of sediment release of NH_4^+ and PO_4^{3-} increase, but the nature of the relationship differs for N and P (Fig. 2.5). This difference in the two relationships results from different biogeochemical controls. Gradual declines in O_2 and increases in sulfide restrict nitrification (Joye and Hollibaugh, 1995; Kemp et al., 1990) and favor dissimilatory nitrate reduction to ammonium, DNRA (McCarthy et al., 2008). The presence of sulfide, in combination with low NO_3^- and NO_2^- availability, reduces the potential for denitrification and anammox (Eyre and Ferguson, 2009; Jensen et al., 2008; Rich et al., 2008). In concert, these various effects lead to increased NH_4^+ release to overlying water. In contrast, PO_4^{3-} remineralized under normoxic conditions is bound to insoluble oxides and hydroxides of Fe and Mn (Froelich, 1988) and retained in sediments until a low-O_2 concentration threshold is

crossed (O_2<50 μmol L^{-1}), thereby reducing Fe(III) and Mn(IV) to soluble states and releasing the accumulated PO_4^{3-} to interstitial and overlying water (Sundby et al., 1992). Additionally, the development of hypoxic and anoxic conditions leads to enhanced phosphorus remineralization from organic matter, without an associated affect on nitrogen (Jilbert et al., 2011). Elevated sulfide accumulations as O_2 nears anoxic levels further promote rapid efflux of PO_4^{3-} (Caraco et al., 1989). Significant correlations between summer sediment-water fluxes and water-column NH_4^+ and PO_4^{3-} concentrations (data not shown) suggest that such high sediment-water fluxes under low O_2 cause elevated water-column nutrient levels.

Patterns of bottom-water nutrient pools and O_2 levels are also spatially linked. As evident in isopleths of mean (1985-2007) distributions of PO_4^{3-}, NH_4^+, and O_2 along the Bay's central channel during June (Fig. 2.6), bottom-water NH_4^+ and PO_4^{3-} accumulations are focused in the northern portion of (200-250 km) the hypoxic region, where O_2 depletion is most intense. The focusing of nutrients and hypoxia in this time and place is readily explained. A large fraction of the organic matter produced during spring is deposited here (Malone et al., 1988), resulting in decomposition, nutrient cycling, and O_2 depletion. In addition, stratification tends to be strongest in June (Murphy et al., 2011), leading to restricted O_2 replenishment and nutrient dilution in bottom-waters (Fig. 2.6). Landward, bottom-layer transport of O_2 into this region (Pritchard, 1967) is also limited by low O_2 concentrations in seaward source water. Thus, a combination of physical, ecological, and biogeochemical processes creates an epicenter of O_2-influenced nutrient cycling in the upper-middle Bay. As bottom-water hypoxia spreads seaward during summer, NH_4^+ and PO_4^{3-} pools increase in those regions (Fig. 2.8).

Seasonal and regional patterns in NH_4^+ and PO_4^{3-} accumulation differ markedly in their relationship to O_2-depletion patterns. Although June-July NH_4^+ and PO_4^{3-} concentrations were highest in the mid-Bay (200 km), PO_4^{3-} continues to increase through August, while NH_4^+ declines (Figs. 7, 8). This is due to a delay in PO_4^{3-} release from sediments that has been well described, as ions retained in sediments under oxidized conditions via sorption to Fe and Mn oxyhydroxides are subsequently released in large quantities with the onset of anoxia during July and August (Reed et al., 2011). The reason for declining NH_4^+ concentrations during July and August is less clear. One explanation for this pattern is that deposition rates of high-quality organic matter in July and August are lower than in spring, which is consistent with the transition from larger, fast-sinking winter-spring diatom-dominated communities to smaller, slowly-sinking, flagellated phytoplankton in summer (Marshall and Nesius, 1996). Alternatively, higher water-column nutrient recycling rates (Glibert, 1982) and a larger contribution of zooplankton fecal material to particle sinking fluxes in summer, may lead to the deposition of relatively nutrient-poor material during this time. Regardless of the explanation, this seasonal asynchrony in N and P cycling contributes to the N-limited conditions for phytoplankton production in the mesohaline Bay during late spring and summer (Fisher et al., 1999).

Changes in vertical profiles of NH_4^+ and PO_4^{3-} under increasingly hypoxic conditions highlight the potential enhancement of nutrient availability in near-surface waters. For example, in comparing two adjacent years with large differences in freshwater flow and nutrient load, and consequently, volume of hypoxic water (1998=4.2 km^3; 1999=2.6 km^3), it is apparent that in 1998, the increased pycnocline strength and

height in the water column allowed for a sharper decline in O_2 and a shallower depth of hypoxia than in 1999 (Fig. 2.7). Moreover, NH_4^+ and PO_4^{3-} concentrations were generally higher at a given depth below the pycnocline, especially NH_4^+, where concentrations in excess of 10 μmol L^{-1} were present above 10 m. Converting Secchi Depth (z_{sd}) measurements from this station (CB4.3, Table 2.1) of 2.05 m for July 1998 to an estimate of k_d (k_d=1.5/z_{sd}), the 1% light depth would be 6.3 m. Thus high-NH_4^+ water penetrated into or just beneath surface waters where phytoplankton actively grow during a high hypoxia year; in contrast, high NH_4^+ water did not overlap with the 1% light depth in 1999 (Fig. 2.7). Given such elevated nitrogen concentrations at depths above the pycnocline and within the euphotic zone, surface-layer phytoplankton production is likely to be stimulated (Fisher et al., 1999).

Although this discussion has thus far demonstrated temporal/spatial synchrony of hypoxia and NH_4^+ and PO_4^{3-} pools and recycling fluxes, the hypothesized feedback effect of low-O_2 conditions on nutrient cycling also suggests that the relative portion of nutrient inputs that are recycled would increase with hypoxia. A straightforward test of O_2 effects on nutrient recycling enhancement is to compute bottom-water accumulations of NH_4^+ and PO_4^{3-} (in June, July, and August) per unit TN and TP load in winter-spring. This metric, NP NL^{-1} and PP PL^{-1}, respectively, is needed to remove covariance effects, as high nutrient loads will also tend to increase nutrient concentrations and associated phytoplankton production, sinking, and O_2 depletion (Malone et al., 1988). Elevated rates of TN and TP loading are associated with high river flow, which also increases stratification strength and reduces O_2 replenishment to bottom-waters (Murphy et al., 2011). On decadal time-scales, NP NL^{-1} in June was higher on average after 1985

throughout the Bay and significantly higher in landward regions (Fig. 2.2 & 2.3; Table 2.3). Thus, expanded hypoxic volumes were related to elevated NH_4^+ accumulation over this 50-year period. Although NP NL^{-1} was also higher in the post-1985 period in July and August, indicating that hypoxia can lead to elevated nutrient recycling throughout summer, these increases were not significant (Table 2.3).

Because temporal gaps in the historical dataset (Fig. 2.3) limit further quantitative analysis and historical TP loading estimates do not exist, we focused further analysis on recent years (1985-2007) for which there were consistent and extensive data for PO_4^{3-}, NH_4^+, and O_2 concentrations. Significant correlations between hypoxic volume and both NP NL^{-1} and PP PL^{-1} during June in Regions II-III indicate that a larger fraction of spring nutrient loads are recycled from sediments and accumulate in bottom-water when O_2 depletion is more severe (Fig. 2.10). Other potential causative variables (nutrient load, stratification, algal biomass) showed no relationships to the elevated nutrient availability, thus leading to a conclusion that hypoxia was the principal causative factor.

Thus, there appears to be a positive feedback, whereby increased hypoxia generates larger summer nutrient pools, which could fuel higher summer algal growth and subsequent sinking and deposition that sustains more hypoxia for a longer duration. This feedback appears, however, to be spatially dependent. The fact that the strongest relationships between hypoxic volume and either NP NL^{-1} or PP PL^{-1} were for June data in the upper-middle Bay (for both the recent and historical data sets) is likely related to several factors. First, June is a time when the annual spring diatom bloom, which is commonly deposited in this region (Hagy et al., 2005), is being rapidly metabolized (Cowan and Boynton, 1996), thereby releasing large amounts of NH_4^+ and PO_4^{3-} from

organic material. Secondly, stratification is at its seasonal peak during June, and this reduces vertical mixing that may otherwise replenish O_2 and deplete bottom-water nutrients (Murphy et al., 2011). Third, hypoxic conditions first develop in the upper regions of the Bay (>175 km) in the central, deep channel (Fig. 2.6), thus exposing these sediments to hypoxic conditions for a longer period compared to other regions. This latter point is supported by a positive correlation between the date of hypoxia initiation and both NP NL^{-1} and PP PL^{-1} in the upper-middle Bay regions (III-V), where hypoxia developed earlier when NP NL^{-1} and PP PL^{-1} were higher. Such relationships are weaker in other Bay regions for various reasons. For example, the most landward regions are often vertically well-mixed (Table 2.1) and algal growth is light-limited in spring (Fisher et al., 1999). Similarly, lower Bay regions have relatively shallow depths (Fig. 2.1, Table 2.1) and low organic matter deposition (Hagy et al., 2005).

An implicit assumption of the proposed feedback effect is that NH_4^+ and PO_4^{3-} can be transported vertically to surface waters to stimulate phytoplankton growth without an associated downward transport of O_2 to relieve hypoxia. The dominant vertical transport processes in the two-layer circulation of Chesapeake Bay (Pritchard, 1967) are upward vertical advection and upward or downward turbulent mixing, the latter of which depends on solute concentration gradients. Although vertical mixing in summer would generate both upward transport of NH_4^+ and downward transport of O_2, the relatively strong summer stratification in the mesohaline Bay's central channel (Scully, 2010a) suggests that vertical advection would be more important in transporting both nutrients and O_2 into the surface layer and would thus fail to alleviate hypoxia.

Computations made with a salt-balance model in this region over summers of 1986-2006 (Hagy, 2002) suggest that upward advective salt fluxes were 1.5 to 20 times higher than non-advective fluxes (i.e., turbulent mixing). Similar analysis for a Bay tributary revealed that upward transport of NH_4^+ from bottom- to surface-layer is an important nutrient source to surface water phytoplankton during summer (Testa et al., 2008). Additionally, vertically-migrating dinoflagellates, which can acquire nutrients at or below the pycnocline during night and move to illuminated surface water during the day (Tyler and Seliger, 1981), represent a potentially important upward flux of nutrients in summer. Thus, substantial upward transport of nutrients into surface-waters could occur without increasing bottom-water O_2 via several mechanisms.

The seasonal timing of hypoxia-enhanced bottom-water nutrient accumulation matches the time of year which has experienced the most rapid increase in hypoxic volumes over the last half century. Previous analyses of hypoxic volumes in Chesapeake Bay indicated that volumes of hypoxic water in June have increased more than two-fold over the last 6 decades (1950-2007), while hypoxic volumes in late July and August have shown declines in the last 25 years (Murphy et al., 2011). Thus, the abrupt increase in mean summer hypoxia per unit TN load (Fig. 2.2) reflects the large increases in hypoxia during June. Early summer increases in hypoxia match seasonally with concurrent long-term increases in NP NL^{-1} and provide evidence for the large-scale enhancement of nutrient recycling associated with increased hypoxia. Although, this increase in hypoxia been linked with increases in stratification (Murphy et al., 2011) and shifts of summer wind fields (Scully, 2010a), our analysis suggests that enhanced NH_4^+ and PO_4^{3-}

availability under elevated hypoxic volumes could also have supported an increase in hypoxia per unit TN load.

Although similar large-scale enhancements of nutrient accumulation and availability in response to low O_2 conditions have been reported in the literature (Meier et al., 2011; Mort et al., 2010; Van Cappellen and Ingall, 1994), the present study demonstrates the regional importance of these feedbacks over longer time periods. Considering the potential importance of such feedbacks in relation to coastal eutrophication (Conley et al., 2002; Eiola et al., 2009), comparable studies in other systems would further improve understanding of the linkages between nutrient cycling and O_2 depletion. In cases where such links have been made, hypoxia-induced shifts in PO_4^{3-} and inorganic N availability have reportedly also altered the competitive balance among phytoplankton species (Vahtera et al., 2007). Thus, feedbacks between hypoxia-induced nutrient recycling and phytoplankton growth may be more complex than posited here.

Acknowledgements

I thank the Environmental Protection Agency Chesapeake Bay Program and the Maryland Department of Natural Resources for providing monitoring data. Rebecca Murphy provided helpful suggestions and supported and shared R scripts for our spatial interpolations. Randall Burns and Eric Pearlman developed, maintained, and supported the database system we used in this analysis. Insightful discussions with Bill Ball, Walter Boynton, Damian Brady, Dominic Di Toro, and Jeff Cornwell were valuable in the formulation of our ideas. The reviews of two anonymous individuals greatly improved the quality of this manuscript. This study was funded by the National Science

Foundation, Bioengineering and Environmental Systems, under grant BES-0618986, the U.S. Department of Commerce, National Oceanographic and Atmospheric Administration grant NA07NOS4780191, and the Horn Point Laboratory Bay and Rivers Graduate Fellowship. This is contribution #4630 of the University of Maryland Center for Environmental Science.

Table 2.1: Monitoring station details in the modern (1985-2007) Chesapeake Bay Program-Maryland Department of Natural Resources dataset. *See* Fig. 2.2 for map with station locations within Chesapeake Bay. Surface salinity is 1985-2007 mean and hypoxia metrics over 1985-2007.

Station	Latitude	Longitude	Total depth (m)	Surface salinity	Hypoxia present? (1985-2007)	Region	Pycnocline depth (m)	Distance from Atlantic (km)
CB2.1	39.440	-76.025	6	0.48	no	I		259-300
CB2.2	39.347	-76.175	10	2.25	yes	I		259-300
CB3.1	39.248	-76.238	10	4.49	yes	II	5	241-259
CB3.2	39.163	-76.306	10	6.54	yes	II	5	241-259
CB3.3C	38.996	-76.359	26	9.13	yes	III	7	222-241
CB4.1C	38.826	-76.399	33	10.77	yes	IV	12	185-222
CB4.2C	38.646	-76.421	28	11.82	yes	IV	12	185-222
CB4.3C	38.555	-76.428	28	12.15	yes	V	12	139-185
CB4.4	38.415	-76.346	32	12.90	yes	V	12	139-185
CB5.1	38.319	-76.292	36	13.55	yes	V	12	139-185
CB5.2	38.137	-76.228	33	14.08	yes	VI	12	93-139
CB5.3	37.910	-76.171	29	14.38	yes	VI	12	93-139
CB5.4	37.800	-76.175	34	16.46	yes	VI	12	93-139
CB5.5	37.692	-76.189	21	16.71	yes	VII	8	46-93
CB6.1	37.589	-76.162	13	17.55	yes	VII	8	46-93
CB6.2	37.487	-76.156	14	18.06	yes	VII	8	46-93
CB6.3	37.412	-76.159	16	18.61	yes	VII	8	46-93
CB6.4	37.237	-76.208	13	19.82	yes	VIII	6	18-46
CB7.3	37.117	-76.125	12	21.88	no	IX	7	0-18
CB7.4	36.996	-76.020	13	25.21	no	IX	7	0-18

Table 2.2: Sources of historical NH_4^+ data used in this analysis. Included are the analytical methods used for each dataset, as well as sample frequencies and dates of coverage. *See* reference list for full citations of data reports.

Years	No. of samples	Source	Website for data and metadata
1964-1979	1710	Chesapeake Bay Institute data bank compilation of cruise data, 1949-1982	http://archive.chesapeakebay.net/data/historicaldb/nutr_cbi_databank49-82.htm ftp://ftp.chesapeakebay.net/Historical/Nutrient/cbpbay_sum.txt
1969-1973	1237	Historical review of water quality and climatic data from Chesapeake Bay with an emphasis on enrichment, 1936-1974	http://archive.chesapeakebay.net/data/historicaldb/nutr_hist_wq36-74.htm ftp://ftp.chesapeakebay.net/Historical/Nutrient/cbpwils_sum.txt
1968-1980	1293	Water quality and nutrient data from Upper Bay and Maryland Tributaries EPA Storage and Retrieval (STORET) database, 1966-1981	http://archive.chesapeakebay.net/data/historicaldb/nutr_storet66-81.htm ftp://ftp.chesapeakebay.net/Historical/Nutrient/cbpstor2_sum.txt
1968-1980	10,073	Section 106 ambient water quality monitoring for Maryland tidal waters, 1965-1981	http://archive.chesapeakebay.net/data/historicaldb/nutr_cbpmd106.htm ftp://ftp.chesapeakebay.net/Historical/Nutrient/cbpmd106_sum.txt
1977-1978	380	Physio-chemical, plant pigment, and nutrient data from the Continental Shelf to the Upper Bay, 1977-1978	http://archive.chesapeakebay.net/data/historicaldb/nutr_cbpnshelf77-78.htm ftp://ftp.chesapeakebay.net/Historical/Nutrient/cbpnutr_sum.txt
1979	308	1979 Water quality survey of the Chesapeake Bay, EPA Annapolis field office	http://archive.chesapeakebay.net/data/historicaldb/nutr_wqbay79.htm ftp://ftp.chesapeakebay.net/Historical/Nutrient/cbpafob_sum.txt
1980	1462	Chesapeake Bay nutrient dynamics Study, 1980	http://archive.chesapeakebay.net/data/historicaldb/nutr_cbnutrdyn80.htm ftp://ftp.chesapeakebay.net/Historical/Nutrient/cbpdelia_sum.txt
1985-2007	155,120	Chesapeake Bay Program database	http://www.chesapeakebay.net/data_waterquality.aspx

Table 2.3: Mean NH_4^+ pools (10^3 kg) in bottom-waters (±SE) in 4 regions of Chesapeake Bay (delineated by km from Atlantic Ocean) where data were available before (*df*=7) and after (*df*=22) 1985 in the months of June, July, and August. *p*-values for means comparisons (*t*-tests) are included. Significant differences in mean NH_4^+-N pools indicated by bold text.

Region	Period	June	July	August
200-250 km	1965-1980	**284.6 (51.1)**	382.1 (59.5)	237.3 (51.4)
	1985-2007	**430.3 (20.9)**	451.0 (30.2)	373.4 (32.6)
	p-value	**0.004**	0.275	0.058
150-200 km	1965-1980	329.1 (63.5)	399.9 (55.8)	259.7 (67.7)
	1985-2007	431.3 (30.5)	416.6 (62.1)	318.5 (31.5)
	p-value	0.119	0.788	0.412
100-200 km	1965-1980	699.5 (142.5)	797.3 (107.7)	539.5 (151.1)
	1985-2007	792.9 (59.9)	761.2 (59.5)	602.7 (59.0)
	p-value	0.482	0.750	0.651
75-250 km	1965-1980	1190.5 (229.8)	1385.6 (187.5)	931.4 (245.5)
	1985-2007	1382.5 (86.8)	1385.8 (94.85)	1146.7 (100.5)
	p-value	0.340	0.998	0.361

Table 2.4: Regression statistics (*r*, *p*-value) for Type 1 linear models of hypoxic volume and NP NL^{-1} and PP PL^{-1} by region in Chesapeake Bay for years 1985-2007 (*n*=23). Regions II and III are correlated with the hypoxic volume in the region north of 225 km from the Atlantic Ocean, Regions IV and V are correlated with the hypoxic volume in the region between 150 and 225 km, and Regions VI and VII are correlated with the hypoxic volume less than 150 km from the Atlantic Ocean. Bold numbers indicate significant correlations ($p<0.05$).

Region	June N	July N	Aug. N	June P	July P	Aug. P
II	**0.70 (0.0002)**	0.22 (0.31)	-0.01 (0.95)	0.33 (0.12)	-0.26 (0.23)	-0.29 (0.18)
III	**0.75 (<0.001)**	0.06 (0.98)	-0.11 (0.63)	**0.61 (0.002)**	-0.13 (0.54)	-0.23 (0.29)
IV	0.17 (0.42)	0.05 (0.82)	-0.33 (0.12)	0.35 (0.107)	0.05 (0.83)	**-0.46 (0.03)**
V	0.25 (0.26)	0.08 (0.73)	-0.24 (0.27)	0.23(0.29)	0.07 (0.94)	**-0.47 (0.02)**
VI	0.27 (0.33)	0.35 (0.11)	-0.25 (0.25)	0.22 (0.42)	-0.16 (0.47)	-0.19 (0.38)
VII	0.44 (0.11)	0.35 (0.12)	-0.08 (0.71)	-0.003 (0.99)	-0.18 (0.42)	-0.12 (0.59)

Figure Legends

Figure 2.1: (A) Map of Chesapeake Bay with bathymetry included. Circles indicate the location of monitoring stations, boxes indicate locations of sediment-water flux measurements and regions (I-IX) where nutrient mass calculations were made are included. (B) Longitudinal and vertical distribution of sampling locations for measurements (1-2 month^{-1}) of NH_4^+ and PO_4^{3-} in the Chesapeake Bay Water Quality Monitoring Program from 1985 to present. Distributions of dissolved O_2, salinity, and temperature measurements were similar, but vertical profiles were sampled at 1-m depth intervals.

Figure 2.2: Time series of hypoxic (O_2<62.5 μmol L^{-1}) water volume per unit winter-spring Susquehanna River TN load (January to April) from 1950 to 2007 and (inset) correlations between TN load and hypoxic water volume in two periods (1950-1985, open circles) and (1986-2007, closed circles). Hypoxic volume and TN loads were calculated as described in Methods.

Figure 2.3: Time series of NH_4^+-N pools per unit winter-spring Susquehanna River TN load (January to April) from 1960 to 2007. Inset shows relationship between TN load and NH_4^+-N pools in two periods (1965-1980, open circles) and (1985-2007, closed circles).

Figure 2.4: Comparisons of computed NH_4^+-N pools calculated for the years 1985-2007 using data from the full sampling density vs. that using data from sub-sampling the full data set in ways that are consistent with sampling in 8 available years prior to 1985. Each figure includes cross-plots of computed NH_4^+-N pools at both data densities for the regions of Chesapeake Bay between 75-250 km from the Atlantic Ocean for (A) June, (B) July, and (C) August. Dotted lines represent equivalence in the two computations.

Figure 2.5: Relationships between measured bottom-water O_2 concentrations and sediment-water fluxes of (A) NH_4^+ and (B) PO_4^{3-} at two stations in mainstem Chesapeake Bay (*see* Figure 1): Point No Point (38.14 N, -76.23 W) and R-64 (38.56 N, -76.43 W). Unpublished data are from W. R. Boynton and E. Bailey.

Figure 2.6: Interpolated longitudinal and vertical distributions of mean (A) NH_4^+, (B) PO_4^{3-}, and (C) dissolved O_2 in June 1985-2007 along the axis of Chesapeake Bay.

Figure 2.7: Vertical profiles of (A) dissolved O_2, (B) salinity, (C) PO_4^{3-}, and (D) NH_4^+ in July of 1998 and 1999. The depth of the maximum Brunt-Väisälä frequency, which is defined as the pycnocline depth, is indicated by a dotted line for both years. Data are from station CB4.3C (Table 2.1; 38.56 N, -76.43W, Region V). Grey shaded areas are the photic depth (light >1% of surface irradiance) computed from Secchi depth in July 1998.

Figure 2.8: Longitudinal distributions of mean (±SE) values of (A) PO_4^{3-}, (B) NH_4^+, and (C) O_2 in sub-pycnocline water in Chesapeake Bay. Data were averaged over the 1985-2007 period for April, June, and August.

Figure 2.9: Relationships for sub-pycnocline concentrations of (A) NH_4^+ and (B) PO_4^{3-} vs. dissolved O_2 in the middle region (38.5 N, -76.5 W) of Chesapeake Bay, with data labeled separately for the 5 months (April-August).

Figure 2.10: Correlations between both (A) PP PL^{-1} and (B) NP NL^{-1} and hypoxic volume during June in mesohaline Chesapeake Bay (Region III, 38.75 N, -76.4 W). Data are monthly means for each year between 1985 and 2007. Mg = megagram (10^6 g).

Fig 2.1

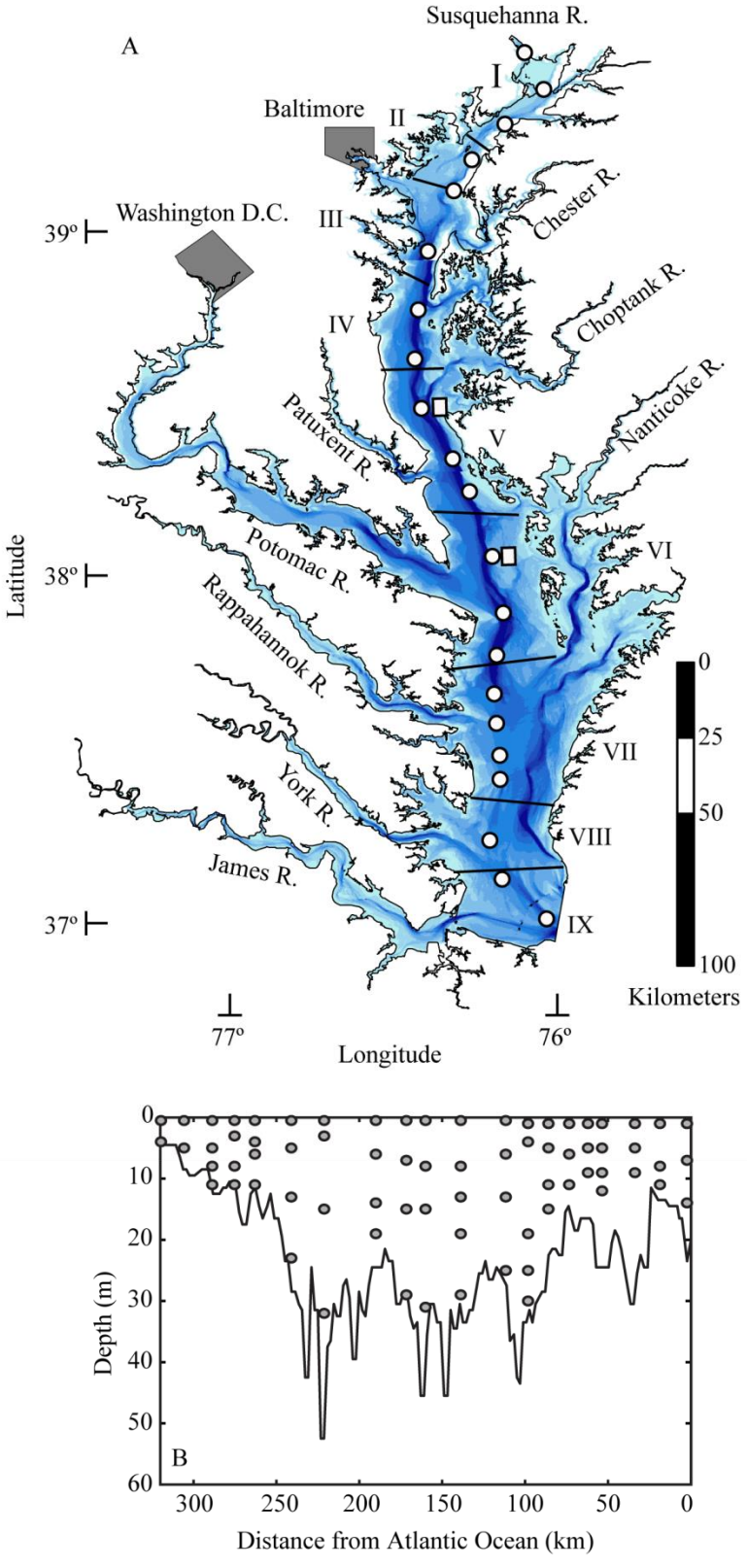
A
Susquehanna R.
I
Baltimore
II
Washington D.C.
III
Chester R.
39º
Choptank R.
IV
Nanticoke R.
Patuxent R.
V
Potomac R.
VI
38º
Rappahannok R.
Latitude
0
25
50
100
Kilometers
VII
York R.
VIII
James R.
37º
IX
77º
76º
Longitude
B
Depth (m)
0
10
20
30
40
50
60
300
250
200
150
100
50
0
Distance from Atlantic Ocean (km)

Fig 2.2

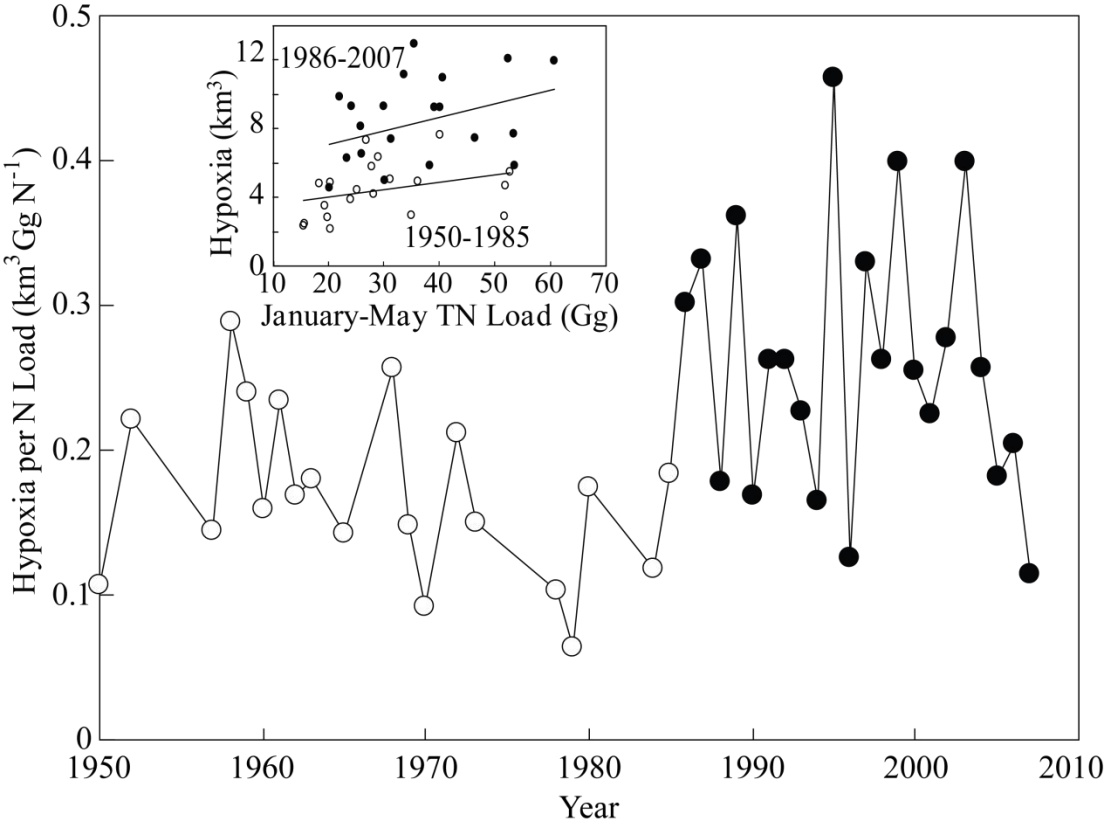
Hypoxia per N Load (km3 Gg N-1)
Year
1950
1960
1970
1980
1990
2000
2010
0
0.1
0.2
0.3
0.4
0.5
Hypoxia (km3)
January-May TN Load (Gg)
1986-2007
1950-1985
0
4
8
12
10
20
30
40
50
60
70

Fig 2.3

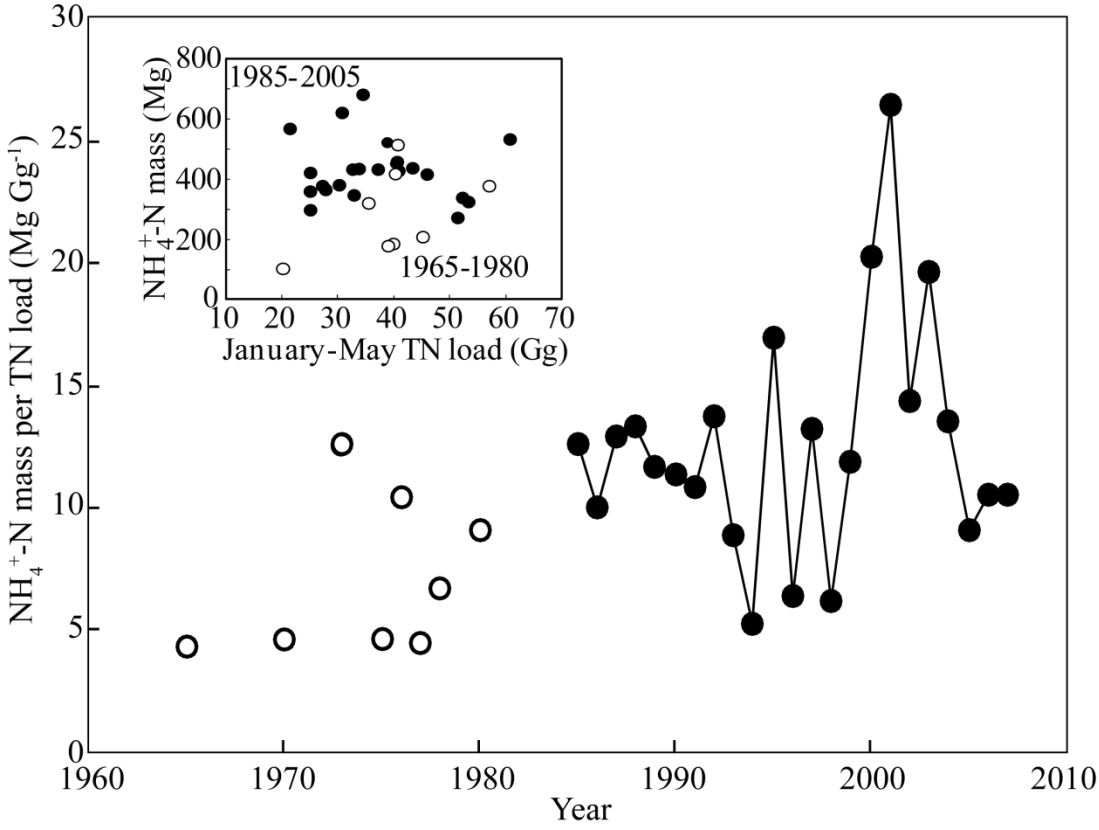
30
25
20
15
10
5
0
1960
1970
1980
1990
2000
2010
Year
NH4+-N mass per TN load (Mg Gg-1)
800
600
400
200
0
10
20
30
40
50
60
70
January-May TN load (Gg)
NH4+-N mass (Mg)
1985-2005
1965-1980

Fig 2.4

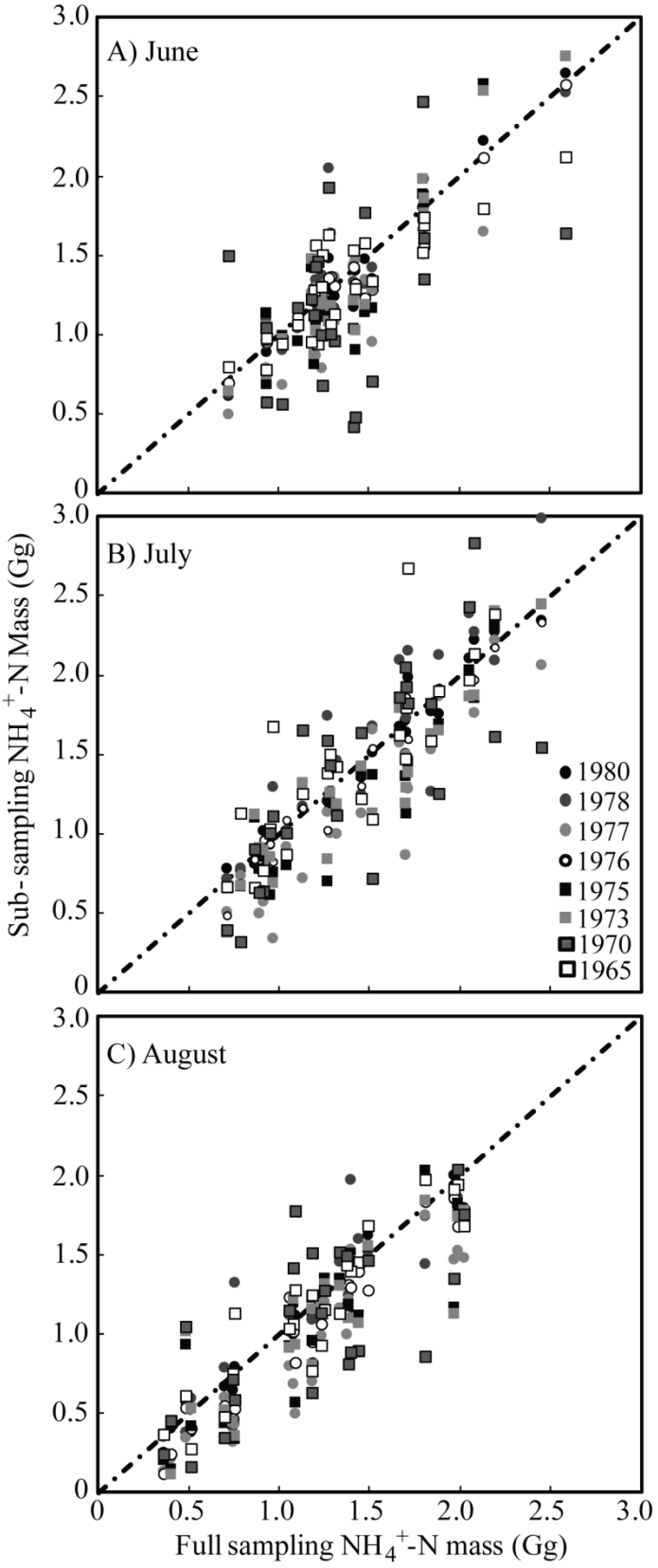
A) June
B) July
C) August
1980
1978
1977
1976
1975
1973
1970
1965
Sub- sampling NH_4^+-N Mass (Gg)
Full sampling NH_4^+-N mass (Gg)
0
0.5
1.0
1.5
2.0
2.5
3.0

Fig 2.5

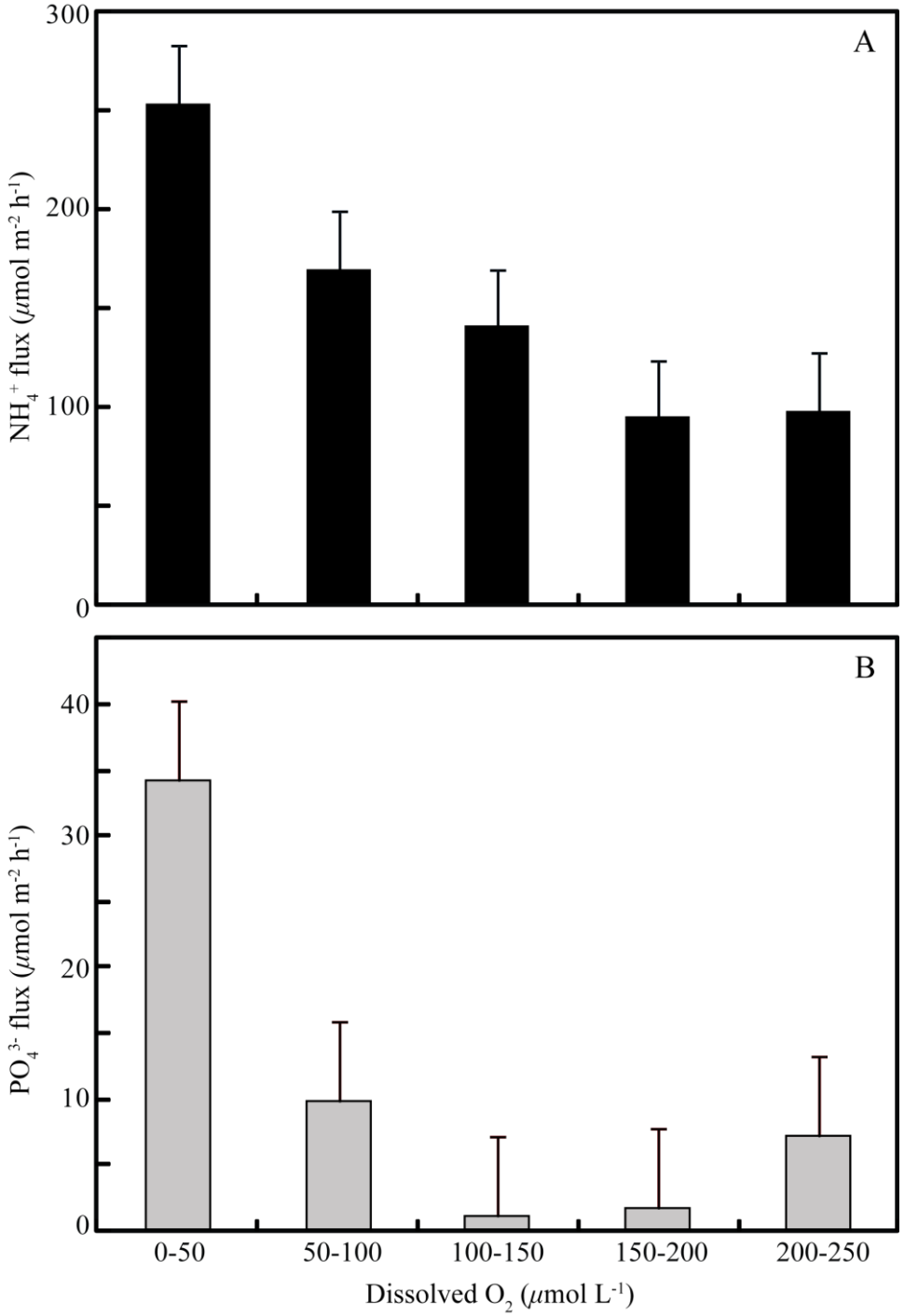
A
B
300
200
100
0
40
30
20
10
0
NH_4^+ flux (μmol m^{-2} h^{-1})
PO_4^{3-} flux (μmol m^{-2} h^{-1})
0-50
50-100
100-150
150-200
200-250
Dissolved O_2 (μmol L^{-1})

Fig 2.6

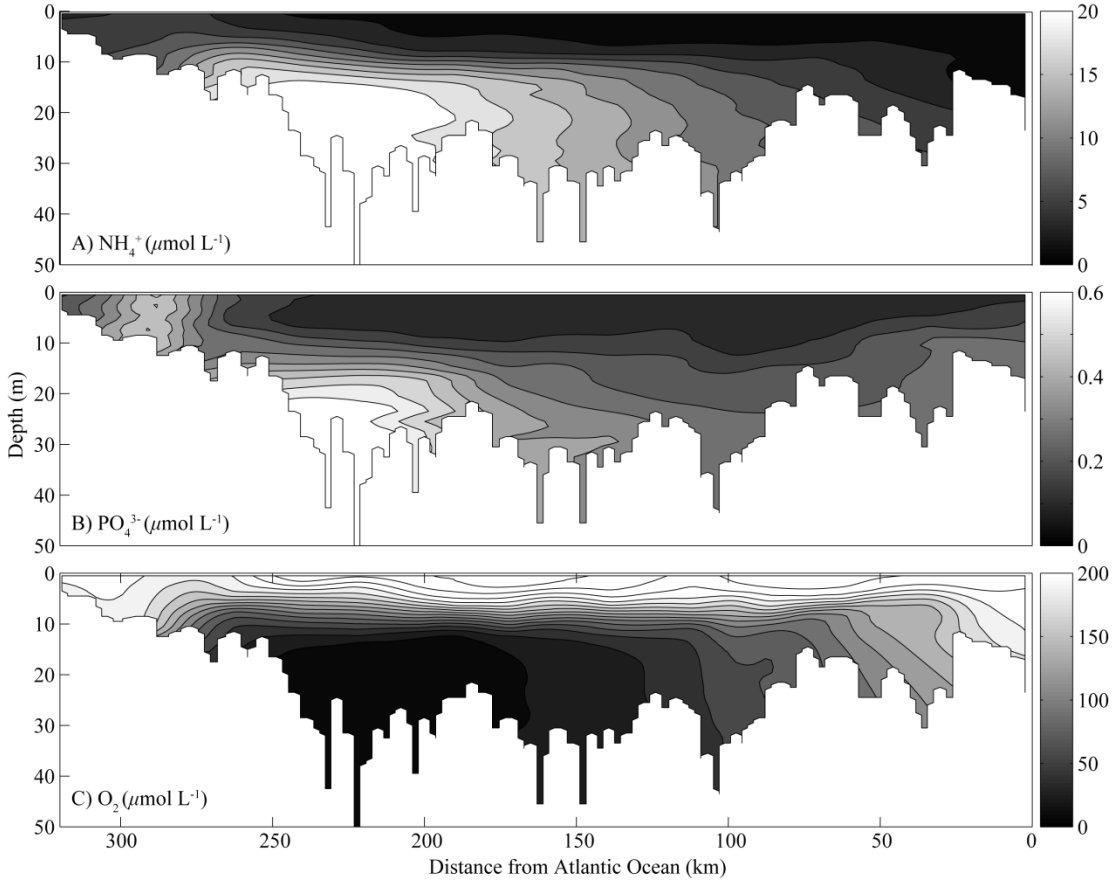
A) NH_4^+ (μmol L^{-1})
B) PO_4^{3-} (μmol L^{-1})
C) O_2 (μmol L^{-1})
Depth (m)
Distance from Atlantic Ocean (km)
0
10
20
30
40
50
300
250
200
150
100
50
0
20
15
10
5
0.6
0.4
0.2
200
150
100

Fig 2.7

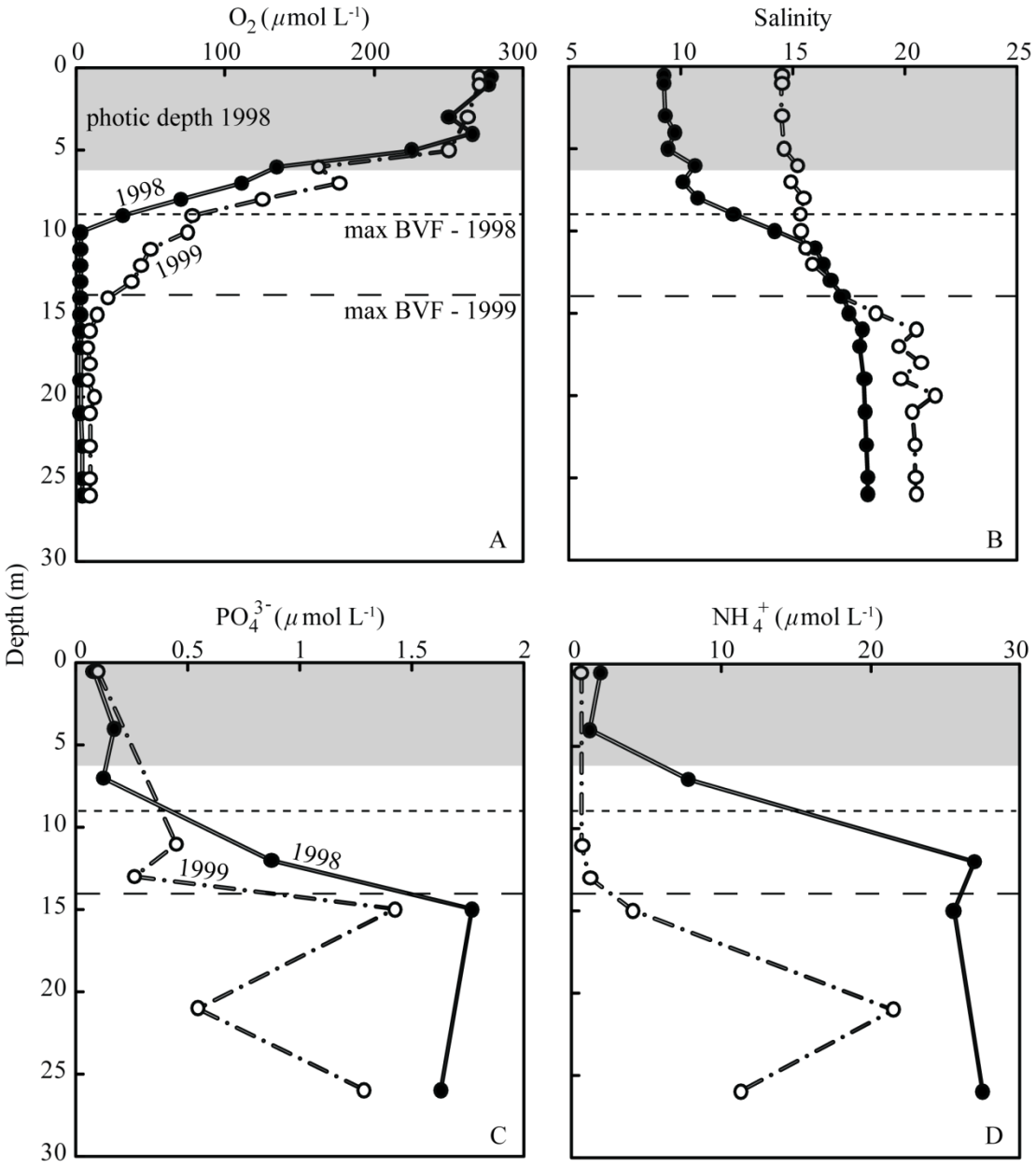
O2 (μmol L-1)
0
100
200
300
Salinity
5
10
15
20
25
Depth (m)
photic depth 1998
1998
1999
max BVF - 1998
max BVF - 1999
A
B
PO4 3- (μmol L-1)
0
0.5
1
1.5
2
NH4 + (μmol L-1)
0
10
20
30
C
D

Fig 2.8

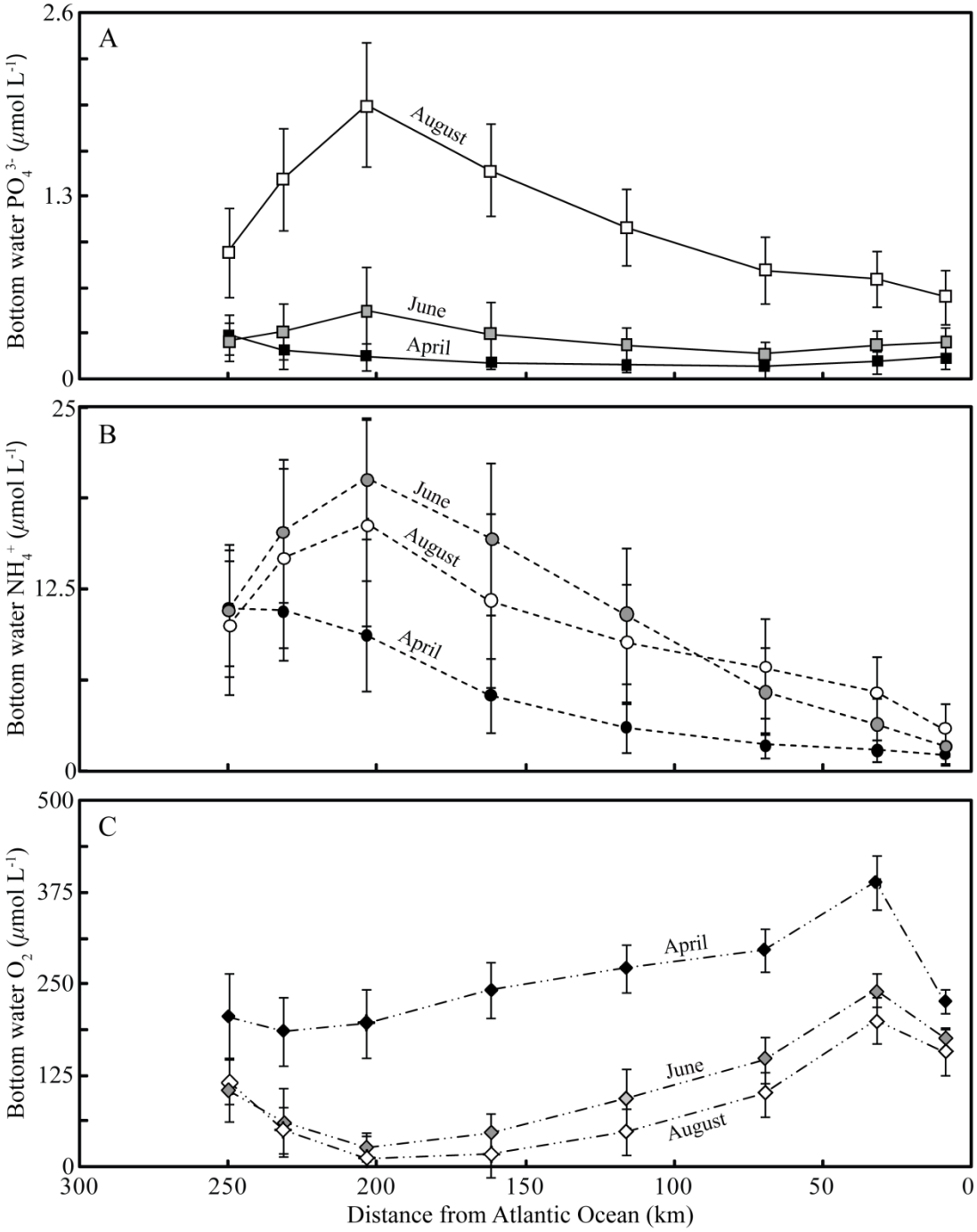
A
B
C
August
June
April
Bottom water PO_4^{3-} (μmol L^{-1})
Bottom water NH_4^+ (μmol L^{-1})
Bottom water O_2 (μmol L^{-1})
2.6
1.3
0
25
12.5
0
500
375
250
125
0
300
250
200
150
100
50
0
Distance from Atlantic Ocean (km)

Fig 2.9

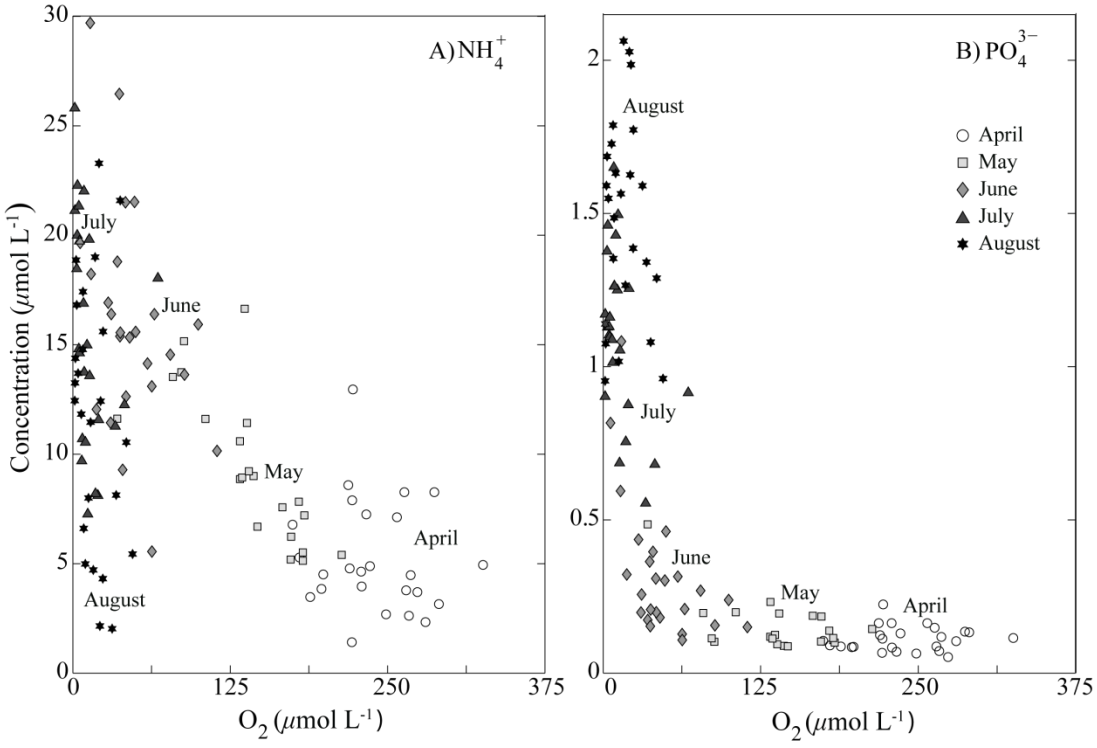
A) NH_4^+
B) PO_4^{3-}
Concentration (μmol L^{-1})
O_2 (μmol L^{-1})
July
June
May
April
August
April
May
June
July
August
0
125
250
375
0
5
10
15
20
25
30
0
0.5
1
1.5
2

Fig 2.10

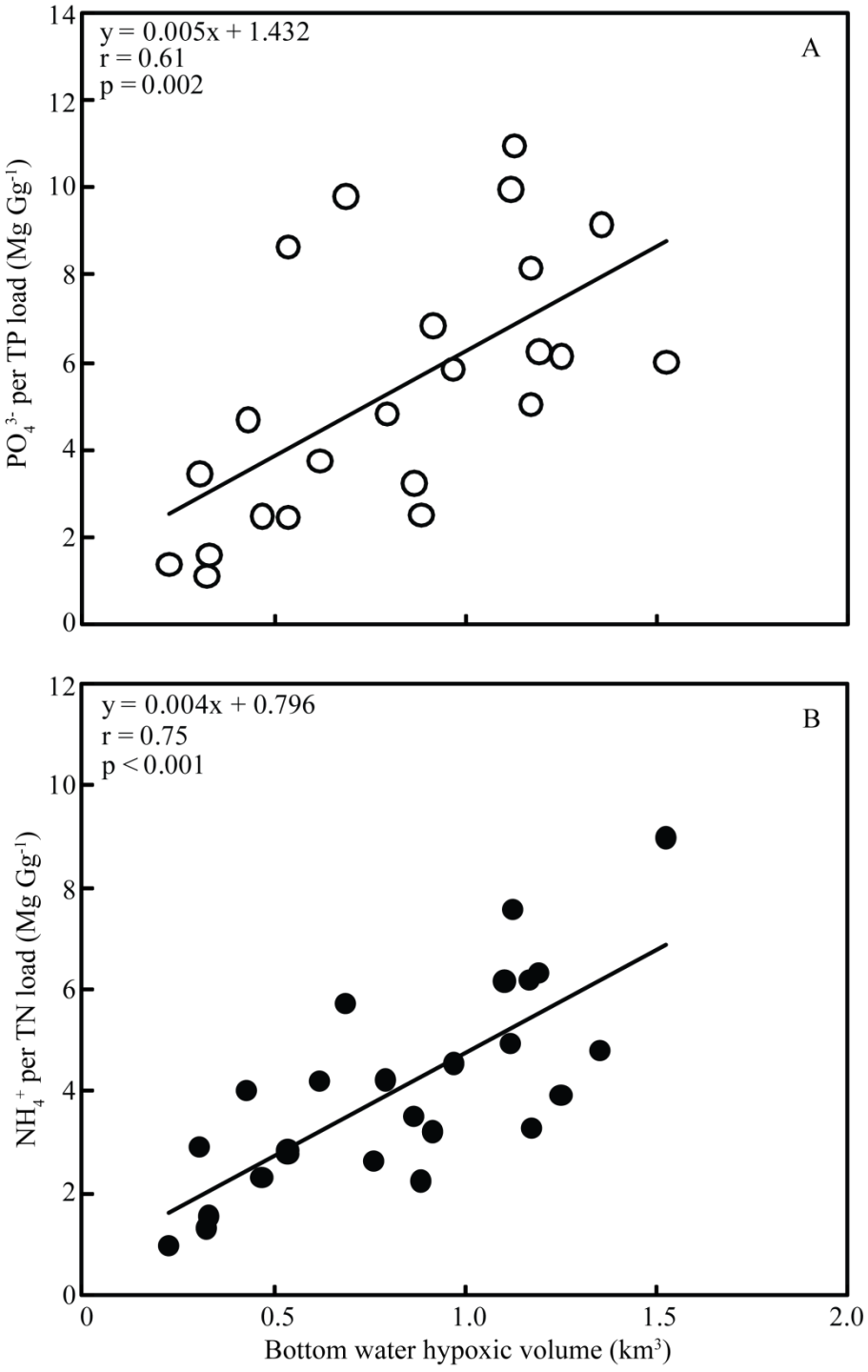
y = 0.005x + 1.432
r = 0.61
p = 0.002
A
PO_4^{3-} per TP load (Mg Gg^{-1})
y = 0.004x + 0.796
r = 0.75
p < 0.001
B
NH_4^+ per TN load (Mg Gg^{-1})
Bottom water hypoxic volume (km^3)

CHAPTER 3: SPATIAL AND TEMPORAL PATTERNS IN WINTER-SPRING OXYGEN DEPLETION IN CHESAPEAKE BAY BOTTOM WATERS

Abstract

Although seasonal hypoxia is a well-studied phenomenon in many coastal systems, most previous studies have focused on variability and controls on low-oxygen water masses during summer when hypoxia is most extensive. Surprisingly little attention has been given to investigations of what controls the development of hypoxic water in the months leading up to seasonal maxima. Thus, we investigated aspects of winter-spring oxygen depletion using a 25-year time-series (1985-2009) by computing rates of water-column O_2 depletion and the dates of hypoxia onset for bottom-waters of Chesapeake Bay. On average, hypoxia (O_2 < 62.5 μM) initiated in the northernmost region of the deep, central channel in early May and extended southward over ensuing months; however, the date of hypoxia onset varied by > 50 days (April 6 to May 31 in the upper Bay). Water-column O_2 depletion rates were consistently highest in the upper Bay, and elevated Susquehanna River flow resulted in more rapid O_2 depletion and earlier hypoxia onset. Winter-spring chlorophyll-*a* concentration in the bottom water was the primary driver of inter-annual variability in hypoxia onset dates and water-column O_2 depletion rates in the upper and middle Bay, while stratification strength was a more important driver in the lower Bay. Hypoxia initiated earlier in 2012 (April 6) than recorded previously, which may be related to extraordinary climatic conditions in the winter-spring of 2012 and the carry-over of large organic matter loads associated with a tropical storm in September 2011. Early summer hypoxic volumes were significantly correlated to winter-spring O_2-depletion rates and hypoxia onset, but were poorly correlated to mid-summer hypoxic volumes, suggesting that climatic fluctuations and organic matter

production during late spring and summer are also important in controlling incipient summer hypoxia.

Introduction

Seasonal depletion of dissolved oxygen (O_2) from coastal waters is a widespread phenomenon that appears to be growing globally (Díaz and Rosenberg, 2008; Rabalais and Gilbert, 2009). Although there is mounting evidence that eutrophication (i.e., anthropogenic nutrient and organic enrichment of aquatic ecosystems) is contributing to the expansion of occurrence, intensity, and duration of hypoxic ("hypoxia" = $O_2 < 62.5$ μM, 2 mg l^{-1}, 30% saturation) conditions in coastal waters worldwide (Díaz and Rosenberg, 2008; Kemp et al., 2009), short- and long-term patterns and trends in climatic forcing also exert control over O_2 in bottom waters (Justíc et al., 2005; Scully, 2010b; Wilson et al., 2008). Considering the potential impacts of hypoxia on growth and mortality of many marine fish and invertebrates (Vaquer-Sunyer and Duarte, 2008), predator-prey interactions and food web structures (Decker et al., 2004; Nestlerode and Diaz, 1998), and biogeochemical processes (Conley et al., 2002; Kemp et al., 1990; Testa and Kemp, 2012), this phenomenon has received increasing attention in recent decades.

It is well known that O_2 concentrations are gradually depleted from deeper waters of Chesapeake Bay from late winter until summer, resulting in the hypoxic and anoxic conditions that to characterize the estuary from mid June-September (Hagy et al., 2004). O_2 concentrations usually reach their seasonal peak in January-February, when solubility is high, vertical mixing strong, and O_2 consuming processes are temperature-limited (Taft et al., 1980). Beginning in February and March, O_2 concentrations in deeper water (> 10 m) tend to follow a near-linear decline until June at rates of 0.94 to 4.69 mmol m^{-3} d^{-1}

(Boynton and Kemp, 2000). Such rapid O_2 declines lead to the onset of hypoxic conditions as early as April and anoxia in June near the head of the hypoxic zone (39^{o}N, 76.3^{o}W). As the summer progresses, hypoxic conditions expand southward, beyond the Potomac River by May and in above-average years, to the Rappahannock River by July.

Earlier studies suggested that the rate of spring O_2 decline and the onset of hypoxic conditions are highly variable from year to year (Boynton and Kemp, 2000; Hagy et al., 2004). It has been suggested that such high inter-annual variability in the seasonal development of O_2-depleted bottom waters is driven by a suite of biological and physical variables, including the magnitude of the spring diatom bloom, volume of winter-spring river flow, spring temperature, wind conditions, and associated vertical and horizontal O_2 transport (Boynton and Kemp, 2000; Hagy et al., 2004; Officer et al., 1984; Scully, 2010b). The response of O_2 depletion to external forcing may, however, be highly non-linear. For example, elevated winter-spring river flow should favor O_2 depletion by increasing vertical stratification and reducing vertical diffusion (Boicourt, 1992), while elevating phytoplankton biomass (Malone et al., 1988). Elevated flow, however, will also enhance landward, longitudinal O_2 transport (Kemp et al., 1992; Kuo et al., 1991), pushing the location of the spring bloom seaward (Hagy et al., 2005).

Despite the high variability and importance of the initialization of hypoxia in spring, most of the hypoxia research in Chesapeake Bay has focused on the summer (June-August) period when the volume of hypoxia is at its seasonal peak (Hagy et al., 2004; Murphy et al., 2011; Scavia et al., 2006). In part, this summer focus is due to the availability of historical O_2 data from 1950-1980 (Hagy et al., 2004) and an emphasis on summer of hypoxia effects on living resources (Breitburg, 2002). Consequently, the

spatial and temporal patterns in the development of hypoxia during spring and the processes that control these patterns are poorly understood. Although previous studies addressed questions on the magnitude and controls on spring O_2 depletion rates (Boynton and Kemp, 2000; Hagy et al., 2004; Taft et al., 1980), comprehensive analyses of spatial and temporal pattenrs have been heretofore lacking. Similarly, very few studies exist addressing hypoxia seasonality in other coastal systems (Rabalais and Turner, 2006).

The goal of this paper was to utilize a large and spatially/temporally-resolved dataset for

O_2 concentrations (and other key variables) to understand the dynamics of seasonal hypoxia development in Chesapeake Bay. We used concentration time-series along the Bay axis to compute rates of water-column O_2 uptake, the date of hypoxia initiation, and the volume of hypoxia. Regional and seasonal variations in these processes were also examined. Variations in these rates and dates were related to a suite of physical and biological variables and to summer hypoxia extent, providing a basis for understanding key controls over space and time.

Methods

Vertical Profiles of Concentrations

Vertical profiles of O_2, water temperature, salinity, and chlorophyll-*a* were obtained from the Chesapeake Bay Program Water Quality database for the 1985-2009 period (http://www.chesapeakebay.net/data_waterquality.aspx), with profiles collected at 20 stations located along the estuary's central channel (Fig. 3.1, Table 3.1). Measurements of O_2, temperature, and salinity were generally made at 1-m depth intervals, while measurements of chlorophyll-*a* were made at 4-5 depths for each station

(2-10 m intervals). Profiles were generally sampled monthly between of November and March and bi-monthly between April and October.

Climatic Data

We compiled several climatic datasets to characterize the major external controls on O_2 dynamics. Daily Susquehanna River flow into the Chesapeake Bay was downloaded from the USGS Chesapeake Bay River Input Monitoring Program website for the years 1985 to 2009 (http://va.water.usgs.gov/chesbay/RIMP/). Wind direction and speed data were collected from the Naval Air Station (PNAS) near the mouth of the Patuxent River in Maryland. The NAS wind data are used because they provide the most centrally located wind observations over the main stem of the bay. The wind direction was calculated from the hourly north and east wind components after the data are filtered with a 36-hour low-pass filter. In computing average wind speeds, only those records where wind blew with a speed greater than 2 m s^{-1}. Wind directions were categorized into 8 compass directions.

Stratification

We computed pycnocline depth for each region as the vertical position in the water column (depth in m, *z*) where the square of the Brunt-Väisälä frequency (N^2) was at its maximum value (Pond and Pickard, 1983) and that value was used as an index of pycnocline strength, where

$$N^2(z) = \frac{g}{\sigma_z} \cdot \frac{\partial \sigma}{\partial z}$$

and g = gravitational constant, 9.81 m s^{-2}, σ_z is the water density at depth (kg m^{-3}), and $\frac{\partial \sigma}{\partial z}$ is the density gradient at depth z, which was calculated using a 2-m window around

z. Density was computed (Fofonoff, 1985) from profiles of temperature and salinity data at 1-m depth intervals using the Chesapeake Bay Program Water Quality database.

Interpolations

We interpolated spatial distributions for O_2, water temperature, salinity, and chlorophyll-*a* concentrations to a 2-D length-depth grid using ordinary kriging (Murphy et al., 2010; Murphy et al., 2011). The statistical package R (R Development Core Team, 2009) with the geoR package (Ribeiro and Diggle, 2009) was used for all interpolations, as described in (Murphy et al., 2011). The resulting 2D distributions were assumed to be constant laterally at a given depth and organized to correspond to tabulated cross-sectional volumes (Cronin and Pritchard, 1975).

For O_2, interpolated concentration data were multiplied by the cross-sectional volumes to compute "hypoxic volumes" for all available profile sets in the years 1985-2009 by summing the volume of all cells with an O_2 concentration < 62.5 μM.

O_2 Depletion metrics

The first day of the year where bottom water O_2 concentrations fall below 62.5 μM provides the most straightforward index of the tendency for hypoxia to occur in a given year. This date was calculated by (1) averaging bottom-water O_2 concentrations for each sampling date, (2) interpolating temporally through time to extrapolate fortnightly and monthly data to a daily concentration using shape-preserving piecewise cubic interpolations (where interpolation is monotonic when data are monotonic, and no artificial maxima or minima are generated), and (3) calculating the day where interpolated O_2 concentrations fall below 62.5 μM (Fig. 3.2). Hypoxia onset dates were calculated for each station in each year from 1985 to 2009.

The second calculation from the O_2 concentrations was the calculated slope of a linear temporal decline in O_2 concentration (non-interpolated) between March and May for each year between 1985 and 2009. Because each station has its own unique depth, bottom-water O_2 was selected from the deepest depth sampled. For each year and station, a linear regression model was fit to the March-May time-series of averaged O_2 concentrations versus time and the slope was calculated (Fig. 3.2). This slope estimate represents a daily O_2 depletion rate, and it reflects the effects on O_2 of various biological, physical, and chemical mechanisms. We made the same computations on time-series of O_2 deficit ($O_{2Saturation}$-$O_{2Observed}$) to examine the impacts of changes in solubility (driven primarily by temperature) on our depletion rates (data not shown); these slopes were highly correlated with the slopes from the observations ($r > 0.90$). For a few years, the O_2 time-series from March to May was not linear, and these often include short-term increases in concentration (e.g., Fig. 3.4); where these situations occurred, only observations made during the monotonic decrease were included in the slope calculation. Correlation coefficients (r-values) for the linear model fits to observed concentrations exceeded 0.90 at all stations/sites.

Statistical Analysis

We investigated the potential for multiple interacting controls on the date of hypoxia onset (hereafter DHO) and the rate of O_2-depletion (hereafter ROD) using simple linear regression and multiple linear regression models (SASv9.2, PROC REG). The independent variables used to construct the models included mean January to May Susquehanna River flow, March-May wind speed and direction, January to April bottom-water chlorophyll-*a*, March to May water temperature, and April and May pycnocline

strength (N^2) and vertical position (depth of maximum N^2). Three multiple linear regression approaches were used, including r^2 selection of all predictor sets, forward selection, and backward selection. Selection of optimal models was based on maximizing the adjusted r^2 of the model and minimizing the Mallow's CP and Akaike information criterion. We tested for normality of residuals using Shapiro-Wilk's *W* and box and normal probability plots. Multicollinearity of predictor variables was examined via variance inflation, condition indexes and eigenvalues of predictor variables.

Results

Spatial and temporal patterns in O_2

Bottom-water dissolved O_2 varies seasonally in Chesapeake Bay, with maximum values in February and minimum concentrations typically occurring between May and July (Fig. 3.3). In most summers, anoxic concentrations occur in upper and middle Bay stations (CB3.3C to CB5.2), while hypoxic or near-hypoxic concentrations occur in the lower Bay, but anoxia is rare (Fig. 3.3). Time-series of bottom-water O_2 at the northern and southern ends of the hypoxic zone stations illustrate consistent seasonal patterns with moderate inter-annual variability in O_2 minima and episodic O_2 replenishment during summer in some years (Fig. 3.3).

Data used in this analysis, which are based on routine measurements at 2-4 week intervals, are likely to miss some short-term dynamics in O_2 concentrations. Although similar data were not available for the mainstem Bay where we focused our study, continuous dissolved O_2 measurements (sampling at 15-minute intervals) were made from a fixed buoy deployed adjacent to the routine monitoring station in the lower Patuxent estuary (LE1.2) during spring of 2004 (Fig. 3.1 & 3.4; Alliance for Coastal

Technologies, http://www.act-us.info/). Rates of ROD and DHO calculated from these two datasets over the April to May period are similar, but several multi-day periods of high variability in O_2 occurred between the fortnightly samples, similar to those used for the majority of calculations in this study (Fig. 3.4).

The 25-year (1985-2009) monthly mean (March-July) spatial patterns in dissolved O_2 reveal the seasonal development of hypoxic water as well and the shifting locations of low-O_2 water with depth and distance along the Bay axis (Fig. 3.5). Parallel time/space patterns in the variance around these mean conditions are also revealing (Fig. 3.5). O_2 first begins to decline in bottom-water within the upper Bay between 200 and 300 km from the Atlantic Ocean in March-April (Fig. 3.5). From this location, O_2 further declines through June and the low-O_2 water mass appears to migrate seaward over the course of spring, where it is generally retained below 10-12 m depth (Fig. 3.5). The standard deviation in O_2 around these 25-year means also reveals both spatial and seasonal shifts in O_2 variability. In March and April, O_2 is most variable in the upper Bay where O_2 is initially depleted and where vertical gradients in O_2 concentration are strong (Fig. 3.5). In contrast, O_2 variability is highest in the middle of the water column in May and June (in the vicinity of the pycnocline) throughout most of the central channel of the Bay (Fig. 3.5). The standard deviation is extremely high near the pycnocline in June, where vertical gradients in O_2 are at seasonal peaks.

Hypoxia onset and O_2 depletion rates

The estimated date of hypoxia onset was highly variable from year to year at a given station, but the spatial pattern in hypoxia onset was consistent. For example, at station CB3.3C near the Bay Bridge, the date that O_2 fell below 62.5 μM ranged from

April 14 to May 31 (46 days) between 1985 and 2009, but hypoxia always initiated at this station before it arrived at other stations (Fig. 3.6). Each year from 1985-2009, hypoxia developed in the most landward bottom waters of the Bay (near CB3.3C), but in only half of those 25 years did hypoxia develop as far south as the mouth of the Rappahannock River (CB6.1). After initiating at station CB3.3C, hypoxia gradually developed at seaward stations over the ensuing four months, reaching the Rappahannock River by late June/early July (Fig. 3.6). Hypoxia initiated 15-25 days earlier in the five years of highest Susquehanna River flow relative to the five lowest-flow years (Fig. 3.7). Although the spatial pattern of hypoxia onset was relatively unchanged in high- versus low-flow years, differences between high and low Susquehanna River flows were greater north of the Potomac River (Cb3.3C to CB5.2) than south (CB5.3 to CB6.2; Fig. 3.7). When hypoxia onset dates were divided into two groups (five highest and five lowest Susquehanna River flow years), onset date was significantly earlier in the high flow years at stations CB3.3C-CB4.3C and CB5.3 ($p < 0.05$, Mann-Whitney U Test).

Overall, interannual variability in the ROD was greater than that of hypoxia initiation, but the spatial patterns and flow responses were similar. Whereas hypoxia onset was earlier in landward regions of the Bay, O_2-depletion rates were higher (Fig. 3.6). The water-column O_2-depletion rates computed in this study were comparable to those made in previous studies using a similar approach in Chesapeake Bay at select locations (Table 3.2). Median water-column O_2-depletion rates were similar north of the Potomac River (CB3.3C to CB5.2) but declined in seaward regions. O_2-depletion rates were generally insensitive to Susquehanna River flow in the upper Bay and lower Bay stations (CB3.3C-CB4.1C, CB5.3-CB6.4), but rates were significantly elevated (by 30%)

in high-flow years in middle Bay regions (CB4.2C-CB5.2; Fig. 3.7). No significant differences were detected between the means when O_2-depeltion rates were divided into two groups based on Susquehanna River flow ($p > 0.05$, Mann-Whitney U Test; Fig. 3.7).

Winter-spring chlorophyll-*a* concentrations explained more variability in hypoxia onset and O_2-depletion than other variables in upper and middle-Bay regions (Table 3.3 & 3.4; Fig. 3.8). Although Susquehanna River flow during several winter-spring periods was significantly correlated with DHO and ROD (Table 3.3, 3.4), we sought explanatory variables that were more specific to biological or physical processes. Bottom-water chlorophyll-*a* concentrations averaged over the January to April period were significantly correlated to DHO (r = -0.47 to -0.73, $p < 0.05$; CB4.1C-CB5.2) and O_2-depletion rate (r = -0.43 to -0.51, $p < 0.05$; CB4.2C-CB5.2). In contrast, the Brunt-Väisälä Frequency was significantly correlated to DHO in only lower Bay stations (r = -0.43 to -0.781, $p < 0.05$; CB5.2-CB5.4) and across several stations for O_2-depletion rate (Table 3.4).

At a limited number of stations, multiple linear regressions resulted in improved predictability of DHO and O_2-depletion rates. For example, at station CB5.2, both January to April bottom-water chlorophyll-*a* and April to May mean Brunt-Väisälä Frequency (maximum value in the water-column) were significant predictors of DHO (Fig. 3.8). For the majority of stations, however, only a single predictor variable explained a significant fraction of variability in the O_2-depletion metrics (Table 3.3, 3.4). Variables representing mean wind speed, wind direction, water temperature and pycnocline depth were not statistically correlated to inter-annual variability in DHO or ROD.

One of the motivating questions in this effort was to understand the relationship between winter-spring O_2 depletion and summer hypoxic volume. That is, does the onset and distribution of hypoxia in spring pre-determine and thus predict the summer condition? We correlated DHO and ROD to Bay-wide hypoxic volumes computed for May, June, and July (Fig. 3.9). DHO and ROD were poorly correlated to hypoxic volume during the mid-summer (July) period, but were significantly correlated to May, and to a lesser extent, to June hypoxic volumes (Fig. 3.9). DHO and ROD at CB5.1 to CB5.4 were most strongly correlated to May and June hypoxic volumes, while these metrics from upper and lower-Bay stations correlated weakly with hypoxic volume.

In September of 2011, Tropical Storm Lee resulted in extraordinarily high Susquehanna River flow and suspended sediment loading rates to Chesapeake Bay. The peak Susquehanna flow following Tropical Storm Lee was ~20,000 m^3 s^{-1}, which was the largest flow since Tropical Storm Agnes in June 1972 (~32,000 m^3 s^{-1}). Flow resulting from TS Lee was estimated to scour 3.6 x 10^9 kg of sediment from the lower Susquehanna River reservoirs (http://chesapeake.usgs.gov/featuresedimentscourconowingo.html) delivering this and other material to Chesapeake Bay. In the following winter-spring period of 2012, water-column O_2 concentrations were at record-low levels (Fig. 3.10) and hypoxia initiated at upper Bay stations earlier than ever recorded in available monitoring data. These O_2 patterns may have been affected by record-high bottom-water temperatures in the winter-spring of 2012 (Fig. 3.10). In addition, chlorophyll-*a* concentrations (Fig. 3.10) and stratification strength were also relatively high during the winter of 2011-2012. For

example, maximum N^2 at CB4.1C was 0.015 and 0.01 s^{-2} in February and March, respectively, which is near the long-term (1985-2009) maximum for these months.

Discussion

This analysis illustrates spatial and temporal patterns of winter-spring oxygen depletion over a 25-year time-series (1985-2009) of monitoring data from Chesapeake Bay. O_2 dynamics during this period have received little prior attention relative to those during summer months. Clear spatial patterns in both dates of hypoxia onset (DHO) and rates of O_2 depletion (ROD) emerged from this analysis, despite substantial interannual variability in these properties. Such high interannual variability was primarily driven by bottom-water chlorophyll-*a* concentration in the upper and middle Bay, while stratification strength was a more important driver in the lower Bay. A record early-initiation of hypoxia in the upper-Bay in 2012 may have been caused by extraordinary winter-spring climatic conditions and the carry-over of large organic matter loads associated with a tropical storm in September 2011, indicating the potential for proximal and remote controls on hypoxia initiation. Interestingly, these metrics of spring O_2 depletion were poorly correlated to mid-summer hypoxic volumes, highlighting the dynamic nature of O_2 in Chesapeake Bay.

Spatial and Temporal Patterns of O_2 Depletion

Although the pattern of winter-spring declines in bottom-water dissolved O_2 were generally consistent across stations along the entire longitudinal axis of Chesapeake Bay, the rate of decline and minimum O_2 concentration varied spatially. Such patterns are well-described for this system and reflect the combined effects of elevated temperature and associated solubility declines, respiration of spring bloom-generated algal material,

and reduced ventilation caused by winter-spring river flows (Boynton and Kemp, 2000; Hagy et al., 2004; Taft et al., 1980). A striking regional pattern in O_2 decline is the consistent early development *anoxia* in the upper Bay stations, but only occasional and short-lived *hypoxia* in the lower Bay stations (Fig. 3.3). This results from the fact that autochthonous and allocthonous organic material tends to accumulate in the upper and middle Bay regions in spring (Hagy et al., 2005; Zimmerman and Canuel, 2001). This also results from gravitational circulation that limits oxygenation of upper and middle Bay bottom water from overlying surface water via vertical mixing and lateral advection/mixing (Malone et al., 1986; Scully, 2010b) or from the lower Bay via longitudinal advection (Kemp et al., 1992; Kuo et al., 1991). Thus, spatial patterns in winter-spring O_2 depletion are driven by a combination of biological and physical processes.

Although these declines in O_2 concentration were apparently gradual when analyzing monthly to fortnightly data, higher frequency measurements reveal that this general decline may be occasionally interrupted by brief events of both rapid depletion and ventilation (Fig. 3.4). Diurnal variability in these data suggest tidal effects (Fig. 3.4), but day-to-day and weekly variability is driven by mixing events, where for example, O_2 increases near April 28 and May 4 are associated parallel salinity decreases, indicating downward mixing of high-O_2 and low-salinity water. Although it is likely that such higher frequency variability also characterizes the time-series in the main channel of Chesapeake Bay (Boicourt, 1992; Breitburg, 1990), as in other systems (Rabalais et al., 2007), limited data exist to sufficiently examine this variability. At this particular station and sampling period, computations using the high-frequency data (DHO = May 21, ROD

= 6.05 mmol m^{-3} d^{-1}) and fortnightly observations (DHO = May 22, ROD =5.24 mmol m^{-3} d^{-1}) are comparable, suggesting that fortnightly data reasonably reflect broad regional and seasonal patterns of winter-spring O_2 declines.

Longer-term variability in the distribution of O_2 reveals seasonally-shifting controls on O_2 consumption. During March and April in the upper region of Chesapeake Bay where O_2 depletion first occurs, the standard deviation of the 1985-2009 mean is highest in deeper water (Fig. 3.5), where accumulations of chlorophyll-*a* commonly develop (data not shown) just seaward of the limit of salt intrusion (Sanford et al., 2001). This region is also adjacent to the estuarine turbidity maximum, where organic matter and phytoplankton may be concentrated (Lee et al., 2012). In contrast, variability during May and especially June is highest at mid-depth in the middle region of Chesapeake Bay. Such variability may be due to fluctuations in pycnocline location, which commonly occurs around 10 m depth and is characterized by strong gradients in O_2 (Murphy et al., 2011). Alternatively, thin layers and/or oxic/anoxic interfaces at or near the pycnocline have been found to be hot spots for particle aggregation and microbial metabolism (Durham and Stocker, 2012), potentially driving O_2 variation via oxic respiration or chemautotrophy associated with sulfide or ammonium oxidation (Casamayor et al., 2001). This spatial pattern in the primary controlling mechanisms of O_2 variability (organic matter availability in the upper Bay, stratification strength in the lower Bay), is consistent with the statistical analysis of interannual variability in DHO and ROD (Table 3.3, 3.4).

Interannual Variability in O_2 Depletion

Like many processes in Chesapeake Bay and other coastal ecosystems, interannual variations in freshwater input are a primary driver of biogeochemical processes, including O_2 depletion. Although Susquehanna River flow is statistically the strongest predictor of DHO and ROD at some stations (Table 3.3, 3.4), flow impacts both the biology and physics of Chesapeake Bay, which cannot be satisfactorily separated with simple statistics. Such widespread control of inter-annual variability in the development and spatial-temporal extent of O_2 depleted waters by freshwater input is a result of flow impacts on a suite of biological and physical variables, including the magnitude of the spring diatom bloom, spring water temperature, and associated vertical and horizontal O_2 transport (Hagy et al., 2004; Officer et al., 1984; Taft et al., 1980). For example, elevated winter-spring river flow should favor O_2 depletion by increasing stratification strength and reducing vertical diffusion (Boicourt, 1992), while elevating phytoplankton biomass as fuel for respiration (Boynton and Kemp, 2000; Malone et al., 1988). Elevated flow, however, will also tend to increase O_2 concentrations via enhanced landward, longitudinal O_2 transport (Kemp et al., 1992)**,** while pushing the location of the spring bloom seaward (Hagy et al., 2005), which should increase ROD in lower Bay regions. ROD was indeed elevated in mid-Bay regions during high-flow years (Fig. 3.7), suggesting that the O_2-depleting effects of elevated organic material and stratification strength may outweigh the O_2-replenishment effects of enhanced longitudinal advection, at least in the mid-Bay region.

Winter-spring O_2 depletion appears to be driven primarily by phytoplankton-derived organic matter in the upper and middle regions of the Bay. O_2 depletion was most

strongly linked to bottom-water chlorophyll-*a*, where peak phytoplankton biomass occurs in the water-column during the winter-spring period (data not shown). Statistical analyses from this study (Table 3.3, 3.4), as well as previous conceptual models of O_2 dynamics in Chesapeake Bay (Boynton and Kemp, 2000) support this assertion. Such strong associations between O_2-depletion and phytoplankton during this period result from the winter-spring bloom dominating phytoplankton biomass production in Chesapeake Bay (Harding and Perry, 1997; Malone et al., 1988), low grazing rates on the spring bloom (White and Roman, 1992) and thus high deposition of fresh organic material (Kemp et al., 1999), and increases in temperature that elevate respiration rates (Malone, 1987; Sampou and Kemp, 1994). Indeed, O_2-depletion rates in Chesapeake Bay were significantly related to chlorophyll-*a* deposition rates derived from sediment traps over the course of several years (Boynton and Kemp, 2000), and biomarker studies indicate that sediment organic matter is most labile during the spring bloom (Zimmerman and Canuel, 2001). Thus, there is strong evidence for the association of winter-spring O_2 declines with the bottom-water biomass of phytoplankton over a large section of Chesapeake Bay.

Although the relationships between bottom chlorophyll and both ROD and DHO are strong in several regions of the Bay, we do not presume that physical transport effects are small. Several investigators have illustrated the importance of stratification, lateral advection and mixing, and longitudinal advection as important controls on O_2 distributions in Chesapeake Bay (Goodrich et al., 1987; Li and Li, 2011; Sanford and Boicourt, 1990; Scully, 2010b). Correlation analysis reveals that stratification strength is the strongest predictor of hypoxia onset and O_2-depeltion at several stations in the middle

and lower Bay, and the highest variability in summer O_2 concentrations occurs within or adjacent to the pycnocline (Fig. 3.5). Stratification strength may be a larger contributor to ROD and DHO in more seaward reaches of the Bay because phytoplankton biomass (Harding and Perry, 1997) and deposition (Hagy et al., 2005) tend to be lower in this region, thus limiting the biological control on O_2 depletion. The control of bottom-water O_2 by physical mechanisms may also be stronger in summer when stratification strength reaches its seasonal maxima at several middle and lower Bay stations (Murphy et al., 2011). Thus, in the lower Bay where hypoxia onset occurs later in the year when stratification strength is at or near its peak (e.g., June, Fig. 3.6), variations in vertical mixing may exert a stronger control on hypoxia in this region than others (Table 3.3).

It is clear, however, that spring O_2-depletion metrics do not significantly correlate with summer hypoxic volumes. Even late-spring (May) and summer (July) hypoxic volumes are uncorrelated with DHO and ROD, suggesting that the summer hypoxic water mass is a dynamic feature that responds to short-term forcing from both physical and biological forcing. Previous investigations using both modeling and observation approaches illustrate this variability due to wind forcing, advection, and respiration in Chesapeake Bay and the Gulf of Mexico (Rabalais et al., 2007; Scully, 2010b). One important implication of this observed disconnect between spring and summer O_2 conditions is that contemporaneous inputs of organic matter are likely required for maintenance of summer hypoxia, in contrast to the long-standing view that summer hypoxia is sustained by the spring diatom bloom (Malone, 1987; Pomeroy et al., 2006). Given that we found the spring bloom to be the primary driver of spring ROD and DHO, we would expect some relationship between these metrics and the summer hypoxic

volumes if spring bloom-derived organic matter was the primary fuel to sustain low-oxygen conditions throughout the year. The fact that these relationships do not exist, and the fact that the metrics do correlate significantly with late-spring/early summer hypoxia, suggest that, by summer, most of this labile material has been respired. Observations of high summer productivity (Malone et al., 1988) and substantial organic matter sinking rates across the pycnocline (Kemp et al., 1999) suggest that summer organic matter production is also important in fueling summer hypoxia. The observations and modeling studies to necessary to test this assertion currently do not exist in Chesapeake Bay.

Winter-Spring O_2 Depletion in 2012

The onset of hypoxia in upper Chesapeake Bay in 2012 (April 6) occurred 8 days before than the earliest of onset dates from the previous 26 years, and this presents a useful case-study for the controls on winter-spring O_2 depletion. The passing of Tropical Storm Lee over much of the Susquehanna River watershed in September of 2011 resulted in extraordinary levels of freshwater flow and the highest suspended sediment loads to Chesapeake Bay recorded in thirty years (Hirsch, 2012). Although the lability and character of this suspended material is uncertain at this time, it is reasonable to assume that large amounts of organic material were deposited to sediments in much of the middle and upper Bay (Cheng et al., 2013). Previous investigators have speculated that organic material deposited to sediments in autumn might remain intact in sediments over the winter (due to low temperatures) and be respired the following spring (Boynton and Kemp, 2000; Taft et al., 1980).

Observations of bottom-water dissolved O_2 at several stations in the upper and middle Bay reveal historically low concentrations in February and March of 2012.

Although water temperature was historically high during these months (2.1 ^{o}C above previous maximum), associated declines in solubility do not explain such low O_2 concentrations (Fig. 3.10). Stratification strength approached the 26-year maximum at station CB3.3C and CB4.1 during this period (0.01-0.015 s^{-2}), suggesting that high stratification due to low wind stress during March (data not shown) could have led to reduced O_2. The remaining explanation is that respiration of organic matter derived the previous fall was responsible. Particulate organic carbon concentrations in the water-column at stations CB3.3C and CB4.1C were 1.5 to 2 times the long-term mean, while chlorophyll-*a* was 3 times the long-term mean at CB4.1C (data not shown), suggesting that respiration rates in the water column (due to both elevated temperature and organic matter availability) were above-average during winter-spring 2012.

The last potential driver of reduced O_2 concentrations is elevated sediment O_2 demand (SOD). Previous modeling of sediment biogeochemistry in Chesapeake Bay suggested that labile organic material deposition from the previous year can accumulate and carry-over to the following spring (Brady et al., 2012). A simple sediment biogeochemical model was used to examine the seasonal response of sediments to a large September depositional event, where a month-long pulse of POM equivalent to 30% of the total annual POM flux was simulated. Four total simulations were run, including (1) a control, where fall POM deposition was equivalent to the long-term mean, (2) the month-long, elevated POM flux, (3) the elevated POM flux with temperatures elevated by 2.5 ^{o}C in the following January to April period, and (4) run #3 with dissolved oxygen reduced to hypoxic conditions (47 μM O_2) begging on April 1st of the following year (Fig. 3.11). Runs #3 and #4 are consistent with observed water-column conditions in

2012. Organic matter diagensis rates for all organic matter pools were set to 0.01 d^{-1}, which is consistent with moderately labile organic matter (Burdige, 1991; Westrich and Berner, 1984). The simulations suggest that a depositional event associated with TS Lee combined with the observed water temperatures could have doubled SOD in the following winter-spring period, from 15 to 30 mmol O_2 m^{-2} d^{-1} (Fig. 3.11). The effect of the observed early onset of hypoxia in the beginning of April reduced SOD by roughly 30%, resulting in SOD comparable to what was observed (Fig. 3.11). However, SOD likely only contributes to 10% of total sub-pycnocline O_2 demand at station CB3.3C, considering a ~20 meter aphotic water-column, water-column respiration of 15 mmol O_2 m^{-3} d^{-1} (Sampou and Kemp, 1994), and SOD of 30 mmol O_2 m^{-3} d^{-1}.

Thus, we conclude that the unusually early hypoxia onset in upper Chesapeake Bay in 2012 was likely due to an interaction of high stratification, elevated temperature, and a carry-over of organic material from the fall of 2011. To adequately address this hypothesis, however, analyses should involve coupled physical-biological model simulations to separate effects of physical circulation from water-column and benthic biogeochemical processes. Such a model would compute both water-column and sediment responses to the loads from TS Lee, and if coupled to a sediment transport model (Cheng et al., 2013), could examine the impacts of sediment organic matter re-suspension on water-column respiration rates.

Summary

We computed rates of winter-spring, water-column O_2 depletion rates and the date of hypoxia onset for 12 stations and 25 years in Chesapeake Bay. Bottom-water, winter-spring chlorophyll-*a* was the strongest single driver of O_2 depletion rates and hypoxia

onset days, especially in the middle and upper Bay regions. This suggests that respiration of the annual spring bloom is the primary driver of early season O_2 depletion. However, metrics of early season O_2 depletion (as well as early season hypoxic volumes) are poorly correlated with summer hypoxic volumes, suggesting that (1) summer phytoplankton production is needed to sustain summer hypoxic volumes and (2) that climatic variations in later spring and summer are strong controls of hypoxic volume. Ongoing numerical modeling studies will between elucidate the mechanisms behind organic matter production and O_2 depletion.

Acknowledgements

This study was funded by the United States National Oceanographic and Atmospheric Administration (NOAA) Coastal Hypoxia Research Program (CHRP-NAO7NOS4780191), the National Science Foundation-funded Chesapeake Bay Environmental Observatory (CBEO-3 BERS-0618986), the State of Maryland Department of Natural Resources (K00B920002), and the Horn Point Laboratory Bay and Rivers Graduate Fellowship. We would like to thank the EPA Chesapeake Bay Program and the Maryland Department of Natural Resources for providing monitoring data; Rebecca Murphy for help and support in interpolation approaches; Randall Burns and Eric Pearlman for development, maintenance, and support of the CBEO testbed; Bill Ball, Walter Boynton, Damian Brady, Dominic Di Toro, and Jeff Cornwell for many insightful discussions. This work is NOAA Coastal Hypoxia Research Program (CHRP) Publication # 13X and the University of Maryland Center for Environmental Science Publication # XXXX.

Table 3.1: Monitoring station characteristics and hypoxia metrics in the modern (1985-2009) Chesapeake Bay Program-MD Department of Natural Resources dataset. See Figure 1 for map with station locations within Chesapeake Bay. Surface salinity, hypoxia onset, and O_2 depletion are means (±SD) over 1985-2009 period.

Station	Latitude	Longitude	Depth (m)	Surface Salinity	Hypoxia Onset	% Years Hypoxic	O_2 Depletion Rate (mmol O_2 m^{-3} d^{-1})
CB3.3C	38.996	-76.359	26	9.13	May 4 (±13)	100	3.19 (±0.78)
CB4.1C	38.826	-76.399	33	10.77	May 8 (±15)	100	3.16 (±0.63)
CB4.2C	38.646	-76.421	28	11.82	May 17 (±16)	100	3.34 (±0.69)
CB4.3C	38.555	-76.428	28	12.15	May 19 (±17)	100	3.31 (±0.63)
CB4.4	38.415	-76.346	32	12.90	May 23 (±18)	100	3.16 (±0.75)
CB5.1	38.319	-76.292	36	13.55	May 24 (±18)	100	3.09 (±0.91)
CB5.2	38.137	-76.228	33	14.08	June 1 (±17)	100	2.94 (±0.78)
CB5.3	37.910	-76.171	29	14.38	June 19 (±20)	100	2.66 (±0.59)
CB5.4	37.800	-76.175	34	16.46	June 22 (±26)	96.0	2.38 (±0.72)
CB5.5	37.692	-76.189	21	16.71	June 30 (±23)	84.0	2.44 (±0.75)
CB6.1	37.589	-76.162	13	17.55	July 5 (±13)	76.0	2.09 (±0.72)
CB6.2	37.487	-76.156	14	18.06	July 20 (±27)	52.0	1.88 (±0.84)

Table 3.2: Comparisons of water-column O_2-depletion metrics from this study with previously estimated rates using several varied approaches. O_2-depletion rates are in units of mmol O_2 m^{-3} d^{-1}

Approach	Months	Years	O_2 Depletion Rate	Source
Slope of Spring Decline	March-May	1985-2009	0.63-5.31	This Study
Slope of Spring Decline	Feb-June	1964-1977	1.25-4.69	(Taft et al., 1980)
Slope of Spring Decline	March-May	1985-1992	2.50-5.00	(Boynton and Kemp, 2000)
Slope of Spring Decline	unknown	1985-2001	2.34-6.13	(Hagy et al., 2004)
Residual of Process Budget	March-May		1.88-4.06	(Kemp et al., 1992)

Table 3.3: Table of correlation coefficients (r, top value) and associated *p*-values (bottom value) for correlations between the Date of Hypoxia Onset (DHO) and potential controlling variables, including Susquehanna River flow, April-May Brunt-Väisälä frequency, and chlorophyll-*a* concentration. For each controlling variable, two periods of aggregation are included. Numbers in bold indicate significance ($p<0.05$).

Hypoxia Onset	CB3.3C (n=25)	CB4.1C (n=25)	CB4.2C (n=25)	CB4.3C (n=25)	CB4.4 (n=25)	CB5.1 (n=25)	CB5.2 (n=25)	CB5.3 (n=25)	CB5.4 (n=23)	CB5.5 (n=20)	CB6.1 (n=18)	CB6.2 (n=13)
Susquehanna Flow (Jan-Mar)	**-0.69** **<0.001**	**-0.57** **0.003**	**-0.54** **0.006**	**-0.55** **0.005**	**-0.47** **0.019**	**-0.54** **0.006**	-0.36 0.074	-0.29 0.162	-0.14 0.512	-0.18 0.442	-0.14 0.563	-0.002 0.995
Susquehanna Flow (Feb-Apr)	-0.38 0.059	**-0.51** **0.009**	**-0.64** **0.001**	**-0.63** **0.001**	**-0.58** **0.003**	**-0.60** **0.002**	-0.35 0.082	-0.35 0.086	-0.31 0.142	-0.23 0.315	-0.26 0.286	-0.37 0.220
Chlorophyll-*a* (Jan-Apr)	**-0.53** **0.007**	**-0.73** **<0.001**	**-0.62** **0.001**	**-0.61** **0.001**	**-0.52** **0.008**	**-0.42** **0.036**	**-0.47** **0.018**	-0.21 0.310	-0.18 0.399	**-0.48** **0.034**	-0.42 0.081	-0.23 0.456
Brunt-Väisälä Frequency (Apr)	**0.40** **0.048**	-0.13 0.536	-0.10 0.626	-0.15 0.478	-0.16 0.430	-0.19 0.354	-0.38 0.059	-0.21 0.315	**-0.64** **0.001**	-0.24 0.286	0.29 0.223	-0.06 0.855
Brunt-Väisälä Frequency (May)	0.08 0.715	-0.03 0.890	-0.32 0.114	-0.22 0.280	-0.07 0.753	-0.19 0.364	-0.37 0.066	-0.36 0.080	**-0.53** **0.010**	-0.29 0.211	**0.50** **0.036**	-0.28* 0.360

*Date of Hypoxia Onset at this station was significantly correlated to regional mean (CB5.4-CB6.4) of the given variable

Table 3.4: Table of correlation coefficients (r, top value) and associated p-values (bottom value) for correlations between the March to May water-column O_2 depletion rate (ROD) and potential controlling variables, including Susquehanna River flow, Brunt-Väisälä frequency, water temperature, and chlorophyll-*a* concentration. For each controlling variable, two periods of aggregation are included. Numbers in bold indicate significance ($p<0.05$).

O_2 Depletion	CB3.3C (n=25)	CB4.1C (n=25)	CB4.2C (n=25)	CB4.3C (n=25)	CB4.4 (n=25)	CB5.1 (n=25)	CB5.2 (n=25)	CB5.3 (n=25)	CB5.4 (n=24)	CB5.5 (n=24)	CB6.1 (n=24)	CB6.2 (n=24)
Susquehanna Flow (Jan-Mar)	-0.20 0.345	-0.12 0.580	0.03 0.870	0.29 0.168	0.26 0.218	0.30 0.143	0.36 0.075	-0.12 0.561	-0.19 0.422	-0.10 0.669	-0.04 0.855	0.04 0.860
Susquehanna Flow (Feb-Apr)	0.07 0.745	0.28 0.190	**0.40** **0.048**	**0.50** **0.012**	**0.45** **0.025**	**0.45** **0.023**	0.38 0.060	0.14 0.496	0.03 0.889	0.13 0.560	0.08 0.709	0.19 0.390
Chlorophyll-*a* (Jan-Apr)	-0.14 0.496	-0.003 0.990	**0.43** **0.030**	**0.51*** **0.011**	**0.48*** **0.014**	0.34 0.092	**0.43*** **0.032**	0.23 0.275	0.39 0.099	0.06 0.789	0.22 0.323	0.32 0.149
Brunt-Väisälä Frequency (Apr)	0.33 0.112	0.28 0.189	0.12 0.578	0.004 0.985	0.004 0.984	0.05 0.808	**0.47** **0.017**	0.12 0.580	0.13 0.591	0.08 0.722	-0.05 0.825	-0.25 0.258
Brunt-Väisälä Frequency (May)	-0.24 0.248	0.18 0.393	0.23 0.269	0.18 0.407	0.17 0.405	0.30* 0.150	**0.46*** **0.021**	0.25 0.220	0.16 0.503	0.33 0.139	**0.53** **0.009**	0.39 0.074

*Water-column O_2 depletion rate at this station was significantly correlated to regional means (CB4.3C-CB5.2) of the given variable

Figure Legends

Figure 3.1: Map of Chesapeake Bay with bathymetry (see "Depth" key) and major tributaries included (also note horizontal "Distance" key). Circles indicate the location of monitoring stations, where the "CB" prefix to each number have been omitted. Open square indicates the location of station LE1.2, where continuous observations of dissolved O_2 were made.

Figure 3.2: Seasonal cycle of bottom-water O_2 saturation and concentration at CB5.1 (Fig. 3.1) in 2004 and illustration of how rate water-column O_2 depletion and date of hypoxia onset were derived from the time-series data (see text).

Figure 3.3: Time-series of bottom-water O_2 concentration at two stations near the upper (CB3.3C) and lower ends of the Chesapeake Bay hypoxic zone over 1985-1995. Gray shaded area indicates the hypoxia concentration threshold (62.5 μM).

Figure 3.4: Comparison of six-week time-series of bottom-water O_2 (16 m deep) measured continuously (YSI data sonde every 15 minutes, small gray lines and circles) and measured fortnightly (14 d, open circles/dashed line) at a station in the lower Patuxent River estuary in the spring of 2004 (Station LE1.2, 38.38, -76.51, see Fig. 3.1).

Figure 3.5: Two-dimensional isopleths depicting distributions of dissolved O_2 concentration with depth and distance along the Bay axis over the years 1985-2009 for four months (March, April, May, June) for the 25-year mean values (left panels) and standard deviations around the means (right panels).

Figure 3.6: Box plots of hypoxia onset day (top panel) and water-column O_2 depletion rate (bottom panel) at 12 stations along the Chesapeake Bay axis for the years 1985 to 2009 (see Fig. 3.1).

Figure 3.7: Patterns of hypoxia onset day (top panel) and water-column O_2 depletion rate shown as mean values (± standard errors) for the five years of highest (open circles) and five years of lowest (closed circles) winter-spring Susquehanna River flow. Asterisks between lines indicate significant differences between high-flow and low-flow groups.

Figure 3.8: Correlations of January to April bottom-water algal biomass (chlorophyll-*a*, top panel) and April to May mean stratification strength (Brunt-Väisälä Frequency, N^2, middle panel) with hypoxia onset day at station CB5.2 (see Fig. 3.1). Bottom panel is observed hypoxia onset day plotted against predictions from a multiple linear regression with chlorophyll-*a* and N^2.

Figure 3.9: Correlation coefficient of water-column O_2 depletion rate versus hypoxic volume (during May, June, and July) as they vary along the main Chesapeake Bay channel during three months. Asterisks near the circles indicate significant correlations.

Figure 3.10: Seasonal cycles of monthly mean water quality conditions in the bottom-waters over 1985-2009 at station CB3.3C in Chesapeake Bay (see Fig. 3.1: for (a) temperature, (b) oxygen solubility, (c) O_2 concentration, and (d) chlorophyll-*a*. Mean values are shown as a solid line, the shaded area in the top three panels shows the range (i.e., 25-year maximum and minimum value for each respective month), and the shaded area in the bottom panel is the 25-year standard deviation. Filled circles are observations from 2012, where hypoxia onset occurred on April 6 and the water-column O_2 depletion rate was 1.55 mmol m^{-2} d^{-1}.

Figure 3.11: Time series of sediment O_2 demand (SOD) from July-July in a simulation experiment with a two-layer sediment biogeochemical model (Brady et al., 2013) at station CB3.3C in Chesapeake Bay. The black line represents the "control" experiment, based on average conditions, the large dashed line represents the model forced with a month-long elevation of POM deposition representing the impact of Tropical Storm Lee in September 2011, the small dashed line in black represents the TS Lee experiment with January to April temperatures elevated by 2.5 ^{o}C, and the gray dotted line represents the TS Lee + Temperature experiment with hypoxia beginning on April 1.

Fig. 3.1

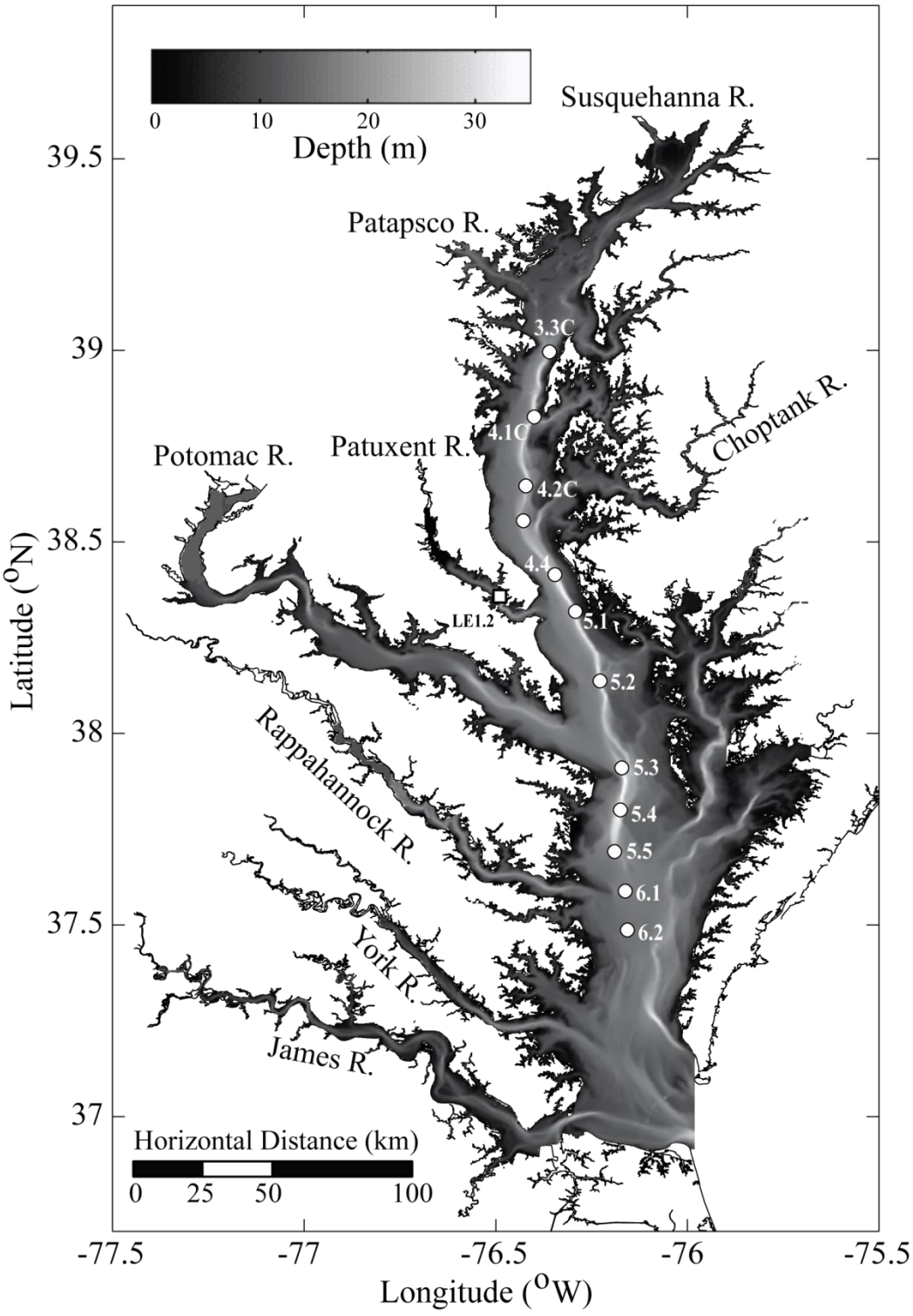
Susquehanna R.
0
10
20
30
Depth (m)
39.5
Patapsco R.
39
3.3C
4.1C
Choptank R.
Potomac R.
Patuxent R.
4.2C
38.5
4.4
LE1.2
5.1
5.2
Latitude (°N)
38
Rappahannock R.
5.3
5.4
5.5
6.1
37.5
6.2
York R.
James R.
37
Horizontal Distance (km)
0
25
50
100
-77.5
-77
-76.5
-76
-75.5
Longitude (°W)

Fig. 3.2

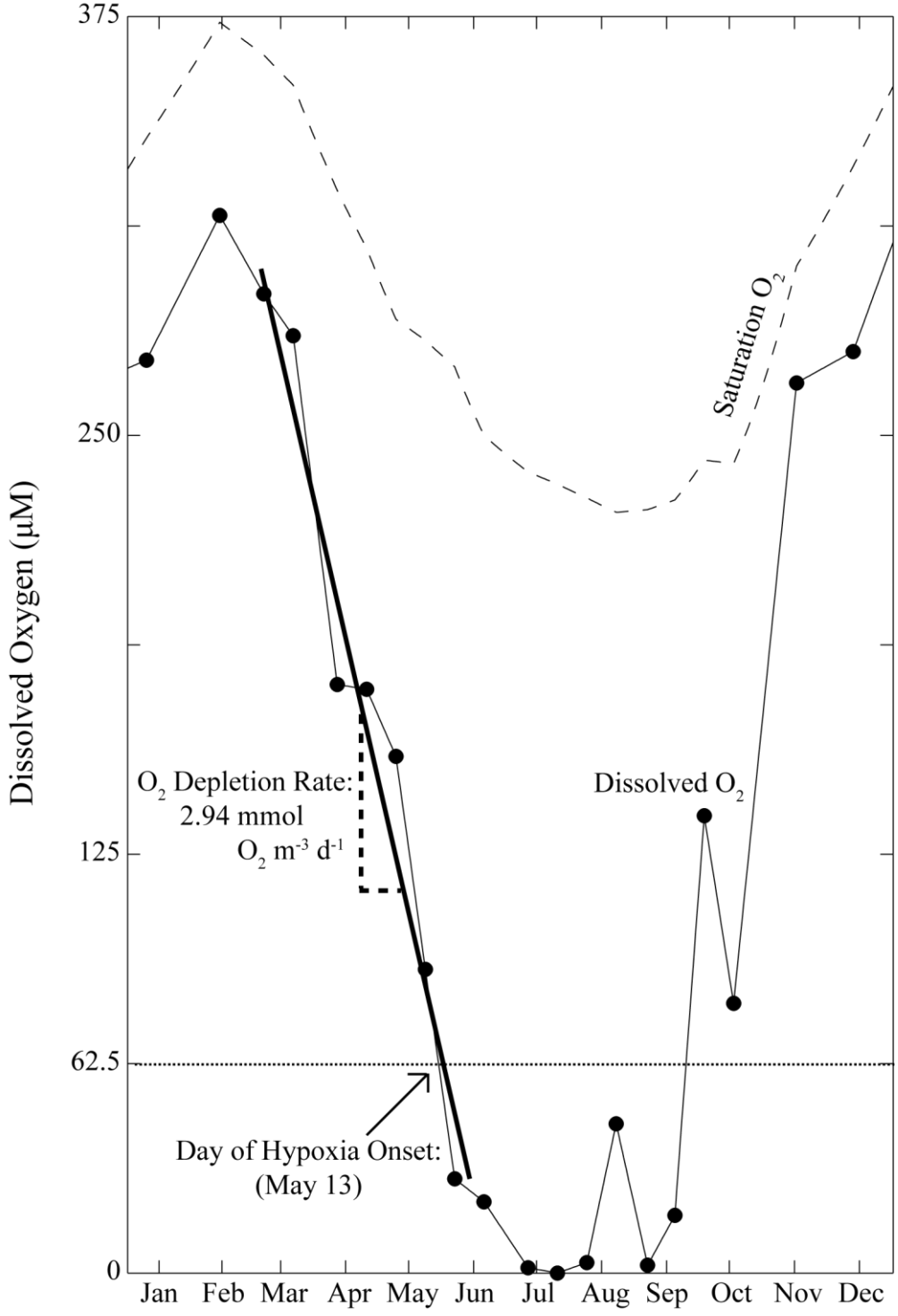
375
250
125
62.5
0
Dissolved Oxygen (μM)
Jan
Feb
Mar
Apr
May
Jun
Jul
Aug
Sep
Oct
Nov
Dec
Saturation O2
Dissolved O2
O2 Depletion Rate:
2.94 mmol
O2 m-3 d-1
Day of Hypoxia Onset:
(May 13)

Fig. 3.3

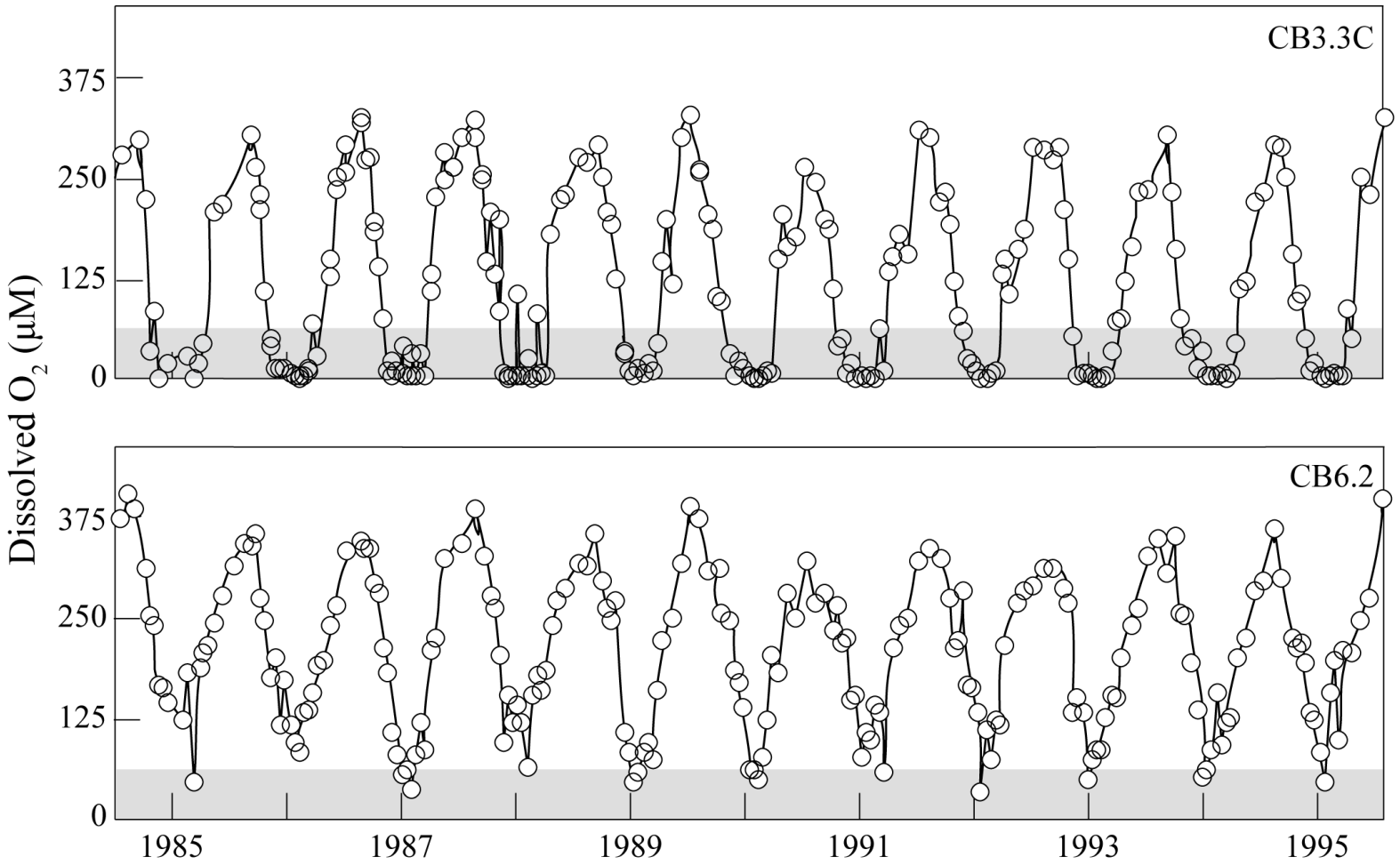
CB3.3C
CB6.2
Dissolved O_2 (μM)
375
250
125
0
1985
1987
1989
1991
1993
1995

Fig. 3.4

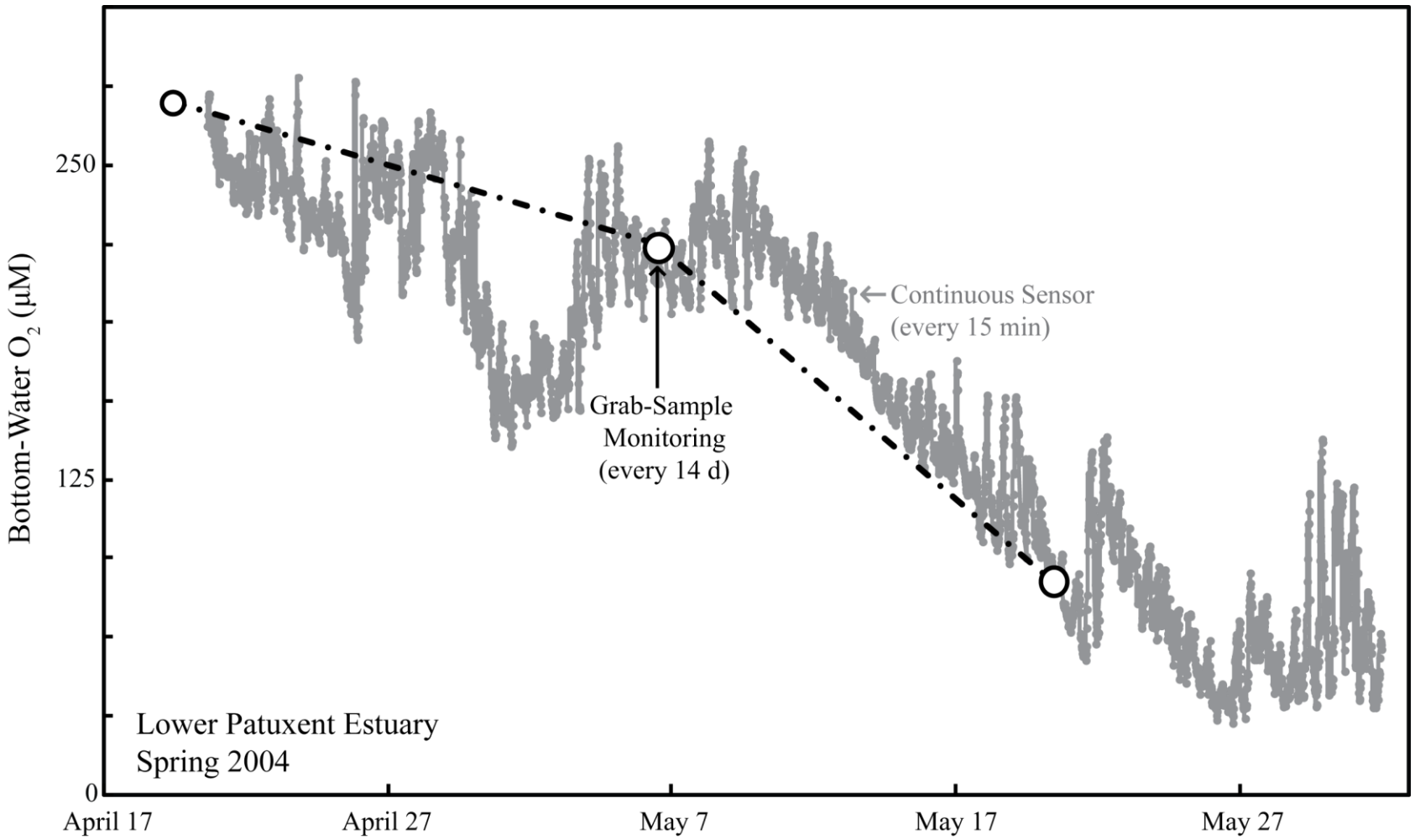
Bottom-Water O_2 (µM)
250
125
0
April 17
April 27
May 7
May 17
May 27
Continuous Sensor
(every 15 min)
Grab-Sample
Monitoring
(every 14 d)
Lower Patuxent Estuary
Spring 2004

Fig. 3.5

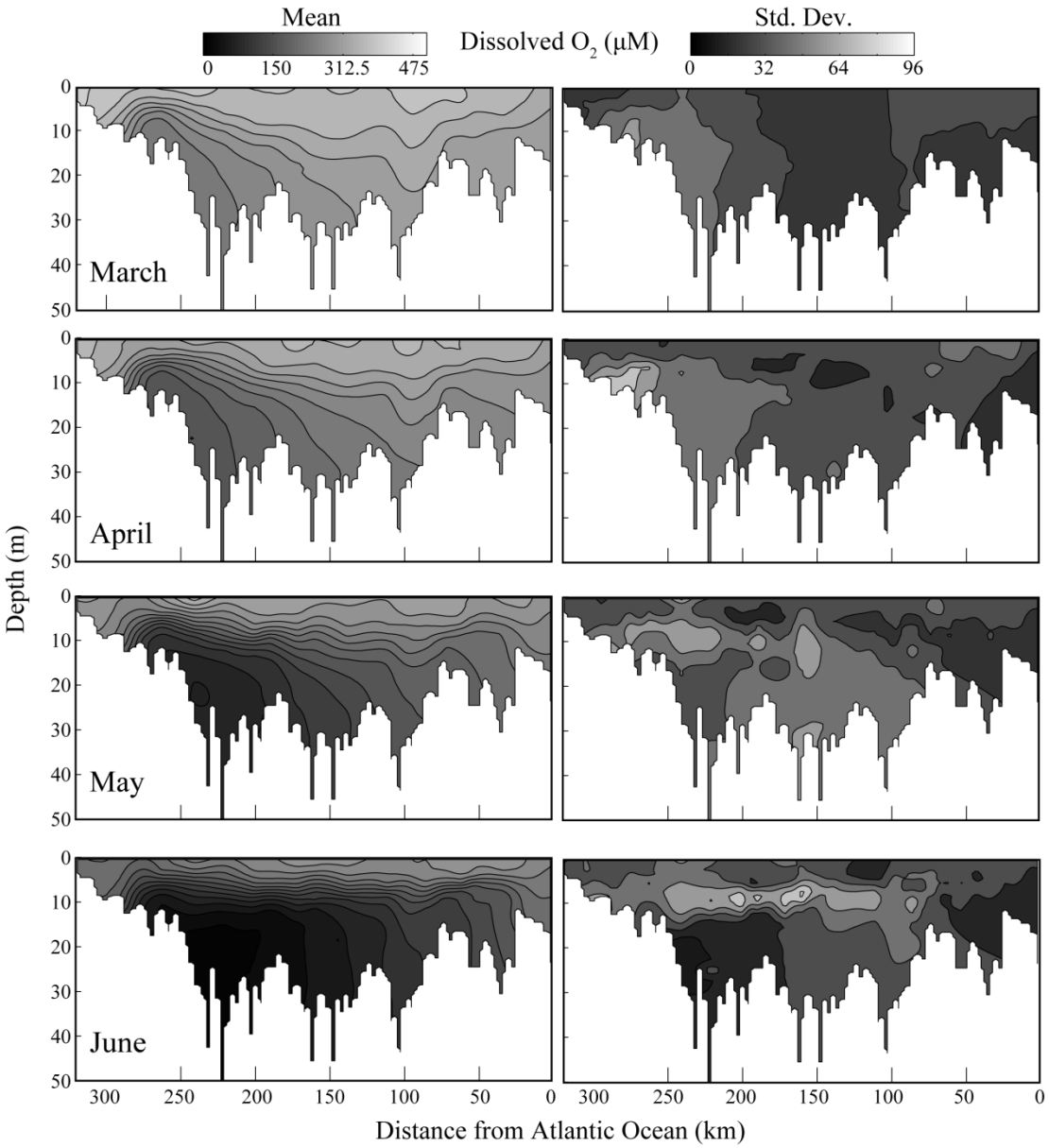
Mean
Dissolved O_2 (μM)
Std. Dev.
0 150 312.5 475
0 32 64 96
March
April
May
June
Depth (m)
0 10 20 30 40 50
300 250 200 150 100 50 0
Distance from Atlantic Ocean (km)

Fig. 3.6

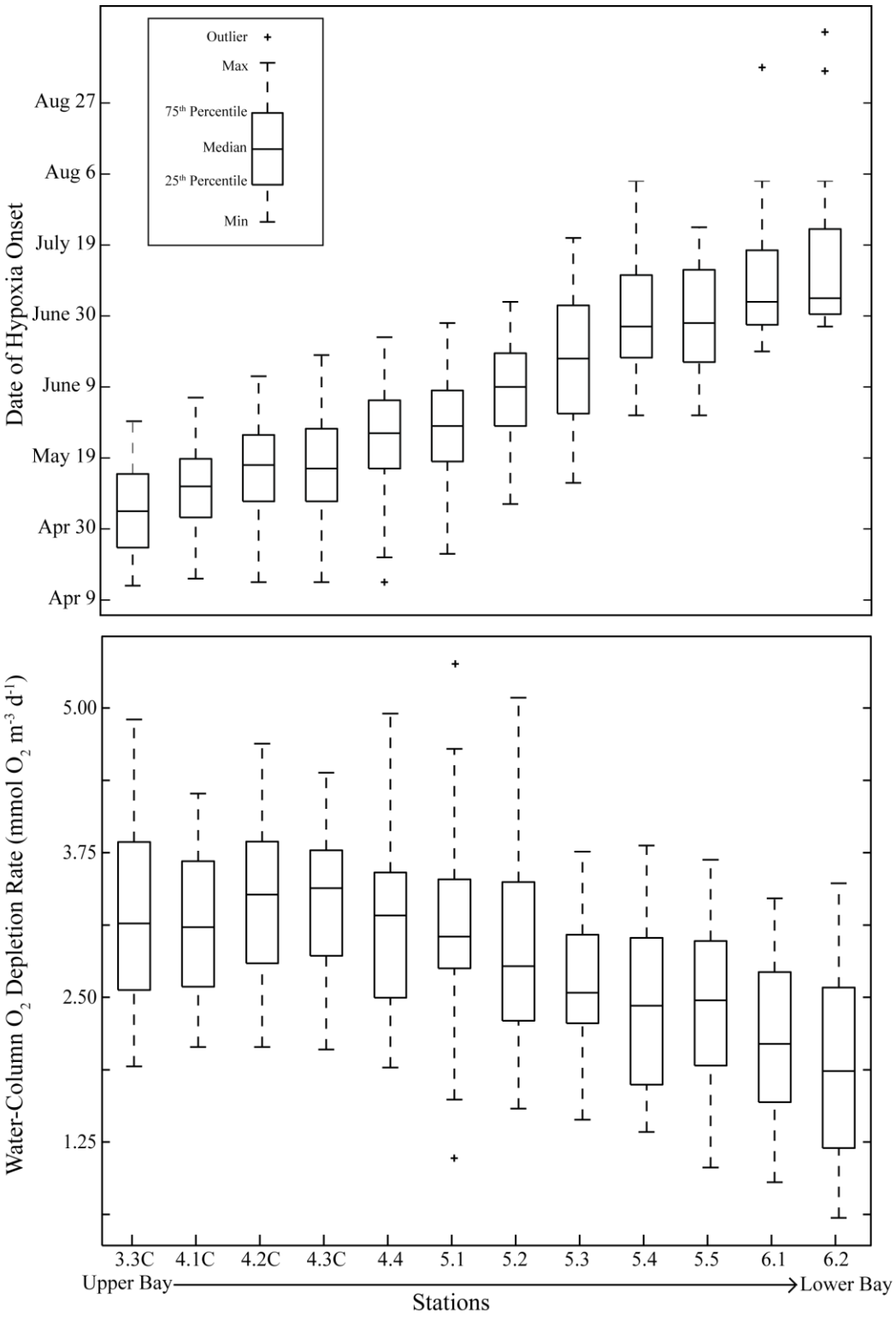
Outlier
Max
75th Percentile
Median
25th Percentile
Min
Aug 27
Aug 6
July 19
June 30
June 9
May 19
Apr 30
Apr 9
Date of Hypoxia Onset
5.00
3.75
2.50
1.25
Water-Column O2 Depletion Rate (mmol O2 m-3 d-1)
3.3C
4.1C
4.2C
4.3C
4.4
5.1
5.2
5.3
5.4
5.5
6.1
6.2
Upper Bay
Lower Bay
Stations

Fig. 3.7

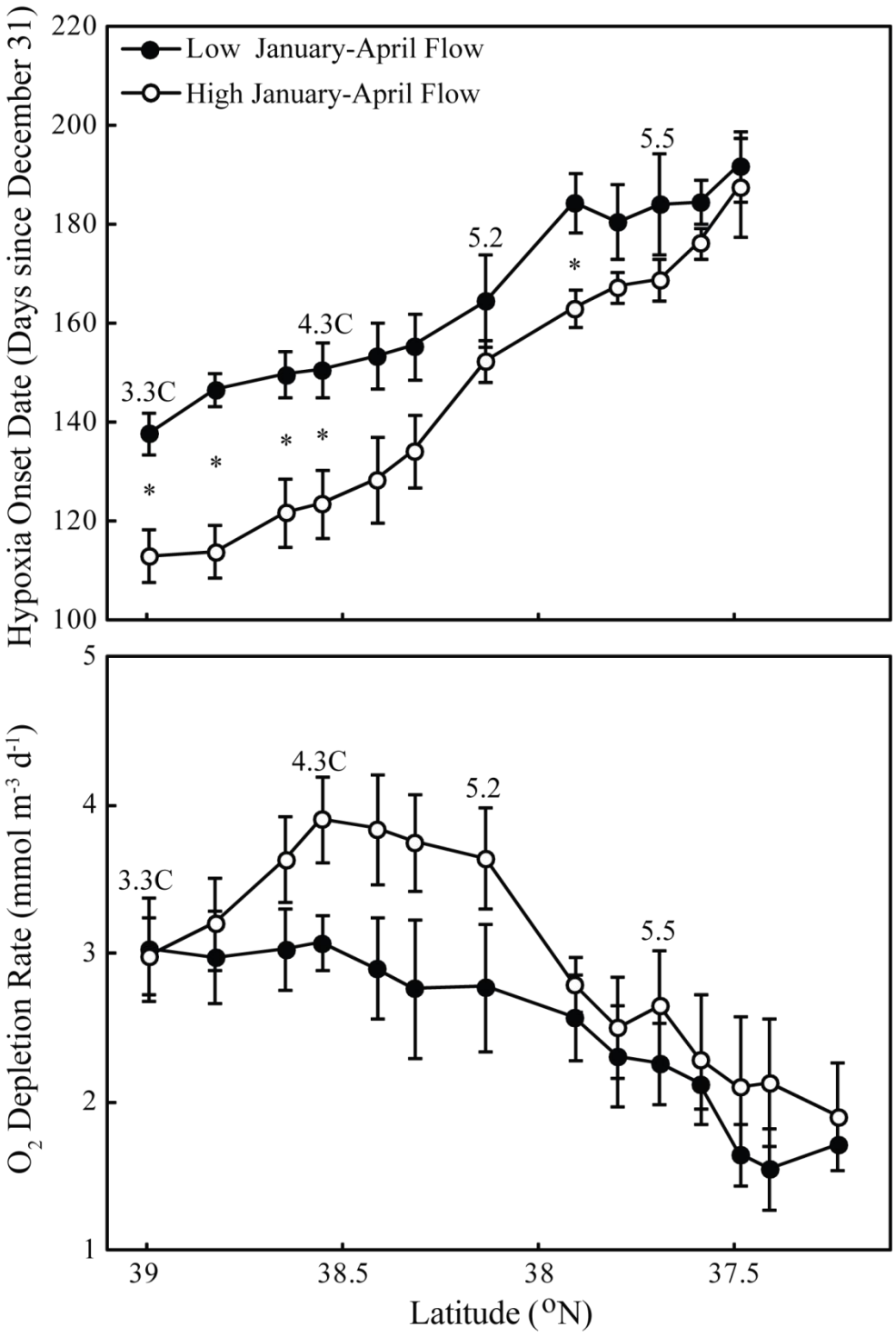
Low January-April Flow
High January-April Flow
Hypoxia Onset Date (Days since December 31)
220
200
180
160
140
120
100
3.3C
4.3C
5.2
5.5
*
O2 Depletion Rate (mmol m-3 d-1)
5
4
3
2
1
39
38.5
38
37.5
Latitude (°N)

Fig. 3.8

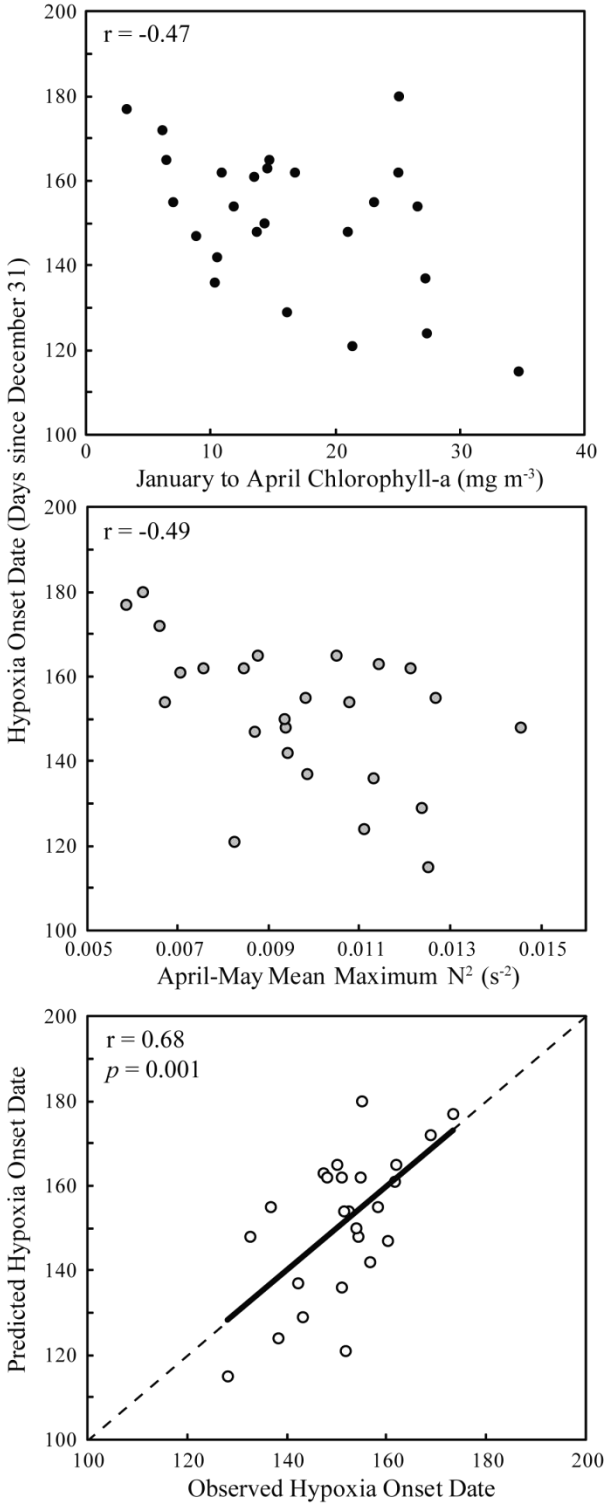
r = -0.47
Hypoxia Onset Date (Days since December 31)
January to April Chlorophyll-a (mg m-3)
r = -0.49
April-May Mean Maximum N2 (s-2)
r = 0.68
p = 0.001
Predicted Hypoxia Onset Date
Observed Hypoxia Onset Date

Fig. 3.9

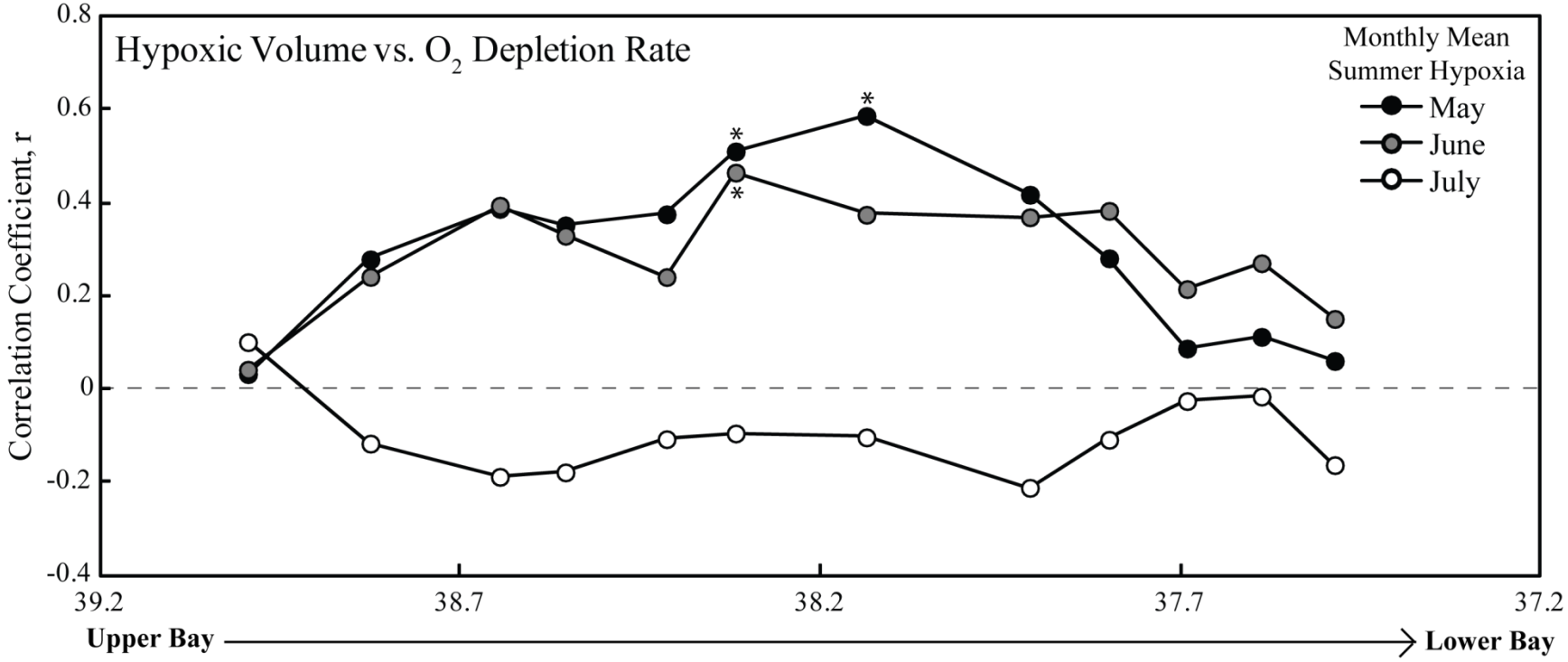
Hypoxic Volume vs. O_2 Depletion Rate
Monthly Mean
Summer Hypoxia
May
June
July
Correlation Coefficient, r
0.8
0.6
0.4
0.2
0
-0.2
-0.4
39.2
38.7
38.2
37.7
37.2
Upper Bay
Lower Bay
*
*
*

Fig. 3.10

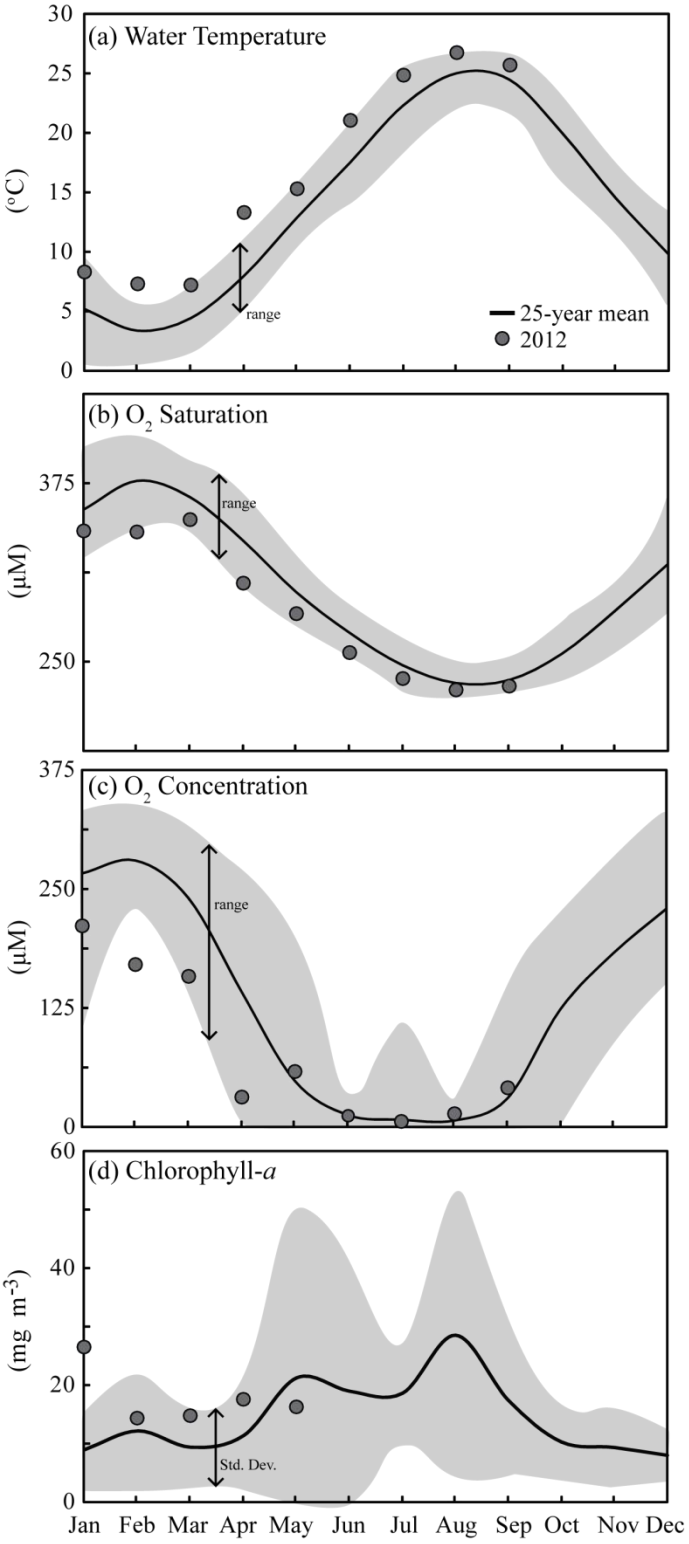
(a) Water Temperature
(°C)
30
25
20
15
10
5
0
range
25-year mean
2012
(b) O2 Saturation
(µM)
375
250
range
(c) O2 Concentration
(µM)
375
250
125
0
range
(d) Chlorophyll-a
(mg m-3)
60
40
20
0
Std. Dev.
Jan Feb Mar Apr May Jun Jul Aug Sep Oct Nov Dec

Fig. 3.11

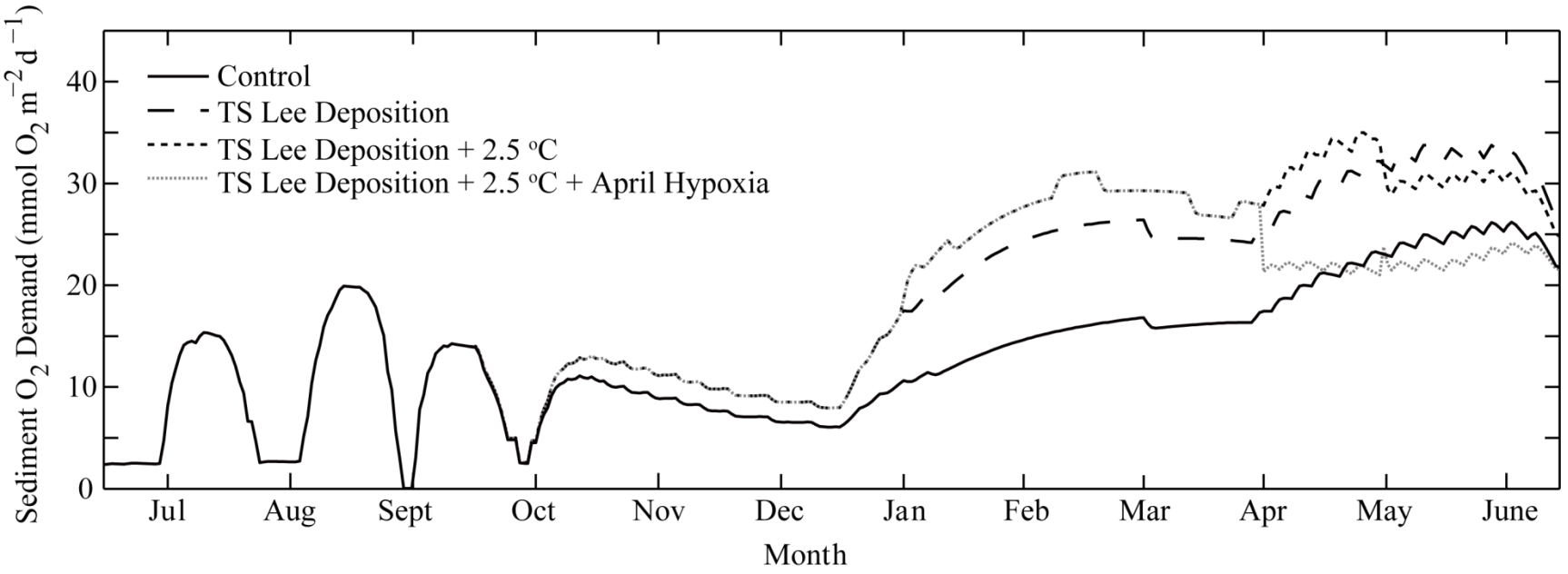
Control
TS Lee Deposition
TS Lee Deposition + 2.5 °C
TS Lee Deposition + 2.5 °C + April Hypoxia
Sediment O_2 Demand (mmol O_2 m^{-2} d^{-1})
0
10
20
30
40
Jul
Aug
Sept
Oct
Nov
Dec
Jan
Feb
Mar
Apr
May
June
Month

CHAPTER 4: SEDIMENT FLUX MODELING: SIMULATING NITROGEN, PHOSPHORUS, AND SILICA CYCLES

Abstract

Sediment-water exchanges of nutrients and oxygen play an important role in the biogeochemistry of shallow coastal environments. Sediments process, store, and release particulate and dissolved forms of carbon and nutrients and sediment-water solute fluxes are significant components of nutrient, carbon, and oxygen cycles. Consequently, sediment biogeochemical models of varying complexity have been developed to understand the processes regulating porewater profiles and sediment-water exchanges. We have calibrated and validated a two-layer sediment biogeochemical model (aerobic and anaerobic) that is suitable for application as a stand-alone tool or coupled to water-column biogeochemical models. We calibrated and tested a stand-alone version of the model against observations of sediment-water flux, porewater concentrations, and process rates at 12 stations in Chesapeake Bay during a 4 - 17 year period.

The model successfully reproduced sediment-water fluxes of ammonium (NH_4^+), nitrate (NO_3^-), phosphate (PO_4^{3-}), and dissolved silica ($Si(OH)_4$ or DSi) for diverse chemical and physical environments. A root mean square error (RMSE)-minimizing optimization routine was used to identify best-fit values for many kinetic parameters. The resulting simulations improved the performance of the model in Chesapeake Bay and revealed (1) the need for an aerobic-layer denitrification formulation to account for NO_3^- reduction in this zone, (2) regional variability in denitrification that depends on oxygen levels in the overlying water, (3) a regionally-dependent solid-solute PO_4^{3-} partitioning that accounts for patterns in Fe availability, and (4) a simplified model formulation for DSi, including limited sorption of DSi onto iron oxyhydroxides. This new calibration balances the need for a universal set of parameters that remain true to biogeochemical

processes with site-specificity that represents differences in physical conditions. This stand-alone model can be rapidly executed on a personal computer and is well-suited to complement observational studies in a wide range of environments.

Introduction

Sediments are important contributors to the nutrient, oxygen, and carbon cycles of shallow coastal ecosystems. Both autochthonous and allocthonous organic matter deposited to sediments drive sediment biogeochemical processes and resultant nutrient fluxes (Jensen et al., 1990), feed benthic organisms (Heip et al., 1995), and can control sediment oxygen demand (Kemp and Boynton, 1992b). In very shallow ecosystems (< 5 m), sediments may be populated by submerged vascular plants and/or benthic algal communities, both of which modify sediment biogeochemical reactions via nutrient uptake and sediment oxygenation (McGlathery et al., 2007; Miller et al., 1996). In moderately shallow systems (5-50m), sediments are sites of organic matter processing, leading to nutrient recycling (Cowan et al., 1996), oxygen consumption (Kemp et al., 1992; Provoost et al., 2013), and associated sediment-water exchange. Therefore, models of sediment diagenetic processes that simulate porewater nutrient concentrations and exchanges of particulate and dissolved substances between the water column and sediments have been developed (Boudreau, 1991; Soetaert and Middelburg, 2009; Vanderborght et al., 1977a). Such models are valuable tools for understanding and managing nutrients and aquatic resources (Cerco and Cole, 1993).

Sediment process model structures range from relatively simple empirical relationships (Fennel et al., 2006) to more complex process simulations that include time-varying state variables (Boudreau, 1991). Simple model representations include assigning

a constant sediment-water flux of O_2 or nutrients (Scully, 2010a) or using basic parameterizations of sediment-water flux as a function of overlying water conditions (Fennel et al., 2006; Hetland and DiMarco, 2008). More complex process models may simulate one or two layers, each of which represent a particular chemical environment (Di Toro, 2001; Emerson et al., 1984; Gypens et al., 2008; Slomp et al., 1998; Vanderborght et al., 1977b). Process models may also resolve depth into numerous layers, allowing for simulations of pore-water constituent vertical profiles (Boudreau, 1991; Cai et al., 2010; Dhakar and Burdige, 1996). Depth resolution in such complex models is usually associated with a higher computational demand (Gypens et al., 2008), thus intermediate complexity formulations (in terms of depth resolution) are commonly used when sediment biogeochemical models are coupled to water-column models to simulate integrated biogeochemical processes (Cerco and Noel, 2005; Sohma et al., 2008), although depth-resolved models have been used (Luff and Moll, 2004).

A sediment biogeochemical model was previously developed to link with spatially articulated water-column models describing biogeochemical processes at a limited computational cost (Brady et al., 2013; Di Toro, 2001). This sediment flux model (SFM) separates sediment reactions into two layers to generate fluxes of nitrogen, phosphorus, silica, dissolved oxygen (O_2), sulfide, and methane. SFM has been successfully integrated into water quality models in many coastal systems, including Massachusetts Bay (Jiang and Zhou, 2008), Chesapeake Bay (Cerco and Cole, 1993; Cerco and Noel, 2005), Delaware's Inland Bays (Cerco and Seitzinger, 1997), Long Island Sound (Di Toro, 2001), and the WASP model widely used by the United States Environmental Protection agency (Isleib and Thuman, 2011). SFM can also be used as a stand-alone diagnostic tool

in sediment process studies, especially over seasonal to decadal time scales (Brady et al., 2013). For example, it has been used to simulate sediment dynamics in the Rhode Island Marine Ecosystem Research Laboratory (MERL) mesocosms (Di Toro, 2001; Di Toro and Fitzpatrick, 1993). Such a stand-alone sediment modeling tool, when combined with high-quality time series observations, can be used for parameter optimization, scenario analysis, and process investigations.

The purpose of this study is: (1) to calibrate and validate a stand-alone version of SFM predictions with a multi-decadal time-series of water-column concentrations and sediment-water exchanges of dissolved inorganic nitrogen, silica, and phosphorus, (2) to utilize SFM to analyze sediment process observations at a range of Chesapeake Bay stations exhibiting differing overlying-water column characteristics (e.g., organic matter deposition rates and oxygen, temperature, and salt concentrations), and (3) to illustrate how SFM can be used to understand process interactions inferred from field rate measurements. A previous companion paper focused on the ammonium (NH_4^+), O_2, sulfide, and methane modules in SFM (Brady et al., 2013). Here, we focus our process studies on nitrate (NO_3^-), phosphate (PO_4^{3-}), and dissolved silica ($Si(OH)_4$; hereafter DSi) fluxes, as well as denitrificaion.

Methods

SFM was previously calibrated and validated for Chesapeake Bay using sediment-water flux measurements, overlying-water nutrient and O_2 concentrations, and process rates (e.g., denitrification) that were available at that time (1985-1988) for 8 sites (Chapter 14 in Di Toro, 2001). More than two decades later, this study used expanded data availability to re-calibrate and validate SFM, improve its simulation skill for

Chesapeake Bay, and demonstrate its utility as a stand-alone tool available for use in other aquatic systems. In this paper we describe and analyze SFM performance in the northern half of Chesapeake Bay using data collected during 4-17 years at 12 stations (Fig. 4.1). SFM can be run on a personal computer, executing a 25-year run on the time-scale of seconds, and a MATLAB interface is available for input generation, model execution, post-processing, and plotting.

General Model Description

The model structure for SFM involves three processes: (1) the sediment receives depositional fluxes of particulate organic carbon and nitrogen, as well as biogenic and inorganic phosphorus and silica, from the overlying water, (2) the decomposition of particulate matter produces soluble intermediates that are quantified as diagenesis fluxes, (3) solutes react, transfer between solid and dissolved phases, are transported between the aerobic and anaerobic layers of the sediment, or are released as gases (CH_4, N_2), and (4) solutes are returned to the overlying water (Fig. 4.2). The model assumes that organic matter mineralization is achieved by denitrification, sulfate reduction, and methanogenesis, thus aerobic respiration is not explicitly modeled. To model these processes, SFM numerically integrates mass-balance equations for chemical constituents in two functional layers: an aerobic layer near the sediment-water interface of variable depth (H_1) and an anaerobic layer below that is equal to the total sediment depth (10 cm) minus the depth of H_1 (Figs. 4.2,4. 3, & 4.4). The SFM convention is to use subscripts with "0" when referring to the overlying water, with "1" when referring to the aerobic layer, and with "2" when referring to the anaerobic layer.

The general forms of the equations are presented in Table 4.1 (Eqs. 1 & 2). For example, one can replace C_{T1} with NO_3^- (1) to compute the change in NO_3^- concentration in the aerobic layer (Eq. 1 in Table 4.1). The governing expressions are mass balance equations that include biogeochemical reactions ($\frac{\kappa_1^2}{K_{L01}} C_{T1}$), burial ($\omega_2 C_{T1}$), diffusion of dissolved material between the aerobic sediments and overlying water column ($K_{L01}(f_{d0}C_{T0} - f_{d1}C_{T1})$) and between sediment layers ($K_{L12}(f_{d2}C_{T2} - f_{d1}C_{T1})$), and the mixing of particulate material between layers; ($\omega_{12}\left(f_{p2}C_{T2} - f_{p1}C_{T1}\right)$: see Eqs. 1 and 2 in Table 4.1).

Aerobic Layer Depth and Surface Mass-Transfer

The thickness of the aerobic layer, H_1, is solved numerically at each time step of the simulation by computing the product of the diffusion coefficient (D_{O_2}) and the ratio of overlying-water O_2 concentration ($[O_2(0)]$) to sediment oxygen demand (*SOD*): $H_1 = D_{O_2} \frac{[O_2(0)]}{SOD}$. This relationship has been verified by measurements (Cai and Sayles, 1996; Jørgensen and Revsbech, 1985). The inverse of the second term on the right hand side of Equation 1 is the surface mass transfer coefficient (Eq. 5 in Table 4.1), which is used as the same mass transfer coefficient for all solutes since differences in the diffusion coefficients between solutes are subsumed in the kinetic parameters that are fit to data (Brady et al., 2013; Di Toro, 2001). It should be noted that in the time varying solution, H_1 and H_2 are within the derivative since the depths of the layers are variable, where dynamic entrainment and loss of mass can be quantified (see Chapter 13 in Di Toro, 2001). The depth of the anaerobic layer (H_2) is simply calculated as the difference between total sediment depth (10 cm) and H_1.

Dissolved and Particulate Mixing

Dissolved and particle mixing between layers 1 and 2 (K_{L12} and ω_{12}, Eqs. 6 & 7 in Table 4.1) are modeled as a function of passive transport and proxies that reflect the activities of benthic organisms. K_{L12} enhancement due to benthic faunal activity is parameterized directly, that is, the dissolved mixing coefficient (D_d) is fit to values that typically increase K_{L12} to 2-3 times molecular diffusion (Matisoff and Wang, 1998). The rate of mixing of sediment particles (ω_{12}; Eq. 7 in Table 4.1) by benthic animals is quantified by estimating the apparent particle diffusion coefficient (D_p; Chapter 13 in Di Toro 2001). In the model, particle mixing is controlled by temperature (first term in Eq. 7 in Table 4.1; (Balzer, 1996)), carbon input (second term in Eq. 7 in Table 4.1; (Robbins et al., 1989)), and oxygen (third term in Eq. 7 in Table 4.1; (Díaz and Rosenberg, 1995)). To make the model self-consistent, that is to use only internally-computed variables in the parameterizations, the model assumes that benthic biomass and therefore, particle mixing is correlated with the amount of labile carbon (i.e., POC_1) present in the sediment, an assumption that is supported by the literature (Tromp et al., 1995). However, if excess carbon loading creates unfavorable oxygen conditions that reduce macrofaunal density and therefore, bioturbation (Baden et al., 1990), particle mixing is reduced by a term called "benthic stress" (S in Eq. 7 in Table 4.1). As O_2 decreases, (1 - $k_S S$) approaches zero. After the stress has passed, the minimum is carried forward for the rest of the year to simulate the observation that benthic communities do not recover until recruitment occurs in the following year (Díaz and Rosenberg, 1995).

Diagenesis

Diagenesis of particulate organic matter (POM) is modeled by partitioning the settling POM into three reactivity classes, termed the "G model" (Westrich and Berner, 1984). Each class represents a fixed portion of the organic material that reacts at a specific rate (Burdige, 1991). For SFM, three G classes represent three levels of reactivity: G_1 is rapidly reactive (20 day half-life & 65% of settling POM), G_2 is more slowly reactive (1 year half-life & 20% of settling POM); G_3 (15% of settling POM) is, for this model, non-reactive (see Table 4.2 for parameters associated with diagenesis). The diagenesis expression is as follows (similar equations govern diagenesis of particulate organic nitrogen and phosphorus):

$$H_2 \frac{d\mathrm{POC}_i}{dt} = -k_{\mathrm{POC},i}\theta_{\mathrm{POC},i}^{(T-20)}\mathrm{POC}_i H_2 - \omega_2 \mathrm{POC}_i + f_{\mathrm{POC},i}\, J_{\mathrm{POC}} \quad \text{Eq. 1}$$

where POC_i is the POC concentration in reactivity class *i* in the anaerobic layer, $k_{\mathrm{POC},i}$ is the first order reaction rate coefficient, $\theta_{\mathrm{POC},i}$ is the temperature coefficient, ω_2 is the sedimentation velocity, J_{POC} is the depositional POC flux from the overlying water to the sediment, and $f_{\mathrm{POC},i}$ is the fraction of J_{POC} that is in the *i*th G class. The aerobic layer is not included, due to its small depth relative to the anaerobic layer: $H_1 \approx 0.1$ cm, while $H_2 \approx 10$ cm. Deposition rates for particulate nitrogen (J_{PON}), phosphorus (J_{POP}), and silica (J_{PSi}) are proportional to J_{POC} based on Redfield stoichiometry (Table 4.2).

Organic matter deposition rates (including particulate biogenic C, N, P, and Si) for each year and station were estimated using a Hooke-Jeeves pattern search algorithm (Hooke and Jeeves, 1961) to minimize the root mean square error (RMSE) between modeled and observed NH_4^+ flux. These estimates of deposition matched well with

observations made using several methods and a detailed discussion of this approach is included in a companion paper (Brady et al., 2013).

Reaction Rate Formulation

Rate coefficients for aerobic-layer reactions (e.g., nitrification, denitrification, sulfide oxidation, etc.) are relatively similar (Eq. 1 in Table 4.1). These reactions are modeled to be dependent on the depth of H_1. For example, the nitrification rate expression in the mass balance equations for NH_4^+ is a product of the aerobic layer nitrification rate ($k_{NH_4^+,1}$) and the depth of the aerobic layer (Fig. 4.3a):

$$k_{NH_4^+,1} H_1 = \frac{D_{NH_4^+} k_{NH_4^+,1}}{K_{L01}}$$

The product $D_{NH_4^+} k_{NH_4^+,1}$ is made up of two coefficients, neither of which is readily measured. The diffusion coefficient in a millimeter thick layer of sediment at the sediment water interface may be larger than the diffusion coefficient in the bulk of the sediment due to the effects of overlying water shear. It is therefore convenient to subsume two relatively unknown parameters into one parameter that is calibrated to data, called $\kappa_{NH_4^+,1}$ (Fig. 4.3a):

$$\kappa_{NH_4^+,1} = \sqrt{D_{NH_4^+} k_{NH_4^+,1}}$$

$\kappa_{NH_4^+,1}$ is termed the reaction velocity, since its dimensions are length per time. Squared reaction velocities are then incorporated in the reaction term of the mass balance equations (Table 4.1).

Ammonium Flux

NH_4^+ concentrations are computed for both aerobic and anaerobic layers via mass balances of biogeochemical and physical processes. Figure 3a shows the sources and

sinks of NH_4^+ in the model. NH_4^+ is produced by organic matter diagenesis (J_{N2} in Fig. 4.3a, Eq. 10 in Table 4.1) in the anaerobic layer, while in the aerobic layer, NH_4^+ is converted to NO_3^- via nitrification using a reaction velocity, $\kappa_{NH_4^+,1}$, (Fig. 4.3a) with Michaelis-Menten kinetics (Eq. 8 in Table 4.1). Mass-transfer coefficients are employed to model diffusion of NH_4^+ between the anaerobic and aerobic layers (K_{L12}) and between the aerobic layer and the overlying water (K_{L01}). A more extensive treatment of the NH_4^+ model is given in a companion publication (Brady et al., 2013).

Nitrate Flux

There are two sources of NO_3^- in SFM: (1) NO_3^- enters from the overlying water column as controlled by surface mass transfer (K_{L01}) and the concentration gradient, and (2) NH_4^+ is oxidized in the aerobic layer (i.e., nitrification; Eq. 13 in Table 4.1, Fig. 4.3b; see Chapter 4 of Di Toro 2001). In turn, NO_3^- can be returned to the overlying water column as NO_3^- flux ($J[NO_3^-]$) or converted to nitrogen gas (i.e., denitrification, Eqs. 11 & 12 in Table 4.1). There is no biogeochemical NO_3^- source in the anaerobic layer (Fig. 5.3. Although it is conventional to confine denitrification to the anaerobic layer (Gypens et al., 2008), denitrification is modeled in both the aerobic and anaerobic layers in SFM (Fig. 4.3b). The close coupling between nitrification and denitrification has been suggested by some authors (Blackburn et al., 1994) and there is evidence for denitrification in the oxic layer within anoxic microsites (Jenkins and Kemp, 1984).

Phosphate Flux

The PO_4^{3-} model differs from the nitrogen models in two important ways: (1) there are no reactions for PO_4^{3-} once it is released during diagenesis (Eqs. 14 & 15 in Table 4.1) and (2) the PO_4^{3-} model includes both organic and inorganic phases (Fig. 4.4a).

There are two sources of PO_4^{3-} to SFM: (1) PO_4^{3-} produced by organic matter diagenesis ($a_{P,C}J_C$ in Fig. 4.4a, Eq. 16 in Table 4.1) in the anaerobic layer and (2) PO_4^{3-} that is sorbed onto particles and deposited to sediments (J_{PIP}). Observations of the latter source are scarce, so we initially assumed that sorbed PO_4^{3-} deposition is equivalent to (J_{POP}), which is supported by the observation that POP is roughly 50% of the particulate phosphorus pool in Chesapeake Bay (Keefe, 1994). Because $J_{PIP}$is likely to be spatially-variable (Keefe, 1994), we optimized J_{PIP} to the sediment-water PO_4^{3-} flux (see below).

Models of phosphorus in marine sediments have traditionally focused on predicting the interstitial concentration of PO_4^{3-} (Rabouille and Gaillard, 1991; Van Cappellen and Berner, 1988), as well as the PO_4^{3-} flux (Slomp et al., 1998). Because SFM is used to predict sediment-water PO_4^{3-} fluxes, it accounts for the fact that a fraction of the PO_4^{3-} released during diagenesis is trapped in sediments in particulate form via precipitation or sorption to amorphous iron oxyhydroxides (Sundby et al., 1992). The model also accounts for the dissolution of iron oxyhydroxides under low oxygen conditions and subsequent release of PO_4^{3-} into porewater (Conley et al., 2002). Thus, the model can account for the temporary storage of PO_4^{3-} near the sediment water interface until oxygen is seasonally-depleted, resulting in iron oxyhydroxides dissolution and subsequently large sediment-water PO_4^{3-} fluxes (Lehtoranta et al., 2009; Testa and Kemp, 2012). SFM distinguishes between solid and dissolved pools of PO_4^{3-} using partition coefficients specific to both layer 1 and 2 (Eqs. 3 and 4 in Table 4.1). The partition coefficient in layer 1 is larger than in layer 2 under oxic conditions, representing the higher concentration of oxidized Fe and allowing for PO_4^{3-} trapping. Once oxygen falls below a

critical concentration (Eq. 22 in Table 4. 1, Table 4.2), a larger fraction of the total PO_4^{3-} is transitioned to the dissolved pool.

Dissolved Silica Flux

The DSi model includes the same partitioning formulation (including O_2-depencency) as the PO_4^{3-} model (Eq. 22 in Table 4.1) and also has no reactions in layer 1 and 2 (Eqs. 17 and 18 in Table 4.1, Fig. 4.4b). Similar partitioning formulations are absent from previous silica models (Vanderborght et al., 1977a), but are present in more recent formulations (Rabouille and Gaillard, 1990), based upon evidence for DSi sorption to Fe oxyhydroxides (hereafter FeOOH) (Sigg and Stumm, 1981).

Unlike phosphorus, nitrogen and carbon, silica diagenesis is a dissolution reaction rather than a microbially-mediated respiratory process. The particulate silica deposited to sediments that may be dissolved originates from two sources: (1) biogenic silica in diatom algal material (J_{PSi}) and (2) detrital silica associated with terrestrially-derived particles ($J_{Detr_{Si}}$, Eqs. 17 & 18 in Table 4.1, Table 4.2). Silica dissolution has been found to be a function of the degree of undersaturation, pH, temperature, particulate silica concentration, salinity, and the nature of the surfaces of the solid-phase silica (Conley et al., 1993; Van Cappellen and Linqing, 1997b; Yamada and D'Elia, 1984). In SFM, the diagenesis of particulate silica is a function of a first-order rate constant (k_{Si}) with a temperature dependency (θ_{Si}), a Michaelis-Menten dependency on particulate silica (P_{Si}), and a first-order dependency on the degree of undersaturation (Eq. 18 in Table 4.1, Table 4.2). The original calibration of SFM considered silica solubility to be independent of temperature (Di Toro, 2001). In this analysis, a temperature dependency on silica

solubility was added (Eq. 18 in Table 4.1), as has been suggested in the literature (Lawson et al., 1978; Van Cappellen and Linqing, 1997a).

Overlying Water Concentrations

Data for overlying water-column nutrient and O_2 concentrations nearest the sediment-water interface in Chesapeake Bay, which are required boundary conditions for the stand-alone SFM simulations, were retrieved for each station and date from the Chesapeake Bay Program (CBP) Water Quality database (http://www.chesapeakebay.net/data_waterquality.aspx). Measurements of bottom water salinity, dissolved O_2, NH_4^+, NO_3^-, and PO_4^{3-} made as part of the Sediment Oxygen and Nutrient Exchange (SONE) experiments (Boynton and Bailey, 2008) were augmented by CBP data by combining the time series and using piecewise cubic hermite interpolation (PCHIP) to derive daily overlying water-column values. DSi data were only available in the CBP dataset. The fine temporal resolution of the combined SONE and CBP monitoring time series insures that the onset of hypoxia and winter temperature regimes (not measured in the SONE dataset) were properly simulated. To calculate initial sediment nutrient conditions, the time series of POM deposition and overlying water concentrations were repeated until there was 15 years of input. The synthetic 15 year time series was used as the model input, followed by the actual years. This insures that the initial conditions for SFM particulate and dissolved constituents are consistent with the depositional fluxes and parameters.

Calibration and Validation Datasets

Observed sediment-water fluxes of NH_4^+, nitrite + nitrate ($NO_2^- + NO_3^-$), PO_4^{3-}, and DSi were estimated from time-course changes in constituents during incubations of intact

plexiglass sediment cores (Boynton and Bailey, 2008). Although not presented in this paper, the organic matter deposition rates used in this analysis were validated against available observations, as were rates of sediment oxygen demand, sulfate reduction, and porewater concentrations (Brady et al., 2013). Cores for the measurement of sediment denitrification were collected by box coring in both the upper Chesapeake Bay ("Still Pond") and in the mid-bay ("R-64"); the methods for core incubation are described in detail elsewhere (Kana et al., 2006). Briefly, triplicate cores from each site that had aerobic overlying water conditions were bubbled with air for ~2 hours while submersed in a temperature controlled bath. Tops caps with suspended magnetic stirrers were attached and time courses of solute (NH_4^+, NO_x^-) and gas (O_2, N_2, Ar) concentrations were determined. The rate of gas flux was determined from high precision N_2:Ar or O_2:Ar ratios using membrane inlet mass spectrometry. While the fluxes of N_2 are referred to as denitrification, they are actually the summation of all gaseous N transformation processes and may include processes such as anammox (Rich et al., 2008) or N fixation associated with sulfate reduction (Bertics et al., 2013); fluxes of N_2O were not measured.

Error Metrics and Parameter Optimization

Model-data comparisons were facilitated using multiple skill assessment metrics (Stow et al., 2009a). RMSE, mean error (sum of residuals divided by the number of observations), and reliability index (RI) were computed for each flux/station combination. Mean error is a measure of aggregate model bias while RMSE takes into account the magnitude of model-data discrepancies. Finally, the RI quantifies the average factor by which model predictions differ from observations. An RI of 2, for instance,

would indicate that SFM predicts the observation within a factor 2, on average (Stow et al., 2009a).

We first ran SFM at 12 stations for all years where observations of sediment-water fluxes were available using the parameter set from the original calibration of SFM in Chesapeake Bay (Di Toro, 2001). We then calibrated several components of the model to optimize model-data fits. Specifically, we ran 50 simulations with 50 different values for 11 parameters to find the minimum root mean square error (RMSE) between modeled and observed solute fluxes for the nutrient flux (NO_3^-, PO_4^{3-}, and DSi) associated with each parameter. This optimization routine requires the range of potential parameter values and the number of simulations to be run using parameter values equally spaced between the range. The pattern search range for each parameters was centered around the parameter value from the original model calibration (Di Toro, 2001). This process is repeated for each station and the RMSE for each variable (e.g., $J[NO_3^-]$) and parameter (e.g., $\kappa_{NO_3^-,1}$) is saved after each run. Parameter ranges were constrained in each case based on published values and chosen after careful consideration of model-data residuals. Optimization simulations were performed for 11 parameters, which is a subset of the total parameter set, including: (1) the aerobic and anaerobic layer denitrification reaction velocity ($\kappa_{NO_3^-,1}$, $\kappa_{NO_3^-,2}$), (2) the PO_4^{3-} and DSi partition coefficients in layer 1 and 2 ($\Delta\pi_{PO_4^{3-},1}$, $\pi_{PO_4^{3-},2}$, $\Delta\pi_{Si,1}$, $\pi_{Si,2}$), (3) the particulate inorganic PO_4^{3-} and DSi depositional fluxes, (4) the half-saturation constant for P_{Si} dependency of silica dissolution ($K_{M,PSi}$), and (5) the first-order silica diagenesis rate constant (k_{Si}).

Results

Sediment-Water Nitrogen Fluxes

Using the original model calibration, which was based on measurements made during 1985-1988, SFM sediment-water NO_3^- fluxes matched observations at three sites with similar characteristics (e.g., Still Pond in Fig. 4.5a), but under-estimated net influxes to sediments at other sites (e.g., R-64 in Fig. 4.5b, Table 4.3). Specifically, SFM simulated NO_3^- fluxes well at sites with low salinity, in close proximity to freshwater discharges from major river, and relatively high (normoxic) O_2 levels throughout the year (Windy Hill, Still Pond, and Maryland Point; Table 4.3). However, at the other nine sites, which are generally deeper and experience seasonal hypoxia and anoxia, the original SFM calibration was unable to capture the large spring NO_3^- fluxes into the sediment that occurred in years after 1988 (e.g., Fig. 4.5b, Table 4.3).

The parameter optimization routine to minimize the RMSE between observed and modeled NO_3^- fluxes yielded different results for the aerobic and anaerobic denitrification velocity ($\kappa_{NO_3^-,1}$ and $\kappa_{NO_3^-,2}$). Although model results were relatively insensitive to changes in the anaerobic-layer denitrification velocity (data not shown), alterations of the aerobic-layer denitrification velocity resulted in substantial improvements in the NO_3^- flux predictions across the nine relatively hypoxic sites (Fig. 4.5c, Table 4.3). The value of $\kappa_{NO_3^-,1}$ from the original calibration (0.1 m d^{-1}) resulted in the lowest RMSE at Windy Hill, Still Pond, and Maryland Point (low salinity, normoxic), while higher values of $\kappa_{NO_3^-,1}$ reduced RMSE at the other sites (higher salinity, seasonally-hypoxic; Fig. 4.5c, Table 4.3). Increasing the denitrification velocity 2-4 times more than the original calibration resulted in a 38% reduction in RMSE across hypoxic sites (Table 4.3).

Importantly, the optimized value of $\kappa_{NO_3^-,1}$ correlated significantly (r = -0.81, p = 0.002) with the model-computed depth of the aerobic layer (Fig. 4.5c inset).

We restructured the formulation for denitrification to make it uniform across varying environmental conditions. The strong correlation between H_1 and optimized $\kappa_{NO_3^-,1}$ (Fig. 4.5c inset) indicates that the depth-dependence of aerobic layer NO_3^- removal (via denitrification) is responsible for the station specific optimization of $\kappa_{NO_3^-,1}$. In the NO_3^- mass balance, the squared aerobic layer denitrification velocity ($\kappa_{NO_3^-,1}$) is divided by the surface mass-transfer coefficient (K_{L01}; Eq. 1 in Table 4.1). Because $\kappa_{NO_3^-,1} = \sqrt{D_{NO_3^-}\, k_{NO_3^-,1}}$ and $K_{L01} = \frac{D_{NO_3^-}}{H_1}$, the NO_3^- removal term is $\left(D_{NO_3^-}\, k_{NO_3^-,1}\right)\left(\frac{D_{NO_3^-}}{H_1}\right)^{-1}$[$NO_3^-$(1)], or in a more simplified form, $k_{NO_3^-,1}\, H_1$ [NO_3^-(1)]. This formulation implies that denitrification is occurring uniformly over the depth of the aerobic layer, yet if anaerobic microsites are unequally distributed, or denitrification occurs only at the interface of the aerobic and anaerobic layers, this implication would not be valid. Thus, we executed a second optimization without the depth dependence, where aerobic-layer denitrification is simply $k_{NO_3^-,1}$ [NO_3^-(1)]. The results of this second optimization indicated that a spatially invariant denitrification velocity of 0.2 m d^{-1}, which we call $k_{NO_3^-,1g}$, resulted in an overall 33% decrease in RMSE across all observations at all sites (Fig. 4.6, Table 4.3).

Denitrification

In addition to model-data comparisons of NO_3^- fluxes, it was also possible to validate model-computed denitrification rates (using the depth-independent formulation) with observations made at several stations within Chesapeake Bay (Fig. 4.7). Denitrification has been measured across a wide range of conditions (i.e., overlying-water NO_3^-, salinity,

O_2, and depth) in Chesapeake Bay over the past several decades (Kana et al., 1998; Kemp et al., 1990) using a variety of methods. A collection of measurements made in the Choptank River estuary over a large gradient (3-300 μM) of overlying-water NO_3^- (Kana et al., 1998) demonstrated a strong dependence of denitrification on NO_3^- availability in the overlying water (Piña-Ochoa and Álvarez-Cobelas, 2006). When seasonally-averaged, modeled denitrification rates for each station are plotted against overlying-water NO_3^-, the overall relationship and rate magnitudes compare favorably to observations (Fig. 4.7a).

At stations R-64 and Still Pond, denitrification rates estimated over an annual cycle in 200 and 2001 match the seasonality and magnitude of SFM predictions (Fig. 4.7b and c). In general, two different seasonal patterns of denitrification were predicted by SFM for two distinct environmental types; at stations with high NO_3^- and no seasonal hypoxia, denitrification followed the annual temperature cycle (e.g., Still Pond), whereas stations with low summer NO_3^- and seasonal hypoxia or anoxia, denitrification displayed the bimodal cycle (e.g., R-64; Fig. 4.7b).

Phosphate Flux

Unlike NO_3^-, the original model calibration resulted in sediment-water PO_4^{3-} fluxes that agreed with the data reasonably well (Fig. 4.8, Table 4.3), as evidenced by a reliability index of 1.41 (well below 2). However, model estimates of PO_4^{3-} fluxes were particularly high during the summer at anoxic stations compared with observed fluxes (Fig. 4.8b). Optimization routines suggested station-specific values for the aerobic ($\Delta\pi_{PO_4^{3-},1}$) and anaerobic ($\pi_{PO_4^{3-},2}$) layer partition coefficients significantly improved model fit during this important seasonal period of internal phosphorus loading. Model-

observation fits resulted in an overall RMSE reduction of 25% when $\Delta\pi_{PO_4^{3-},1}$ and $\pi_{PO_4^{3-},2}$were higher at low salinity sites in close proximity to river inputs (Still Pond, Maryland Point; Fig. 4.8c, Table 4.3) and when $\Delta\pi_{PO_4^{3-},1}$ and $\pi_{PO_4^{3-},2}$were lower at most other sites (Fig. 4.8c, Table 4.3). In some cases (e.g., R-78, Point No Point), the model was insensitive to changes in the partitioning coefficients. Station-specific values of $\Delta\pi_{PO_4^{3-},1}$ were related to the amount of oxalate-extractable Fe observed in the top 3 cm of sediments (Cornwell and Sampou, 1995) at four sites in Chesapeake Bay (Fig. 4.8c inset). Where Fe concentrations were higher, the aerobic layer partitioning coefficient optimized at a higher values (Fig. 4.8c inset). When the optimized parameters were included in SFM simulations, the model better represented the observed sediment-water fluxes, particularly during summer (Fig. 4.9, Table 4.3). When the PO_4^{3-} flux was optimized to J_{PIP}, RMSE was slightly improved (Table 4.3), with J_{PIP} contributing between 25% and 50% of total phosphorus deposition (data now shown).

Nitrogen and Phosphorus Recycling

O_2 concentration exerts strong control over nitrogen and phosphorus cycling in sediments. To explore the role overlying water O_2 in the removal of nutrients by sediments, sediment-water fluxes of NH_4^+ and PO_4^{3-} were plotted against the deposition of organic N and P (Fig. 4.10). Between 25% and 50% of the deposited nitrogen was removed (via burial or denitrification), while in general, 25% of the phosphorus was removed (via burial or storage). Nitrogen removal was higher at stations where summer O_2 concentrations generally do not become anoxic (Fig. 4.10).Thus, at Still Pond and Maryland Point, where O_2 concentrations are above 3 mg O_2 L^{-1} year-round and partitioning coefficients (i.e., Fe concentrations) are high (Fig. 4.10), phosphorus removal

was > 50%. Another method of assessing O_2 effects on nitrogen cycling is to compute the "nitrogen recycling efficiency" ($NRE = \frac{J[NH_4^+]}{J[NH_4^+] + J[N_2] + J[NO_3^-]}$) from the model nitrogen fluxes (Boynton and Kemp, 2008), which represents NH_4^+ recycling relative to the total efflux of inorganic N solutes. This index, computed from model simulations, was negatively correlated to overlying water O_2 at all sites in Chesapeake Bay ($r > 0.95$, $p < 0.001$; Fig. 4.10, inset).

Dissolved Silica Flux

The original calibration of the silica model generally resulted in an underestimation of the sediment-water DSi flux, especially during warmer months (Fig. 4.11). SFM originally considered silica solubility to be constant in time. However, when SFM was run at all stations with silica solubility formulated as an exponential function of temperature $Si_{sat} = Si_{sat,20}\theta_{Si}^{(T-20)}$ (Lawson et al., 1978), the model improved slightly (Table 4.3). Optimizations indicated that the model was insensitive to changes in $K_{M,PSi}$ and k_{Si} (data not shown), where values were applicable to all Chesapeake Bay stations. Optimization routines suggested that the inorganic (i.e., non-biogenic) silica deposition rate ($J_{Detr_{Si}}$) of 1.8 mmol Si m^{-2} d^{-1} was 22% to 46% of biogenic silica fluxes at all stations except R-78 (67%).

SFM includes an O_2-dependent sorption of DSi onto particles (partitioning), which represents DSi binding onto FeOOH under oxygenated conditions (as with PO_4^{3-}). The anaerobic-layer partition coefficient, $\pi_{Si,2}$, was similar to PO_4^{3-} in the original calibration, yet there is a limited literature to suggest strong binding of DSi to FeOOH under the conditions found in most estuarine sediments. Thus, we optimized the model for $\Delta\pi_{Si,1}$ and $\pi_{Si,2}$, and found that RMSE, ME, and RI of DSi flux were uniformly reduced across

all stations when the partition coefficients were reduced from 10 to 5 ($\Delta\pi_{Si,1}$) and from 100 to 15 ($\pi_{Si,2}$) at the anoxic sites (Table 4.3), with a 36% reduction in RMSE across sites. The optimized values or $\Delta\pi_{Si,1}$ (15) and $\pi_{Si,2}$ (50) were higher at the oxic, low-salinity sites (Still Pond, Maryland Point; Table 4.2 & 4.3). The resulting seasonal pattern of DSi more closely fit that of the observations (Fig. 4.11).

Discussion

This paper illustrates the simulation skill and flexibility of application for the stand-alone version of SFM with a focus on analyzing sediment-water fluxes of NH_4^+, NO_3^-, N_2, PO_4^{3-}, and DSi. Here we have demonstrated a range of ways that the model can complement field measurements to estimate unmeasured processes and simulate inter-annual variations in biogeochemical processes.

Nitrogen Cycling

After model reformulation and parameter optimization, SFM simulated NO_3^- fluxes that agreed well with observations across many stations with varying salinity, O_2, and organic matter deposition rates. The same is true for NH_4^+ fluxes, which are described in detail in a companion publication (Brady et al., 2013). For NO_3^- simulations, it was clear the original value of $\kappa_{NO_3^-,1}$ and the associated NO_3^- flux were underestimated for the majority of stations we tested in Chesapeake Bay. This "missing" NO_3^- uptake could result from an under-prediction of denitrification rates or a result of the fact that SFM does not include dissimilatory nitrate reduction to ammonium, or DNRA (An and Gardner, 2002). Because we lack sufficient information to model DNRA in Chesapeake Bay, but have access to denitrification measurements, we explored how under-estimated denitrification rates might be contributing to the "missing NO_3^- uptake. Optimized values

for $\kappa_{NO_3^-,1}$ were inversely correlated to the depth of the aerobic layer across the stations in our analysis; that is, where the aerobic layer depth was large, $\kappa_{NO_3^-,1}$was low. Because SFM assumes that denitrification is occurring uniformly throughout each layer, the NO_3^- loss rate associated with denitrification will be larger for a given value of $\kappa_{NO_3^-,1}$ as the aerobic layer depth increases. Thus, we removed the depth-dependence from the aerobic-layer denitrification formulation.

Although denitrification is considered to be a strictly anaerobic process, evidence exists for denitrification within the aerobic zone associated with "anoxic microsites" in organic aggregates (Jenkins and Kemp, 1984; Jørgensen, 1977). The inclusion of aerobic-layer denitrification in SFM, although absent from conventional sediment diagenesis models (Jahnke et al., 1982; Vanderborght et al., 1977b), has been included in more recent work (Brandes and Devol, 1995). If the aerobic-layer denitrification is occurring in anoxic microsites, we have no reason to assume that these sites would not be equally distributed. However, denitrification may be active in sections of sediments where there is close spatial coupling between the anoxic zone and the high- NO_3^- zone, which is nearly always aerobic (Blackburn et al., 1994). If this was the case, modeled denitrification would only occur in a relatively thin section of the sediment at the interface of the aerobic and anaerobic layer, and thus the denitrification loss term in SFM should be depth-independent. We applied such a formulation in SFM and found good model-data agreement across sites at a single value for the aerobic layer denitrification rate (Fig. 4.6, Table 4.3). It should be noted that sediment models that resolve porewater profiles with high vertical resolution do not need such a formulation, as interfaces within strong, opposing concentration gradients are well-represented.

Modeled denitrification rates agreed well with observations (Kana et al., 1998) and indicate the potential to model seasonal cycles of an important process that is effort intensive to measure (Fig. 4.7). Measurements of sediment denitrification were found to be strongly tied to overlying-water NO_3^- in the Choptank River (Kana et al., 1998), as well as many other locations (Dong et al., 2000; Pelegrí and Blackburn, 1995; Seitzinger et al., 1993). SFM simulations fit this pattern across all sites in Chesapeake Bay and during three seasons (Fig. 4.7a). The intercept of a linear model fit of overlying-water NO_3^- and denitrification rates indicates the degree of nitrification (Kana et al., 1998). We compared this intercept (as derived for each station and month) to SFM-modeled nitrification rates and found that the intercept value was highly correlated ($r > 0.8$) with the modeled rates (Di Toro, 2001). From a seasonal perspective, denitrification appears to have two maxima at seasonally-hypoxic stations (Fig. 4.7b), one in April-June and another in October-November (Kemp et al., 1990). This has been observed in other systems as well (Jørgensen and Sørensen, 1988) and primarily results from NO_3^- limitation during periods of the year (i.e., summer) when sediment nitrification is limited by low O_2 and high sulfide concentrations (Henriksen and Kemp, 1988). Conversely, at stations with ample NO_3^- concentrations in overlying water year-round (e.g., Maryland Point, Still Pond), high denitrification rates were maintained throughout summer and followed the annual temperature cycle (Fig. 4.7c).

Previous studies have used cross-system comparisons to estimate the fraction of external nitrogen loading that is lost to the atmosphere via denitrification as roughly 50% (Seitzinger, 1988). An analysis of SFM data indicated that between 50% and 75% of the PON flux to sediments was released as NH_4^+ (Fig. 4.10), indicating that 25% to 50% of

the depositional flux was either lost to the atmosphere via coupled nitrification-denitrification or it was buried in sediments. For the majority of sites in Chesapeake Bay, denitrification on average accounted for 25% of the PON flux, while burial of PON has been reported to be 15% to 25% of PON deposition (Boynton et al., 1995; Kemp et al., 1990). Interestingly, the $J[NH_4^+]/J_{PON}$ ratio was higher at 8 of the 12 stations we modeled that experienced seasonal hypoxia or anoxia relative to those that did not; this indicates that hypoxia-driven summertime declines in denitrification resulted in a larger fraction of J_{PON} being released as NH_4^+ (Fig. 4.10) as has been observed previously in many other coastal ecosystems (Kemp et al., 1990; Seitzinger and Nixon, 1985).

Recent research has indicated that previously under-appreciated aspects of the nitrogen cycle maybe be important in marine ecosystems (Burgin and Hamilton, 2007). These include, but are not limited to, dissimilarity reduction of nitrate to ammonium (DNRA), anaerobic ammonium oxidation (anammox), and nitrogen fixation associated with sulfate reduction (Bertics et al., 2010; Brunet and Garcia-Gill, 1996; Dalsgaard and Thamdrup, 2002; Gardner et al., 2006; Rich et al., 2008). SFM does not include these processes, primarily because we do not yet have the data to support model formulation and validation of these processes, especially in Chesapeake Bay. Some of these processes may be indirectly modeled; for example, N_2 production due to anammox may be "parameterized" in the modeled denitrification. It is clear from our experience here that future modeling studies may add equations and parameters to simulate these processes explicitly as more information on controlling processes becomes available.

Phosphorus Cycling

SFM-simulated PO_4^{3-} fluxes agreed well with observations across many stations, but the comparisons were slightly more complex due to solute-particle interactions. The adsorption of PO_4^{3-} onto FeOOH (as well as manganese oxides) is an important mechanism of temporary phosphorus storage in marine sediments (Slomp et al., 1998; Sundby et al., 1992), which can dominate dissolved PO_4^{3-}dynamics near the sediment-water interface (Krom and Berner, 1981) and control seasonal cycles of sediment-water PO_4^{3-}fluxes (Cowan and Boynton, 1996). Optimization routines indicated a spatial-dependence of the optimal aerobic-layer partitioning coefficients and the relationship of these coefficients to observed oxalate-extractable Fe availability illustrates elevated PO_4^{3-} sorption within Fe -richsediments near the land-water interface (Spiteri et al., 2008; Upchruch et al., 1974). Lower PO_4^{3-} retention via sorption (i.e., lower partitioning coefficient) is also consistent with the removal of Fe via precipitation with sulfides in more saline regions of the estuary (Caraco et al., 1989; Jordan et al., 2008), although these dynamics are not specifically modeled in SFM. Although the incorporation of site-specific parameters into models is not ideal, we justify spatially-varying partition coefficients because Fe is not modeled explicitly and because partition coefficients could potentially be predicted from known Fe concentrations.

Although many previous models of PO_4^{3-} have emphasized diagenetic production and the resultant vertical porewater profiles (Rabouille and Gaillard, 1991; Van Cappellen and Berner, 1988) , other models have examined the influence of PO_4^{3-} sorption and desorption on the availability and sediment-water fluxes (Slomp et al., 1998). The evolution of seasonal increases in sediment-water PO_4^{3-} fluxes in Chesapeake Bay often

lags by a month or more after NH_4^+ increases (Cowan and Boynton, 1996). This phenomenon has been explained by the adsorption of diagenetically-produced PO_4^{3-} to FeOOH in the aerobic layer under oxic condtions, which buffers porewaters and results in low concentrations and sediment-water fluxes. Similar interactions do not limit NH_4^+ sediment-water fluxes, thus diagenetically-produced NH_4^+ is free to diffuse to the overlying water. Under reduced oxygen conditions characteristic of several regions of Chesapeake Bay, iron is reduced, thereby releasing the stored PO_4^{3-} to the water column later in summer (Testa and Kemp, 2012). The use of oxygen-dependent partitioning coefficients allows for the representation of these processes; when such coefficients are removed, the annual PO_4^{3-} flux cycle closely resembles that of NH_4^+ (data not shown). This formulation otherwise represents an instantaneous partitioning between solid and dissolved PO_4^{3-}, where other formulations consider different adsorption rates as a function of the crystalline structure of the FeOOH (Slomp et al., 1998). We lack the data necessary to model detailed FeOOH structure.

An analysis of SFM data indicated that roughly 75% of the POP flux to sediments was released as PO_4^{3-} (Fig. 4.10), indicating that 25% of the depositional flux was either buried or stored in the active sediment. The $J[PO_4^{3-}]/J_{POP}$ ratio was higher at 2 of the 12 stations we modeled and these two stations were where partitioning coefficients were higher and overlying-water O_2 concentrations remained above 100 μM year-round. This indicates that burial processes are similar across sites and that relatively high O_2 can maintain PO_4^{3-} in sediments.

Silica cycling

The calibration process for the silica sub-model in SFM resulted in simulated DSi fluxes that agreed well with observations across many stations and provided insights on key processes affecting sediment silica biogeochemistry. First, the addition of a temperature-dependent silica solubility formulation is consistent with experimental work (Lawson et al., 1978; Van Cappellen and Linqing, 1997a) and removed the constraint on porewater DSi accumulation imposed by the fixed solubility (900 μM) in the original model. In turn, model porewater DSi concentrations increased in warmer periods to generate the sediment-water concentration gradient necessary to better match observed DSi fluxes (Fanning and Pilson, 1974; Schink et al., 1974). Such controls contribute to the strong temperature-dependency on sediment-water DSi fluxes in Chesapeake Bay (Yamada and D'Elia, 1984) .

Porewater DSi accumulation is also strongly dependent on the dissolution rate constant (k_{Si}), but reported values of this parameter vary between 10^{-7} and 10^{-9} s^{-1} (Rabouille and Gaillard, 1990; Vanderborght et al., 1977a; Wong and Grosch, 1978). Such variation is due to differences in the diatom species being dissolved, the residence time of the algal cells in the water column prior to deposition, alterations of the siliceous material within the sediment (Rabouille and Gaillard, 1990; Schink et al., 1975), and other factors. Considering the temperature dependence for this first-order reaction constant in SFM, the optimized value for k_{Si} in SFM varies from 4.3 x 10^{-7} to 7.5 x 10^{-6} over the course of the year, which is somewhat faster than other values reported in the literature during warm months. However, SFM considers the deposition of relatively

fresh organic matter, which may explain the faster dissolution rates compared to natural samples of diverse siliceous material from less productive regions (Schink et al., 1975).

The major improvement to the silica model in SFM, however, resulted from reducing the solid-solute partitioning coefficients that represent the sorption/desorption of DSi with FeOOH. As O_2-dependent partitioning allows for the storage of diagenetically-produced PO_4^{3-} and DSi in sediments until low O_2 conditions lead to FeOOH dissolution and PO_4^{3-}/DSi release. Although sorption dynamics between PO_4^{3-} and FeOOH are well-described (Sundby et al., 1992), silica is less affected by these interactions than PO_4^{3-} (Mayer and Gloss, 1980) and DSi fluxes have been found to be relatively insensitive to O_2 (Yamada and D'Elia, 1984). Indeed, most sediment silica models do not include sorption of DSi to FeOOH (Schink et al., 1975; Wong and Grosch, 1978). When we reduced the partitioning coefficients at all sites, the model representation of DSi fluxes improved substantially, with a more representative seasonal cycle (Fig. 4.11). With the partitioning formulation active, SFM predicts large and short-lived peaks in DSi flux in late spring at stations where O_2 reaches anoxic and hypoxic levels (e.g., R-64, Point No Point). This is due to temporary storage of DSi sorbed to FeOOH during spring followed by abrupt and large sediment-water effluxes of DSi when O_2 declines below 62.5 μM (data not shown). With the removal of this temporary storage mechanism for SFM, DSi is stored in lower quantities during spring and is released gradually through summer as it dissolves, and the resulting fluxes match observations (Fig. 4.11, Table 4.3).

Model Improvements

There are some limitations of the SFM sub-models described here that could be improved in the future. Although SFM's two-layer vertical resolution limits its ability to

simulate fine scale, vertically distinct processes, its simplicity adds to the model's flexibility as a linked component in 3D biophysical models and as a tool in stand-alone applications (Vanderborght et al., 1977a, b). SFM now includes a benthic algal sub-module (Cerco and Seitzinger, 1997) that considers the interactions between benthic algae and sediment-water fluxes. This addition allows the use of SFM in shallow-water ecosystems where light reaches the sediments. Although the denitrification formulations in SFM originally lacked a limitation by organic carbon (Di Toro, 2001), we have added this dependency to SFM, thereby improving its applicability in more carbon-limited systems. We related the regional-specificity in the optimized phosphorus partition coefficients to the concentration (and thus availability of sorption sites) of FeOOH. A more mechanistic alternative is an iron model that has been developed within the SFM framework (Chapter 21 in Di Toro, 2001) and could be integrated with the nutrient and O_2 sub-modules of SFM in the future. The parameter optimization scheme described here allows for relatively fast (i.e., less than one hour) sensitivity tests and parameter adjustment for applications in new systems. Finally, an explicit representation of aerobic respiration could be included, as well as recently emphasized pathways within the nitrogen cycle, such as DNRA and anammox.

An important goal in the calibration and development of any model is the balance between generality, realism, and precision (Levins, 1966). Because SFM is ideally applicable to a wide-variety of ecosystems, it occasionally became necessary to sacrifice precision in any one environment to develop a more general set of equations to represent a given suite of key processes. Beyond these key processes, there are many reactions we know exist in reality, but to date have not been sufficiently studied and cannot be

meaningfully represented in a model. Thus, although all models necessarily simplify a complex-ecosystem into a set of mathematical formulations that can practically represent system behavior, it is advantageous to develop general models with the flexibility to add realism as the state-of-the-science progresses. Although calibration exercises can result in parameter sets that enhance model precision while sacrificing generality (as in this study), ultimately some level of human judgment must be involved in evaluating trade-offs (Cerco and Noel, 2005) and exploring the potential to gain biogeochemical insight from the modeling process.

Acknowledgements

I would like to thank my co-authors on the manuscript version of this chapter, published in *Estuarine, Coastal, and Shelf Science*, including Damian Brady, Dominic Di Toro, Walter Boynton, Jeffrey C. Cornwell, and W. Michael Kemp. I would also like to thank James Fitzpatrick for the many discussions we have had related to topics covered in this manuscript and the US EPA Chesapeake Bay Program and the Maryland Department of Natural Resources for collecting many of the data presented in this work. Partial funding for our contribution to this work came from the United States National Oceanographic and Atmospheric Administration (NOAA) Coastal Hypoxia Research Program (CHRP-NAO7NOS4780191), the National Science Foundation (Chesapeake Bay Environmental Observatory; CBEO-3 BERS-0618986 and Biocomplexity Research; OCE-9981617), and by the State of Maryland Department of Natural Resources (K00B920002). This work is NOAA Coastal Hypoxia Research Program (CHRP) Publication # 13X and the University of Maryland Center for Environmental Science Publication # XXXX.

Table 4.1: The model equations are listed below. The solutions are found by numerically integrating the equations (Di Toro 2001). *Parameter definitions are located at the bottom of this table.

Mass balance equations (these are the general equations for C_{T1} and C_{T2}):

1
$$\frac{d\{H_1 C_{T1}\}}{dt} = -\frac{\kappa_1^2}{K_{L01}} C_{T1} + K_{L01}(f_{d0} C_{T0} - f_{d1} C_{T1}) + \omega_{12}\left(f_{p2} C_{T2} - f_{p1} C_{T1}\right) + K_{L12}(f_{d2} C_{T2} - f_{d1} C_{T1}) - \omega_2 C_{T1} + J_{T1}$$

2
$$\frac{d\{H_2 C_{T2}\}}{dt} = -\kappa_2 C_{T2} - \omega_{12}\left(f_{p2} C_{T2} - f_{p1} C_{T1}\right) - K_{L12}(f_{d2} C_{T2} - f_{d1} C_{T1}) + \omega_2 (C_{T1} - C_{T2}) + J_{T2}$$

3 where
$$f_{di} = \frac{1}{1 + m_i \pi_i} \qquad i = 1, 2$$

4
$$f_{pi} = 1 - f_{di}$$

5
$$K_{L01} = \frac{D_{O_2}}{H_1} = \frac{SOD}{[O_2(0)]}$$

6
$$K_{L12} = \frac{D_d \theta_{D_d}^{(T-20)}}{(H_1 + H_2)/2}$$

7
$$\omega_{12} = \frac{D_p \theta_{D_p}^{(T-20)}}{H_1 + H_2} \frac{POC_1}{POC_R} min_{(each\ year)}(1 - k_s S)$$

where
$$\frac{dS}{dt} = -k_s S + \frac{K_{M,D_p}}{K_{M,D_p} + [O_2(0)]/2}$$

Kinetic source and reaction terms for ammonium, nitrate, phosphate, and silica

Ammonium (NH_4^+)

8 $$\kappa_1^2 = \kappa_{NH_4^+,1}^2 \theta_{NH_4^+}^{(T-20)} \left(\frac{K_{M,NH_4^+} \theta_{K_{M,NH_4^+}}^{(T-20)}}{K_{M,NH_4^+} \theta_{K_{M,NH_4^+}}^{(T-20)} + [NH_4^+(1)]} \right) \left(\frac{[O_2(0)]/2}{K_{M,NH_4^+,O_2} + [O_2(0)]/2} \right)$$

9 $$\kappa_2 = 0$$

$$J_{T1} = 0 \text{ and}$$

10 $$J_c = \sum_{i=1}^{2} -k_{\mathrm{POC},i} \theta_{\mathrm{POC},i}^{(T-20)} \mathrm{POC}_i H_2$$

$$J_{T2} = a_{N,C} J_c$$

Nitrate (NO_3^-)

11 $$\kappa_1^2 = \kappa_{NO_3^-,1}^2 \theta_{NO_3^-}^{(T-20)}$$

12 $$\kappa_2 = \kappa_{NO_3^-,2} \theta_{NO_3^-}^{(T-20)}$$

13 $$J_{T1} = \kappa_{NH_4^+,1}^2 \theta_{NH_4^+}^{(T-20)} \frac{[NH_4^+(1)]}{K_{L01}} \left(\frac{K_{M,NH_4^+} \theta_{K_{M,NH_4^+}}^{(T-20)}}{K_{M,NH_4^+} \theta_{K_{M,NH_4^+}}^{(T-20)} + [NH_4^+(1)]} \right) \left(\frac{[O_2(0)]/2}{K_{M,NH_4^+,O_2} + [O_2(0)]/2} \right)$$

$$J_{T2} = 0$$

Phosphate (PO_4^{3-})

14 $$\kappa_1^2 = 0$$

15 $$\kappa_2 = 0$$

16 $$J_{T1} = 0 \text{ and } J_{T2} = a_{P,C} J_C + J_{PIP}$$

Particulate Silica (P_{Si})

17
$$\frac{d\{H_2[P_{Si}]\}}{dt} = -S_{Si}H_2 - \omega_2[P_{Si}(2)] + J_{PSi} + J_{Detrital_{Si}}$$

$$S_{Si} = k_{Si}\theta_{Si}^{(T-20)}\frac{[P_{Si}(2)]}{K_{M,PSi}+[P_{Si}(2)]}(Si_{sat,20}\theta_{Si}^{(T-20)} - f_{d2}[Si(OH)_4(2)])$$

18
$$J_{PSi} = a_{Si,C}J_c$$

$$J_{Detr_{Si}} = \textit{Non-algal particulate } J_{PSi} \textit{ flux}$$

Silicate ($Si(OH)_4$)

19
$$\kappa_1^2 = 0$$

20
$$\kappa_2 = 0$$

$$J_{T1} = 0$$

21
$$J_{T2} = k_{Si}\theta_{Si}^{(T-20)}\frac{[P_{Si}(2)]}{K_{M,PSi}+[P_{Si}(2)]}(Si_{sat,20}\theta_{Si_{sat}}^{(T-20)} - f_{d2}[Si(OH)_4(2)])\,H_2$$

Partitioning: PO_4^{3-} and $Si(OH)_4$

$If\ [O_2(0)] < [O_2]_{critPO_4^{3-},Si}$:

$$\pi_{PO_4^{3-},Si,1} = \pi_{PO_4^{3-},Si,2}\Delta\pi_{PO_4^{3-},Si,1}^{\frac{[O_2(0)]}{[O_2]_{critPO_4^{3-},Si}}}$$

22
$If\ [O_2(0)] \geq [O_2]_{critPO_4^{3-},Si}$:

$$\pi_{PO_4^{3-},Si,1} = \pi_{PO_4^{3-},Si,2}\,\Delta\pi_{PO_4^{3-},Si,1}$$

* H_1, H_2 = depth of layer 1 and 2 (cm); $C_{T0,}$ C_{T1}, C_{T2} = total (dissolved +particulate) concentration in layers (mmol m^{-3}); POC_1 = Layer 1 particulate organic carbon concentration (mmol m^{-3}), POC_R = reference particulate organic carbon concentration (0.1 mg C g $solids^{-1}$); f_{d1}, f_{d2} = dissolved fraction of total concentration in each layer; f_{p1}, f_{p2} = particulate fraction of total concentration in each layer; K_{L12}= mass transfer coefficient between layers 1 and 2; K_{L01}= ratio of SOD to overlying water dissolved O_2, or mass transfer coefficient between layer 1 and the overlying water-column; K_{L12}= mass transfer coefficient between layer 1 and 2 (m d^{-1}); ω_2 =sedimentation velocity (m d^{-1}); ω_{12}= particle mixing velocity between layers 1 and 2 (m d^{-1}); k_s= first-order decay coefficient for accumulated benthic stress (d^{-1}); S = benthic stress term (d); J_{T1} = source of solute to layer 1 (mmol m^{-2} d^{-1}); J_{T2} = source of solute to layer 2 (mmol m^{-2} d^{-1}); κ_1, κ_2= reaction velocity for first-order removal reaction rate constant in layer 1 and 2 (m d^{-1}); m_1, m_2 = solids concentration in layer 1 and 2 (kg L^{-1}); π_1, π_2 =partition coefficient in layer 1 and 2 (L kg^{-1}); D_p = diffusion coefficient of particulate solutes due to particle mixing (cm^2 d^{-1}); D_d = diffusion coefficient of dissolved solutes (cm^2 d^{-1}); $\theta_{D_{p,d}}$ = temperature coefficient for D_p or D_d; $K_{M,i}$ = half saturation coefficient (i = relevant parameter or variable, in concentrations units of relevant variable); $a_{N,C}$ = stoichiometric ratio of NH_4^+, released to POC mineralized (mol N mol C^{-1}); $a_{Si,C}$ = stoichiometric ratio of $Si(OH_4)$ released to POC mineralized (mol O_2 mol C^{-1}). Where specific solutes are shown (e. g, $[NO_3^-(i)]$), i = layer). Parameter values listed in Table 4.2. C_{T1} and C_{T2} were computed for NH_4^+, NO_3^-, PO_4^{3-} (= dissolved + particulate phosphate), and $Si(OH_4)$ (= dissolved + particulate silica). $[O_2]_{critPO_4^{3-},Si}$ is the O_2 concentration below which the aerobic layer partition coefficient is a function of O_2.

Table 4.2: Sediment Flux Model Parameters.

Variable	Value	Units	Variable	Value	Units
Recycle Fractions					
			Benthic Stress		
$f_{POC,N,P,1}$	0.65		k_S	0.03	d^{-1}
$f_{POC,2}$	0.20		$K_{M,Dp}$	62.5	μM O_2*
$f_{PON,2}$	0.25		**Ammonium**		
$f_{POP,2}$	0.20		$\kappa_{NH_4^+,1}$	0.131	m d^{-1}
$f_{POC,3}$	0.15		$\theta_{NH_4^+}$	1.123	
$f_{PON,3}$	0.10		K_{M,NH_4^+}	52.0	μM N
$f_{POP,3}$	0.15		$\theta_{K_{M,NH_4^+}}$	1.125	
Diagenesis			$K_{M,NH_4^+O_2}$	11.5	μM O_2
$k_{POC,N,P,1}$	0.01-0.0351[†]	d^{-1}	a_{O_2,NH_4^+}	2.0	mol O_2 mol^{-1} N
$\theta_{POC,N,P,1}$	1.10		**Nitrate**		
$k_{POC,N,P,2}$	0.0018	d^{-1}	$\kappa_{NO_3^-,1}$	0.1-0.3[‡]	m d^{-1}
$\theta_{POC,N,P,2}$	1.15		$\kappa_{NO_3^-,2}$	0.25	m d^{-1}
k_{Si}	0.5	d^{-1}	$\theta_{NO_3^-}$	1.08	
θ_{Si}	1.10		a_{O_2,NO_3^-}	1.25	mol O_2 mol^{-1} N
$a_{O_2,C}$	1.0	mol O_2 mol^{-1} C	**Silica**		
$a_{N,C}$	0.167	mol N mol^{-1} C	$Si_{sat,20}$	1390	mmol Si m^{-3}
$a_{P,C}$	0.009	mol P mol^{-1} C	$\theta_{Si_{sat}}$	1.023	
$a_{Si,C}$	0.171	mol Si mol^{-1} C	$K_{M,PSi}$	3560	mmol Si m^{-3}
Solids			$\Delta\pi_{Si,1}$	5-15[§]	L kg^{-1}
ω_2	0.7	cm y^{-1}	$\pi_{Si,2}$	15-50[§]	L kg^{-1}
m_1	0.5	kg L^{-1}	$J_{Detr_{Si}}$	1.8	mmol Si m^{-2} d^{-1}
m_2	0.5	kg L^{-1}	$[O_2]crit_{Si}$	62.5	μM O_2
Mixing			**Phosphate**		
D_d	0.7	cm^2 y^{-1}	$\Delta\pi_{PO_4^{3-},1}$	100-300[§]	L kg^{-1}
θ_{Dd}	1.08		$\pi_{PO_4^{3-},2}$	50-100[§]	L kg^{-1}
D_p	0.6	cm^2 d^{-1}	$[O_2]crit_{PO_4^{3-}}$	62.5	μM O_2
θ_{Dp}	1.117		**Dimensions**		
POC_R	0.1	mg C g $solids^{-1}$	$H_1 + H_2$	10.0	cm

*Indicates that units are in O_2 equivalents

[†]Diagenesis rate range reflects the new (0.01; Brady et al. 2013) and original (0.035) calibration

[‡]Denitrification reaction velocity range reflects the range of values from the original calibration and optimization routine

[§]Partitioning coefficient range reflects the range of values from the optimization routine

Table 4.3: Root mean square error (RMSE), reliability index (RI), and mean error (ME) for model-data comparison of sediment-water nitrate, phosphate and silicate fluxes. Station depth (m), mean annual salinity, and summer (June-August) O_2 (μM) in bottom-water included for each station. Refer to text for model and parameterization schemes and to Brady et al. (2013) for station location details.

		J[NO_3^-] (μmol N m^{-2} hr^{-1})			J[PO_4^{3-}] (μmol P m^{-2} hr^{-1})			J[Si] (μmol Si m^{-2} hr^{-1})		
Sites	Metric	Original Calibration	$\kappa_{NO_3^-,1}$ Optimized by station	$k_{NO_3^-,1g}$ Optimized for all stations	Original Calibration	$DpPO_4^{3-}$ Optimized by salinity	Optimized Model	Original Calibration	Temperature Dependent Solubility	Partitioning Reduced
Windy Hill	RMSE	23.44	19.34	38.88	18.11	14.18	13.27	276.55	275.48	166.52
Salinity = 1.0	RI	1.29	1.27	1.33	1.88	1.78	1.82	1.66	1.69	1.29
O_2 = 183.1	ME	5.62	-7.67	27.59	9.01	1.42	-2.65	159.23	161.34	50.35
Maryland Point	RMSE	32.32	32.21	43.91	10.24	10.24	10.24	206.66	207.73	183.59
Salinity = 1.9	RI	1.22	1.22	1.33	1.38	1.38	1.38	1.43	1.43	1.39
O_2 = 196.8	ME	1.98	5.62	28.02	-1.11	-1.11	-1.11	45.46	43.26	35.46
Still Pond	RMSE	23.32	21.89	33.53	3.20	3.20	3.20	144.12	144.99	148.29
Salinity = 4.8	RI	1.18	1.18	1.30	1.21	1.21	1.21	1.78	1.78	1.76
O_2 = 167.4	ME	10.75	3.71	23.85	-0.62	-0.62	-0.62	84.51	83.81	11.59
Horn Point	RMSE	21.06	15.01	13.04	42.44	32.71	27.08	394.40	391.92	216.21
Salinity = 11.1	RI	1.21	1.15	1.15	1.62	1.76	1.83	1.62	1.65	1.27
O_2 = 150.4	ME	-11.83	2.71	1.08	-7.31	-11.04	-12.86	282.60	279.96	118.01
Buena Vista	RMSE	20.67	10.11	9.38	34.28	28.52	26.05	419.70	411.15	225.46
Salinity = 11.5	RI	1.21	1.12	1.13	1.33	1.30	1.32	1.49	1.48	1.25
O_2 = 107.6	ME	-14.16	2.59	-2.73	19.22	9.24	3.86	345.67	341.94	124.18

Marsh Point	RMSE	20.61	10.54	11.06	48.73	39.41	34.00	306.66	306.01	179.15
Salinity = 13.2	RI	1.17	1.11	1.13	1.47	1.56	1.84	1.86	1.85	1.23
O_2 = 54.8	ME	-14.43	0.29	-2.89	1.55	1.84	1.42	153.42	151.64	14.51
St. Leonard Creek	RMSE	18.13	14.76	12.42	11.89	12.22	12.98	346.03	345.33	211.19
Salinity = 13.6	RI	1.17	1.15	1.12	1.29	1.44	1.47	1.85	1.87	1.29
O_2 = 94.2	ME	-10.09	0.88	0.71	2.27	-2.85	-5.96	268.37	267.81	108.48
Broome Island	RMSE	24.79	11.32	13.34	52.58	35.13	26.17	309.26	307.91	188.14
Salinity = 13.8	RI	1.25	1.15	1.18	1.70	1.62	1.58	1.67	1.68	1.34
O_2 = 75.7	ME	-19.00	1.12	-6.21	-5.06	-6.82	-8.02	204.26	202.50	58.75
Ragged Point	RMSE	19.67	12.73	11.59	23.91	18.92	14.86	204.50	198.99	124.76
Salinity = 15.6	RI	1.23	1.19	1.16	1.38	1.48	1.68	1.78	1.77	1.22
O_2 = 27.5	ME	-11.07	-0.36	-1.52	-6.08	-5.07	-4.64	80.12	79.41	-14.65
R-78	RMSE	11.76	11.26	9.02	11.70	11.33	11.05	158.14	158.14	107.86
Salinity = 17.0	RI	1.46	1.37	1.20	1.48	1.76	1.75	1.77	1.77	1.28
O_2 = 17.5	ME	-3.26	2.32	2.08	2.24	1.68	1.41	107.14	107.14	41.42
R-64	RMSE	20.10	12.48	10.84	20.27	16.64	12.84	267.94	267.98	183.32
Salinity = 19.3	RI	1.17	1.13	1.13	1.32	1.42	1.42	1.73	1.72	1.24
O_2 = 14.9	ME	-12.17	0.74	-4.22	-6.35	-4.48	-3.81	188.37	187.82	109.21
Point No Point	RMSE	14.04	8.38	7.08	13.38	10.56	9.42	260.48	260.48	173.13
Salinity = 20.6	RI	1.25	1.14	1.15	1.27	1.29	1.29	1.96	1.96	1.36
O_2 = 36.9	ME	-10.10	-0.70	-3.36	-5.18	-5.24	-5.54	224.56	224.56	114.17

Figure Legends

Figure 4.1. Map of northern Chesapeake Bay, on the east coast of the United States (inset), showing the locations where Sediment Flux Model (SFM) simulations were compared to Sediment Oxygen and Nutrient Exchange (SONE) observations.

Figure 4.2. Generic schematic diagram of the Sediment Flux Model (SFM), including state variables, transport and biogeochemical processes, and boundary conditions. Note that the depths of the aerobic (H_1) and anaerobic (H_2) layers vary over time.

Figure 4.3. Schematic representation of nitrogen transport and kinetics in the Sediment Flux Model (SFM). Panels a & b represent the dynamics of the NH_4^+ and NO_3^- models, respectively. Note: (1) there is no diagenesis (ammonification) in layer 1 (panel a). (2) there is no source of NO_3^- in the anaerobic layer, as no O_2 is present (Panel b).

Figure 4.4. Schematic representation of the phosphorus and silica transport and kinetics in the Sediment Flux Model (SFM). Panels a and b represent the processes within the phosphorus and silica models, respectively. Note: (1) there is no source of PO_4^{3-} or DSi in the aerobic layer and (2) both PO_4^{3-} and DSi are partitioned between particulate and dissolved phases in both layers, and (3) solubility control for silica dissolution (Panel b).

Figure 4.5. Modeled (lines) versus observed (circles) sediment-water NO_3^- flux at Still Pond (a) and R-64 (b), where aerobic-layer denitrification was modeled using a layer 1 denitrification velocity ($\kappa_{NO_3^-,1}$) of 0.1 m day^{-1} from the original calibration. (c) Comparison of RMSE values for modeled NO_3^- flux across all stations at varying values of the aerobic-layer denitrification velocity, where the optimized value for $\kappa_{NO_3^-,1}$ is highly correlated to model-computed aerobic-layer depth across stations (inset).

Figure 4.6. Modeled (lines) and observed (circles) time series of NO_3^- flux from four stations in Chesapeake Bay (a: Windy Hill, b: Still Pond, c: R-64, d: Point No Point). Gray dashed lines represent model output using a layer 1 denitrification velocity of 0.1 m day^{-1} from the original calibration, while black solid lines represent model output using the depth-independent, aerobic-layer denitrification model of 0.2 m day^{-1}.

Figure 4.7. (a) Relationship between overlying-water NO_3^- and sediment denitrification rates as observed (squares) in the Choptank River estuary (Kana et al., 1998) and modeled for all stations over 3 seasons with SFM (circles). (b) Seasonal cycle of modeled (line is mean, shaded area is ± 1SD) and observed (squares) sediment denitrification at R-64 and (c) Still Pond.

Figure 4.8. Modeled (lines) versus observed (circles) sediment-water PO_4^{3-} flux at Still Pond (a) and R-64 (b), where model computations were made using an aerobic-layer partitioning coefficient of 300 kg l^{-1} from the original calibration. (c) Comparison of RMSE values for modeled PO_4^{3-} flux across all stations at varying values of the aerobic-layer partitioning coefficient, where the optimized value for $\Delta\pi_{PO_4^{3-},1}$is highly correlated to observed oxalate-extractable Fe (inset) in the top 10 cm of sediments (Cornwell and Sampou, 1995).

Figure 4.9. Modeled (lines) and observed (circles) time series of PO_4^{3-} flux from four stations in Chesapeake Bay (a: Windy Hill, b: Still Pond, c: R-64, d: Point No Point). Gray dashed lines represent model output using the original aerobic-layer partition coefficient ($\Delta\pi_{PO_4^{3-},1}$) and black solid lines represent the station-specific optimized $\Delta\pi_{PO_4^{3-},1}$. Grey areas are overlying-water O_2 concentrations at each station during the simulation.

Figure 4.10. Relationship of modeled sediment-water NH_4^+ (top panel) and PO_4^{3-} (bottom panel) fluxes to PON and POP deposition, respectively, at each station in Chesapeake Bay. Open circles are stations characterized by oxygenated conditions throughout the year in the overlying-water, which shaded circles represent stations with seasonal hypoxia or anoxia. Data are means over the model period, which is specific to each station. Lines represent the percentage of N or P removed (via denitrification, burial, or long-term storage) from that deposited. The inset figure is the relationship of "Nitrogen Recycling Efficiency" ($NRE = \frac{J[NH_4^+]}{J[NH_4^+] + J[N_2] + J[NO_3^-]}$) to overlying water O_2 at R-64 and St. Leonard's Creek, where data are monthly means.

Figure 4.11. Modeled (lines) and observed (circles) time series of DSi flux from four stations in Chesapeake Bay (a: Windy Hill, b: Still Pond, c: R-64, d: Point No Point). Gray dashed lines represent model output using the original calibration, while black solid lines represent simulations with modeled temperature-dependent Si_{sat}, optimized parameters (see text), and station-specific optimized $\Delta\pi_{Si,1}$ and $\pi_{Si,2}$.

Fig. 4.1

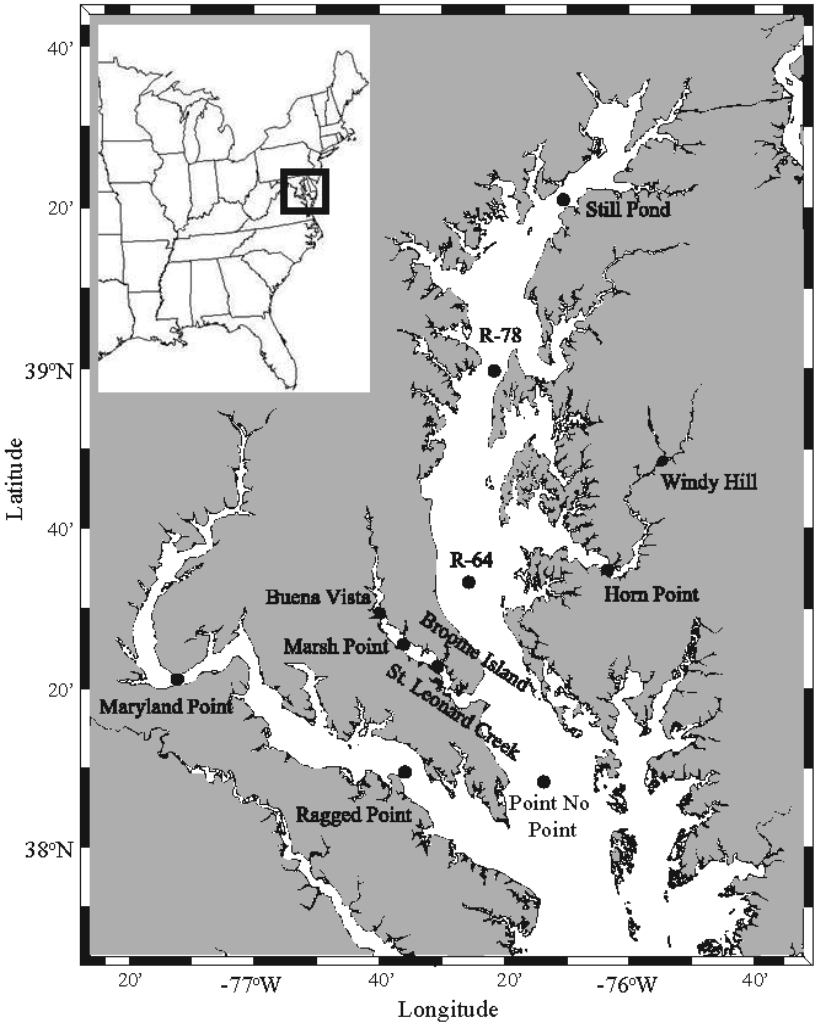
40'
20'
39°N
40'
20'
38°N
Latitude
Still Pond
R-78
Windy Hill
R-64
Horn Point
Buena Vista
Marsh Point
Broome Island
St. Leonard Creek
Maryland Point
Ragged Point
Point No Point
20'
-77°W
40'
20'
-76°W
40'
Longitude

Fig. 4.2

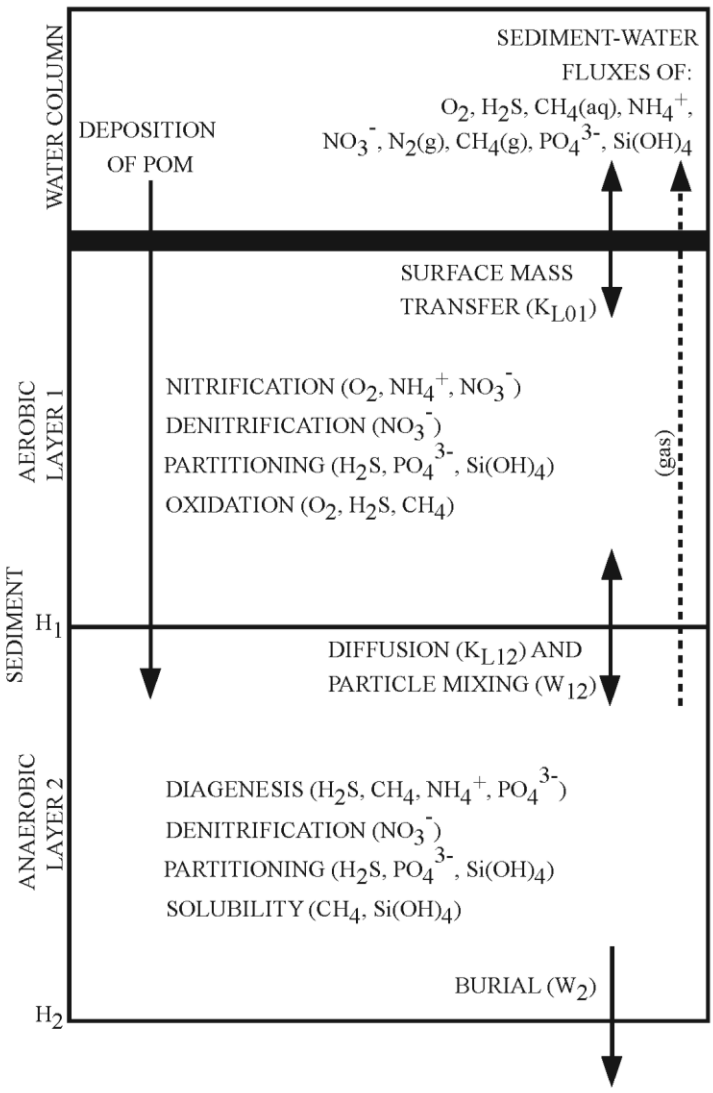
WATER COLUMN
SEDIMENT-WATER
FLUXES OF:
O_2, H_2S, CH_4(aq), NH_4^+,
NO_3^-, N_2(g), CH_4(g), PO_4^{3-}, $Si(OH)_4$
DEPOSITION
OF POM
SURFACE MASS
TRANSFER (K_{L01})
AEROBIC
LAYER 1
NITRIFICATION (O_2, NH_4^+, NO_3^-)
DENITRIFICATION (NO_3^-)
PARTITIONING (H_2S, PO_4^{3-}, $Si(OH)_4$)
OXIDATION (O_2, H_2S, CH_4)
(gas)
SEDIMENT
H_1
DIFFUSION (K_{L12}) AND
PARTICLE MIXING (W_{12})
ANAEROBIC
LAYER 2
DIAGENESIS (H_2S, CH_4, NH_4^+, PO_4^{3-})
DENITRIFICATION (NO_3^-)
PARTITIONING (H_2S, PO_4^{3-}, $Si(OH)_4$)
SOLUBILITY (CH_4, $Si(OH)_4$)
BURIAL (W_2)
H_2

Fig. 4.3

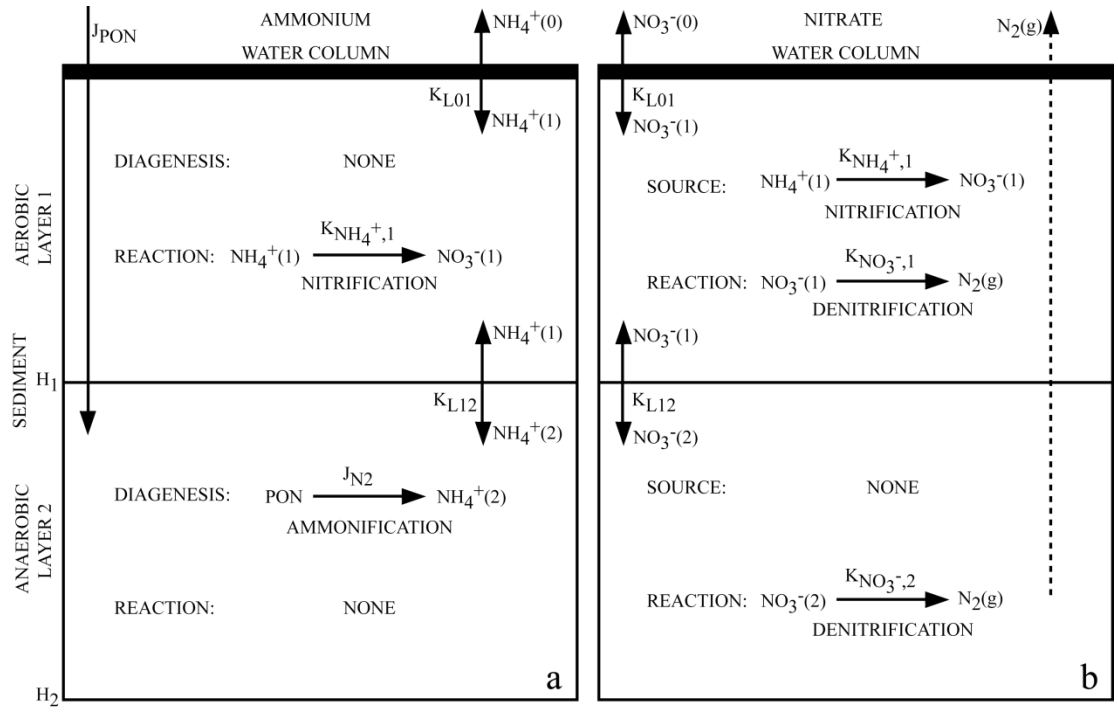
AMMONIUM
WATER COLUMN
J_{PON}
$NH_4^+(0)$
K_{L01}
$NH_4^+(1)$
DIAGENESIS: NONE
AEROBIC LAYER 1
REACTION: $NH_4^+(1) \xrightarrow{K_{NH_4^+,1}} NO_3^-(1)$
NITRIFICATION
SEDIMENT
H_1
$NH_4^+(1)$
K_{L12}
$NH_4^+(2)$
ANAEROBIC LAYER 2
DIAGENESIS: PON $\xrightarrow{J_{N2}}$ $NH_4^+(2)$
AMMONIFICATION
REACTION: NONE
H_2
a
$NO_3^-(0)$
NITRATE
WATER COLUMN
$N_2(g)$
K_{L01}
$NO_3^-(1)$
SOURCE: $NH_4^+(1) \xrightarrow{K_{NH_4^+,1}} NO_3^-(1)$
NITRIFICATION
REACTION: $NO_3^-(1) \xrightarrow{K_{NO_3^-,1}} N_2(g)$
DENITRIFICATION
$NO_3^-(1)$
K_{L12}
$NO_3^-(2)$
SOURCE: NONE
REACTION: $NO_3^-(2) \xrightarrow{K_{NO_3^-,2}} N_2(g)$
DENITRIFICATION
b

Fig. 4.4

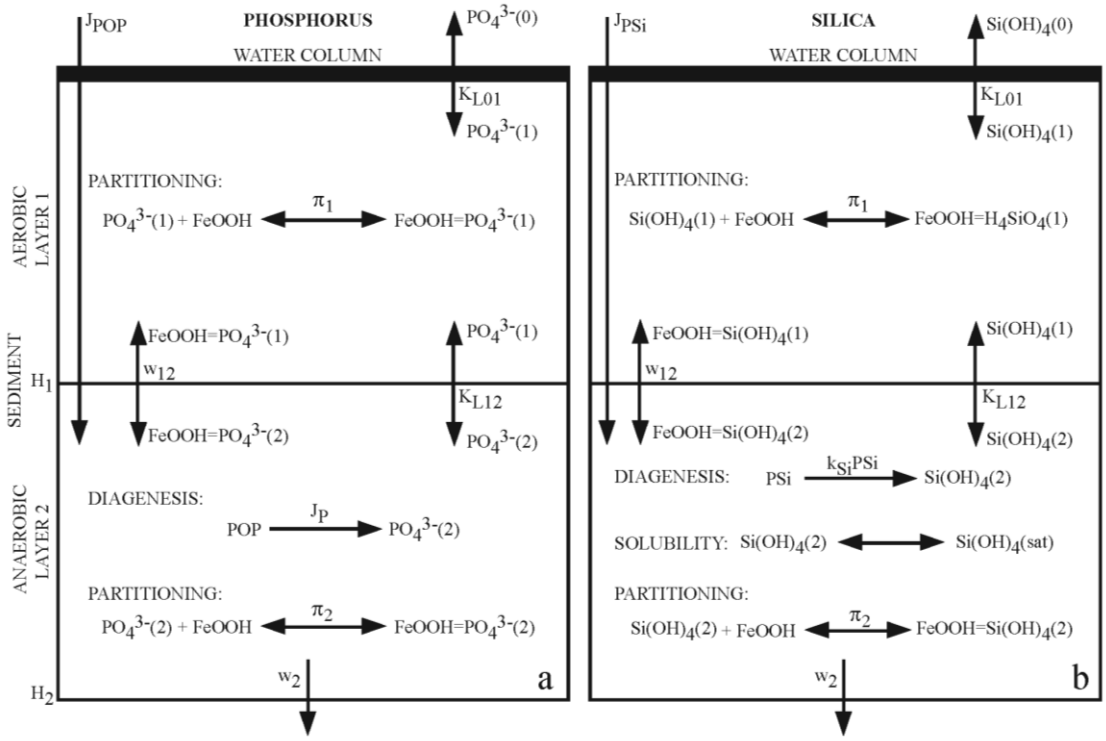
PHOSPHORUS
WATER COLUMN
J_{POP}
$PO_4^{3-}(0)$
K_{L01}
$PO_4^{3-}(1)$
PARTITIONING:
$PO_4^{3-}(1)$ + FeOOH
π_1
FeOOH=$PO_4^{3-}(1)$
AEROBIC LAYER 1
SEDIMENT
H_1
FeOOH=$PO_4^{3-}(1)$
w_{12}
$PO_4^{3-}(1)$
K_{L12}
FeOOH=$PO_4^{3-}(2)$
$PO_4^{3-}(2)$
DIAGENESIS:
POP
J_P
$PO_4^{3-}(2)$
ANAEROBIC LAYER 2
PARTITIONING:
$PO_4^{3-}(2)$ + FeOOH
π_2
FeOOH=$PO_4^{3-}(2)$
H_2
w_2
a
SILICA
WATER COLUMN
J_{PSi}
$Si(OH)_4(0)$
K_{L01}
$Si(OH)_4(1)$
PARTITIONING:
$Si(OH)_4(1)$ + FeOOH
π_1
FeOOH=$H_4SiO_4(1)$
FeOOH=$Si(OH)_4(1)$
w_{12}
$Si(OH)_4(1)$
K_{L12}
FeOOH=$Si(OH)_4(2)$
$Si(OH)_4(2)$
DIAGENESIS:
PSi
$k_{Si}PSi$
$Si(OH)_4(2)$
SOLUBILITY: $Si(OH)_4(2)$
$Si(OH)_4$(sat)
PARTITIONING:
$Si(OH)_4(2)$ + FeOOH
π_2
FeOOH=$Si(OH)_4(2)$
w_2
b

Fig. 4.5

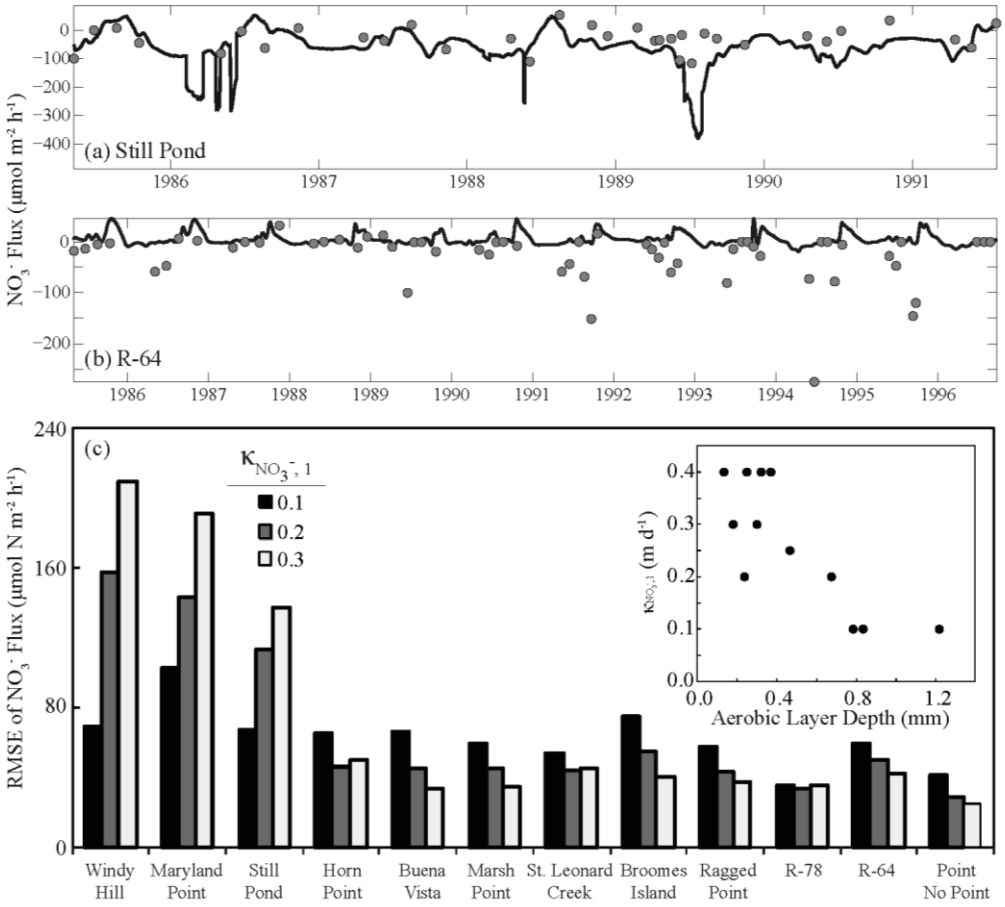
(a) Still Pond
(b) R-64
NO_3^- Flux (μmol m^{-2} h^{-1})
(c)
$\kappa_{NO_3^-,1}$
0.1
0.2
0.3
RMSE of NO_3^- Flux (μmol N m^{-2} h^{-1})
$\kappa_{NO_3,1}$ (m d^{-1})
Aerobic Layer Depth (mm)
Windy Hill
Maryland Point
Still Pond
Horn Point
Buena Vista
Marsh Point
St. Leonard Creek
Broomes Island
Ragged Point
R-78
R-64
Point No Point

Fig. 4.6

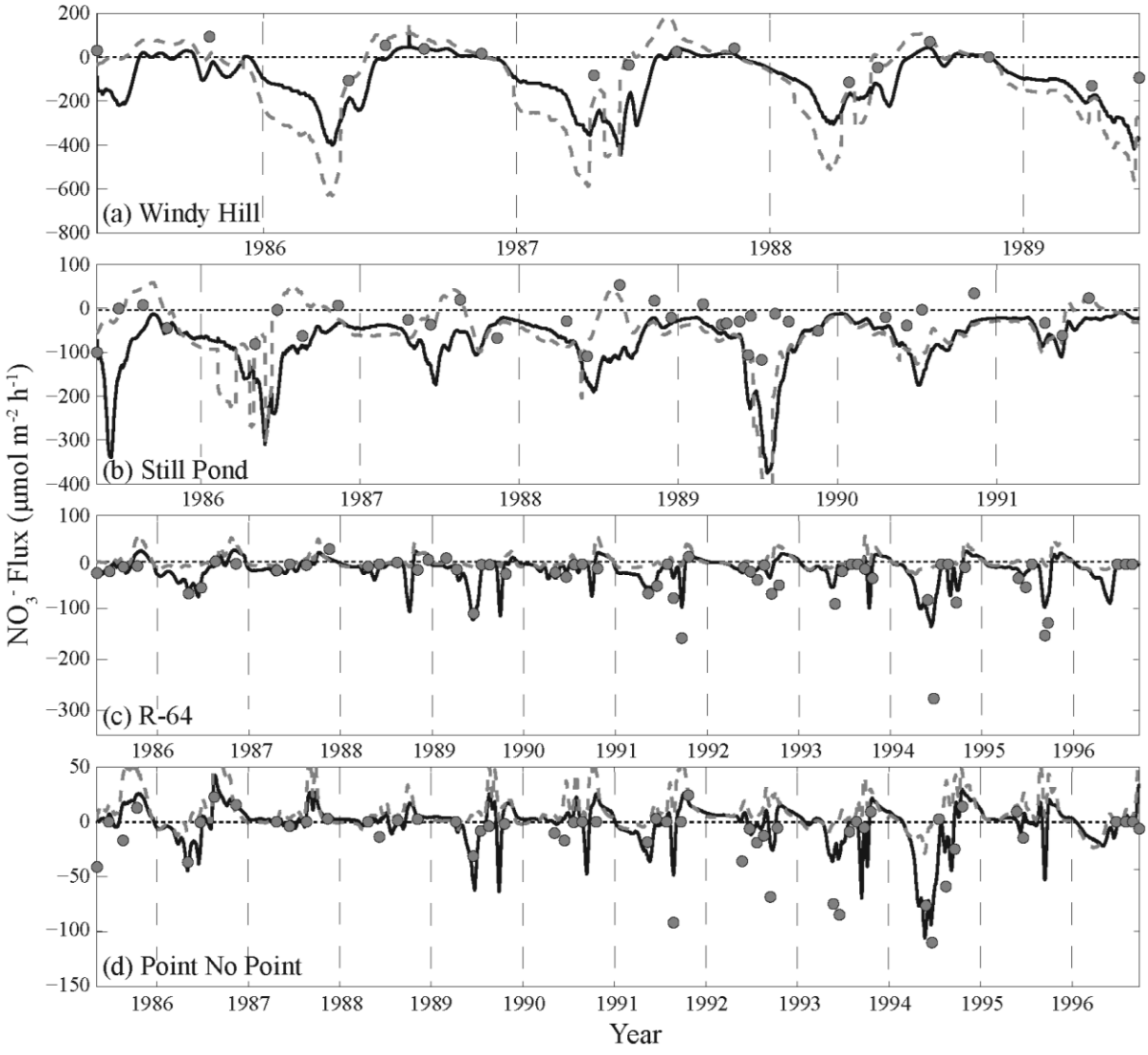
(a) Windy Hill
(b) Still Pond
(c) R-64
(d) Point No Point
NO3- Flux (µmol m-2 h-1)
Year

Fig. 4.7

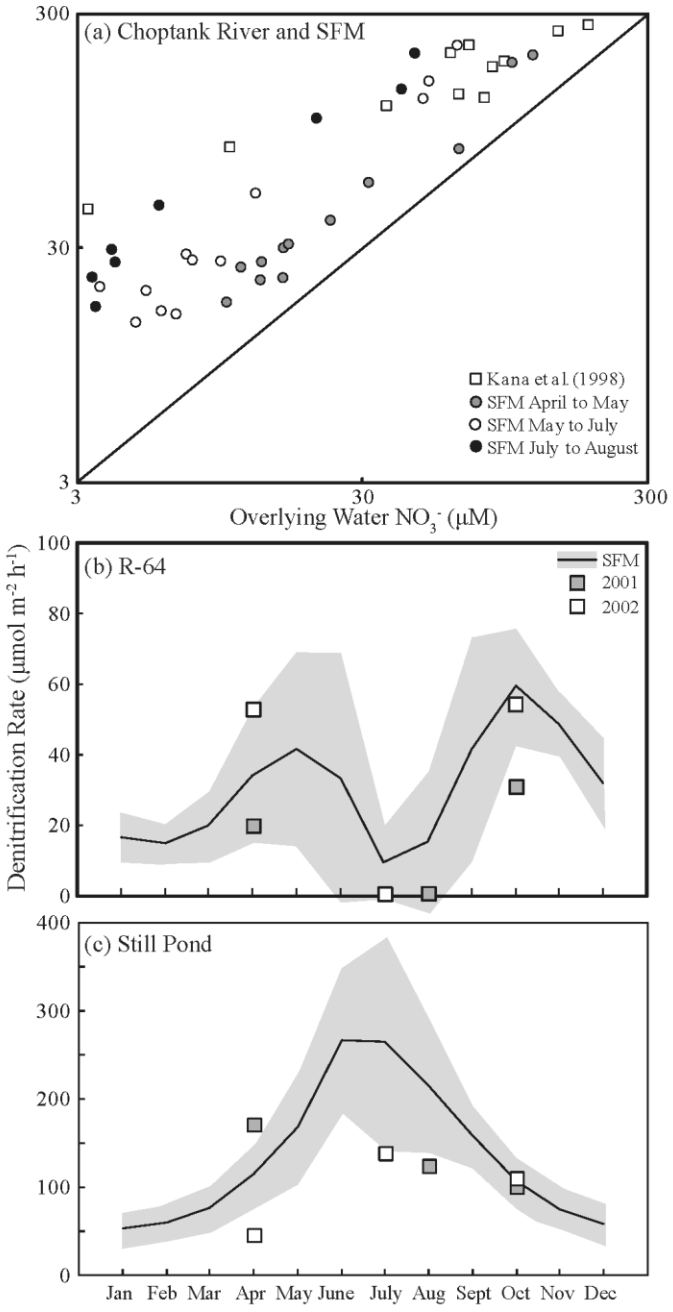
(a) Choptank River and SFM
300
30
3
3
30
300
Overlying Water NO_3^- (µM)
Kana et al (1998)
SFM April to May
SFM May to July
SFM July to August
(b) R-64
SFM
2001
2002
Denitrification Rate (µmol m^{-2} h^{-1})
100
80
60
40
20
0
(c) Still Pond
400
300
200
100
0
Jan Feb Mar Apr May June July Aug Sept Oct Nov Dec

Fig. 4.8

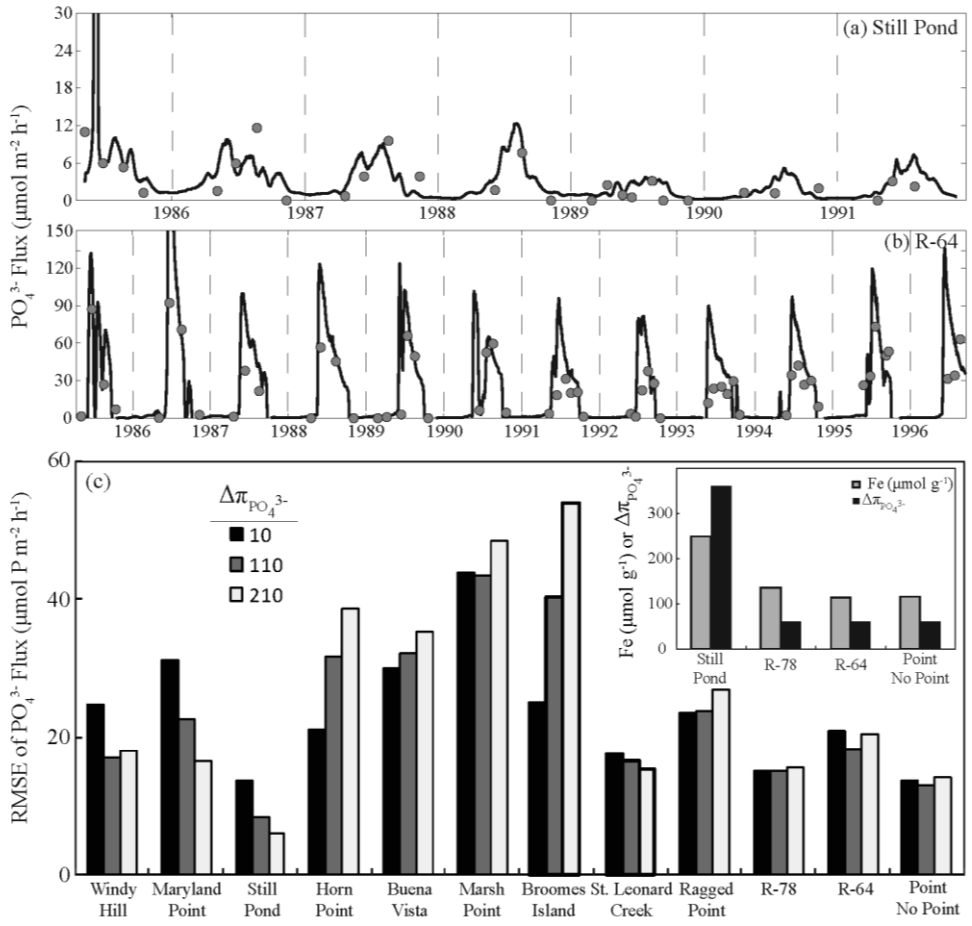
(a) Still Pond
(b) R-64
(c)
PO_4^{3-} Flux (µmol m^{-2} h^{-1})
RMSE of PO_4^{3-} Flux (µmol P m^{-2} h^{-1})
$\Delta\pi_{PO_4^{3-}}$
10
110
210
Fe (µmol g^{-1})
$\Delta\pi_{PO_4^{3-}}$
Fe (µmol g^{-1}) or $\Delta\pi_{PO_4^{3-}}$
Still Pond
R-78
R-64
Point No Point
Windy Hill
Maryland Point
Still Pond
Horn Point
Buena Vista
Marsh Point
Broomes Island
St. Leonard Creek
Ragged Point
R-78
R-64
Point No Point

Fig. 4.9

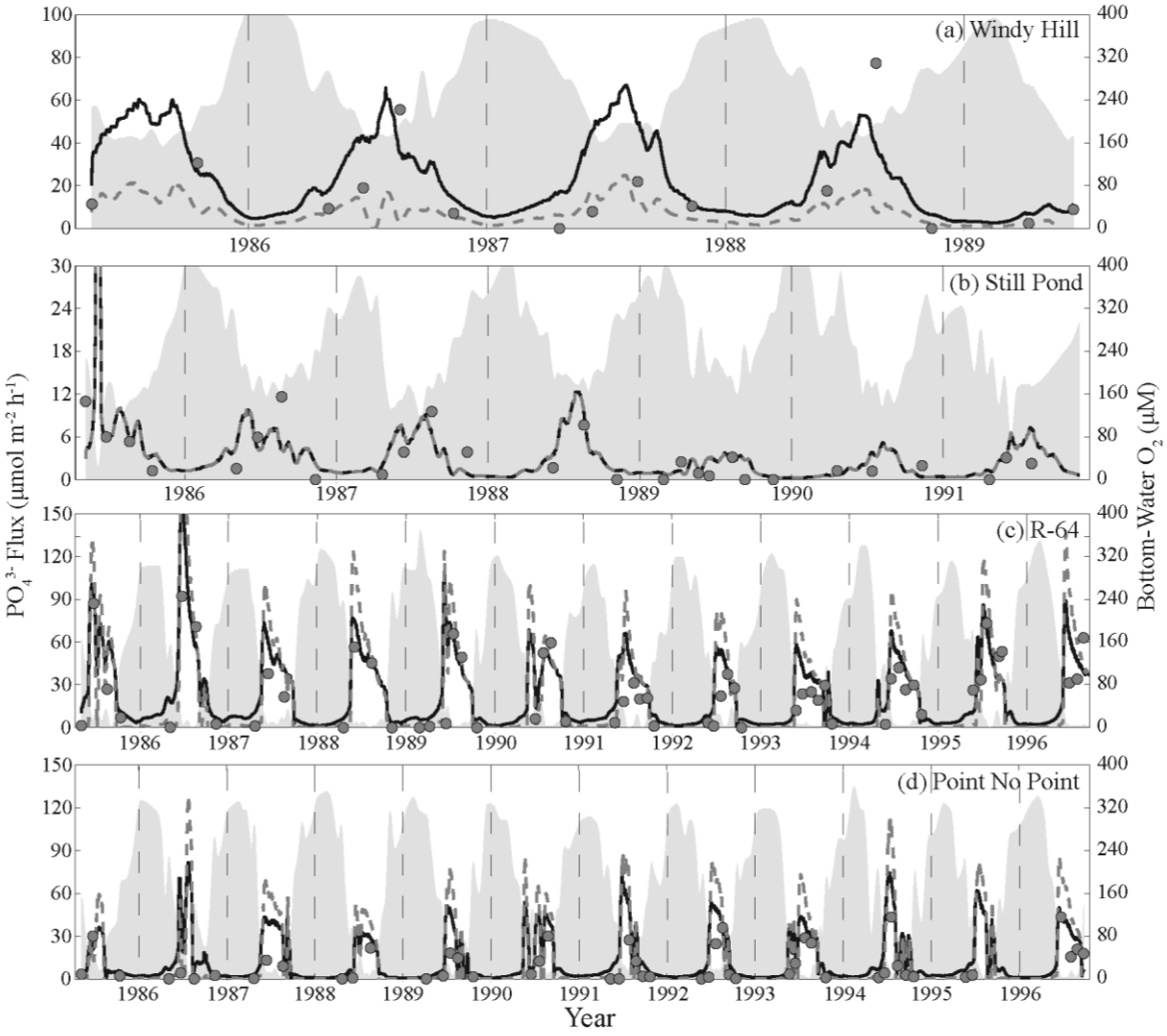
(a) Windy Hill
(b) Still Pond
(c) R-64
(d) Point No Point
PO_4^{3-} Flux (µmol m^{-2} h^{-1})
Bottom-Water O_2 (µM)
Year
1986
1987
1988
1989
1990
1991
1992
1993
1994
1995
1996

Fig. 4.10

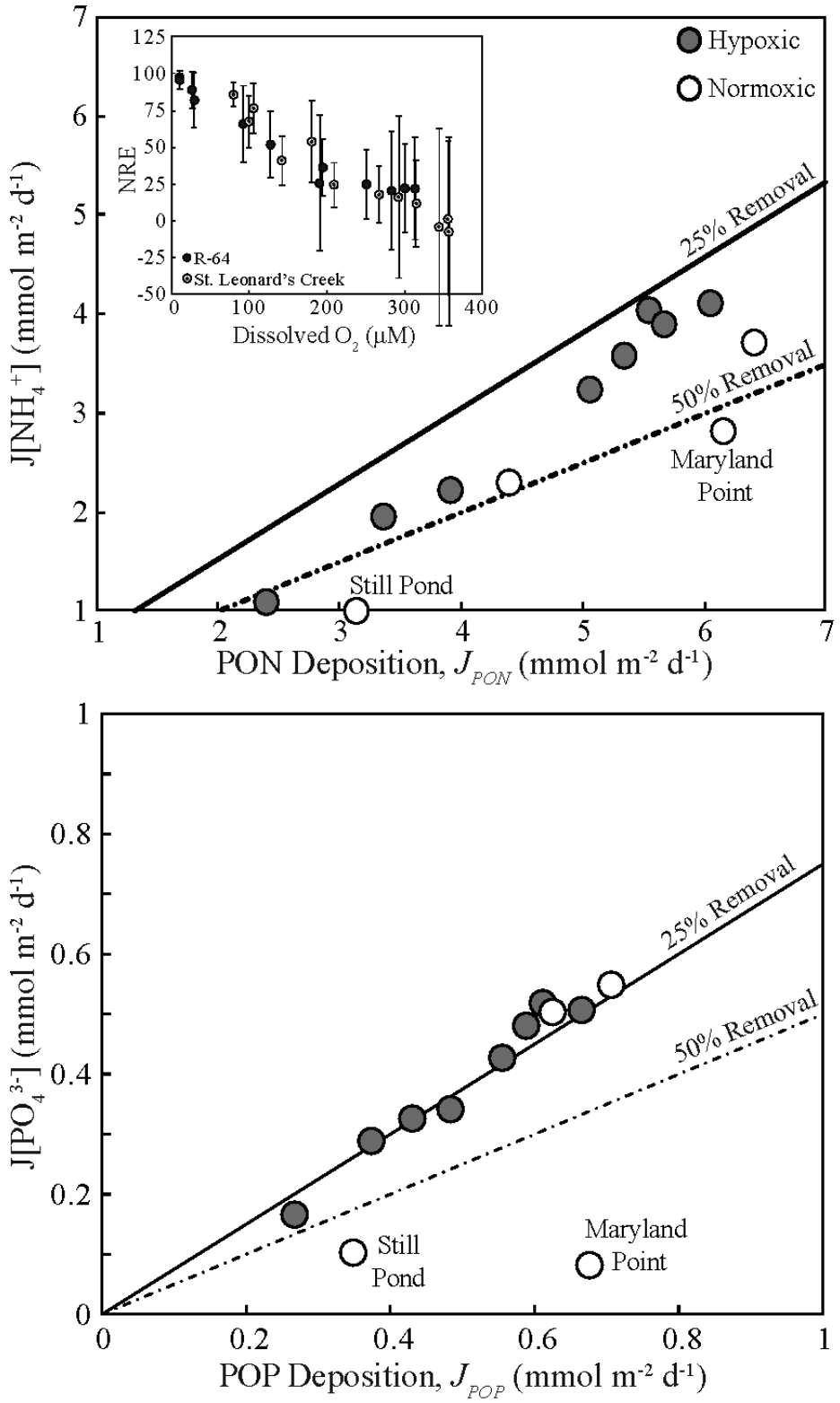
Hypoxic
Normoxic
25% Removal
50% Removal
Maryland Point
Still Pond
J[NH4+] (mmol m-2 d-1)
PON Deposition, JPON (mmol m-2 d-1)
NRE
R-64
St. Leonard's Creek
Dissolved O2 (µM)
J[PO43-] (mmol m-2 d-1)
POP Deposition, JPOP (mmol m-2 d-1)

Fig. 4.11

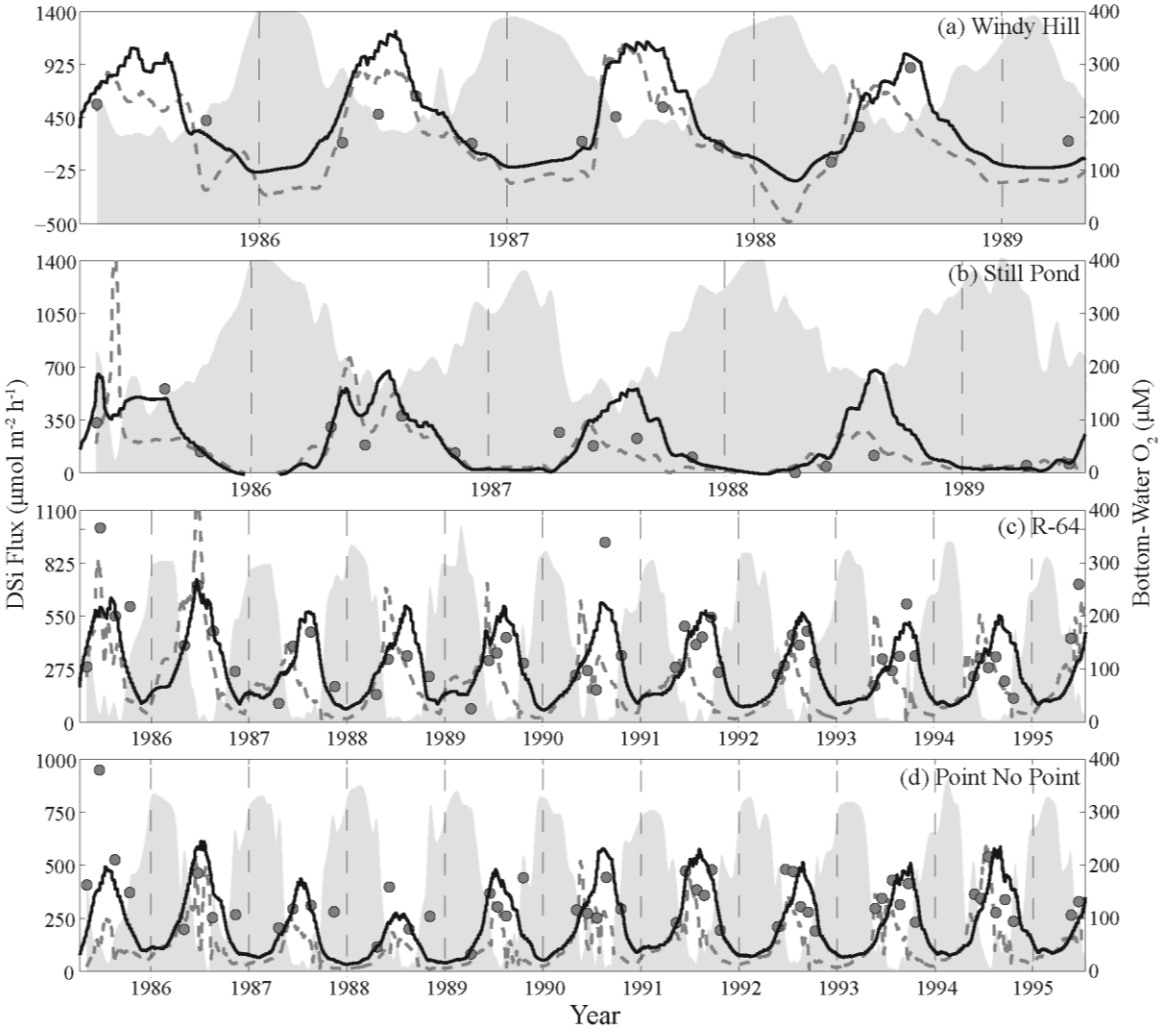
(a) Windy Hill
(b) Still Pond
(c) R-64
(d) Point No Point
DSi Flux (µmol m-2 h-1)
Bottom-Water O2 (µM)
Year
1986
1987
1988
1989
1990
1991
1992
1993
1994
1995

CHAPTER 5: QUANTIFYING THE EFFECTS OF NUTRIENT LOADING AND CARBON PRODUCTION ON DISSOLVED O_2 IN CHESAPEAKE BAY USING A COUPLED HYDRODYNAMIC-BIOGEOCHEMICAL MODEL

Abstract

We coupled an implementation of the Regional Ocean Modeling System (ROMS) to a biogeochemical model (RCA) in Chesapeake Bay to understand the controls on organic carbon production and transport and associated oxygen depletion. Model simulations were performed for a 10-year period (1996-2005) and water-column state variables, sediment-water fluxes, and metabolic rates were validated against existing data. A series of nutrient-load experiments were run using the year 2000 to understand system responses to altered loads of nitrogen and phosphorus and the spatial and temporal nature of Chesapeake Bay's response to nutrient loads. ROMS-RCA represented observed seasonal and regional dynamics of water-column and sediment processes, capturing interannual variability in hypoxic volumes. Nutrient loading experiments revealed a non-linear response of hypoxia to nitrogen load, with hypoxic-volume-days maximizing at nitrogen loads twice that of observed. O_2 levels were more sensitive to nitrogen loads than phosphorus loads, consistent with the preponderance of nitrogen limitation in Chesapeake Bay in late spring and summer months. Expanded hypoxic volumes under higher nitrogen loads were associated with increases in water-column production and respiration in seaward regions of Chesapeake Bay during summer (June to August) months. Analysis of the 10-year model run with realistic hydrodynamics and nutrient loading revealed a similar pattern, emphasizing the role of stimulation of phytoplankton growth in more-nutrient-limited lower-Bay regions during summer as a primary mechanism supporting elevated hypoxic volumes. ROMS-RCA is a useful tool for investigating system processes in Chesapeake Bay and other coastal ecosystems.

Introduction

Depletion of dissolved oxygen (O_2) from coastal waters is a widespread phenomenon that appears to be growing globally (Díaz and Rosenberg, 2008; Rabalais and Gilbert, 2009). There is considerable interest in this phenomenon because O_2 concentrations below ~30% saturation ("hypoxia"=O_2 < 2 mg l^{-1}) generally alter behavior, cause reduced growth, and increase the occurrence of mortality for many marine fish and invertebrates (Díaz, 2001; Vaquer-Sunyer and Duarte, 2008). Hypoxia may also affect predator-prey interactions and food web structures, with low O_2 zones providing more tolerant organisms extended habitat for foraging and refuge from predation (Decker et al., 2004; Nestlerode and Diaz, 1998). Low O_2 levels also alter the redox state and associated biogeochemical processes in sediments (Testa and Kemp, 2012), including coupled nitrification-denitrification (Kemp et al., 1990) and inorganic phosphorus sorption to metal oxide-hydroxide complexes (Slomp and Van Cappellen, 2007). Due to the diverse and considerable consequences of low-O_2 conditions, substantial research efforts have focused on this topic.

Key ecological controls on seasonal hypoxia in coastal waters involve the production and delivery of labile organic matter to the region of O_2 depletion. Because hypoxia in stratified coastal systems is confined to the bottom layer, respiration must be fueled by labile organic matter, typically particulate organic carbon (POC) sinking from the upper water-column (Hagy et al., 2005). The origin of the POC that fuels respiratory O_2 sinks can either be from sources within the aquatic system or from external sources, including the adjacent watershed or ocean (Bianchi et al., 2008). External sources of POC include runoff of terrestrial plant debris, import of algal biomass from adjacent rivers or oceans,

and anthropogenic inputs of organics (e.g., sewage effluents). To fuel bottom respiration in stratified waters, however, organic matter must be in the form of particles capable of sinking to the bottom layer and the high rates of POC generally needed to support bottom-layer hypoxia in Chesapeake Bay tend to be from algal production in overlying waters driven by external inputs of inorganic nutrients (Kemp and Boynton, 1992a).

There is substantial evidence that eutrophication (i.e., anthropogenic nutrient and organic enrichment of aquatic ecosystems) is contributing to the expansion of occurrence, intensity, and duration of hypoxic conditions in coastal waters worldwide (Díaz and Rosenberg, 2008; Gilbert et al., 2010). Nutrient additions tend to fertilize growth, sinking and decomposition of phytoplankton in bottom waters of estuaries, bays, and inland seas. For many coastal systems in the industrialized regions of the world, there have been major socio-economic commitments to remediate hypoxic zones by reducing nutrient loading from the adjacent catchment and overlying atmosphere (Boesch et al., 2001; Carstensen et al., 2006). Despite such substantial socio-economic investments (Boesch, 2002; Kronvang et al., 2005), recent analyses of historical data from European and North American coastal systems suggest little evidence for simple and straightforward responses of hypoxia to remediation actions that include reduced nutrient loading (Conley et al., 2009a; Duarte et al., 2009).

Much effort has been invested in building models to simulate O_2 dynamics on several time and space scales in both sediments and the water-column. In general, model structures range from relatively simple statistical models and empirical relationships (Murphy et al., 2011; Turner et al., 2006) to more complex process simulations that focus either on sediment processes or on coupled biophysical dynamics (Boudreau, 1991;

Fennel et al., 2013; Luff and Moll, 2004). Simple models are often focused on evaluating the major drivers of O_2 depletion and how management actions might alleviate low-O_2 zones, while coupled biophysical models are used to help understand ecosystem interactions and feedbacks, where O_2 is one of many biogeochemically-linked model variables (Peña et al., 2009). Coupled biophysical models, however, are built at a variety of scales and complexities. 3-D hydrodynamic models may be built at meso (~1 km) horizontal scales with finer (1-10 m) vertical resolution (including stratification) and are computed at hourly time scales, solving for salinity, temperature, elevation, three velocity components, and vertical mixing or more advanced turbulence schemes (Shchepetkin and McWilliams, 2005). The hydrodynamics may be directly or indirectly coupled to multi-compartment biogeochemical models that include phytoplankton and zooplankton, particulate and dissolved inorganic and organic nutrient pools (N, P, Si, C), and O_2 (Fennel et al., 2006; Lin et al., 2007; Xu and Hood, 2006; Zheng et al., 2004). Such models can include sediment parameterizations (Eiola et al., 2009), or be coupled to relatively simple sediment process models (Fennel et al., 2006; Soetaert et al., 2000; Sohma et al., 2008), or to more advanced models that compute diagenesis and remineralization of carbon, nitrogen, phosphorus, silica, sulfur and O_2 (Brady et al., 2013; Luff and Moll, 2004; Testa et al., 2013).

Biogeochemical and ecosystem models are useful tools that can integrate the varied physical, biological, and anthropogenic drivers of ecosystem variability and associated internal interactions. By their nature, these models integrate and synthesize our understanding of ecosystem processes, and they provide a number of unique capabilities, including (1) simulation of biological activity in the context of the physical regime, (2)

coupling hydrologic and anthropogenic processes on land to compute watershed impacts on the receiving water, (3) providing metrics of uncertainty in predictions, as well numeric goals for management (e.g., Total Maximum Daily Load), and (4) providing new quantitative insights into ecological processes that are otherwise difficult to understand.. This latter point emphasizes the fact that models are useful tools to understand ecosystem processes in a way that are impractical with observational or experimental studies; thus they provide a unique approach to improving our knowledge about coastal processes. Although multiple coupled, hydrodynamic-biogeochemical models currently exist for Chesapeake Bay (Cerco, 2000; Li et al., 2009; Xu and Hood, 2006), these models have yet to be fully utilized to examine spatial and temporal patterns in dissolved O_2 and metabolic processes resulting from altered nutrient loading (Cerco, 1995). The purpose of this manuscript is to provide such an analysis for Chesapeake Bay, in simulating carbon and O_2 transport and transformation using a coupled physical-biogeochemical model.

Methods

General Model Description

The modeling framework involves an offline coupling of the Regional Ocean Modeling System (ROMS) to a water-column and sediment biogeochemical model called RCA for simulation during the years 1996-2005. Hourly average ROMS output are used to force RCA, which is simulated on a 10-minute time-step over an 80 x 120 grid cell domain with 20 vertical layers. Both models have been applied in a number of different coastal ecosystems (Fennel et al., 2006; Isleib and Thuman, 2011; Li et al., 2005; Zhang and Li, 2010).

ROMS in Chesapeake Bay

The hydrodynamic model is an implementation of the Regional Ocean Modeling System, or ROMS (Haidvogel et al., 2000) for Chesapeake Bay (Li et al., 2005). The model has been validated against a wide range of observational data and has shown considerable capability in reproducing estuarine dynamics at tidal, synoptic, and seasonal time-scales (Li et al., 2005; Li et al., 2007). We use an application of this model with 80×120 grid points in the horizontal direction (about ~1 km grid size) and 20 layers in the vertical direction (Fig. 5.1). A quadratic stress is exerted at the bed, assuming that the bottom boundary layer is logarithmic over a roughness height of 0.5 mm (Xu et al., 2002). The vertical eddy viscosity and diffusivity are computed using the k-kl turbulence closure scheme (Warner et al., 2005) with the background diffusivity and viscosity set at $5x10^{-6}$ m^2 s^{-1} (Xu et al., 2012). The hydrodynamic model is forced by freshwater discharge at river heads, by tidal and nontidal elevations at the offshore boundary, and by wind, heat, and freshwater fluxes across the air-sea surface. At the offshore open boundary, we employ Chapman's condition for surface elevation, Flather's condition for barotropic velocity, an Orlanski-type radiation condition for baroclinic flow, and a combination of radiation condition and nudging for tracers (with a relaxation time scale of 1 day) (Marchesiello et al., 2001).

Tidal forcing at the open ocean boundary consists of 10 constituents (M2, S2, N2, K2, K1, O1, P1, Q1, Mf, and Mm) that are linearly interpolated from the Oregon State University global inverse tidal model of TPXO7 (Egbert and Erofeeva, 2002). Non-tidal water elevations are acquired from detailed observations at NOAA Duck station. Salinity and temperature at the oceanic open boundary are obtained from monthly Levitus

climatology. At the riverine boundaries of 8 major tributaries, daily discharge along with zeros salinity and seasonal water temperature are prescribed using USGS and Chesapeake Bay Program (CBP) monitoring data. Atmospheric forcing is applied via standard bulk formulae (Fairall et al., 2003) to North American Regional Reanalysis (NARR) from National Center for Environmental Prediction products (Mesinger et al., 2006), including 3-hourly winds, net shortwave and downward longwave radiation, air temperature, relative humidity, and pressure. In addition, Chesapeake Bay Program monitored surface water temperature throughout the Bay, and we produced a SST field based on linear interpolation of monitoring data from 23 stations along the Bay. Modeling SST is relaxed toward this temperature field.

Biogeochemical Model

We coupled ROMS simulations with a water-column biogeochemical model called RCA, which includes a two-layer sediment biogeochemical model (Isleib and Thuman, 2011; Zhang and Li, 2010). The sediment model is described in detail elsewhere (Brady et al., 2013; Testa et al., 2013), so it is not described in the narrative below. RCA is the most recent extension of the family of water quality models that originated as the Water Quality Analysis Simulation Program (WASP) used by the United States Environmental Protection Agency (http://www.epa.gov/athens/wwqtsc/html/wasp.html). The model includes two phytoplankton groups (a winter "diatom" group and a summer 'dinoflagellate" group), as well as state variables representing particulate and dissolved organic carbon, nitrogen and phosphorus, dissolved inorganic nitrogen, phosphorus, and silica, biogenic particulate silica, and dissolved O_2 (Fig. 5.2).

RCA also includes a state variable that represents O_2 equivalents associated with sulfide and methane released from sediments. Nitrification and denitrification are modeled in both the water-column and sediments.

External Forcing

RCA is driven by loads of dissolved and particulate material from river flows, non-point sources, atmospheric deposition, and direct anthropogenic loads from point sources. In-river concentrations were obtained from routine monitoring stations (www.chesapeakebay.net) within the eight major rivers entering the ROMS-RCA domain. Below fall line, non-point loads were obtained from the Chesapeake Bay Watershed Model (http://www.chesapeakebay.net/about/programs/modeling/53/), which is an application of the Hydrologic simulation Program - Fortran (HSPF) (Bicknell et al., 1996). Land-water cells from the watershed model were matched to ROMS-RCA cells and if multiple cells resided in a single ROMS-RCA cell, the loads were added together. Point source loads for each ROMS-RCA cell were obtained from the Chesapeake Bay Program Nutrient Point-Source Database (http://www.chesapeakebay.net/data/downloads/bay_program_nutrient_point_source_database). Atmospheric deposition of NH_4^+ and NO_3^- was added uniformly to surface cells across the model domain and estimated from the National Atmospheric Deposition Program (http://nadp.sws.uiuc.edu/sites/siteinfo.asp?net=NTN&id=MD13) station near Wye, Maryland.

Phytoplankton Growth

RCA simulates light, temperature, and nutrient influences on phytoplankton growth for two distinct phytoplankton groups (with an optional 3rd group) with different kinetics

(Table 5.1 & 5.2). These two groups represent a winter-spring diatom community (Group 1) and a summer mixed community (Group 2) that represents dinoflagellates. RCA uses phytoplankton carbon as an aggregate measure of algal biomass, and this biomass (in carbon units) is readily converted to chlorophyll-*a* using group-specific carbon-chlorophyll ratios (Table 5.2). The specific phytoplankton growth rate, $G_{p,i}$, is related to the maximum growth rate at optimal light, temperature, and nutrient conditions ($g_{max,i}$) via Equation 1 in Table 5.2. The temperature effect on growth rate relates the growth rate at ambient temperature (T) to the growth rate at a phytoplankton-group-specific optimal temperature ($T_{opt,i}$) using shaping parameters b_1 and b_2 (Equations 1 & 2 in Table 5.1, Table 5.2). The effect of light availability on phytoplankton growth is simulated as a function of phytoplankton-group-specific photo-inhibition ("saturating" light level, $I_{s,i}$) and light attenuation in the water column due to the effects of turbidity and algal self-shading (k_d). A depth-averaged growth rate factor (g_I or "Light effect" in Table 5.1) is computed by integrating the specific growth rate over depth (Equation 3 in Table 5.1). Incident solar radiation at the water surface is evaluated at any time, t, as below (Eq. 1):

$$I_o(t) = \frac{I_{tot}}{0.635f} sin\left[\frac{\pi(t_d - t_{sunrise})}{f}\right] \quad \text{Eq. 1}$$

where I_{tot} is the total daily incident solar radiation (ly d^{-1}), f = fraction of daylight for a given day (daylight hours/24), t_d is the time of day, and $t_{sunrise}$ is the time of sunrise. The light availability at a given depth, $I_o(H)$, is a function of depth, surface light intensity, and the light extinction coefficient, k_d, as below (Eq. 2):

$$I_o(H) = I_o(t) exp^{-k_d H} \quad \text{Eq. 2}$$

where H is the cell depth. The light attenuation factor, k_d, is computed as a function of the background attenuation due to non-algal, inorganic and organic particles and colored

dissolved organic matter (CDOM), as well as self-shading due to phytoplankton biomass. The non-algal light attenuation factor is estimated from empirical formulations developed for Chesapeake Bay, where light attenuation is statistically predicted from observed distributions of total suspended solids (TSS) and salinity, which represents CDOM (Xu et al., 2005). Surface-water TSS data collected fortnightly to monthly as part of the Chesapeake Bay Monitoring Program (www.chesapeakebay.net) were interpolated spatially using kriging and temporally (simple linear fit) to obtain daily values for each model cell, while salinity values obtained from the ROMS hydrodynamic simulation (SAL) were used to compute CDOM contributions to k_d. Statistical models (Eq. 3) were then used to compute a non-algal light attenuation factor, $k_{d,base}$:

$k_{d,base}$ = 1.80 + 0.0673[TSS] - 0.0960[SAL] where SAL <=15 Eq. 3a

$k_{d,base}$ = 1.17 + 0.0060[TSS] - 0.0225[SAL] where SAL >15 Eq. 3b

For each cell and time-step, the total light attenuation factor, k_d, is then computed from $k_{d,base}$ and the modeled algal biomass (Eq. 4):

$$k_d = k_{d,base} + k_{d,chla} * C{:}CHL_i * PHYTb_i \quad \text{Eq. 4}$$

where $k_{d,chla}$ is the chlorophyll-*a* self-shading coefficient (mg^2 mg chl-*a*), $C{:}CHL_i$ is the carbon to chlorophyll ratio for each phytoplankton group (50 and 75 respectively for Group 1 and 2), and $PHYTb_i$is the phytoplankton biomass for each phytoplankton group (g m^{-3}). The effect of nutrient limitation is simulated via a Michaelis-Menten formulation for three inorganic nutrients, nitrogen, phosphorus, and silica (Equation 4 in Table 5.1), with phytoplankton-group-specific half-saturation coefficients (Table 5.2). The minimum value for the Michaelis-Menten formulation is used as the growth-reduction term at each time-step (Table 5.1).

Phytoplankton Respiration, Sinking, and Grazing Loss

RCA represents phytoplankton respiration due to two components: (1) basal respiration and (2) respiratory losses associated with photosynthesis (Laws and Chalup, 1990). The sum of these two formulations represents phytoplankton respiration (R_p; Equation 5 in Table 5.1, Table 5.2). Zooplankton are not explicitly modeled in RCA, and thus the dynamics of zooplankton grazing associated with seasonal changes in species, biomass, reproduction, and micro- and macro-zooplankton interactions are excluded from the model (Kimmel and Roman, 2004; Roman et al., 2001; Stoecker and Egloff, 1987). Rather, RCA includes a temperature-dependent grazing loss term on phytoplankton that can be specified for each phytoplankton group in the model (R_{GR}; Equation 6 in Table 5.1, Table 5.2). Finally, phytoplankton models have employed a large range of sinking velocities (Lin et al., 2007; Xu and Hood, 2006; Zheng et al., 2004), which represents the fact that phytoplankton sinking rates can vary greatly among species (Bienfang, 1981; Passow, 1991) and environmental conditions. In RCA, phytoplankton biomass loss due to sinking (R_S) is simulated as a base settling velocity that is modulated by temperature and nutrient stress (Bienfang et al., 1982) in each respective cell (Equation 7 in Table 5.2). The total loss rate for phytoplankton (D_P) is the sum of respiration, grazing, and settling (Eq. 5).

$$D_P = R_P + R_{GR} + R_S \qquad \text{Eq. 5}$$

Nutrients are released during phytoplankton respiration and predation processes, as well as during bacterial hydrolysis and mineralization processes. In RCA, phytoplankton respiration and grazing losses are portioned into the resulting carbon and nutrient pools using stoichiometric conversions and fixed fractions of dissolved and particulate pools

(Table 5.2). As bacterial biomass and production is not modeled explicitly, the impacts of bacterial activity on hydrolysis and mineralization is simulated using a non-linear recycling term (Di Toro and Matystik, 1979). This formulation (Equation 8 in Table 5.2) allows first-order, temperature-dependent rates at high organic carbon concentrations, but second-order rates at low organic carbon concentrations that effectively slows bacterial activity under conditions of low organic matter availability and phytoplankton biomass (e.g., Equations 8 & 9 in Table 5.1).

Organic Carbon

RCA includes pools for labile and refractory particulate organic carbon (LPOC, RPOC), labile and refractory dissolved organic carbon (LDOC, RDOC), and a highly labile dissolved carbon pool that represents DOC exudates released from actively growing phytoplankton cells (ExDOC). The distinctions of labile and refractory represent differential time scales of decomposition or oxidation, similar to the "G-model" (Westrich and Berner, 1984). LPOC and RPOC are externally loaded into the model, lost due to sinking (Equation 16 in Table 5.1, Table 5.2) or released during zooplankton grazing and are hydrolyzed into dissolved organic forms (LDOC and RDOC) based on a first-order reaction rate and the saturating recycling term (Equation 9 in Table 5.1, Table 5.2). DOC oxidation has a similar formulation, but includes an O_2-limitation term (Equation 10 in Table 5.1, Table 5.2). Unlike DOC and POC, ExDOC is generated as a fixed fraction of primary production rates (10%) and has a much higher oxidation rate than the other DOC forms.

Nitrogen

RCA includes pools for ammonium (NH_4^+), nitrate (NO_3^-), labile and refractory particulate organic nitrogen (LPON, RPON), and labile and refractory dissolved organic nitrogen (LDON, RDON). PON and DON pools are simulated like the carbon pools (Equations 9 & 11 in Table 5.1, Table 5.2). NH_4^+ enters the system from external sources and is released during grazing, remineralized from DON, and exchanged with the sediment sub-model. NH_4^+ sink terms include phytoplankton uptake and nitrification, which is modeled as a first-order function of $[NH_4^+]$ and an O_2-limitation term (Equation 12 in Table 5.1). This contrasts to other models, which simulate nitrification with a Michaelis-Menten dependence on NH_4^+ (Soetaert and Herman, 1995). NO_3^- enters the system from external sources and is released during grazing, nitrification, and exchanged with the sediment sub-model. NO_3^- sink terms include phytoplankton uptake and denitrification, which is modeled with a Michaelis-Menten dependence on LDOC and a non-linear O_2-contrl term (Equation 13 in Table 5.1, Table 5.2).

Phosphorus

RCA includes pools for phosphate (PO_4^{3-}), labile and refractory particulate organic phosphorus (LPOP, RPOP), and labile and refractory dissolved organic phosphorus (LDOP, RDOP). POP and DOP pools are simulated like the carbon pools (Equations 9 & 11 in Table 5.1, Table 5.2). PO_4^{3-} enters the system from external sources and is released during grazing, remineralized from DOP, and exchanged with the sediment sub-model. The only PO_4^{3-} sink term is phytoplankton uptake.

Silica

RCA includes pools for dissolved silica (DSi) and particulate biogenic silica (BSi). BSi is generated during phytoplankton respiration and grazing and is lost via vertical sinking (Equation 16 in Table 5.1, Table 5.2). BSi is also dissolved into DSi via a first-order dissolution reaction (Equation 14 in Table 5.1, Table 5.2) that includes the saturating recycling term, which is supported by the potential for bacteria to enhance silica dissolution in marine waters (Bidle and Azam, 1999). DSi is also exchanged with the sediment sub-model.

Oxygen

Dissolved oxygen (O_2) sources in RCA includes photosynthetic production, reaeration from the atmosphere, and loading from external sources (e.g., river input). Photosynthetic O_2 production (K_{G_p}) is simulated using stochiometric conversions (Table 5.2) of the phytoplankton growth rates as described previously (Table 5.1). O_2 exchanges between the atmosphere and surface cells are driven by linearly-interpolated hourly wind velocities measured at the Patuxent River Naval Air Station (PRNS). The air-water exchange coefficient (k_a) is computed as below:

$$k_a = KL/H \qquad \text{Eq. 6}$$

where

$$KL = 0.728 * \sqrt{w_s} - 0.317 * w_s + 0.0372 * {w_s}^2 \qquad \text{Eq. 7}$$

and w_s is the interpolated wind speed (m s^{-1}) and $H$is the depth of the surface cell. The air-water exchange of O_2 is then computed as a function of temperature and O_2 relative to saturation:

$$K_{O_2} = k_a \theta_{k_a}^{(T-20)} * (O_{2,sat} - O_2) \qquad \text{Eq. 8}$$

where $O_{2,sat}$ is the saturation concentration of O_2 based on temperature and salinity (μM), O_2 is the surface-layer O_2 concentration (μM), and is the air-water O_2 exchange (mmol l^{-1} d^{-1}). Dissolved O_2 sinks include algal respiration (K_{R_p}), DOC oxidation ($K_{DOC_{ox}}$; LDOC, RDOC, ExDOC), nitrification (K_{nitrif}), oxidation of reduced solutes released from the sediment model (K_{H_sS/CH_4}; H_2S and CH_4), and in the bottom cells (Equations 5, 10, 12, and 15, respectively, in Table 5.1) sediment oxygen demand (K_{SOD}). Thus, the generic O_2 equation becomes:

$$\Delta O_2 = K_{O_2} + K_{G_p} - K_{R_p} - K_{DOC_{ox}} - K_{nitrif} - K_{H_sS/CH_4} - K_{SOD} \quad \text{Eq. 9}$$

where K_{O_2} occurs only in surface cells and K_{SOD} occurs only in bottom cells.

Calibration and Validation Datasets

Validations of the water-column state variables (e.g., chl-*a*, NH_4^+, POC, etc.) were performed using fortnightly-monthly observations of these variables at several depths and stations within Chesapeake Bay (http://www.chesapeakebay.net/data). Rates of water-column respiration were compared to measurements of O_2-uptake in dark bottles at several stations (Sampou and Kemp, 1994; Smith and Kemp, 1995, 2001), while rates of photic-layer net primary production were validated with observations based on oxygen incubations and empirical model computations based on ^{14}C uptake measurements (Harding et al., 2002; Smith and Kemp, 1995). Observed sediment-water fluxes of NH_4^+, nitrite + nitrate (NO_2^- + NO_3^-), PO_4^{3-}, DSi and O_2 were estimated from time-course changes in constituents during incubations of intact plexiglass sediment cores (Boynton and Bailey, 2008) and collected at several stations in Chesapeake Bay (Fig. 5.1).

Model-data comparisons were facilitated using multiple skill assessment metrics (Stow et al., 2009b): RMSE, the correlation coefficient between model simulations and

observations (the model was sampled at time when observations available), and reliability index (RI) were computed for each flux/station combination. Finally, the RI quantifies the average factor by which model predictions differ from observations. An RI of 2, for instance, would indicate that SFM predicts the observation within a factor 2, on average (Stow et al., 2009b).

Results

ROMS-RCA represented the spatial and temporal dynamics of phytoplankton biomass, dissolved and inorganic nutrients, sediment-water fluxes, primary production and respiration, and dissolved O_2 in Chesapeake Bay over multiple years. Model simulations reveal a strong, non-linear sensitivity of Chesapeake Bay hypoxia to nitrogen load, and suggest that seaward expansions of hypoxic water under elevated nitrogen loads are driven by elevated June to August water-column respiration in lower Bay regions. These regions tend to be more nutrient limited than landward regions, and are thus more sensitive to nutrient additions, especially during summer months when nutrient concentrations are at seasonal minima.

Biophysical Setting

Simulations were run during the year 2000, which was a year with generally average conditions in Chesapeake Bay (Fig. 5.3). Both the timing and magnitude of Susquehanna River flow approached the 1985-2010 mean, with peak flows in the March to May period (Fig. 5.3). Susquehanna flow approached long-term minima during February, however, resulting in relatively high salinity in the mesohaline regions of Chesapeake Bay (Fig. 5.3). Water temperatures and wind velocities approached average conditions in the Bay (Fig. 5.3).

Model Validation: Water-Column, Sediment, and Hypoxia

Model performance was evaluated using multiple quantitative metrics involving water-column state variables (e.g., O_2, NH_4^+, etc; Table 5.3). O_2, NO_3^-, and DSi were well represented by the model in both surface and bottom layers, with low RMSE, high r, and RI values approaching 1 (Table 5.3). Modeled particulate and dissolved nitrogen and phosphorus were poorly correlated to observations temporally (i.e., low r values), but had relatively low RMSE and RI values between 1.0 and 1.5 (except for bottom water PP and PN), indicating that modeled concentrations approached observed values (Table 5.3). Surface-water, model-data fits for chl-*a*, NH_4^+ and PO_4^{3-} were poorer than other variables (high RMSE, low r, RI > 1.5), but bottom-water simulations better represented the data, especially for NH_4^+ and PO_4^{3-} (Table 5.3). Surface-layer chl-*a* was generally over-estimated by the model, but seasonal cycles were captured and inter-annual variability due to changes in river flow and nutrient load were broadly captured, especially in the lower Bay (Fig. 5.4). The same was true for bottom-water O_2, although model over-predications of bottom-water O_2 were especially apparent in upper Bay regions (Table 5.3, Fig. 5.4).

Modeled sediment-water fluxes of O_2, NH_4^+, NO_3^-, PO_4^{3-}, N_2, and DSi were compared to observations (Boynton and Bailey, 2008; Cowan and Boynton, 1996) made at several stations in the mainstem of Chesapeake Bay (e.g., Fig. 5.5). The model captured both seasonal and spatial variations in these fluxes, where NH_4^+ (Fig. 5.5) and PO_4^{3-} (data not shown) peak in summer in the middle regions of the Bay, and sediment O_2 fluxes (positive values indicate net sediment uptake) peak in warmer months, except for the middle Bay, where summer hypoxia and anoxia force O_2-limitation of sediment O_2

uptake (Fig. 5.5). Modeled mid-Bay sediment O_2 fluxes remained high in summer (>2x observed values) because modeled bottom-water O_2 concentrations were overestimated (Fig. 5.4). Model computations of N_2, NO_3^-, and DSi also compared favorably with observations across several stations (data not shown), as they have in independent analyses of the sediment flux model in Chesapeake Bay (Brady et al., 2013; Testa et al., 2013).

Model-predicted hypoxic volumes were also compared to volumes computed from spatial interpolations of observed O_2 distributions in Chesapeake Bay collected during fortnightly to monthly surveys (Murphy et al., 2011; Testa and Kemp, 2012). Over a 10-year simulation, ROMS-RCA captured inter-annual variability in hypoxic volume, but tended to under predict hypoxic volumes in three of the four years with below-average winter-spring Susquehanna River flow (1999-2000 and 2002, Fig. 5.6).

Spatial Response to Nutrient Loads

The nutrient load sensitivity tests included a large range of loading rates (observed load scaled by 0.05 to 4) and here we focus on a subset of those simulations for nitrogen (hereafter N), phosphorus (hereafter P), and nitrogen+phosphorus loads (hereafter N+P): (1) 0.25x, (2)1x (observed case), and (3) 2x. A 75% reduction in nitrogen load (Case 0.25x) reduced late-spring, surface-layer chl-*a* concentrations by ~30%, with mid-Bay concentrations falling from 30-35 mg m^{-3} in Case 1x to ~20 mg m^{-3} in Case 0.25x (Fig. 5.7). Conversely, the doubled nitrogen load (Case 2x) cause a seaward migration of the late-spring chl-*a* peak, with concentrations in excess of 30 mg m^{-3} developing south of the York River (37.25 ^{o}N, Fig. 5.7). Phosphorus load reductions of 75% did not reduce chl-*a* as much as N load reductions, especially in lower Bay regions, while doubled P

loads did not result in the seaward expansion of late-spring chl-*a*, as did with N (Fig. 5.7 & 5.8). However, doubled P loads led to higher chl-*a* in middle Bay regions near 38.5 ^{o}N than did the doubled N loads (Fig. 5.7). The 75% reduction in N+P load has a quantitatively similar effect on late-spring chl-*a* as did the same reduction in N loads alone, but doubled N+P loads led to elevated chl-*a* in all regions of the Bay south of 39 ^{o}N (Fig. 5.7).

Seasonally, elevated nitrogen loads led to 20-50% increases summer phytoplankton biomass, primarily in middle and lower Bay regions, where winter-spring algal biomass was less sensitive to N loads (Fig. 5.8). More severe N-limitation during summer in the lower Bay was responsible for the sensitivity of biomass (and thus growth) to N loads during this season, while P-limitation appeared to be more prominent in early spring (Fig. 5.8). Nutrient limitation was weak overall in northern regions of the Bay (data not shown, Fig. 5.7).

Hypoxia Response to Nutrient Loads

Spatial patterns of elevated chl-*a* that resulted from elevated nutrient loads were associated with a larger region of low-O_2 water in Chesapeake Bay. The 75% reduction in N loads resulted in much high bottom-water O_2 levels (Fig. 5.9), and hypoxia did not develop until mid-summer. At higher N loading levels (1x and 2x), hypoxia was present in June, and the low-O_2 volume expanded seaward and landward, occupied a larger fraction of the water-column, and spread laterally (Fig. 5.9). The hypoxic volume also expanded seaward.

Hypoxic volumes generated by the various nutrient loading scenarios reveal nutrient-specific relationships. The metric of hypoxia used in this analysis is hypoxic-volume-

days ($HVD = \sum_{Jan\ 1}^{Dec\ 31} Hypoxic\ Volume * 365$), which integrates the spatial extent and temporal duration of hypoxic water (Hagy et al., 2004). The *HVD* generated by the N1x and N2x experiments were more than 3-fold and 5-fold higher than the N0.25x scenario (Fig. 5.10). *HVD* was less sensitive to P loads, with a 75% P-load reduction only generating a 25% reduction in *HVD*. Conversely, *HVD* was much more sensitive to N+P loads, with a 7-fold difference in *HVD* between NP0.25x and NP2x (Fig. 5.10). These patterns of *HVD* response to different levels and types of nutrient loads are consistent with the phytoplankton biomass responses (e.g., lower-Bay chl-*a* increase with N –load, seaward expansion of high-chl-*a* concentrations with high N-load, overall chl-*a* increase and spatial expansion with elevated N+P load; Fig. 5.7 & 5.8).

A larger set of nitrogen-load simulations were run to quantify the impacts of nitrogen loading, specifically, on hypoxia. In these simulations, the January to May Susquehanna River TN load was varied by 1.5 to 105 Gg, corresponding to the loading notation of 0.05x to 4x (Fig. 5.11). The resulting relationship between TN load and *HVD* was non-linear, and could be fit with a logistic relationship (Fig. 5.11). The logistic fit is valuable because its parameters are informative metrics of the nature of the load-*HVD* relationship. For example, consider the general logistic equation $HVD = min_{HVD} + \frac{max_{HVD} - min_{HVD}}{(1+ce^{-k(Nl-Nlmx)})^{1/c}}$, where min_{HVD} is the minimum HVD, max_{HVD} is the maximum possible *HVD*, *Nl* is the nitrogen load, *Nlmx* is the nitrogen load where the rate of change of *HVD* is greatest, k is the "growth rate" of *HVD*, and c is a fitting parameter. It is clear that 600 km^3-d is the maximum possible HVD in response to TN loads, but more interestingly, an *NLmx* of 24 Gg is where HVD changes most rapidly due to load (compare to observed load in 2000 of 31 Gg), and a *k* value of 0.088 indicates an increase

of 11.4 km^3-d *HVD* for a given 1 Gg increase in load (Fig. 5.11). Over the period from 1996 to 2005, where model runs have been made, observed TN loads fall within the linear part of the curve, and data do not always fall along the curve, revealing the impacts of interannual variability in physical forcing.

Regional and Seasonal Aspects of Metabolic Response to Nutrient Loads

Patterns of water-column and sediment metabolism resulting from the nutrient loading experiments reveal where and when the organic matter production was produced that fueled hypoxia in Chesapeake Bay. On an annual basis, the middle and lower Bay (between Choptank and Rappahannock Rivers) is where the majority of respiration occurs in the Bay. This respiration (water-column + sediments), however, is most sensitive to nitrogen loading in the lower Bay (e.g., CB5.2, CB6.1; Fig. 5.12). Although respiration increases associated with nutrient loading are associated with increases in net primary production (NPP), respiration integrated over the water-column exceeds NPP at all but the upper Bay stations (Fig. 5.12). In the shallower stations flanking the central channel of the Bay, the opposite is true (data not shown). This latter pattern, with net primary production in shallow waters and net respiration in deeper waters, reveals lateral patterns in the respiration budget of Chesapeake Bay. For example, when the Bay is divided into 9 regions (Fig. 5.1), the percentage of the total regional respiration that occurs in areas deeper than 10 meters is 40-80% and is generally more than 60%. For SOD, the percentage is closer to 40, suggesting that SOD is more evenly divided between deep and shallow habitats.

Regional respiration values allow for a computation of relative contributions to total Bay respiration that occur along the longitudinal axis. Here we compute regional totals

for metabolic processes (see Fig. 5.1 for region notation and location), which should not be confused with alternative regional designations in Chesapeake Bay (Harding and Perry, 1997). In comparing three regions of the Chesapeake Bay, representing the upper, middle and lower Bay, it is clear that the larger lower Bay regions contribute the largest fraction of total respiration (Fig. 5.13). But perhaps more interesting is the fact that the lower Bay is most sensitive to nitrogen load and that the *increase* in summer respiration due to elevated nitrogen load in the lower Bay (~150 Gg) is equivalent to the total respiration in the middle Bay region at the highest loading rates (Fig. 5.13). Lastly, increases in respiration in the lower Bay in summer due to nutrient load increases (~150 Gg) are three times the increase that occurred in the spring period (~50Gg; Fig. 5.13).

The same patterns in respiration are illustrated by a statistical analysis of the 1996-2005 model time-series, which includes the effects of changes in nutrient load, but also transport impacts due to interannual differences in circulation. Here, lower Bay summer (June to August) respiration is significantly and positively ($r^2 = 0.48$, $p < 0.01$) correlated to January to May TN loads, while upper Bay respiration is significantly, but negatively ($r^2 = 0.49$, $p < 0.01$) correlated with load (Fig. 5.14). Middle Bay respiration rates are relatively insensitive to nutrient load (data not shown). Conversely, SOD is weakly correlated to TN load and is generally lower at higher nutrient loads (Fig. 5.14). Clearly, there are clear spatial differences in the response of water-column and sediment respiration to changes in nutrient loading.

Discussion

Eutrophication has been a central topic in coastal ecology for decades, where research efforts have included retrospective data analyses (Cloern, 2001), mesocosm studies

(D'Elia et al., 1986; Oviatt et al., 1986), and numerical modeling studies (Cerco, 1995; Soetaert and Middelburg, 2009). For large and complex ecosystems, numerical models can be used as tools to understand eutrophication processes, internal cycling, and responses to external forcing in a way that cannot practically be accomplished using observational studies. In Chesapeake Bay, several modern hydrodynamic-biogeochemical models have been developed to understand phytoplankton dynamics, bio-physical interactions, and dissolved O_2 cycling (Cerco, 1995; Li et al., 2009; Williams et al., 2006; Xu and Hood, 2006). This study presents a new modeling tool and its application to understand metabolic responses to nutrient loading and the associated O_2 dynamics over multiple temporal and spatial scales.

ROMS-RCA reproduced seasonal and spatial patterns of chl-*a*, O_2, and dissolved and particulate material in Chesapeake Bay. The fact that reasonable model-data fits were achieved across a 10-year simulation, during which large variations in climatic forcing and nutrient loading occurred, suggests the model is robust and valuable for simulation experiments. Especially important is the models' ability to reproduce large interannual variations in phytoplankton biomass, dissolved O_2, and sediment-water fluxes associated with variations in freshwater input and nutrient loads. Despite some obvious limitations of the model (over-prediction of surface-water chl-*a* and inorganic nutrients, bottom-water O_2, and under-prediction of hypoxic volume in dry years), the model qualitatively performs as well as similar models in Chesapeake Bay (Cerco, 2000; Xu and Hood, 2006), and can be used for examinations of system behavior in response to external forcing (Li et al., 2009).

A limitation of all coupled hydrodynamic-biogeochemical models that have been applied in Chesapeake Bay with O_2 as a state variable is an over-prediction of bottom water O_2 (Cerco, 1995; Xu and Hood, 2006). This is also true for ROMS-RCA, and the problem is more pronounced in years of below-average freshwater flow (Fig. 5.4 & 5.5). Two obvious sources of this error are (1) an over-prediction of physical replenishment (advection, vertical diffusion) or (2) an under-estimation of biogeochemical O_2 uptake. The application of ROMS utilized here (Li et al., 2005) generates vertical salt gradients (i.e., stratification) that are occasionally much weaker than those observed in Chesapeake Bay, especially along the deep, central channel in the upper Bay during the winter-spring period (Appendix V). Such weak stratification results from the fact that (1) the model domain is somewhat shallower than the Bay in some regions of the central channel (maximum depth = 25 m in ROMS, 52 m in the Bay), restricting the landward transport of salt, as well as (2) the lack of wind-forcing data that represent true over-water wind stress and its spatial variability, as different wind formulations can generate large differences in vertical salt structure (Li et al., 2005). Although better wind fields and higher-resolution model grids will solve some of these problems, the O_2 over-prediction occurs in models that predict stronger stratification (Xu and Hood, 2006). Considering the dependence of biogeochemical model parameterizations on the physical model simulation (Doney et al., 2004; Skogen and Moll, 2005), it is critical to achieve the best hydrodynamic simulations possible.

Biogeochemical O_2 uptake is another obvious source of model error. Although limited water-column respiration data were available for the years 1996-2005, modeled, bottom-water rates of water column-respiration range seasonally from 6 to 30 mmol O_2

m^{-3} d^{-1}, which are representative of measurements made in several regions of Chesapeake Bay (Sampou and Kemp, 1994; Smith and Kemp, 1995, 2003). Modeled sediment-O_2 demand is also comparable to measurements made at several stations in Chesapeake Bay, ranging from 3 to 70 mmol O_2 m^{-2} d^{-1} and following appropriate seasonal cycles (Fig. 5.5). Model-data O_2 discrepancies, however, are largest during winter-spring in the upper portions of the deep, central channel (Fig. 5.4). Bottom-water chl-*a* accumulations in this region during winter-spring have been shown to be the primary driver of O_2-depletion during this time (Boynton and Kemp, 2000) and in general, ROMS-RCA is unable to reproduce this upper-Bay, bottom-water chl-*a* peak. In another model of Chesapeake Bay, these deep-water chl-*a* maxima were reproduced (Xu and Hood, 2006); however, this model did not include a sediment-submodel, and chl-*a* was allowed to accumulate in bottom cells as opposed to being deposited to sediments. In ROMS-RCA, phytoplankton biomass is deposited to sediments, thus removing it from the water-column. In a simulation of the year 2000, where chl-*a* was not allowed to deposit to sediments, bottom-water chl-*a* and POC increased by 50-100% and dissolved O_2 decreased by 20-40 μM during May (data not shown), suggesting that accurate representations of bottom-water chl-*a* will improve the O_2 model. It is unclear what mechanisms may be responsible for maintaining high- chl-*a* in bottom waters, but resuspension associated with the Estuarine Turbidity Maximum (Sanford et al., 2001), turbulence (Huisman et al., 2002), or motility (Sellner, 1991) could all be at play. In fact, winter-spring phytoplankton biomass near station 3.3C (Fig. 5.1) in the year 2000 was dominated by *Heterocapsa rotundata*, a dinoflagellate that is motile, tolerant of low-light, and known to bloom in colder months near the landward shoaling of the deep channels in Chesapeake

tributary estuaries (Sellner, 1991). New model formulations that account for these types of phytoplankton may lead to improved model performance.

Nutrient loading experiments revealed key spatial and temporal aspects of phytoplankton growth and nutrient limitation. That is, modeled phytoplankton biomass responses to nutrient load experiments were consistent with observed patterns of nutrient limitation in Chesapeake Bay. Late-spring phytoplankton biomass was elevated in seaward regions under elevated nitrogen loads, while upper-middle Bay phytoplankton biomass was elevated under elevated phosphorus loads (Fig. 5.7). This pattern is consistent with phosphorus-limitation of algal growth in lower-salinity water in spring, and nitrogen limitation in higher-salinity water during summer (Fisher et al., 1992; Malone et al., 1996). The fact that doubled nitrogen loads had a limited impact on mid-Bay phytoplankton biomass, especially in spring (Fig. 5.8), is associated with phosphorus-limitation in this region and season (Malone et al., 1996). However, doubled nitrogen loads increased summer phytoplankton biomass by 50% in the lower Bay, where nitrogen limitation was present (Malone et al., 1996). Considering this seasonal and regional pattern of nutrient limitation, doubled N+P loads increased phytoplankton biomass Bay-wide, as upper and middle Bay regions were relieved of P-limitation and seaward regions relieved of N-limitation. These results emphasize the already-appreciated need for a dual nutrient reduction strategy for water quality management in Chesapeake Bay and other, similar coastal ecosystems (Boesch et al., 2001; Greene et al., 2009; Paerl et al., 2004).

Elevated nutrient loads were associated with an expansion of low-O_2 water vertically, longitudinally (N-S), and laterally (E-W). The most striking expansion occurred along the

Bay's north-south axis, where elevated net primary production (NPP) and water column respiration in seaward regions (associated with elevated nitrogen loads) caused elevated O_2 demand in this region (Figs. 9, 12, 14). This suggests that nitrogen loads generate larger hypoxic volumes than phosphorus loads because elevated nitrogen increases production and respiration in nitrogen-limited, seaward Bay regions. Patterns of long-term chl-*a* concentration reveal that over the last six decades, chl-*a* has increased more in the lower Bay than other regions (Harding and Perry, 1997), thus linking elevated nitrogen loads over those decades with lower Bay production. Indeed, increases in hypoxic volume in Chesapeake Bay are often realized by a seaward expansion of the volume to the lower Bay (Hagy et al., 2004). Interestingly, although local, photic-layer NPP was nearly sufficient to balance respiration in underlying waters of the very lower Bay (Fig. 5.12), respiration exceeded NPP in middle Bay regions. NPP exceeded respiration in adjacent shallow waters, which flank the central channel, suggesting that lateral transport of organic material was important to meet respiration demands, as was suggested for the Patuxent River estuary (Testa and Kemp, 2008), observed directly in the mainstem of Chesapeake Bay [*Smith and Kemp, unpublished*], and implied by consistently higher chl-*a* in western, shallow water stations relative to central channel stations during summer months (Appendix IV).

Hypoxic-volume-days (*HVD*) were consistently higher under elevated nutrient loads, but the response varied for nitrogen versus phosphorus. *HVD* was more sensitive to nitrogen loads than phosphorus, which results from widespread nitrogen limitation in seaward Bay regions summer months (Fisher et al., 1992) that led to higher NPP and phytoplankton biomass in these regions under elevated nitrogen loads or much lower

NPP and biomass under reduced loads (Fig. 5.7 & 5.12). Relatively lower sensitivity to P-loads results from the fact that P is limiting in winter-spring in the upper and middle Bay, a time where NPP appears to be a less important driver of summer hypoxic volumes (Fig. 5.14). The fact that HVD was more sensitive to combined N+P load changes reveals the potential for alternating nutrient limitation if the load is dominated by either N or P, especially during transitional periods in Chesapeake Bay where P is limiting in spring and N is limiting in summer (Malone et al., 1996). During the N0.05x experiment (very low N loads), nitrogen became the limiting nutrient throughout the year in the middle and lower Bay (Fig. 5.8; N is limiting when "N-Limitation Term" < "P-Limitation Term"). In contrast, during the N2x experiment, N-limitation was maintained in the lower Bay (CB6.1; Fig. 5.8, while P-limitation was predominant in spring in the middle and lower Bay. These results highlight previously-underemphasized seasonal dynamics associated with hypoxia-nutrient load relationships, as well as the interacting role of N and P loads in controlling hypoxic volume, which have been highlighted in other large coastal ecosystems (Conley et al., 2009b; Greene et al., 2009).

HVD responded non-linearly to nitrogen loads over the range of the simulations, where January to May TN loads varied over 2 orders of magnitude. Although the N-load-*HVD* relationship was linear over the range of nitrogen loads that have recently been observed in Chesapeake Bay (Hagy et al., 2004; Murphy et al., 2011), these simulations suggest that *HVD* would saturate (600 km^3-d) at loads approaching twice that of conditions in 2000. However, simple mechanistic models that simulate Chesapeake Bay hypoxia also predict similar, non-linear relationships between TN load and hypoxic volume (Liu et al., 2011; Liu and Scavia, 2010), although estimates at the low-end of the

loading range have not been observed. Although this saturating relationship in the ROMS-RCA output is possibly constrained by the circulation and mixing patterns specific to the year 2000, *HVD* is larger than the 600 km^3-d maximum at saturating N load levels when the P load has been doubled (Fig. 5.10). This suggests that (1) more widespread P-limitation develops at the higher N loads and (2) a physical or bathymetric limit to *HVD* has not been reached even at doubled N+P loads. It is also noteworthy that the highest sensitivity of *HVD* to N-load occurs at a load of 24 Gg, which is below the 1985-2009 mean loading level. If HVD is plotted against N load for each year from the more realistic 1996-2005 simulation, the *HVD* tends to fall below the functional curve in Figure 5.11 for years with below-average Susquehanna Flow (lower *HVD*/load), while *HVD*/load is higher in above-average flow years. As hypoxic volume may be controlled more by physical processes than biogeochemistry in early summer (Murphy et al., 2011; Scully, 2010a), this variation may be explained by inter-annual variations in physical transport.

Several other studies have examined ecosystem responses to nutrient loading changes using coupled physical-biogeochemical models. These studies have generally found a variety of ecosystem responses to changes in nutrients loading, ranging from relatively straightforward dynamics (Billen et al., 2001; Cerco, 1995), to complex responses due to differential responses of phytoplankton communities (Neumann et al., 2002), and the potential for thresholds associated with biogeochemical changes (Murray and Parslow, 1999). Such varied responses are likely due to differences between ecosystems (river versus estuary), models (diversity of kinetically-unique phytoplankton groups), and the range of nutrient loads tested. A consequence of understanding this complexity is that we

must consider that nutrient load-hypoxia relationships are not necessarily linear (Testa and Kemp, 2011), even within a specific ecosystem. Analysis of the N load-hypoxia relationship found here for Chesapeake Bay reveals that in this system, spatial and seasonal patterns of nutrient limitation modulate the response of Chesapeake Bay to nutrient loads, leading to spatial-dependencies and non-linear behavior. In other systems, more linear behavior is generally associated with loads of material that is oxidized directly (e.g., NH_4^+, BOD), such as in systems close proximity to large population centers (Billen et al., 2001; Soetaert et al., 2006).

Perhaps the clearest conclusion of the nutrient load simulations for Chesapeake Bay is the importance of summer NPP and respiration in driving the Bay's response to nitrogen loading. This is significant because recent historical data analyses have suggested that declines in late summer (July-August) hypoxic volume are associated with modest declines in January to May Susquehanna River nitrogen loads (Murphy et al., 2011). Such analyses did not, however, provide data to illustrate the specific mechanisms connecting reduced winter-spring TN loads to July-August hypoxic volumes. As this and other studies (Fisher et al., 1992) have shown, nitrogen limitation is the primary control on phytoplankton growth during summer throughout much of Chesapeake Bay. Model simulations clearly display that NPP, phytoplankton biomass, and respiration during the summer period are more sensitive to nitrogen additions than during spring (Fig. 5.8, 5.12, 5.14), especially in the lower Bay. In addition to this local respiration, lower Bay organic matter production could be transported landward in bottom waters (Appendix VI) to fuel the respiration observed in the middle Bay (Kemp et al., 1997). In a separate model simulation, where summer phytoplankton were not allowed to grow (Appendix III),

bottom-water O_2 was replenished to non-hypoxic levels beginning in mid-June; that is, summer phytoplankton growth and subsequent respiration were necessary to maintain hypoxia throughout summer. Additionally, N-loading enhancement of lower Bay water-column respiration was a primary driver of interannual variations in hypoxic volume in the 10-year simulation in Chesapeake Bay. These simulation results clearly identify nitrogen load as a clear driver of mid-late summer hypoxic volume in Chesapeake Bay.

Acknowledgements

I must thank my co-authors on the manuscript version of this chapter, including Yun Li, Younjoo Lee, Ming Li, Damian Brady, Dominic Di Toro, and W. Michael Kemp. Yun Li coupled ROMS to RCA and Younjoo Lee executed the 10-year ROMS-RCA run and contributed to the RCA calibration. I would like to thank James Fitzpatrick for the many discussions we have had related to topics covered in this manuscript. I would also like to thank the United States Environmental Protection Agency Chesapeake Bay Program and the Maryland Department of Natural Resources for collecting many of the data presented in this work. Partial funding for our contribution to this work came from the United States National Oceanographic and Atmospheric Administration (NOAA) Coastal Hypoxia Research Program (CHRP-NAO7NOS4780191), the National Science Foundation-funded Chesapeake Bay Environmental Observatory (CBEO-3 BERS-0618986), and by the State of Maryland Department of Natural Resources (K00B920002). This work is NOAA Coastal Hypoxia Research Program (CHRP) Publication # 13X and the University of Maryland Center for Environmental Science Publication # XXXX.

Table 5.1. RCA model equations. Parameter definitions are located at the bottom of this table.

Process	Equation	Notes
(1) Phytoplankton Growth (G_p)	$g_{max,i} * g_T * g_I * g_N$	
(2) Temperature effect (g_T)	$e^{-\beta_1(T-T_{opt,i})^2}$ @ $T \leq T_{opt,i}$ $e^{-\beta_2(T_{opt,i}-T)^2}$ @ $T \geq T_{opt,i}$	
(3) Light effect (g_I)	$\frac{e}{k_d H}\left[exp\left(\frac{-I_o}{I_{s,i}}e^{-k_d H}\right) - exp\left(\frac{-I_o}{I_{s,i}}\right)\right]$	H = cell depth (m), k_d = light attenuation Coefficient (m^{-1}), I_o = Surface Light (ly d^{-1})
(4) Nutrient effect (g_N)	$\min\left(\frac{DIN}{K_{M,N,i}+DIN} * \frac{PO_4^{3-}}{K_{M,P,i}+PO_4^{3-}} * \frac{DSi}{K_{M,Si,i}+DSi}\right)$	
(5) Phytoplankton Respiration (R_P)	$k_{rg,i}GPP_i + k_{rb,i}\theta_{rb,i}^{(T-20)}$	
(6) Grazing (R_{GR})	$k_{gz,i}\theta_{gz,i}^{(T-20)}$	
(7) Phytoplankton Sinking Rate (R_S)	$\left(V_{sPHYT,i} + V_{snlim,i} * [1 - g_N]\right)\theta_{vsphyt}^{(T-20)}$	
(8) Saturating Recycling Term	$R_{SAT} = \frac{TDOC}{K_{M,sat}+TDOC}$	TDOC = LDOC + RDOC
(9) Organic Matter Hydrolysis	$k_{POM}\theta_{POM}^{(T-20)} * R_{SAT}$	POM = organic matter species (e.g., RPON)
(10) Organic C Oxidation	$k_{DOC}\theta_{DOC}^{(T-20)} * R_{SAT} * \frac{K_{M,DOC}}{K_{M,DOC}+O_2}$	DOC = LDOC or RDOC

(11) Remineralization	$k_{DOM}\theta_{DOM}^{(T-20)} * R_{SAT}$	DOM = organic matter species (e.g., RDON)
(12) Nitrification	$k_{NIT}\theta_{NIT}^{(T-20)} * [NH_4^+] * \frac{O_2}{K_{M,NIT}+O_2}$	
(13) Denitrification	$\frac{5}{4} * \frac{12}{14} * k_{DNF}\theta_{DNF}^{(T-20)} * \frac{K_{M,NO3}}{K_{M,NO3}+O_2} * \frac{LDOC}{K_{M,sat}+LDOC}$	
(14) Silica Dissolution	$k_{si}\theta_{si}^{(T-20)} * R_{SAT}$	
(15) O_2 Equivalents Oxidation	$k_{ox}\theta_{ox}^{(T-20)} * \frac{O_2}{K_{M,o2}+O_2} * R_{SAT}$	O_2 Equivalents = CH_4 + H_2S
(16) POM Sinking Rate	$V_{sPOM}\theta_{vsPOM}^{(T-20)}$	

Table 5.2. RCA Model Parameters.

Variable	Value	Units	Variable	Value	Units
Phytoplankton Group 1 (diatoms)			**Phytoplankton Group 2 (dinoflagellates)**		
$T_{OPT,1}$	7	^{o}C	$T_{OPT,2}$	25	^{o}C
$g_{max,1}$	3.2	d^{-1}	$g_{max,2}$	3.4	d^{-1}
$I_{S,1}$	200	ly d^{-1}	$I_{S,2}$	350	ly d^{-1}
$K_{M,N,1}$	0.714	µM N	$K_{M,N,2}$	0.571	µM N
$K_{M,P,1}$	0.032	µM P	$K_{M,P,2}$	0.032	µM P
$K_{M,Si,1}$	0.178	µM Si	$K_{M,Si,2}$	0.71	µM Si
$k_{rb,1}$	0.03	d^{-1}	$k_{rb,2}$	0.025	d^{-1}
$\theta_{rb,1}$	1.047		$\theta_{rb,2}$	1.047	
$a_{N,C,1}$	0.167	mol N mol^{-1} C	$a_{N,C,2}$	0.167	mol N mol^{-1} C
$a_{P,C,1}$	0.009	mol P mol^{-1} C	$a_{P,C,2}$	0.009	mol P mol^{-1} C
$a_{Si,C,1}$	0.171	mol Si mol^{-1} C	$a_{Si,C,2}$	0.171	mol Si mol^{-1} C
k_1b_1	0.004		k_2b_1	0.005	
k_1b_2	0.014		k_2b_2	0.015	
$k_{gz,1}$	0.1	d^{-1}	$k_{gz,2}$	0.1	d^{-1}
$\theta_{gz,1}$	1.03		$\theta_{gz,2}$	1.1	
Hydrolysis and Respiration			**Recycle Fractions**		
$k_{LDOC,N,P}$	0.2	d^{-1}	f_{LPOC}	0.35	
$\theta_{LDOC,N,P}$	1.02		f_{LDOC}	0.50	
$k_{RDOC,N,P}$	0.015	d^{-1}	f_{LPON}	0.15	
$\theta_{RDOC,N,P}$	1.02		f_{RPON}	0.05	
$k_{LPOC,N,P}$	0.1	d^{-1}	f_{LDON}	0.60	
$\theta_{LPOC,N,P}$	1.02		f_{RDON}	0.10	
$k_{RPOC,N,P}$	0.025	d^{-1}	$f_{NH_4^+}$	0.10	
$\theta_{RPOC,N,P}$	1.02		f_{LPOP}	0.15	
$k_{ExDOC,N,P}$	0.5	d^{-1}	f_{RPOP}	0.05	
$\theta_{ExDOC,N,P}$	1.02		f_{LDOP}	0.60	
k_{Si}	0.2	d^{-1}	f_{RDOP}	0.10	
θ_{kSi}	1.10		$f_{PO_4^{3-}}$	0.10	
Nitrogen Cycling, Sulfide Oxidation			**Sinking Velocities, Recycling**		
k_{NIT}	0.01	d^{-1}	$Vs_{PHYT,1}$	0.30	m d^{-1}
θ_{kNIT}	1.08		$Vs_{PHYT,2}$	0.20	m d^{-1}
$K_{m,NIT}$	31.25	µM O_2	θ_{Vsphyt}	1.027	
k_{DNF}	0.05	d^{-1}	Vs_{POM}	0.50	m d^{-1}
θ_{kDNF}	1.045		θ_{Vspom}	1.027	
$K_{m,NO3}$	0.714	µM NO_3^-	$Vs_{nlim,1}$	0.2	m d^{-1}
k_{ox}	0.05	d^{-1}	$Vs_{nlim,2}$	0.2	m d^{-1}
θ_{ox}	1.08		$K_{M,\ sat}$	8.3	µM C
$K_{m,O2}$	3.125	µM O_2	$K_{M,DOC}$	6.25	µM O_2

Table 5.3. Root mean square error (RMSE), reliability index (RI), and correlation coefficient (r) for model-data comparison of water-column state variables during the 1996-2005 period. All concentrations in μM except chlorophyll-*a*, which is mg m^{-3}.

Surface		chl-*a*	O_2	NH_4^+	NO_3^-	PON	DON	PO_4^{3-}	PP	DOP	DSi
CB2.2	RMSE	13.96	32.37	8.95	13.75	12.10	6.93	0.99	0.69	0.14	24.73
Salinity = 2.3	RI	1.68	1.06	1.71	1.14	1.46	1.18	1.60	1.43	1.23	1.40
Depth = 13	r	0.14	0.91	-0.08	0.89	0.06	0.19	0.23	-0.03	-0.25	0.61
CB3.1	RMSE	18.07	38.67	13.12	15.95	14.43	6.72	1.01	0.77	0.18	21.61
Salinity = 4.4	RI	2.01	1.06	2.12	1.39	1.60	1.24	1.87	1.59	1.31	1.44
Depth = 13	r	0.03	0.89	0.02	0.89	-0.001	0.24	0.29	-0.20	-0.01	0.64
CB3.3C	RMSE	19.67	98.85	18.80	15.67	15.50	8.53	1.08	0.66	0.21	19.44
Salinity = 9.2	RI	1.78	121	3.37	1.85	1.51	1.27	2.28	1.51	1.31	1.43
Depth = 26	r	-0.21	0.54	-0.07	0.87	-0.18	0.09	0.15	-0.19	0.12	0.66
CB4.1C	RMSE	19.20	84.98	16.34	19.51	14.27	8.69	0.82	0.6	0.22	17.32
Salinity = 11.1	RI	1.77	1.17	3.46	2.27	1.47	1.27	2.35	1.56	1.43	1.50
Depth = 33	r	-0.15	0.53	-0.03	0.84	-0.05	-0.05	0.39	0.01	0.20	0.66
CB4.2C	RMSE	19.31	47.06	11.24	15.49	12.26	9.86	0.62	0.65	0.27	17.75
Salinity = 11.9	RI	1.87	1.11	3.38	2.43	1.50	1.28	2.26	1.64	1.46	1.63
Depth = 28	r	0.05	0.69	0.11	0.79	0.14	-0.01	0.51	0.13	0.19	0.68
CB4.3C	RMSE	19.30	49.9	12.70	14.17	12.35	9.17	0.70	0.69	0.25	20.93
Salinity = 12.2	RI	1.89	1.09	3.48	2.27	1.50	1.27	2.37	1.67	1.42	1.72
Depth = 28	r	0.04	0.68	0.09	0.80	0.11	-0.13	0.38	0.06	0.23	0.65
CB5.2	RMSE	15.80	37.72	8.24	11.35	8.83	7.21	0.48	0.60	0.22	19.38
Salinity = 14.1	RI	1.65	1.08	2.43	1.98	1.26	1.24	1.85	1.48	1.36	1.81
Depth = 33	r	0.39	0.78	0.24	0.77	0.32	0.03	0.37	0.44	0.19	0.59
CB6.1	RMSE	13.16	50.23	3.68	6.23	8.43	9.32	0.43	0.40	0.28	19.46
Salinity = 16.7	RI	1.97	1.14	3.25	2.35	1.44	1.28	3.02	1.65	1.59	2.42
Depth = 14	r	0.33	0.78	0.48	0.66	0.28	0.07	0.11	0.53	0.18	0.47

Bottom		chl-*a*	O_2	NH_4^+	NO_3^-	PON	DON	PO_4^{3-}	PP	DOP	DSi
CB2.2	RMSE	15.36	64.37	12.58	20.08	16.05	5.86	1.04	1.99	0.14	24.99
Salinity = 2.3	RI	1.91	1.14	1.96	1.62	1.54	1.34	1.79	1.86	1.53	2.07
Depth = 13	r	0.26	0.77	-0.10	0.77	0.16	0.16	0.40	0.01	-0.21	0.62
CB3.1	RMSE	22.31	68.70	16.75	19.95	18.82	7.47	1.20	1.76	0.19	25.65
Salinity = 4.4	RI	2.03	1.30	2.05	1.94	1.55	1.34	2.02	1.82	1.60	2.20
Depth = 13	r	0.33	0.83	0.42	0.78	0.37	-0.06	0.50	0.12	-0.05	0.77
CB3.3C	RMSE	15.86	84.47	12.87	7.61	15.24	6.97	0.62	0.80	0.17	22.93
Salinity = 9.2	RI	1.67	1.39	1.64	2.28	1.33	1.16	1.50	1.49	1.37	1.55
Depth = 26	r	0.40	0.83	0.80	0.71	0.41	-0.21	0.84	0.29	0.01	0.84
CB4.1C	RMSE	15.88	79.32	13.74	6.20	14.18	7.10	0.64	0.83	0.16	23.78
Salinity = 11.1	RI	2.47	2.21	2.19	3.51	1.63	1.26	1.86	1.94	1.64	1.87
Depth = 33	r	0.47	0.85	0.78	0.71	0.50	-0.16	0.83	0.43	-0.05	0.84
CB4.2C	RMSE	14.64	66.09	13.60	5.16	12.19	7.41	0.67	0.71	0.18	22.66
Salinity = 11.9	RI	2.40	1.49	2.18	3.09	1.59	1.26	1.91	1.90	1.60	1.86
Depth = 28	r	0.49	0.89	0.80	0.69	0.52	-0.25	0.79	0.42	-0.24	0.78
CB4.3C	RMSE	13.56	56.93	13.72	4.93	10.93	6.32	0.67	0.68	0.15	21.80
Salinity = 12.2	RI	2.11	1.44	2.15	2.94	1.54	1.23	1.94	1.85	1.58	1.86
Depth = 28	r	0.49	0.91	0.82	0.70	0.54	-0.14	0.81	0.36	-0.08	0.83
CB5.2	RMSE	12.68	55.44	10.54	3.77	10.32	5.73	0.65	0.66	0.17	19.27
Salinity = 14.1	RI	2.11	1.69	2.17	2.71	1.52	1.22	1.98	1.81	1.56	1.90
Depth = 33	r	0.63	0.92	0.76	0.67	0.58	-0.20	0.70	0.34	-0.22	0.73
CB6.1	RMSE	12.67	61.05	7.77	3.62	12.39	5.72	0.78	0.70	0.20	15.27
Salinity = 16.7	RI	1.72	1.33	2.08	2.61	1.50	1.20	2.65	1.64	1.42	1.84
Depth = 14	r	0.60	0.90	0.69	0.40	0.49	-0.29	0.69	0.25	-0.30	0.67

Figure Legends

Figure 5.1: Map of Chesapeake Bay bathymetry (left panel), illustration of ROMS-RCA model grid (with 20 vertical sigma-layers) with wet cells in red (middle panel), and map of Chesapeake Bay with the locations of water-column monitoring stations (chl-*a*, O_2, salinity, nutrients, carbon, blue circles) and sediment-water flux observation stations (red squares).

Figure 5.2: Schematic diagram of the major state variables and transformation process in RCA (see methods for further detail).

Figure 5.3: Seasonal patterns of major climatic and hydrographic conditions in Chesapeake Bay during the year 2000. (top) Mean Susquehanna River flow (blue dashed line) with daily minimum and maximum flows (red dashed lines) for the 1985-2010 period, and the Susquehanna hydrograph for 2000 (black solid line). (2^{nd} from top) Mean daily wind speed measured at the Patuxent River Naval Air Station from 1985-2010 (blue line) and for the year 2000 (green line). 1985-2010 annual cycle (solid lines) of water temperature (2^{nd} from bottom) and salinity (bottom) at a station in the middle of Chesapeake Bay (CB4.3C) with 1985-2010 minima and maxima (dashed lines). Circles are for the year 2000.

Figure 5.4: Time-series of observed (red circles) and modeled (black lines) surface-layer chl-*a* (left panel) and bottom-layer dissolved O_2 (right panel) at three stations (CB3.3C in upper Bay, CB4.3C in middle Bay, and CB6.1 in lower Bay) in Chesapeake Bay for the model simulation period spanning 1996-2005.

Figure 5.5: Comparisons of simulated sediment-water NH_4^+ (left panel) and O_2 (right panel) flux (1996-2005 mean is solid black line, minima and maxima are dotted lines) with observations (red circles ± 1 SD) made over various years between 1985 and 1996 in three regions of Chesapeake Bay corresponding to CB3.3C in the upper Bay, CB4.3C in the middle Bay, and CB6.1 in the lower Bay.

Figure 5.6: Time-series (1996-2005) of Susquehanna River Flow (top panel) and observed (red circles) and simulated (blue lines) hypoxic volume (bottom panel) in Chesapeake Bay.

Figure 5.7: Surface-layer distributions of early June modeled chl-*a* for several nutrient load experiments, including alterations of N (left panel), P (middle panel), and N+P (right panel) loading, including a 75% reduction (0.25x, top panels), the year 2000 observed case (1x, middle panels), and a doubling case (2x, bottom panels).

Figure 5.8: Annual cycle of modeled surface-layer diatom group biomass (top panel), summer group biomass (2nd panel from top), nitrogen limitation term (2nd panel from bottom), and phosphorus limitation term (bottom panel) at two stations (CB4.3C, left panels, CB6.1, right panels) in Chesapeake Bay under 3 nitrogen loading simulations (red line=0.05x, blue line=1x, black line=2x).

Figure 5.9: Distributions of modeled dissolved O_2 during June 1-10 in 2000 for three nitrogen loading simulations, including N0.25x (top panel), N1x (middle panel), and N2x (bottom panel). Hypoxic water is indicated by dark red colors.

Figure 5.10: Comparison of modeled hypoxic-volume-days (*HVD*) for several different nutrient loading scenarios (0.25x, 1x, 2x) for nitrogen only (red bars at left), phosphorus only (green bars in middle), and nitrogen+phosphorus (blue bars at right).

Figure 5.11: Relationship between January to May total nitrogen loading and *HVD* from model simulations (green circles) and a logistic curve fit to the data (equation included; see text for description). Logistic curve parameters for the maximum *HVD* (black dotted line) and the N load where the rate of change in *HVD* is highest (Nlmx; vertical green dashed line) are included, as is the observed TN load for the year 2000.

Figure 5.12: Annual computations of modeled photic-layer integrated net primary production (NPP) and sub-photic layer, integrated respiration (including SOD) for 10 nitrogen load simulations at 4 stations in Chesapeake Bay, including CB2.2 (top panel, upper Bay), CB4.3C (2^{nd} panel from top, middle Bay), CB5.2 (2^{nd} panel from bottom, middle Bay), and CB6.1 (bottom panel, lower Bay).

Figure 5.13: Total model-computed, water-column respiration in three regions of Chesapeake Bay (see Fig. 5.1 for regional boundaries) computed for each of 10 nitrogen load experiments during spring (March-May, top panel) and summer (June-August, bottom panel).

Figure 5.14: Correlations between model-computed, sub-photic layer respiration (top panel) and sediment O_2 demand (bottom panel) and January to May Susquehanna River TN load at two stations in Chesapeake Bay (black circles are CB2.2, white circles are CB5.2). Data are June to August means for each year from the 10-year (1996-2005) simulation.

Fig. 5.1

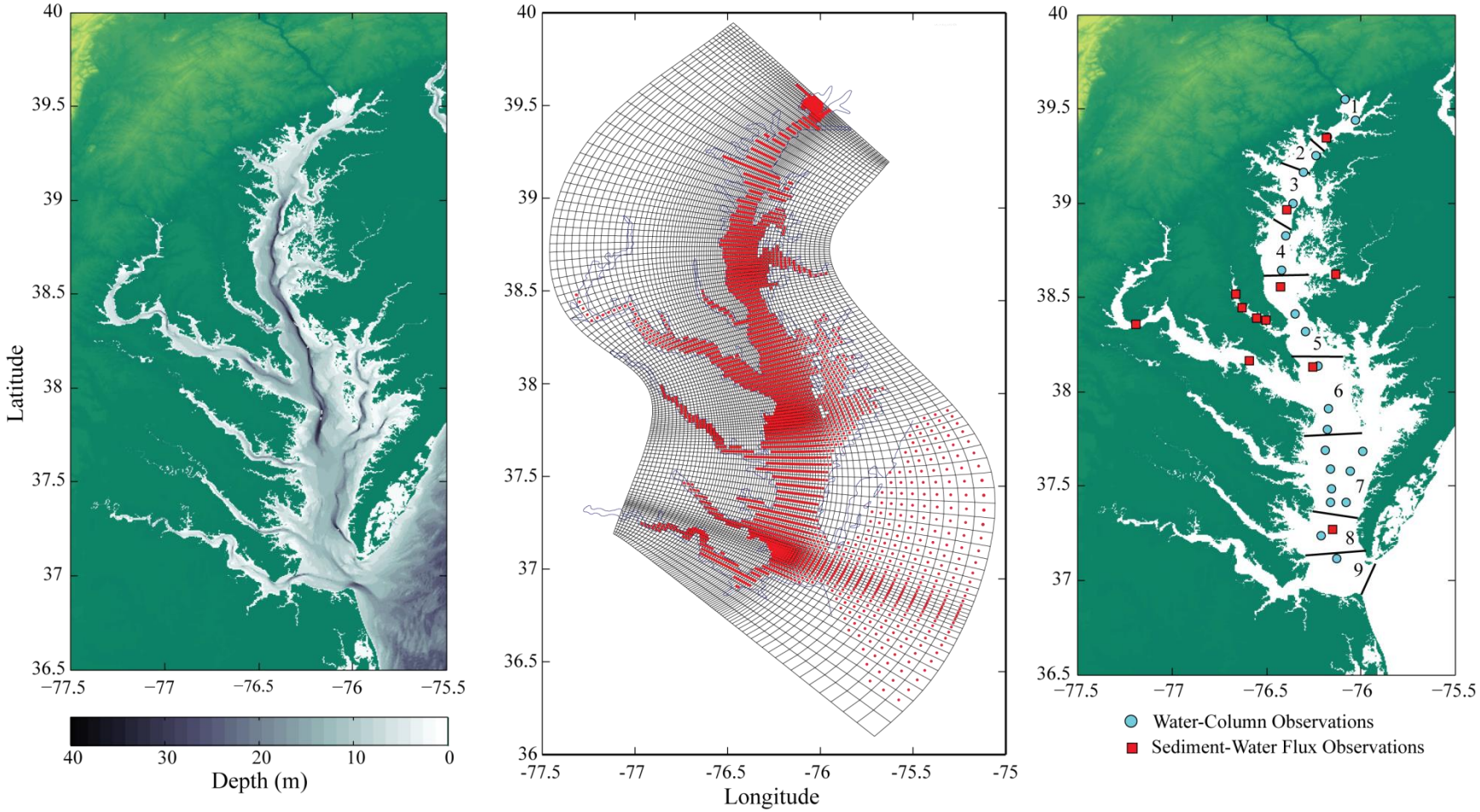
Latitude
Depth (m)
Longitude
Water-Column Observations
Sediment-Water Flux Observations
1
2
3
4
5
6
7
8
9

Fig. 5.2

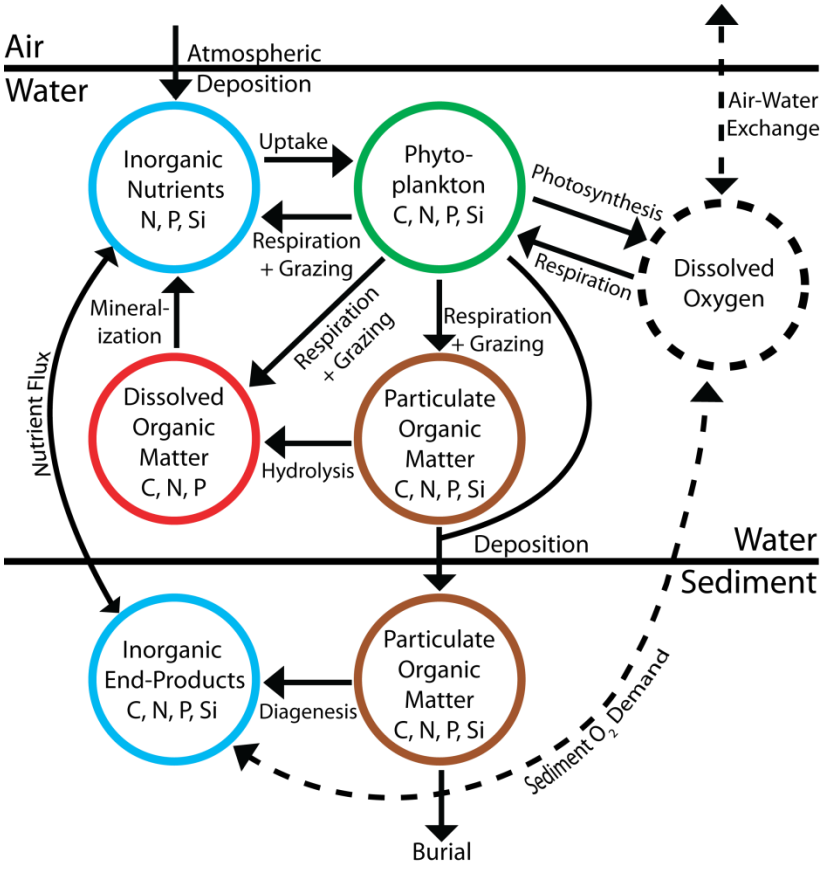
Air
Water
Atmospheric Deposition
Air-Water Exchange
Inorganic Nutrients N, P, Si
Uptake
Phyto-plankton C, N, P, Si
Photosynthesis
Respiration
Dissolved Oxygen
Respiration + Grazing
Mineral-ization
Respiration + Grazing
Respiration + Grazing
Nutrient Flux
Dissolved Organic Matter C, N, P
Hydrolysis
Particulate Organic Matter C, N, P, Si
Deposition
Water
Sediment
Inorganic End-Products C, N, P, Si
Diagenesis
Particulate Organic Matter C, N, P, Si
Sediment O2 Demand
Burial

Fig. 5.3

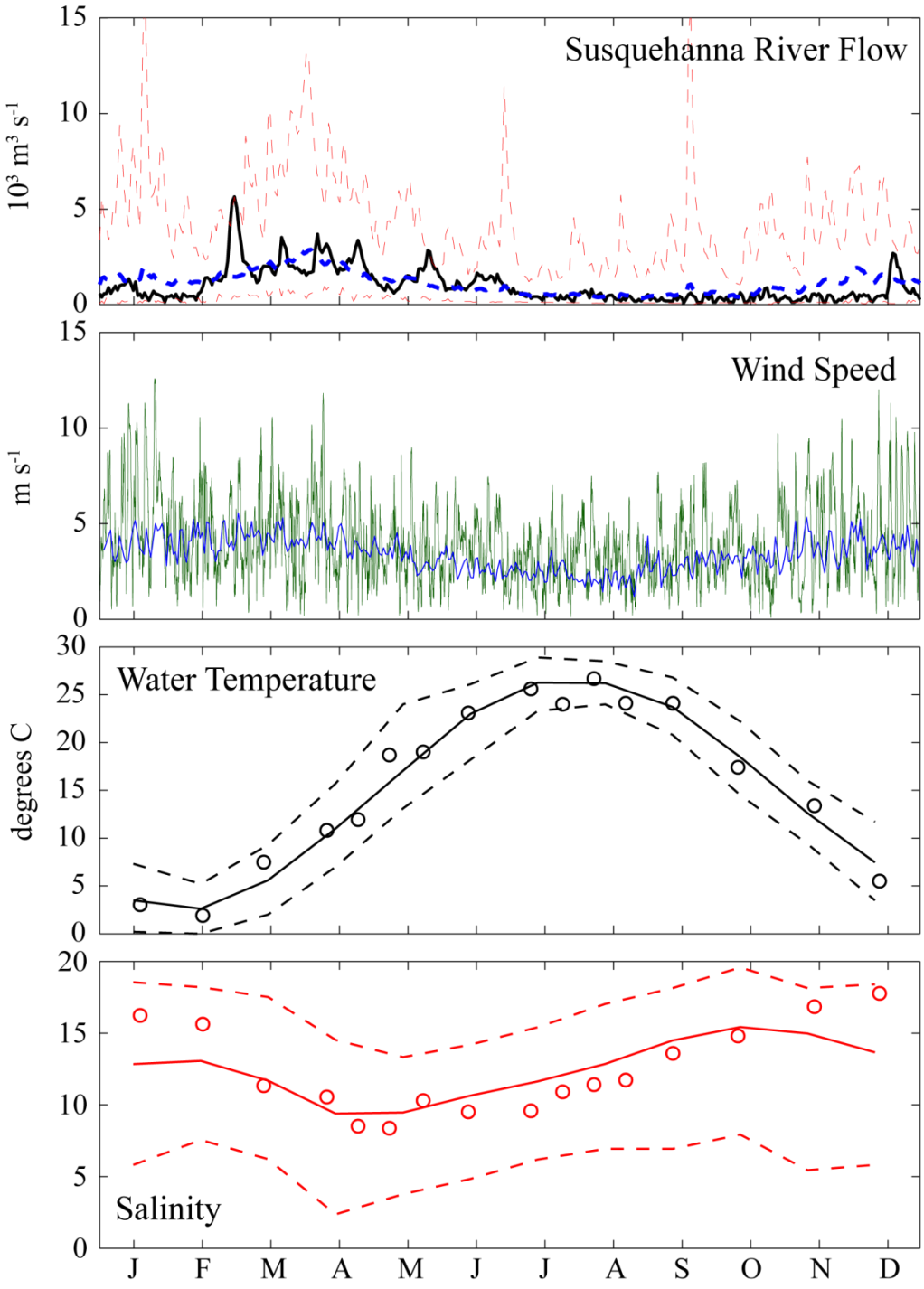
Susquehanna River Flow
10^3 m^3 s^{-1}
Wind Speed
m s^{-1}
Water Temperature
degrees C
Salinity
J F M A M J J A S O N D

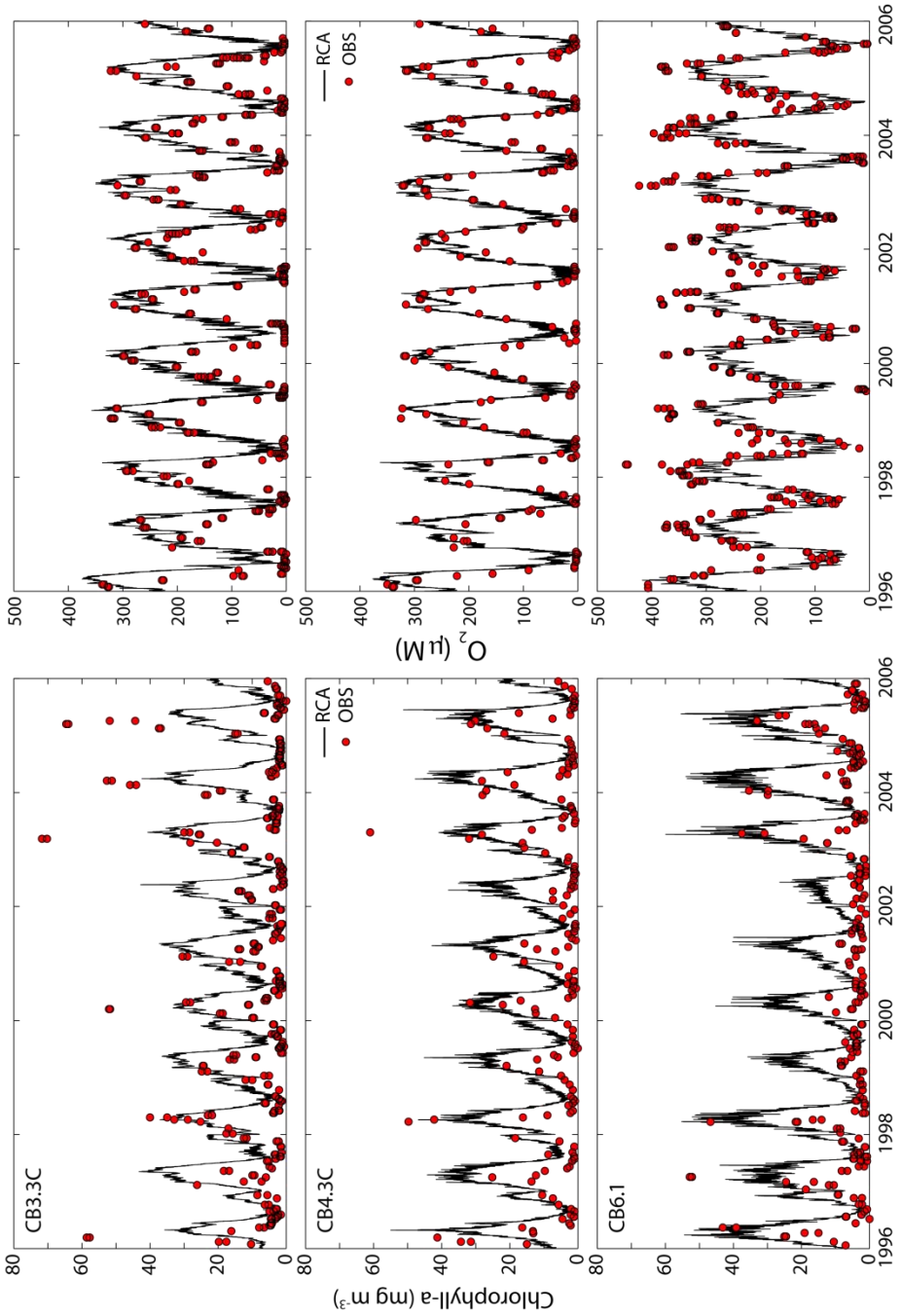
CB3.3C
CB4.3C
CB6.1
RCA
OBS
Chlorophyll-a (mg m-3)
O2 (μM)
0
20
40
60
80
100
200
300
400
500
1996
1998
2000
2002
2004
2006

Fig. 5.4

Fig. 5.5

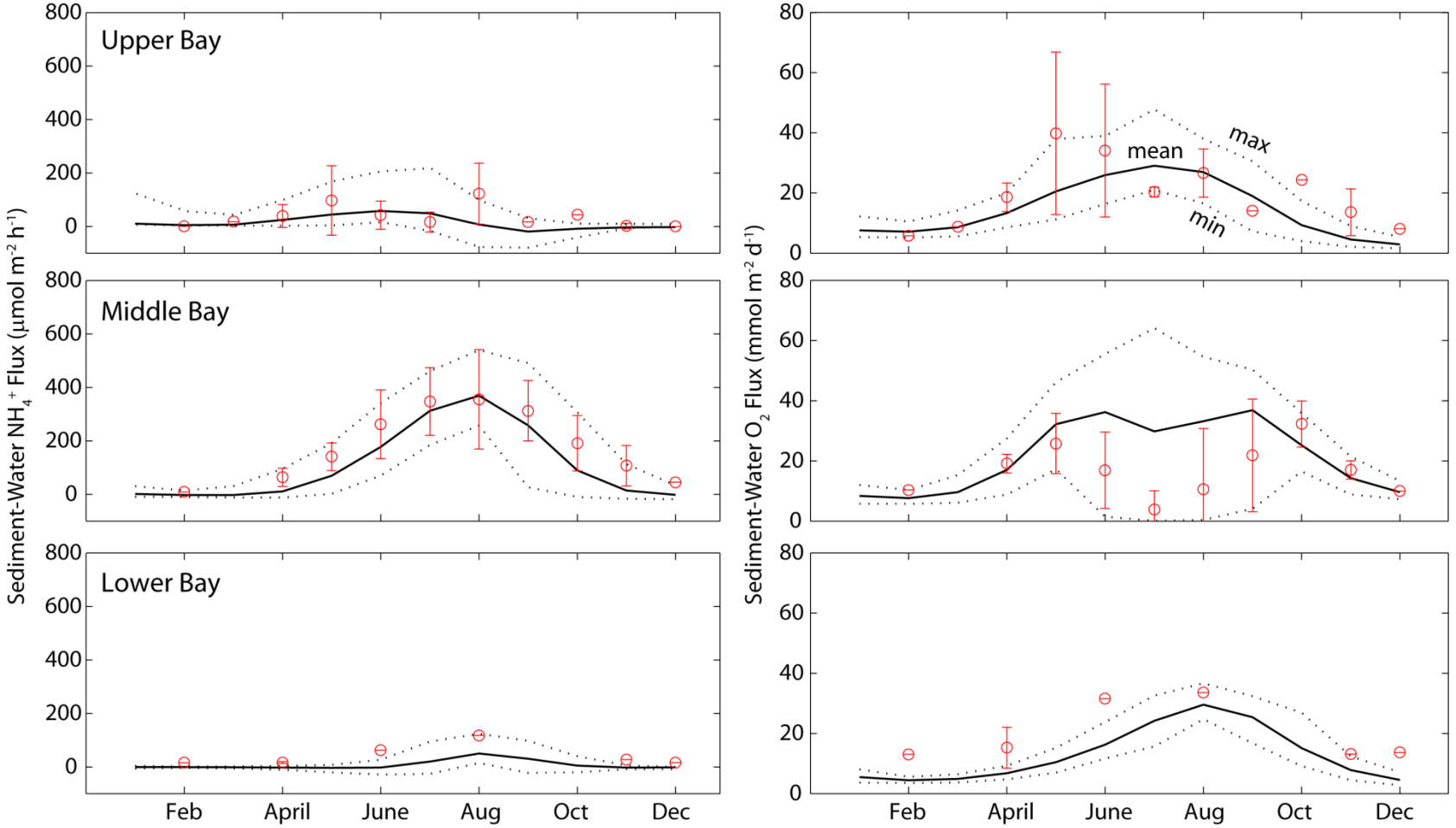
Upper Bay
Middle Bay
Lower Bay
Sediment-Water NH4+ Flux (µmol m-2 h-1)
Sediment-Water O2 Flux (mmol m-2 d-1)
max
mean
min
Feb
April
June
Aug
Oct
Dec

Fig. 5.6

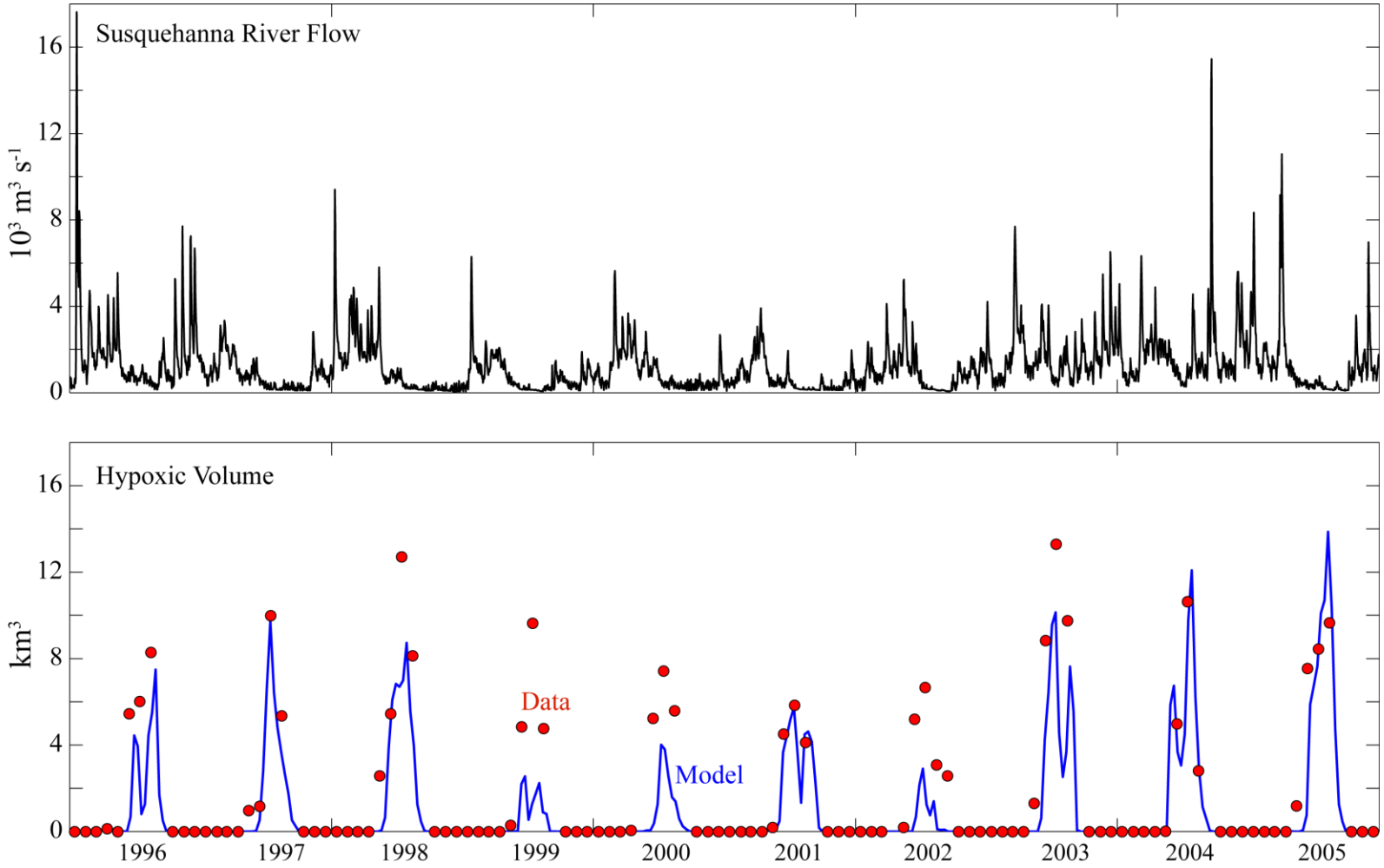
Susquehanna River Flow
10^3 m^3 s^{-1}
0
4
8
12
16
Hypoxic Volume
km^3
0
4
8
12
16
Data
Model
1996
1997
1998
1999
2000
2001
2002
2003
2004
2005

Fig. 5.7

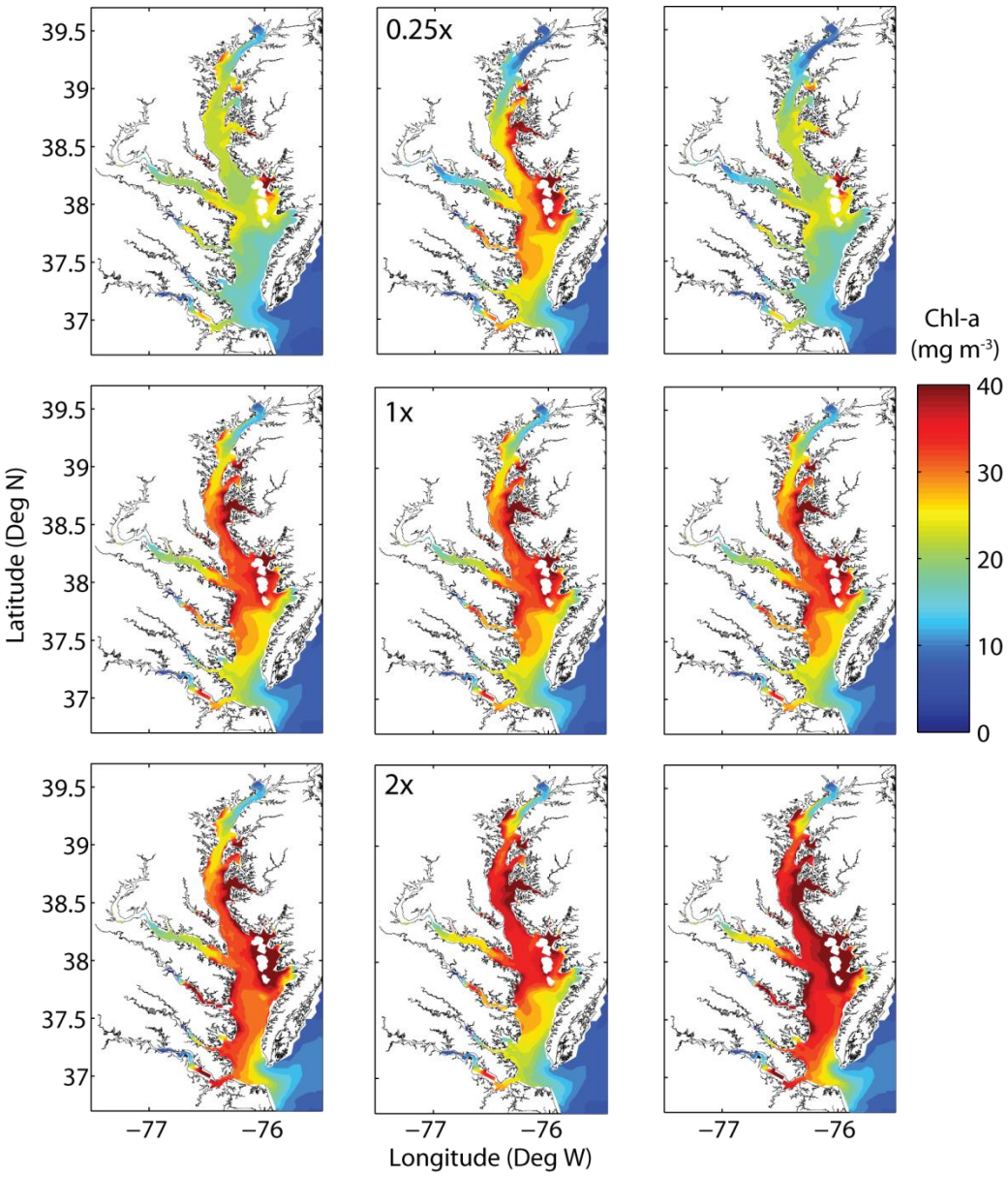
0.25x
1x
2x
Chl-a
(mg m-3)
40
30
20
10
0
Latitude (Deg N)
39.5
39
38.5
38
37.5
37
−77
−76
Longitude (Deg W)

Fig. 5.8

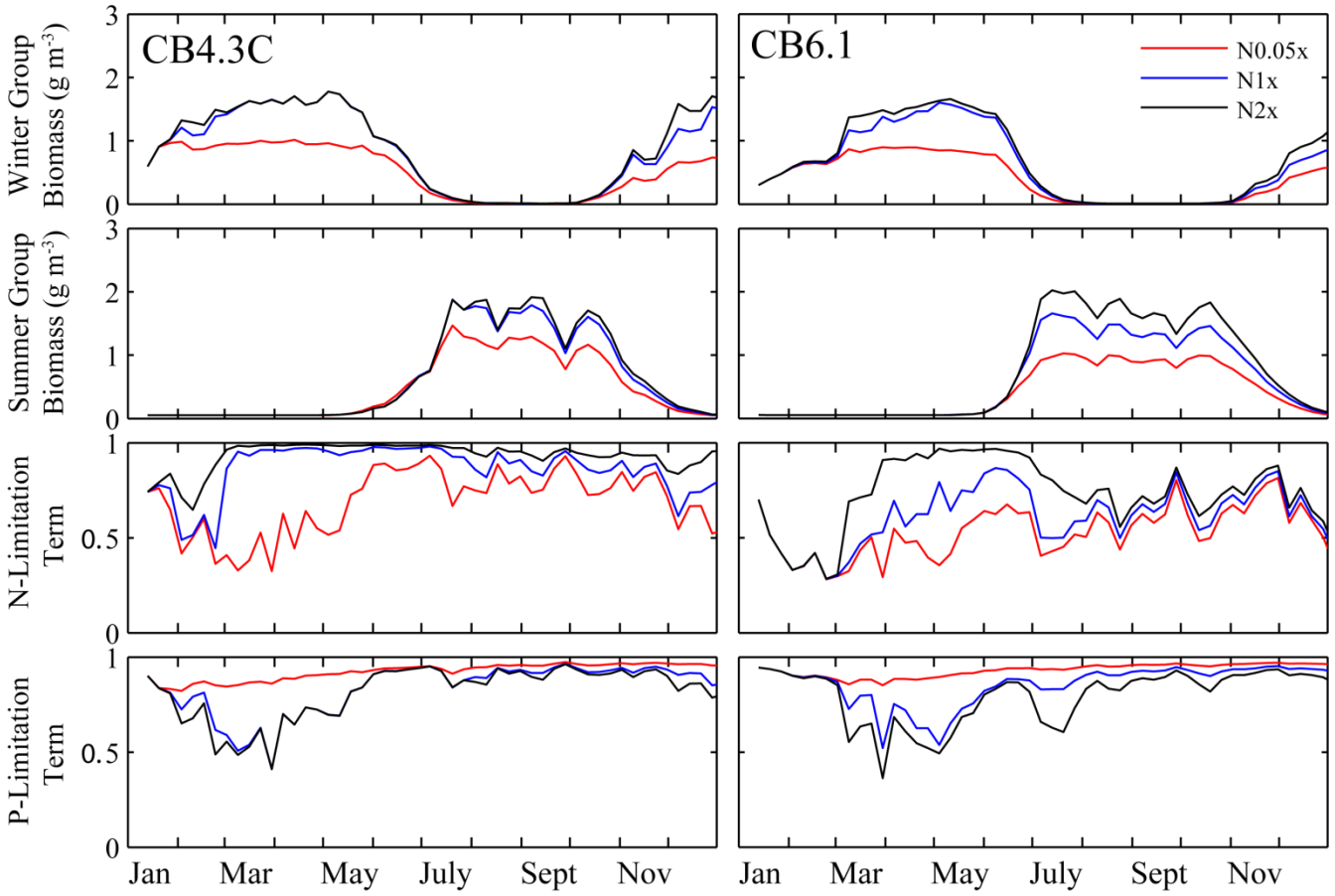
CB4.3C
CB6.1
N0.05x
N1x
N2x
Winter Group Biomass (g m-3)
Summer Group Biomass (g m-3)
N-Limitation Term
P-Limitation Term
0
1
2
3
0.5
Jan
Mar
May
July
Sept
Nov

Fig. 5.9

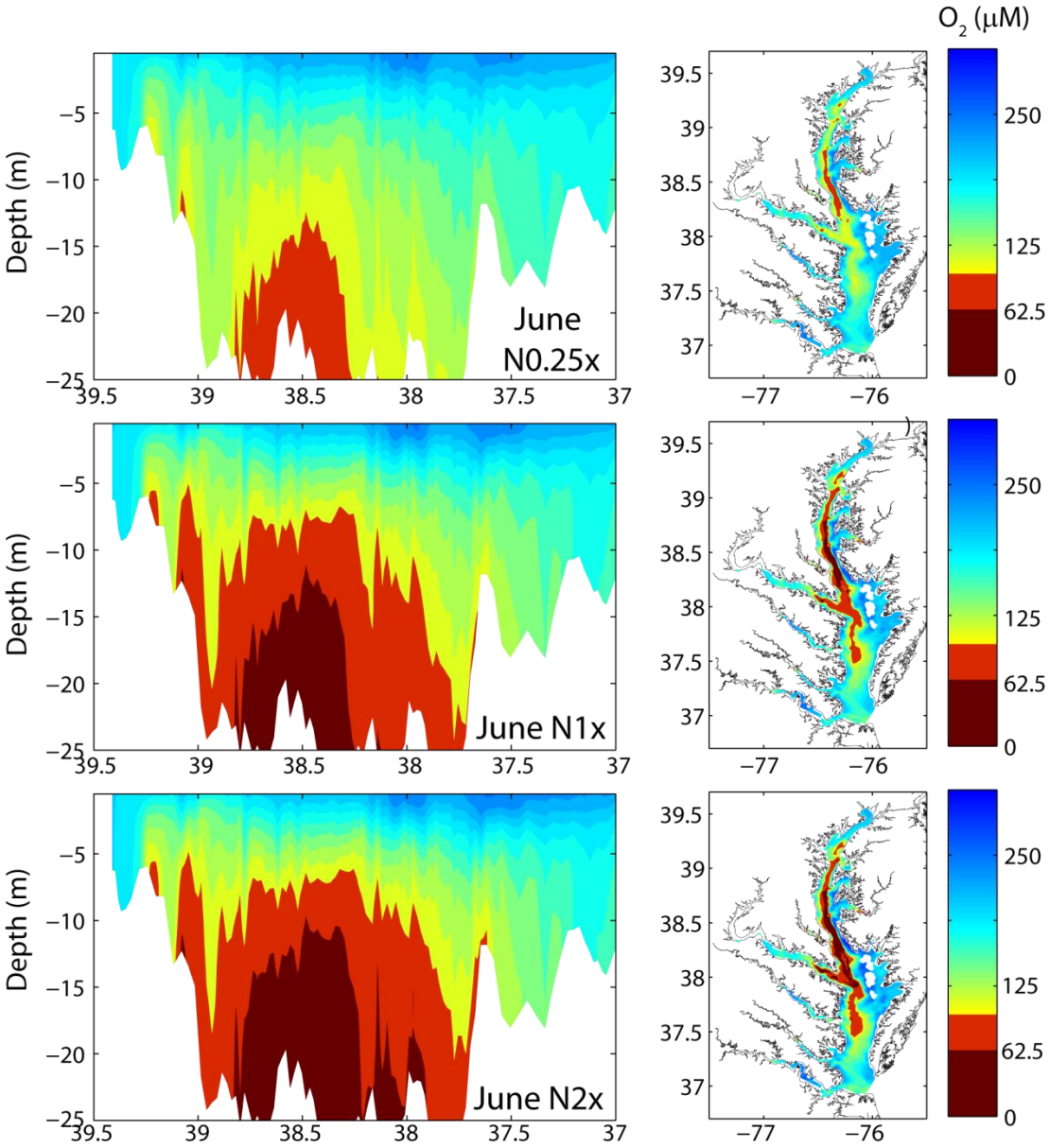
O2 (μM)
Depth (m)
June
N0.25x
June N1x
June N2x
−5
−10
−15
−20
−25
39.5
39
38.5
38
37.5
37
−77
−76
250
125
62.5
0

Fig. 5.10

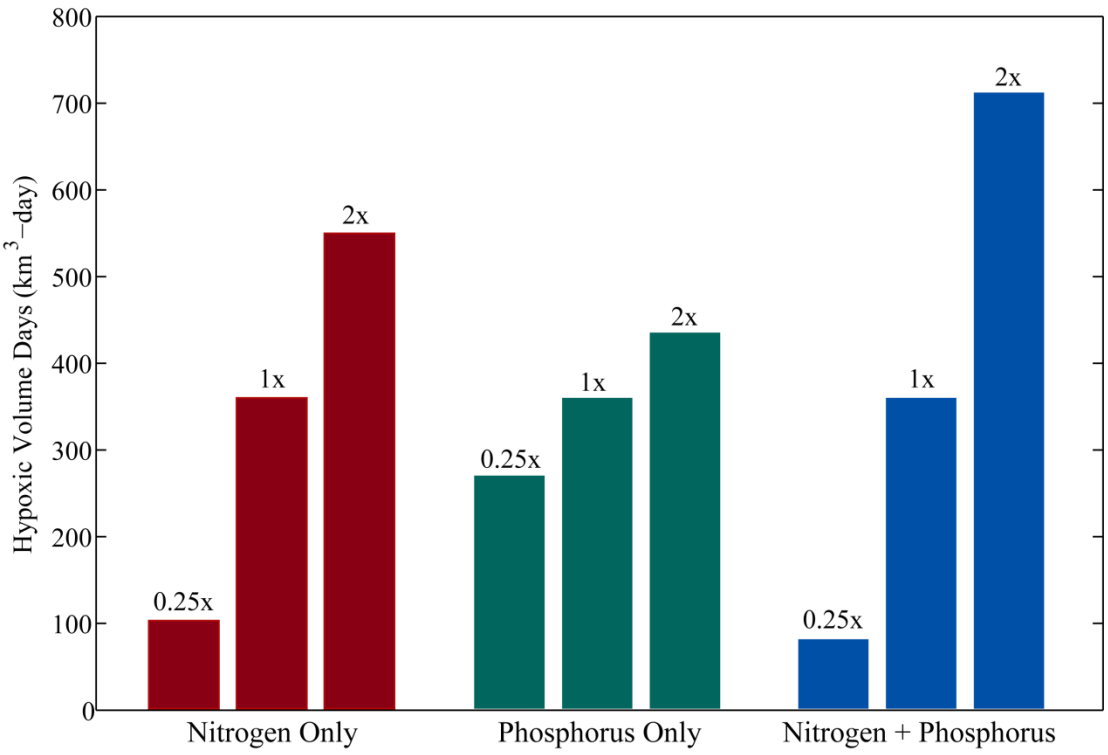
800
700
600
500
400
300
200
100
0
Hypoxic Volume Days (km 3 –day)
0.25x
1x
2x
0.25x
1x
2x
0.25x
1x
2x
Nitrogen Only
Phosphorus Only
Nitrogen + Phosphorus

Fig. 5.11

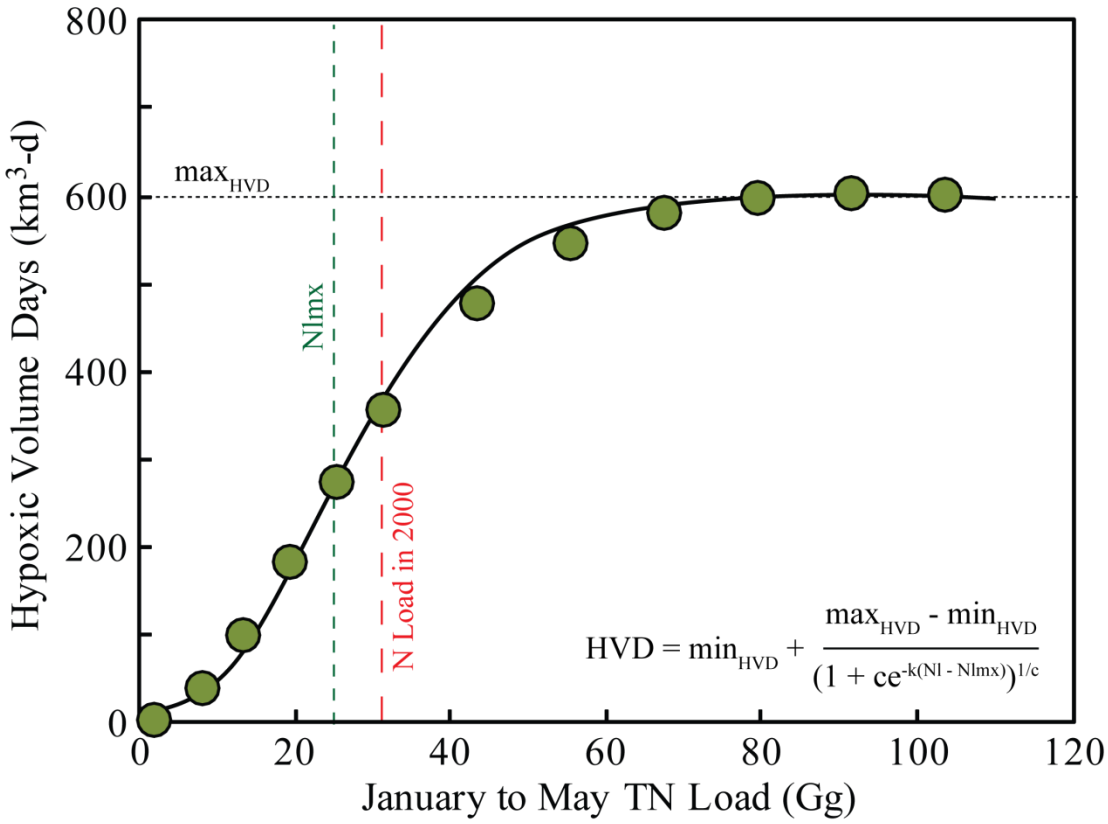
800
600
400
200
0
Hypoxic Volume Days (km3-d)
maxHVD
Nlmx
N Load in 2000
HVD = minHVD + (maxHVD - minHVD) / (1 + ce-k(Nl - Nlmx))1/c
0
20
40
60
80
100
120
January to May TN Load (Gg)

Fig. 5.12

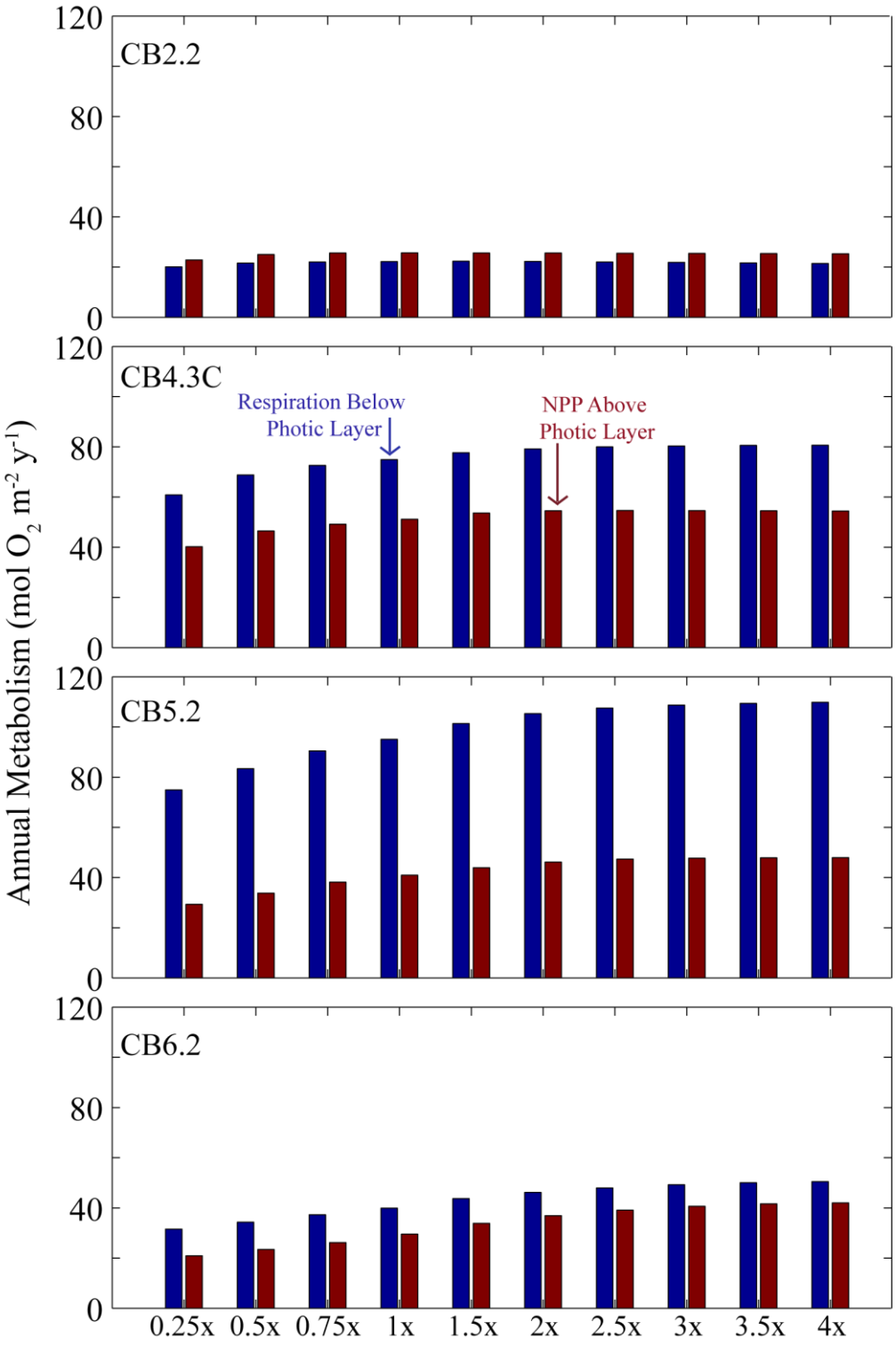
CB2.2
CB4.3C
Respiration Below
Photic Layer
NPP Above
Photic Layer
CB5.2
CB6.2
Annual Metabolism (mol O2 m-2 y-1)
0
40
80
120
0.25x
0.5x
0.75x
1x
1.5x
2x
2.5x
3x
3.5x
4x

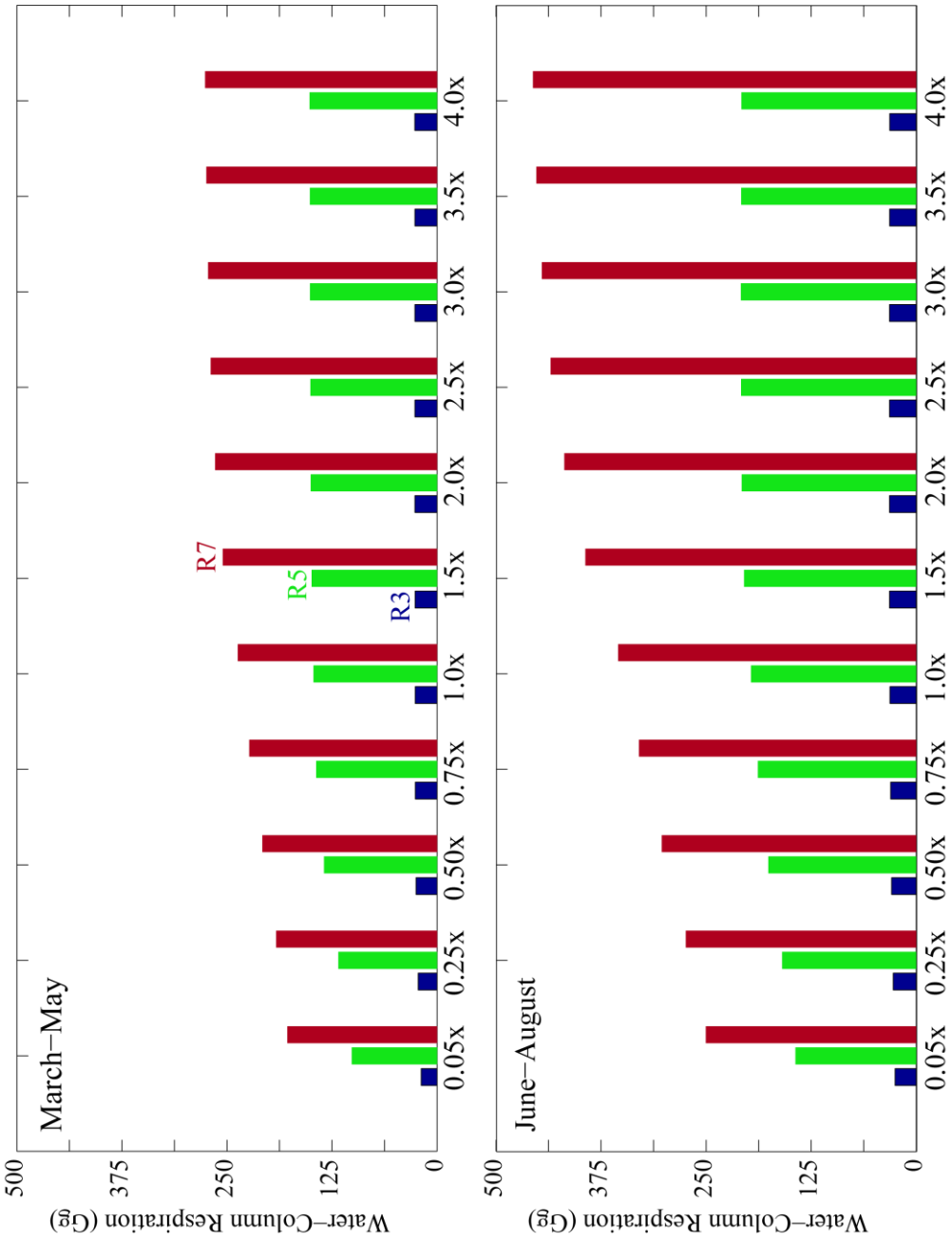
March–May
June–August
Water–Column Respiration (Gg)
0
125
250
375
500
R7
R5
R3
0.05x
0.25x
0.50x
0.75x
1.0x
1.5x
2.0x
2.5x
3.0x
3.5x
4.0x

Fig. 5.13

Fig. 5.14

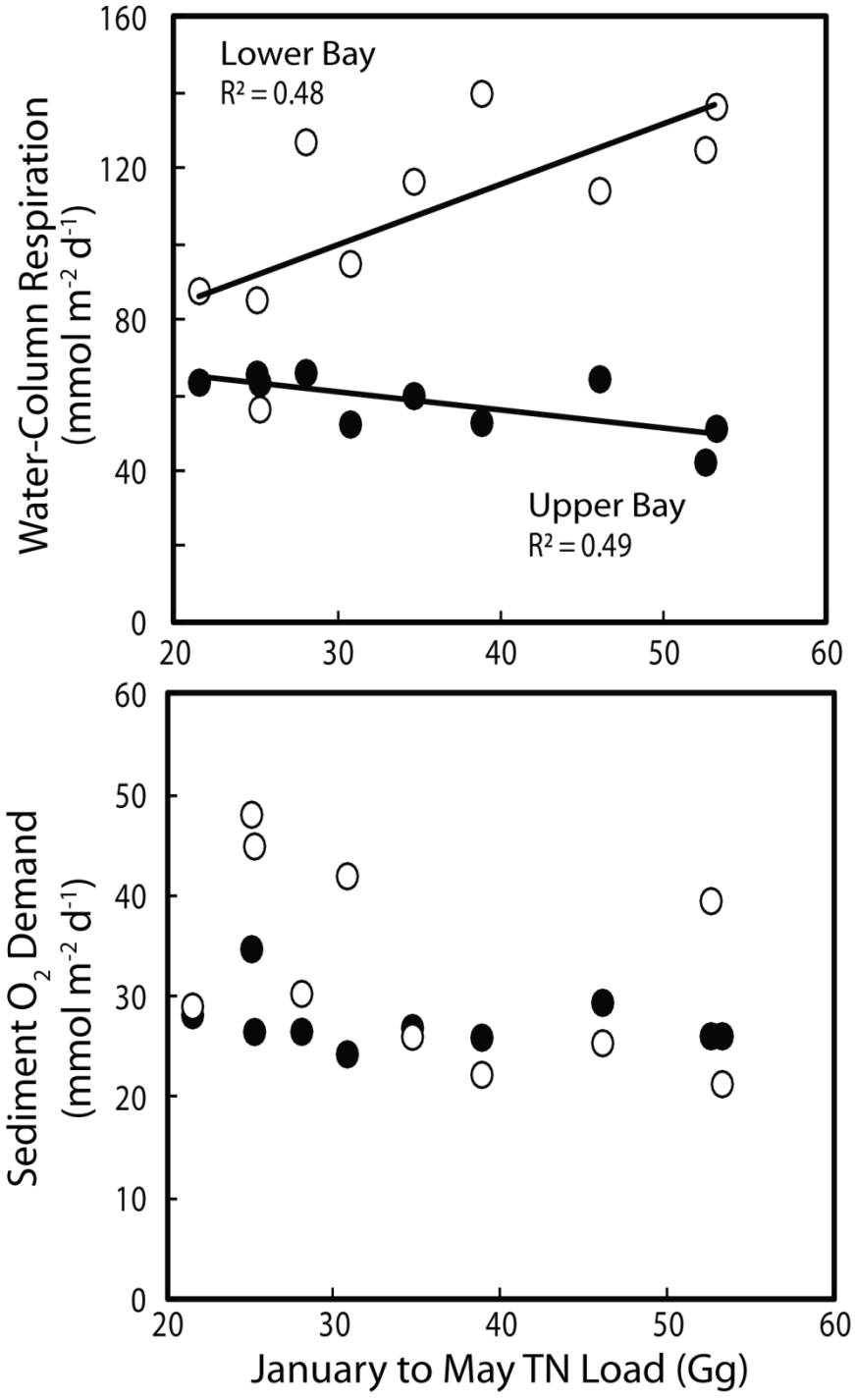
Lower Bay
R² = 0.48
Upper Bay
R² = 0.49
Water-Column Respiration
(mmol m-2 d-1)
Sediment O2 Demand
(mmol m-2 d-1)
January to May TN Load (Gg)
0
40
80
120
160
10
20
30
50
60

SUMMARY AND SYNTHESIS

Dissolved O_2 concentrations in Chesapeake Bay and other aquatic ecosystems result from a dynamic balance between biogeochemical production/consumption and physical replenishment. The biological and physical mechanisms that control O_2 operate over many different time-scales (sub-daily to fortnightly to seasonal to interannual), and are inherently linked. Such strong biophysical interactions have made it difficult to understand the key processes that control O_2 concentrations, primarily because the dominant controls may alternate over time and space, while multiple controls may be operating at any given time. Previous experimental, statistical, and numerical modeling analyses have elucidated many of the key mechanisms controlling O_2 and hypoxia (Boicourt, 1992; Breitburg, 1990; Hagy et al., 2004; Kemp et al., 1992; Murphy et al., 2011; Officer et al., 1984; Scully, 2010a; Seliger and Boggs, 1988; Taft et al., 1980). I have gained many new insights into the controls on hypoxia over the course of the dissertation research presented here; much of this new understanding was accompanied by contemporaneous discoveries by colleagues working on the Chesapeake hypoxia problem. Below, I place my work in the context of historical and recent research to summarize the state of knowledge on hypoxia in Chesapeake Bay and beyond.

Although low oxygen waters have been observed in Chesapeake Bay since as early as the 1930s (Newcombe and Horne, 1938), it was not until the 1980s that sufficient data had accumulated to understand long-term changes in volumes of low-O_2 water (Flemer et al., 1983; Officer et al., 1984; Seliger and Boggs, 1988). Although these early studies identified increased nutrient loading and river flow as primary drivers of hypoxic volume, there were too few data to understand long-term trends. This changed upon the

publication of a 50-year time-series of hypoxic volume calculations for the mid-summer period (Hagy et al., 2004). Although it was clear that there was indeed a long-term increase in Chesapeake Bay hypoxia, there was an apparent doubling of the volume of hypoxia generated for a given nitrogen load, and this doubling appeared to occur abruptly in 1985-1986 (Conley et al., 2009a; Hagy et al., 2004; Kemp et al., 2009). However, when the hypoxic volume data were examined seasonally, it was discovered that this doubling of hypoxia per unit nitrogen load was driven by large increases in the early summer data (e.g. late June, early July), while the later summer data (late July) showed a gradual decline beginning in 1990, consistent with declines in Susquehanna River nutrient loads (Murphy et al., 2011). The cause of the early July increase was linked to elevated stratification (Murphy et al., 2011) and shifts in regional climate cycles and associated impacts on the patterns of summer winds (Kemp et al., 2009; Scully, 2010a).

I also investigated this long-term pattern in hypoxic volume, but tested a different hypothesis for the increased hypoxia-per-unit-N load. The hypothesis states that hypoxic volumes may be self-reinforcing, as increases in hypoxic volume result in higher recycling of inorganic N and P (primarily from sediments), yielding larger water-column N and P accumulations for a given N and P load, supporting higher summer algal production and thus more O_2 depletion (Chapter 2&4, Testa and Kemp 2012). Similar positive feedback mechanisms have been suggested from other coastal ecosystems (Conley et al., 2009a; Kemp et al., 2009). I discovered that during June in upper-middle regions of Chesapeake Bay (e.g., near CB3.3), that larger accumulations of NH_4^+ and PO_4^{3-} in bottom waters per unit N and P load were associated with elevated hypoxic volumes (Chapter 2). The significance of this is that June, or the early summer, is the

time of year when large increases in hypoxic volume occurred (Murphy et al., 2011), thereby connecting hypoxia increases with higher nutrient availability. Subsequent modeling analyses have displayed that summer nutrient availability and associated phytoplankton production are the key mechanisms for supporting and maintaining summer hypoxic volumes (Chapter 5, Appendix II). Future modeling analyses that integrate changes in physical forcing and biogeochemical processes will help quantify the relative importance of these processes during the early summer period.

Hypoxia research in Chesapeake Bay has certainly focused on the summer period (June to August), which is a time when hypoxia is most extensive and its ecological impacts most severe. Relatively less attention has been given to the winter-spring period (February to May), a time when O_2 depletion begins and hypoxia is initiated. Previous work has indentified rates of winter-spring O_2 decline and the date of hypoxia onset (Boynton and Kemp, 2000; Hagy et al., 2004; Taft et al., 1980), but a comprehensive analysis of O_2 depletion over many years and stations has yet to be achieved. The primary results of this analysis, reported in Chapter 3, suggest that bottom-water chlorophyll-*a* is the primary driver of winter-spring O_2 depletion and hypoxia onset in Chesapeake Bay, which is consistent with previous studies (Boynton and Kemp, 2000). However, this chlorophyll-O_2 connection is only strong north of the Potomac River and physical mechanisms appear to exert stronger control in lower Bay regions (Chapter 3). Additionally, it is clear that winter-spring O_2-depletion metrics (and winter-spring chlorophyll-*a*) are only weakly correlated to early summer hypoxic volumes and they have no significant relationship to mid-late summer volumes. Thus, the assumption that the spring bloom is the primary driver and fuel for Chesapeake Bay hypoxia (Malone,

1987; Pomeroy et al., 2006) is too simplistic. Subsequent modeling studies have suggested that concurrent algal production is necessary to maintain hypoxia throughout the summer (Appendix III) and that summertime net primary production and respiration are the primary drivers of interannual variability in hypoxic volume (Chapter 5). It is worth noting that winter-spring Susquehanna River flow has frequently been shown to be an important statistical predictor of summer hypoxia (Hagy et al., 2004; Lee et al., 2013; Murphy et al., 2011); thus these flows (and associated nutrient loads) must connect to summer conditions 3-4 months later. Peak stratification in Chesapeake Bay occurs in June (Murphy et al., 2011) and presumably winter-spring loads are associated with summer nutrient availability, which are two likely mechanisms to connect spring flows and summer hypoxia. I therefore conclude that although the spring bloom controls spring O_2-depletion and hypoxia initiation, summer phytoplankton production (which is strongly limited by nutrient availability) and physical forcing control summertime hypoxic volumes.

One of the key discoveries related to Chesapeake hypoxia in the past five years is that the late-summer hypoxic volume has declined coincident with reductions in winter-spring nutrient loads (Murphy et al., 2011). Despite such strong correlations between hypoxic volume and nutrient load, observations of reduced phytoplankton production or community respiration that mechanistically link reduced nutrient load to reduced hypoxia had been lacking. I executed a suite of model simulations for a given year, where TN loads were varied by two orders of magnitude and the associated dynamics of organic matter production and respiration were examined (Chapter 5), to provide an improved understanding of mechanisms linking nutrient loads and hypoxia. This analysis revealed

that elevated nitrogen loads caused increased phytoplankton growth, biomass, and water-column respiration in lower Bay regions during summer; similar increases were non-existent or muted in middle and upper Bay regions during spring. Although this result is broadly expected, it emphasizes the fact that nitrogen loading represents a dominant control on algal growth in lower Bay regions during summer periods (Fisher et al., 1992; Harding and Perry, 1997; Malone et al., 1996), thus linking N loads and hypoxic volume. These findings not only provide specific mechanisms to support the observation of reduced later-summer hypoxic volumes, but they reinforce our understanding of the need for summer phytoplankton production to maintain summer hypoxic volumes. Future model simulations will realistically simulate the Bay from the late 1980s to the 2000s, with an aim to reproduce the discovery of Murphy et al. (2011) and more fully articulate the mechanisms behind it.

The conclusions of this dissertation are relevant to the dynamics of other temperate costal ecosystems where eutrophication and hypoxia are prevalent and provide some key lessons for water quality management. As mentioned previously, positive feedbacks associated hypoxia effects on nutrient cycling have been suggested for many other systems, and the synthetic approach and quantitative metrics applied in Chapter 2 may be of use in other comparable coastal ecosystems. The potential for such feedbacks, positive or negative, must be included in strategies to manage nutrient loads and also the expectations associated with what those load reductions might achieve. Management agencies are interested in indicators and metrics of water quality, which provide a quantitative basis to measure degradation and restoration associated with nutrient management efforts. Metrics like the winter-spring O_2 depletion rate (Chapter 3,

Appendix I) essentially convert routine hydrochemical measurements into ecological rates, which provide a unique measure of ecosystem response to eutrophication that capture ecosystem responses to nutrient load (Appendix I). Similar metrics can be computed from numerical models, and these approaches can be applied in any system where time-series observations of O_2 are available. Finally, numerical models that include coupled hydrodynamic-biogeochemical simulations are increasingly used in scientific research. These models are valuable not only as predictive simulators, but as diagnostic tools to understand eutrophication and ecosystems responses to external perturbations, such as nutrient loading (Chapter 4&5, Appendix VI). Here, it is clear that these tools have been valuable in Chesapeake Bay to understanding mechanistic controls on hypoxia and the associated water-column and sediment biogeochemical processes. As at least four such models now exists for Chesapeake Bay (Cerco and Meyers, 2000; Xu and Hood, 2006), along with more simple biogeochemical calculations (Li et al., 2013; Scully, 2010b), the potential for ensemble model simulations and comparative analyses is exciting.

APPENDIX I: PATTERNS OF WINTER-SPRING OXYGEN DEPLETION IN THE PATUXENT RIVER ESTUARY

Routine water-quality monitoring data for dissolved O_2 were used to compute rates of March-June water-column O_2 depletion and the day of hypoxia onset at 6 stations (Fig. AI.1) in the Patuxent River estuary for the years 1985-2009. The methodology used to compute these metrics from water-quality monitoring data is described in Chapter 2; the only difference in methodology is the period used to compute O_2 depletion rates (March-May for Chesapeake mainstem, March to June for Patuxent). Such computations have been made by several previous investigators for the mainstem Chesapeake (Boynton and Kemp, 2000; Hagy et al., 2004; Taft et al., 1980), but comparable analyses have never been performed in tributaries.

Mean June-August, bottom-water dissolved O_2 concentrations varied by 2-3 mg l^{-1} from year to year, with gradual declines over the 1985-2009 period (Fig. AI.2; trends not significant). Seasonal minima in dissolved O_2 were lower at station LE1.1 than at other Patuxent stations (Fig. AI.2), and concentrations at RET1.1 increased to generally non-hypoxic values after 1990, which is near the time when Biological Nitrogen Removal (BNR) was initiated at wastewater treatment plants within the watershed (Kemp et al., 2009; Testa et al., 2008). However, concentrations returned to low values consistently after 2002 (Fig. AI.2).

Rates of March-June, water-column O_2 depletion rates were highly variable from year to year at all stations (Fig. AI.3). No clear temporal trends emerged from the patterns, but depletion rates at station RET1.1 were substantially higher prior to 1995, before BNR was fully initiated at all wastewater facilities in the watershed. Hypoxia

onset day also appeared to occur later in the year after 1991, but began arriving earlier after 2002, at the time when summer O_2 concentrations returned to pre-1990 low levels (Fig. AI.3). In general hypoxia initiated during May and June in the Patuxent estuary (although notably later in some years), which is similar to hypoxia onset timing at stations CB5.1-CB5.4 in the mainstem Chesapeake Bay (Fig. AI.3, Chapter 2).

Correlation analysis was used to explore the factors controlling hypoxia onset day and O_2 depletion rates. Potential controlling variables included freshwater input and nutrient (total nitrogen (TN) and phosphorus (TP)) loads to the Patuxent measured at Bowie, Maryland (http://waterdata.usgs.gov/usa/nwis/uv?01594440), water temperature, and chlorophyll-*a*. Overall, April to June TN load (Fig. AI.4) and March to May TP load were most highly correlated with O_2 depletion rates (Fig. AI.5), while no variable significantly correlated with hypoxia onset day. Thus, although no single variable explained more than 50% of the variability in either metric of O_2 depletion, spring nutrient loads appear to be an important driver of spring O_2 depletion.

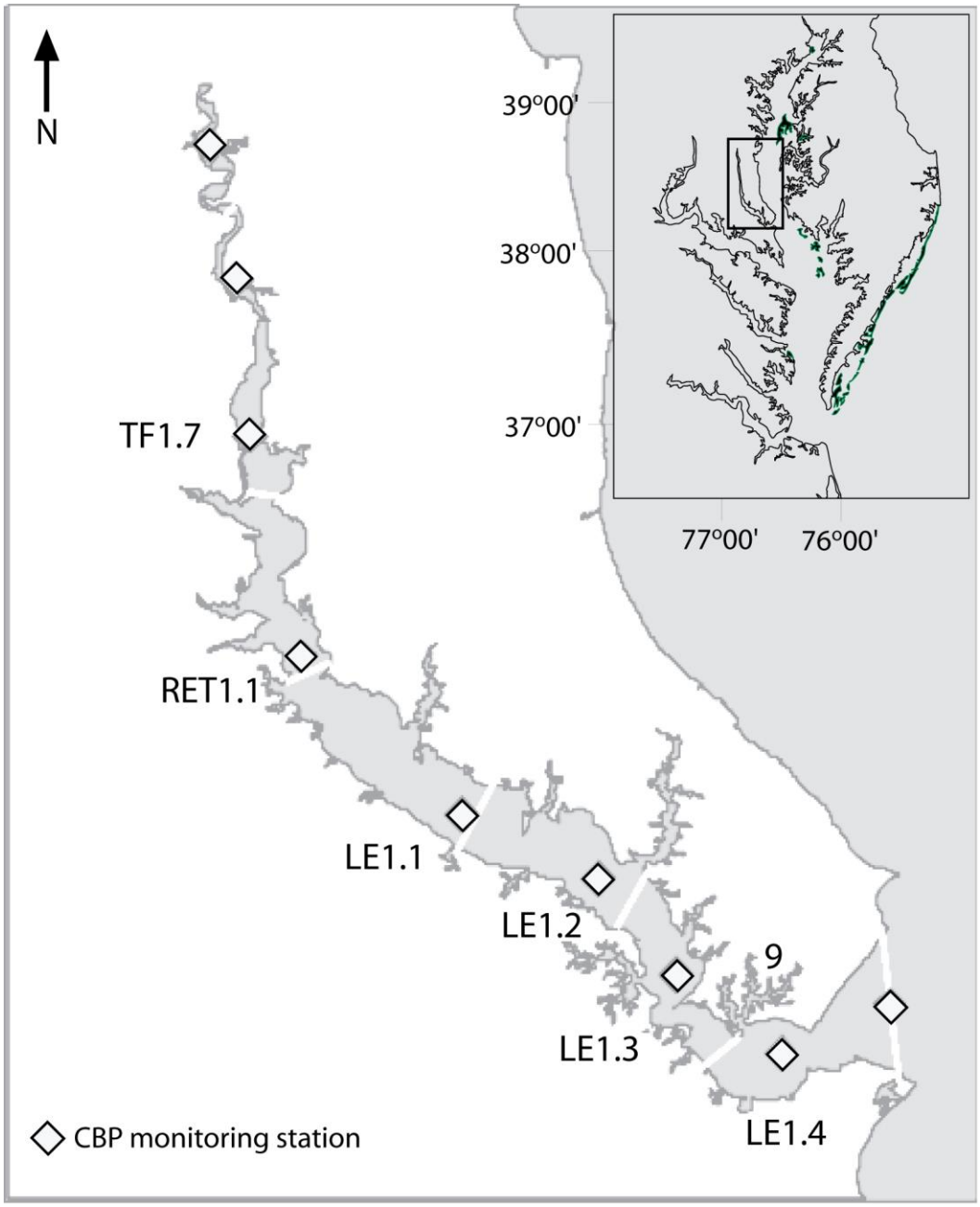

Figure AI.1: Map of the Patuxent River estuary (Chesapeake Bay inset), with the location of water quality monitoring stations.

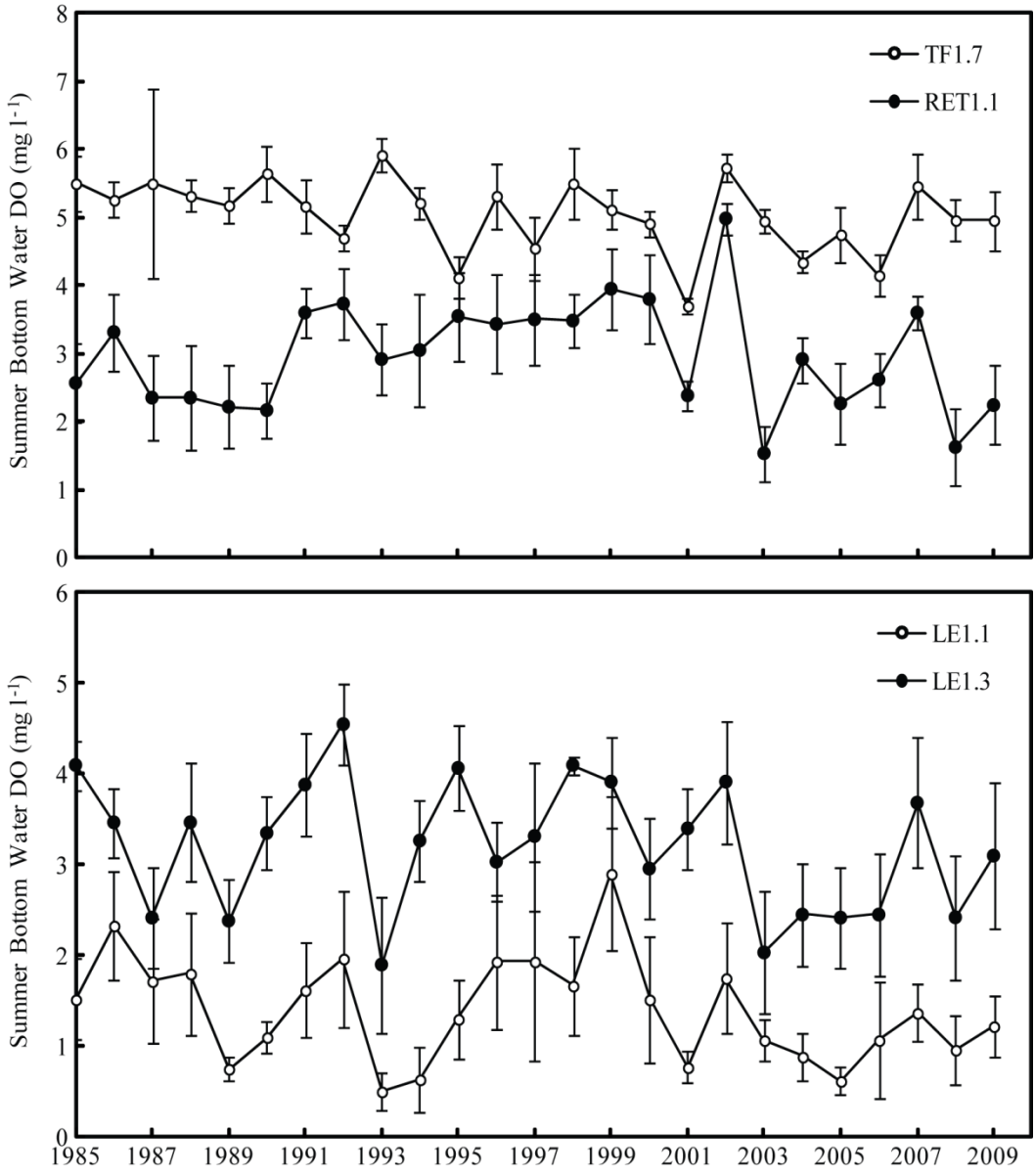

Figure AI.2: Time-series (1985-2009) of mean summer (June to August), bottom-water O_2 concentrations (± SD) at four stations in the Patuxent River estuary.

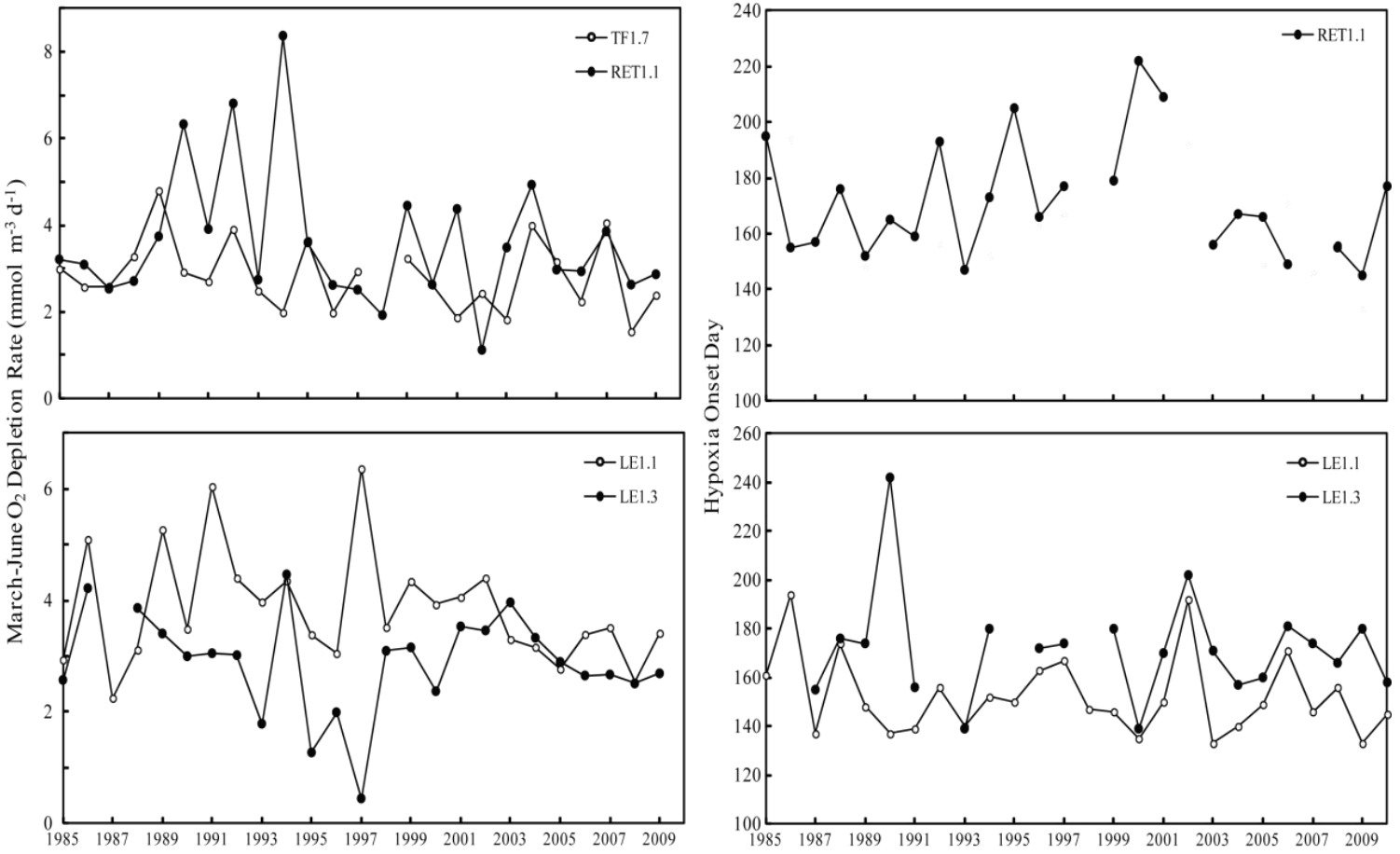

Figure AI.3: Time-series (1985-2009) of April to June, water-column O_2 depletion rates (left panel) and hypoxia onset day (right panel) at four stations in the Patuxent River estuary.

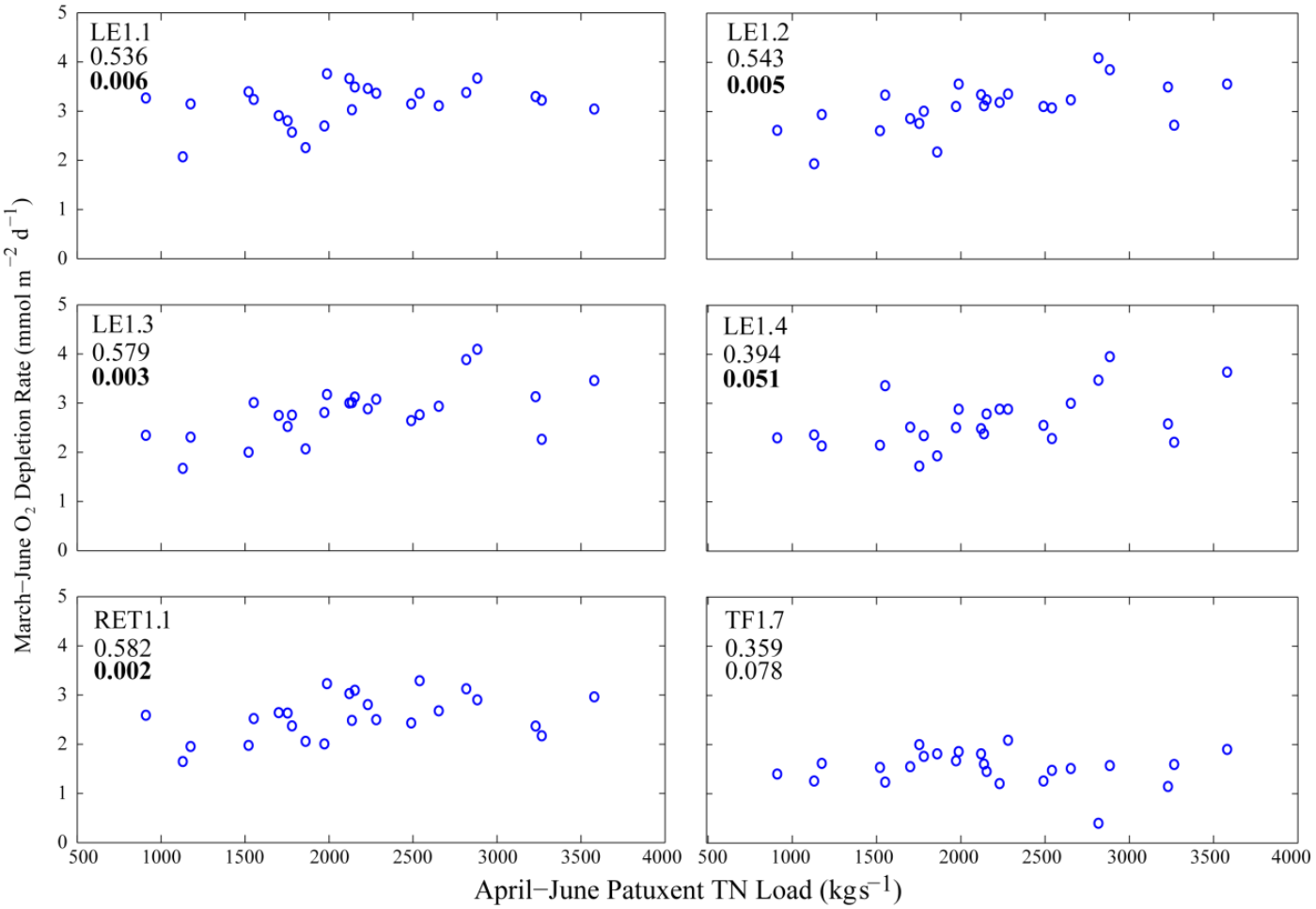

Figure AI.4: Correlations between April to June Patuxent River TN load and water-column O_2 depletion rates at six stations in the Patuxent River estuary.

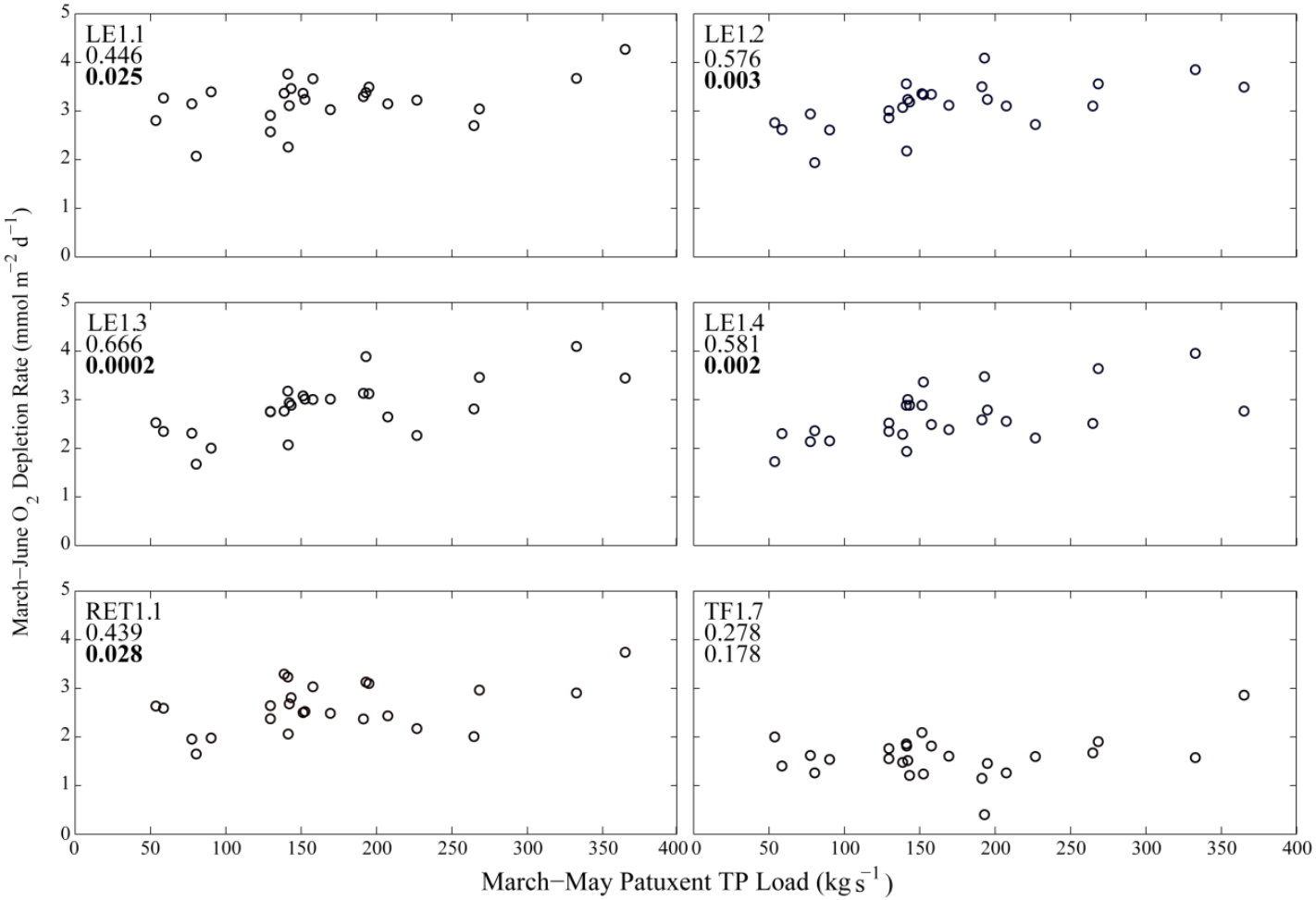

Figure AI.5: Correlations between March to May Patuxent River TP load and water-column O_2 depletion rates at six stations in the Patuxent River estuary.

APPENDIX II: NET ECOSYSTEM PRODUCTION IN SHALLOW AND DEEP HABITATS IN CHESAPEAKE BAY: A MODELING ANALYSIS

Net ecosystem production (or net ecosystem metabolism) is a measure of the total net carbon or O_2 production or consumption in an ecosystem (Stæhr et al., 2012). That is, the combined anabolism and catabolism of all organisms within an ecosystem can be summed to quantify the metabolism of that ecosystem, which represents an integrated measure of a system in terms of its overall rates of production and consumption of organic matter. Net ecosystem production is relevant to the study of hypoxia because when it is positive, it is a direct quantification of the excess, or non-respired, organic matter produced in a region of an ecosystem that could fuel respiration and O_2-depletion in other regions of the system (Kemp and Testa, 2011).

Observational studies have revealed that in Chesapeake Bay during summer, photic-layer NPP is insufficient to support the respiration occurring in the underlying aphotic water in deeper stations, but NPP > (R_{wc} + R_{sed}) at shallower stations (Smith and Kemp, unpublished). It has been hypothesized that excess organic matter produced in shallow shoal habitats is transported laterally to support the excess respiration occurring in the adjacent, deeper regions.

Patterns of net ecosystem production (hereafter NEP) were computed from ROMS-RCA model simulations (Chapter 4) in Chesapeake Bay for the year 2000. Here, NEP for a particular cell or regions is defined as the difference between net primary production (NPP) in the photic layer minus total respiration (water-column (R_{wc}) + sediment (R_{sed})) below the photic layer, thus NEP = NPP – (R_{wc} + R_{sed}). NEP was computed for several stations along the longitudinal axis of Chesapeake Bay, where paired computations were made for stations in the deeper, central channel and for adjacent stations in the shallower, western shoals

(Stations CB3.3, CB4.1, CB4.2, CB4.3). These computations reveal that annually, that NEP is positive in the western, shallow stations and negative in the central, deep stations (Fig. AII.1). Regional respiration computations, where total water-column respiration and sediment O_2 demand are computed for nine regions of Chesapeake Bay (Fig. 2.1), reveal that 50-80% of regional respiration occurs in waters deeper than 10 m (Fig. AII.2). Both sets of computations suggest that the majority of Bay respiration occurs in deeper waters, perhaps simply due to the volume of aphotic water occupying these habitats. The difference between NEP in shallow and deep stations does support the hypothesis that excess organic matter production from shallow habitats must support respiration in adjacent habitats. A second possibility is that excess organic matter in deep, seaward regions is transported landward due to gravitational circulation (Kemp et al., 1997; Smith and Kemp, 1995). Each of these possibilities will be further tested with additional analysis of model data.

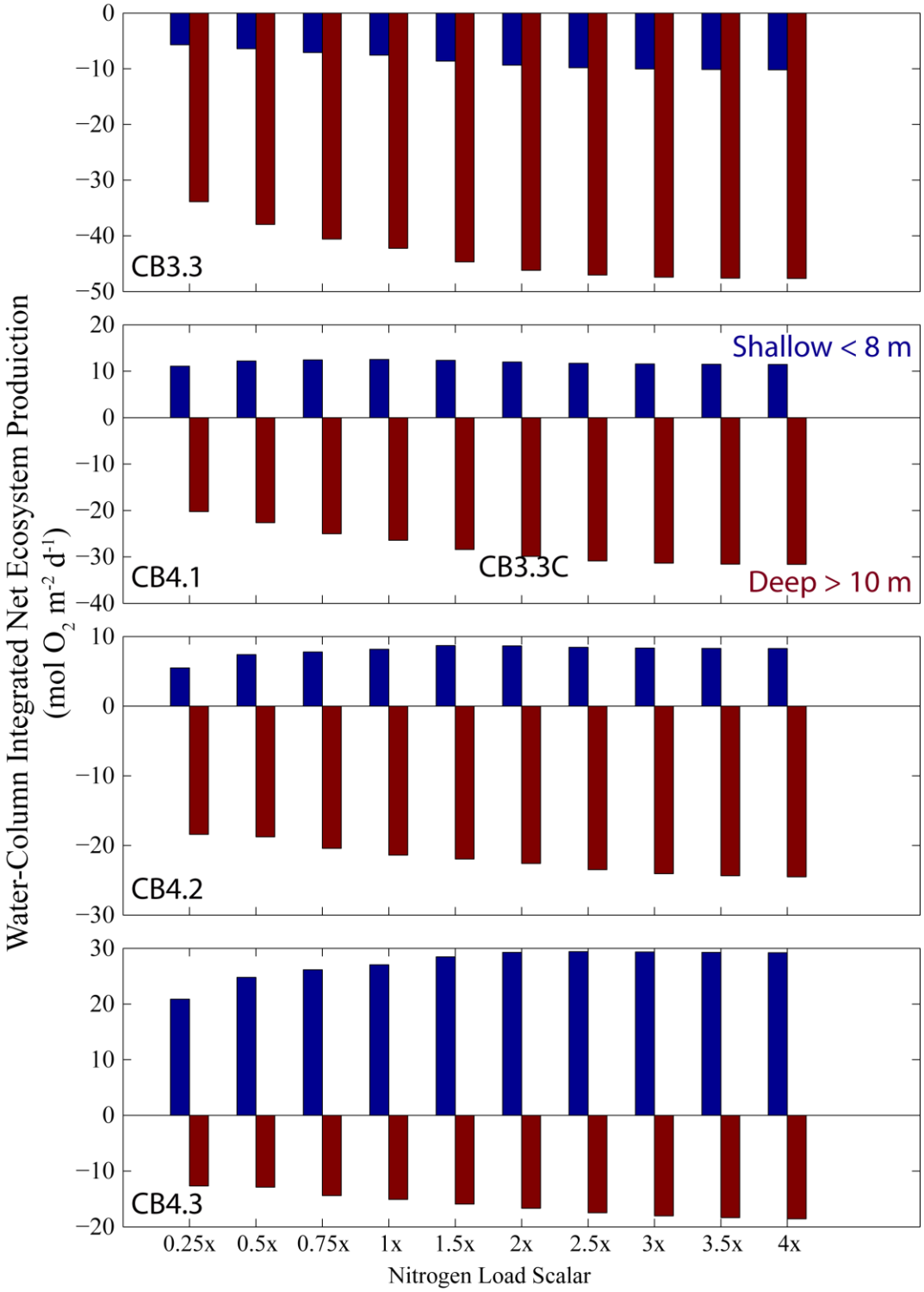

Figure AII.1 Model computations of photic-layer NEP in shallow, western shoal stations (blue bars) and deep, central channel stations (red bars) in Chesapeake Bay. Computations were made for ten different nitrogen loading rates, where x-axis labels indicated how nitrogen load was scaled to the observed load in 2000.

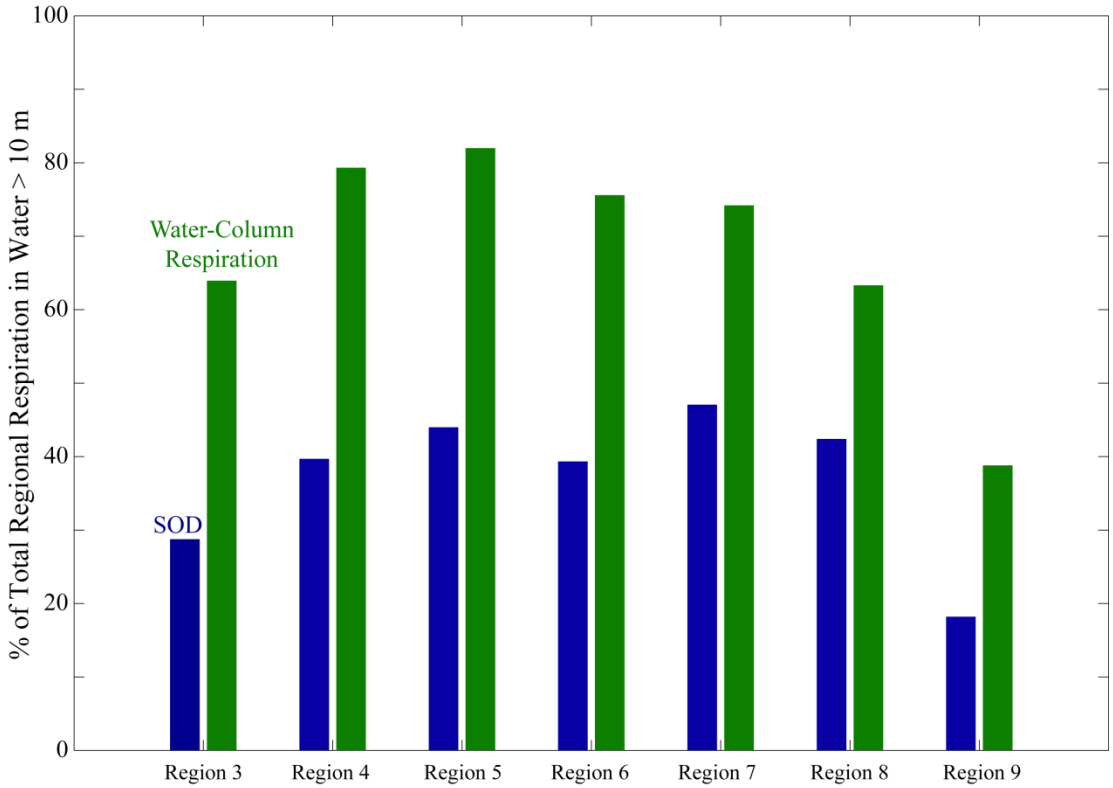

Figure AII.2: Computations of the percent of total respiration in the water-column (green bars) and in sediments (blue bars) that occurred in cells deeper than 10 meters for seven regions of Chesapeake Bay (see Fig. 5.1). Model output from the 1x simulation were used (see Chapter 4).

APPENDIX III: THE ROLE OF SUMMER PHYTOPLANKTON PRODUCTION IN SUPPORTING HYPOXIA IN CHESAPEAKE BAY

A long-standing, and perhaps pervasive view within Chesapeake Bay ecology is that the winter-spring diatom bloom is the primary fuel supporting O_2 depletion and associated hypoxia throughout the summer period (Pomeroy et al., 2006). This perspective is not unfounded, as the winter-spring period is when the largest phytoplankton standing stock occurs (Malone, 1991) and the spring bloom is generally composed of large, fast sinking, and poorly grazed diatom species that can accumulate in the deep water where hypoxia eventually occurs. However, sediment trap measurements have revealed high rates of organic matter sinking during summer (Kemp et al., 1999), primary production rates peak in summer (Harding et al., 2002), and computations based on available measurements of primary production and respiration suggest that winter-spring net primary production is insufficient to support respiration rates for the ensuing 3-4 months (Newell et al., 2007). Clearly, further investigation is needed to answer this question adequately.

Numerical models are ideal tools to answer such a question, as they can be used to track primary production and respiration throughout the Bay over the course of a year and the associated physical transport of that organic material. A first-order test of the potential for the spring bloom to fuel O_2-depletion over the course of a year is to run a simulation where summer phytoplankton production is omitted from the model. Using ROMS-RCA for the year 2000 (Chapter 4), such a simulation was run, where the growth rate of the summer phytoplankton group representing dinoflagellates (Fig. 5.2) was set to zero, effectively removing summer phytoplankton from the model. The result of this test is clearly communicated using time-series of bottom-water O_2 and surface-layer chl-*a* at several

stations in Chesapeake Bay (Fig. AIII.1 & AIII.2). When both winter-spring and summer phytoplankton are included in the simulation, dissolved O_2 reaches hypoxic levels in May, which are maintained until August or September; however, when summer phytoplankton are removed, bottom-water O_2 begins to recover to normoxic levels in later June and early July (Fig. AIII.1). These O_2 patterns are associated with a 50-75% reduction in chl-*a* in surface waters during the July to September period (Fig. AIII.2). Such simulations, although simple, clearly demonstrate the requirement of summer phytoplankton growth to maintain hypoxia in Chesapeake Bay bottom waters throughout the summer.

One obvious caveat with such a simple test is that it ignores one aspect of the spring bloom-summer hypoxia connection: that the spring bloom indirectly fuels summer productivity when its decomposition in early summer results in the release of bioavailable nutrients (Li et al., 2009). Presumably, larger spring blooms lead to higher rates of decomposition and thus elevated release rates of key nutrients. Future studies will further elucidate the details of this key ecological question.

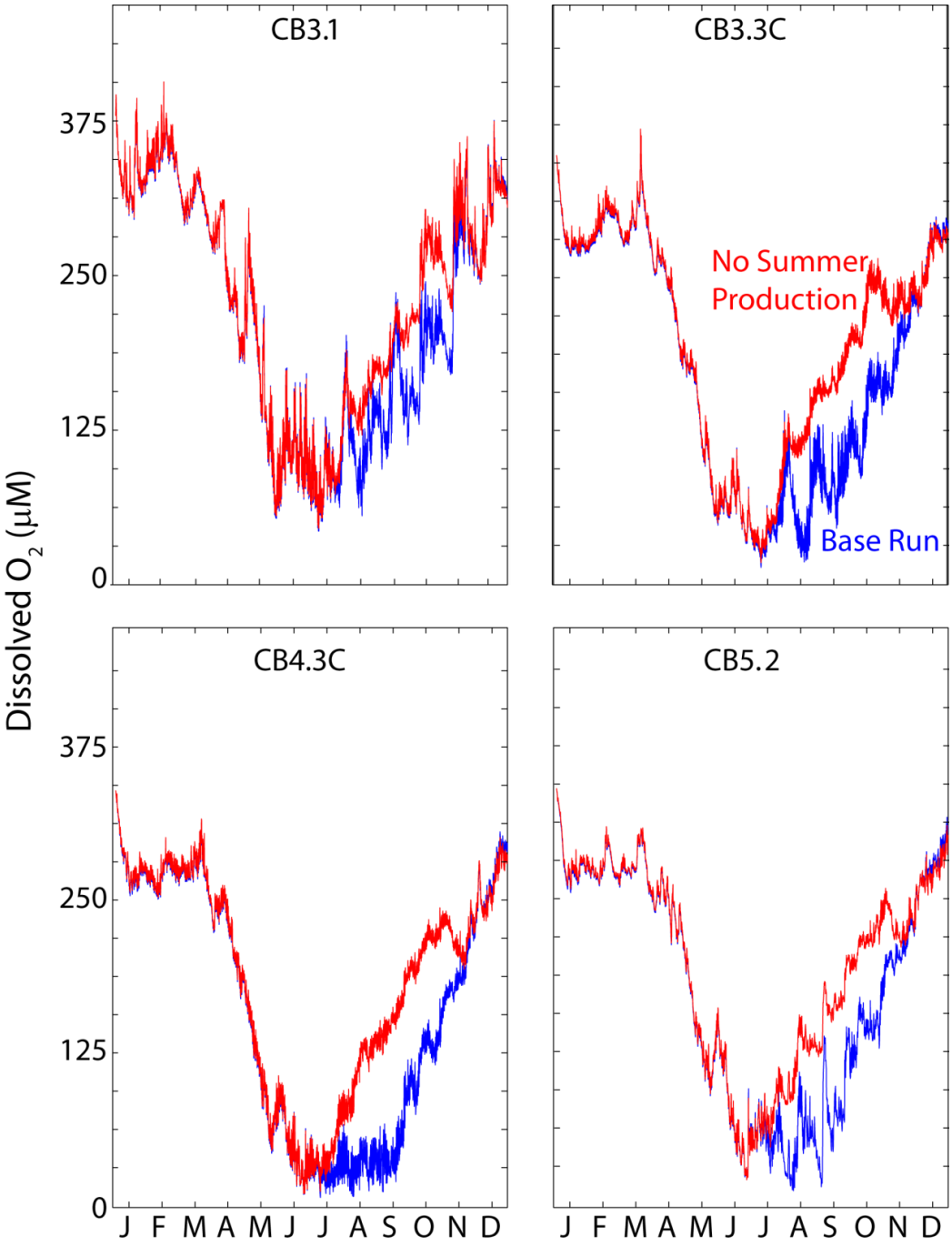

Figure AIII.1: Seasonal cycle of modeled bottom-layer dissolved O_2 at four stations in Chesapeake Bay under two conditions: (1) the "Base Run", or simulation under normal conditions (blue lines), and (2) a simulation where summer phytoplankton growth is prevented ("No Summer Production", red lines).

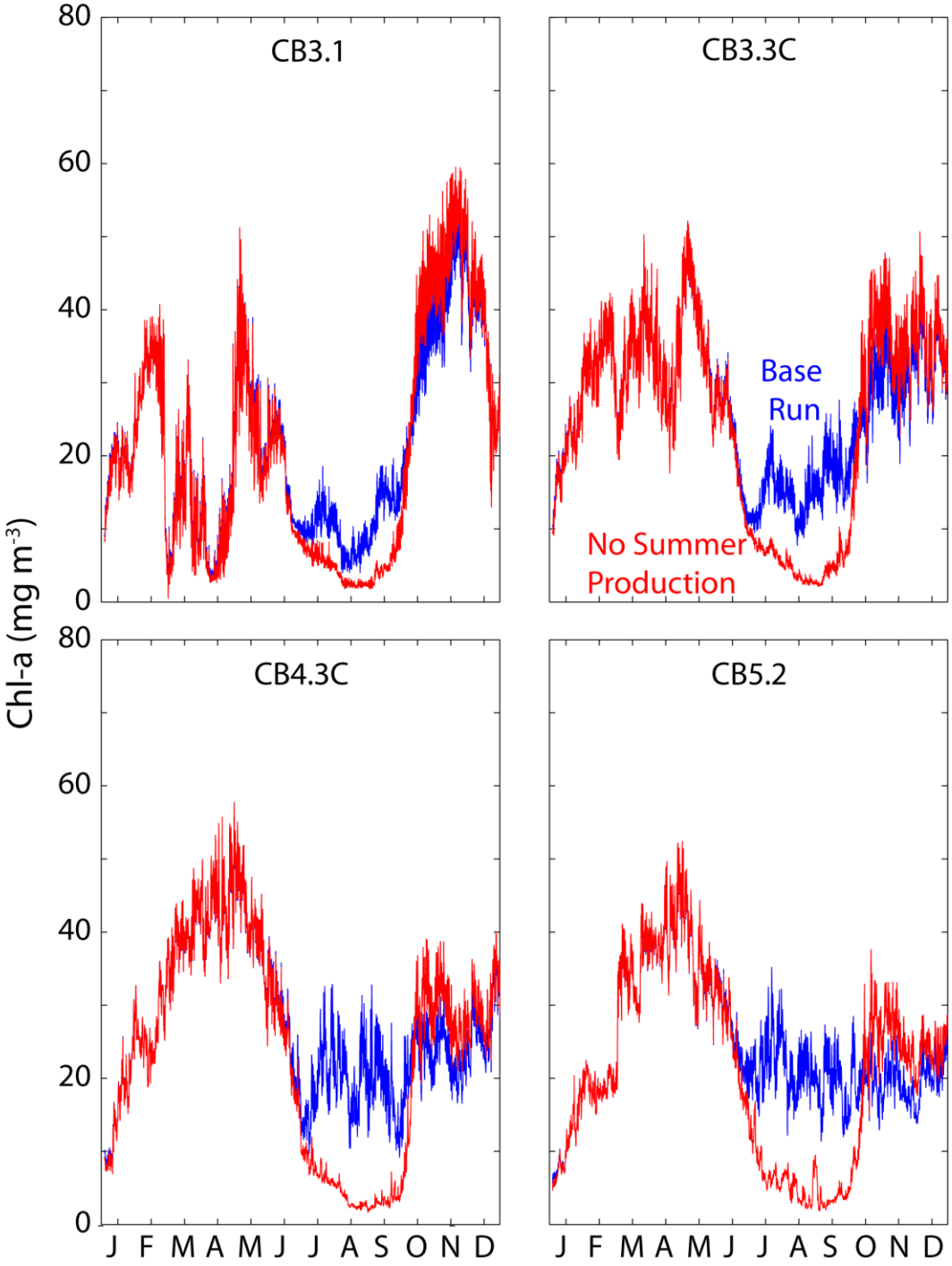

Figure AIII.2: Seasonal cycle of modeled surface-layer chlorophyll-*a* at four stations in Chesapeake Bay under two conditions: (1) the "Base Run", or simulation under normal conditions (blue lines), and (2) a simulation where summer phytoplankton growth is prevented ("No Summer Production", red lines).

APPENDIX IV: PATTERNS OF LATERAL VARIABILITY IN CHLOROPHYLL-A AND DISSOLVED OXYGEN IN MESOHALINE CHESAPEAKE BAY

Observational studies have revealed that during summer in Chesapeake Bay, phytoplankton production is insufficient to support the respiration occurring in the underlying aphotic water in deep (> 10 m) stations, but that excess organic matter is produced at shallower stations (Smith and Kemp, unpublished). As summarized in Appendix 2, it has been hypothesized that excess organic matter produced in shallow shoal habitats is transported laterally to support the excess respiration occurring in the adjacent, deeper regions. It is difficult to test this hypothesis using observation data, as spatially-resolved estimates of phytoplankton metabolism coupled to physical transport rates are needed to understand these spatially-dependent, bio-physical processes. However, a long time-series (1985-2009) of chl-*a* and dissolved O_2 measurements are available at four paired stations in mesohaline Chesapeake Bay (central deep channel stations and adjacent stations on the shallow, western and eastern shoals; Fig. AIV.1), providing the potential to investigate this hypothesis with historical data.

Analysis of these data reveal high interannual variability in surface-water chl-*a* at each station, but a clear tendency for chl-*a* to be higher in western shoal stations than the central or eastern shoal station (Fig. AIV.2). Differences between the stations in the CB3.3 transect are less clear than the three more southerly stations (Fig. AIV.2). Upon averaging these time-series into monthly-means, it is clear that the chl-*a* is much higher in the western shoal stations (e.g., CB3.3W, CB4.3W, etc.) during the summer period (June to August), and that stations are similar to each other in other seasons (Fig. AIV.3). Such patterns support the assertion that phytoplankton biomass (and presumably

productivity) are higher on the western, shallow shoals and may be transported laterally to the central station to support respiration during summer. These patterns are associated with the tendency for bottom-water dissolved O_2 to be much lower in the deep, central stations (Fig. AIV.4), which is the result of several different mechanisms.

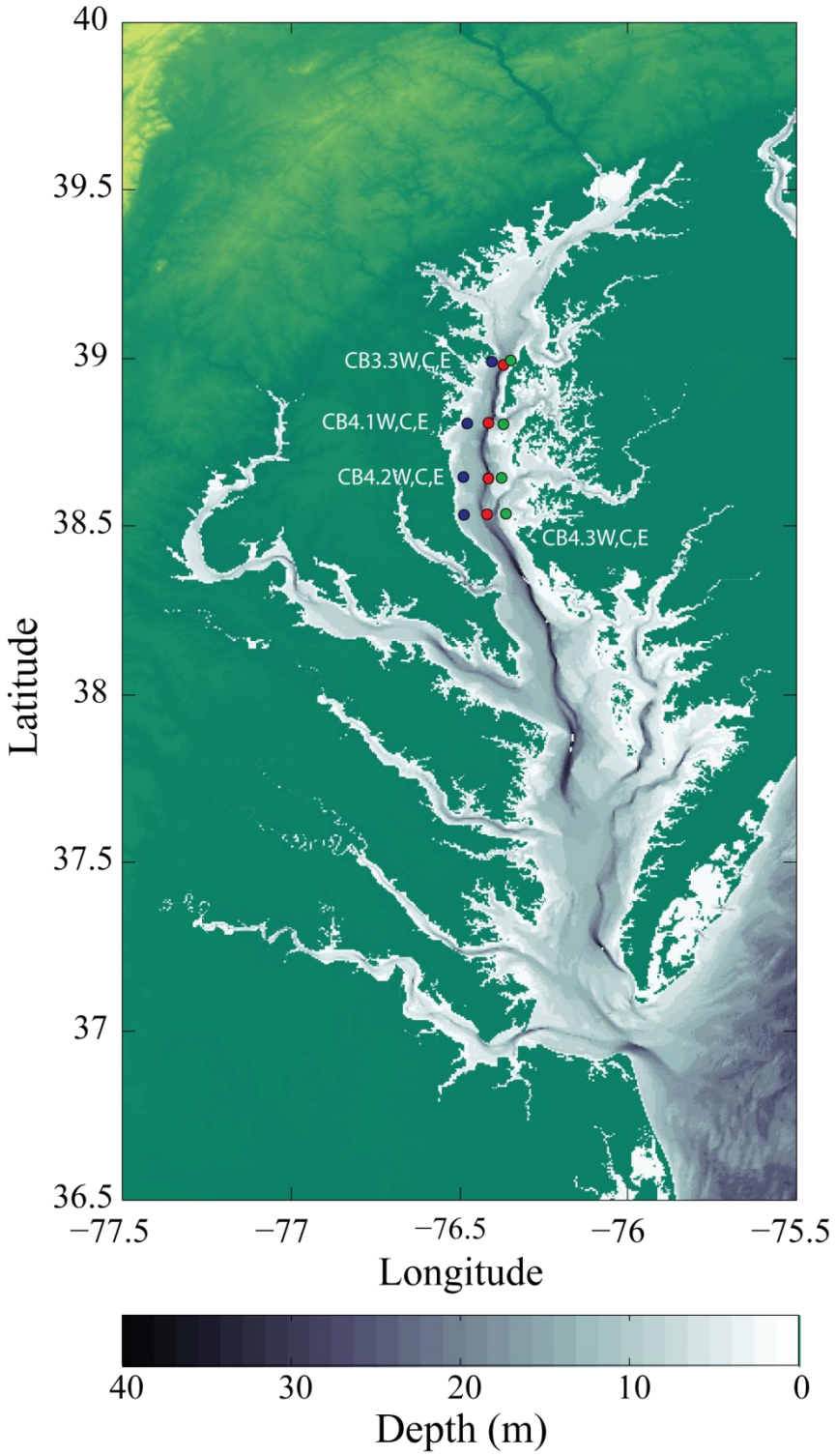

Figure AIV.1: Map of Chesapeake Bay bathymetry, with the location of twelve stations used in the data analysis, including four transects (e.g., CB3.3W, CB3.3C, CB3.3E, etc.).

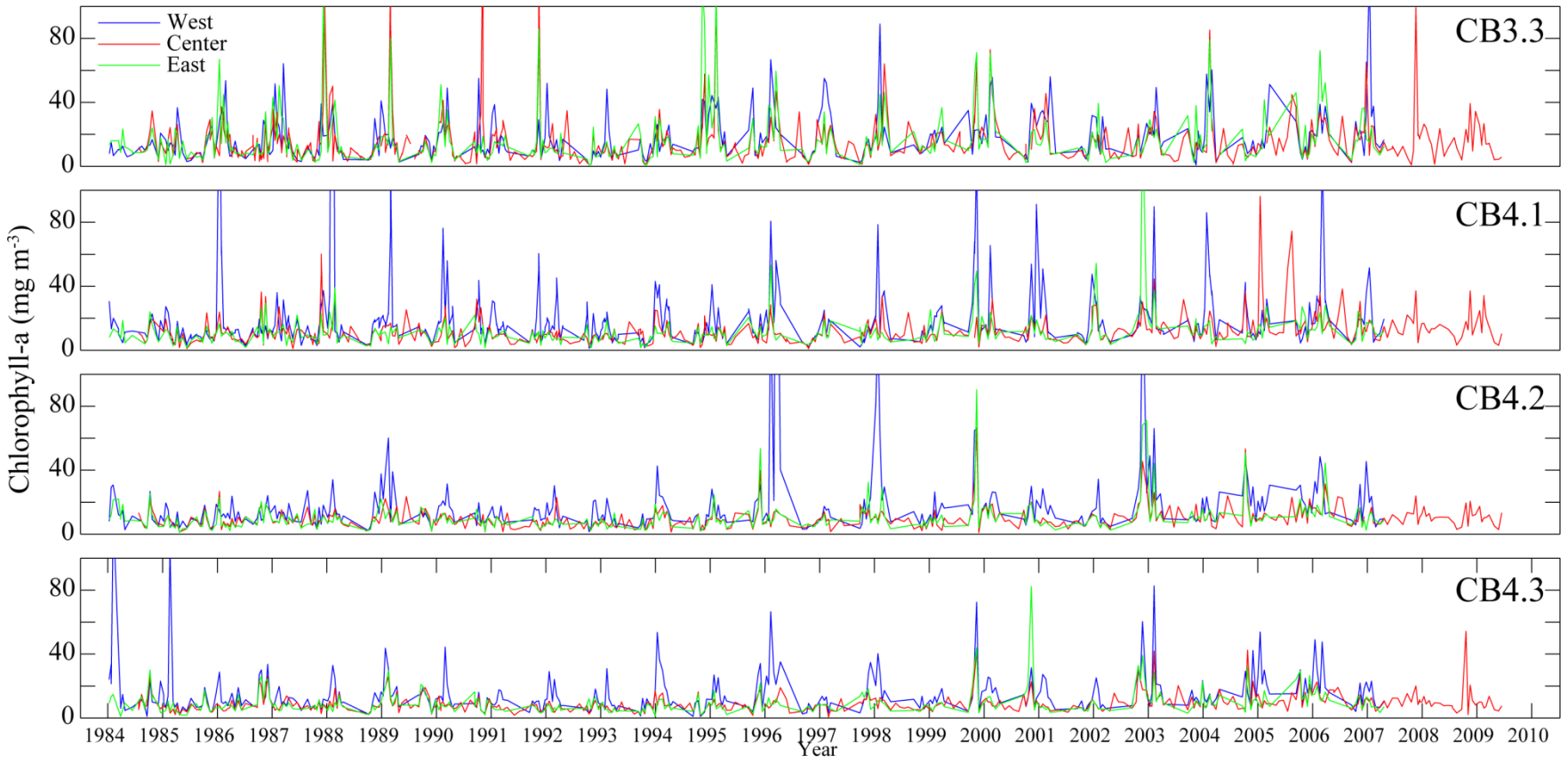

Figure AIV.2: Time-series (1985-2009) of surface-water chl-*a* over four lateral transects in Chesapeake Bay (see Fig. AIV.1), where each transect includes a western shoal station (blue line), a central, deep channel station (red line), and an eastern shoal station (green line).

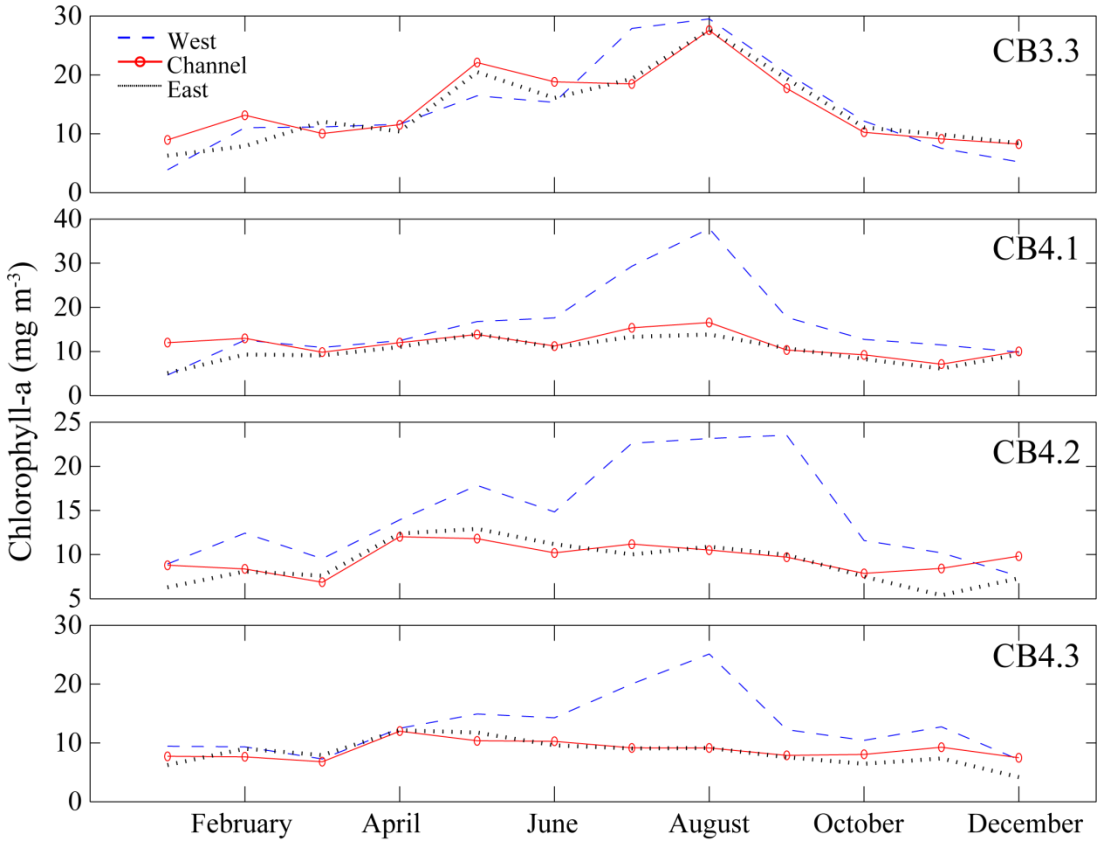

Figure AIV.3: Monthly mean surface-water chl-*a* over the 1985-2009 period over four lateral transects in Chesapeake Bay (see Fig. AIV.1), where each transect includes a western shoal station (blue dashed line), a central, deep channel station (red solid line), and an eastern shoal station (black dotted line).

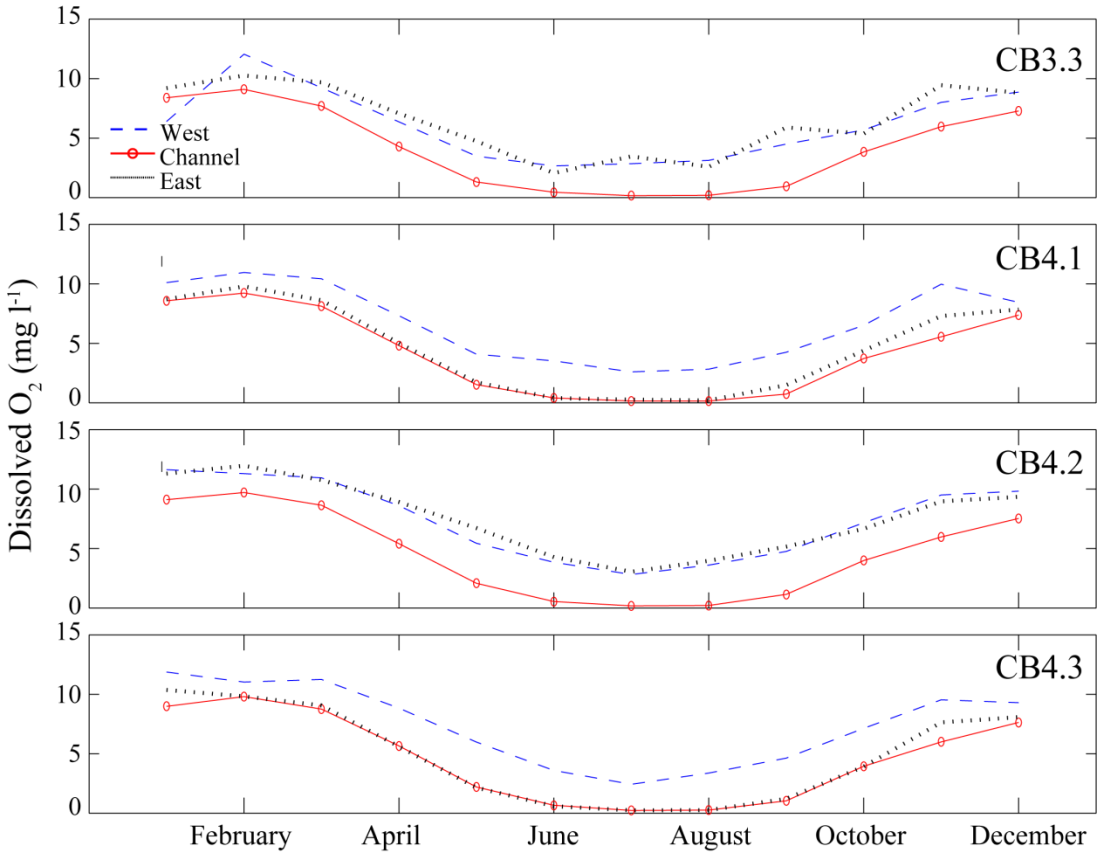

Figure AIV.4: Monthly mean bottom-water O_2 over the 1985-2009 period over four lateral transects in Chesapeake Bay (see Fig. AIV.1), where each transect includes a western shoal station (blue dashed line), a central, deep channel station (red solid line), and an eastern shoal station (black dotted line).

APPENDIX V: THE IMPACTS OF WIND FORCING ON SALT AND OXYGEN DISTRIBUTIONS IN CHESAPEAKE BAY: A MODELING ANALYSIS

Wind stress is a key driver of variability in shallow estuarine systems (Scully, 2010a), with impacts on vertical mixing, horizontal transport, and secondary circulation (Chen and Sanford, 2009; Li and Li, 2011). The nature of the wind used to drive hydrodynamic models can thus have large impacts on the predicted distribution of salt; for example, elevated wind stress can be associated with a deepening of the surface mixed-layer (Li et al., 2005) or elevated mixing on the shallow shoals flanking the main channel of Chesapeake Bay (Scully, 2010b). To understand the impacts of different wind forcing on Chesapeake Bay a series of simulations were performed with several different wind-forcing regimes.

Three different wind forcing data sets were used to drive air-seas fluxes of momentum and heat across the surface of Chesapeake Bay. The first is gridded data (Fig. AV.1) from the North American Regional Reanalysis (NARR) from National Center for Environmental Prediction products (Mesinger et al., 2006). Secondly, the NARR data were amplified by a factor of 1.3, as NARR data underestimate true over-water wind stress in Chesapeake Bay, at least for above-average wind speeds (Ming Li, personal communication). Lastly, spatially-uniform winds based on measurements from Thomas Point Light (TPL) were used (Fig. AV.1), which better represent over-water winds (http://tidesandcurrents.noaa.gov/ofs/cbofs/cbofs.html). For each of the three wind forgings, two difference advections schemes were tested; (1) a 3rd-order upstream horizontal advection with splines vertical advection or (2) the advection scheme known as MPDATA (Smolarkiewicz and Margolin, 1998). Model data for the NARR cases were

run with a background diffusivity of 10^{-6} m^2 s^{-1}, except one case, which was run with 10^{-5} m^2 s^{-1}.

At 3 stations in Chesapeake Bay, salinity predictions tended to be highest (and most representative of the observations, especially in deeper water) with base NARR winds and a background diffusivity of 10^{-6} m^2 s^{-1} (pink lines or "NR bd 10^{-6} MPD"; Fig. AV.2-AV.4). Base NARR winds and a background diffusivity of 10^{-5} m^2 s^{-1} were of intermediate comparability, while simulations with NARR winds scaled by 1.3 ("NR bd 10^{-6} *1.3") tended to generate lower salinity values (Fig. AV.2-AV.4). In the lower Bay, the model response (in terms of salinity) was mixed and small to the different wind forcing. The different advections schemes had little impact on the model simulations for this year and model resolution. The associated O_2 predictions in RCA under the different wind forcing showed similar results (Fig. AV.5 & AV.6), except that the implementation of the MPDATA ("NR bd 10^{-6} MPD") scheme resulted in higher bottom-water O_2 concentrations at CB3.3C and 4.3C than the similar run without MPDATA ("NR bd 10^{-6}") for several periods during late summer and fall (Fig. AV.5 & AV.6). Lastly, Thomas Point winds resulted in an overall freshening of the Bay with a general deepening of the surface mixed layer (Fig. AV.7), but TPL simulations generally resulted in poorer representations of salinity. Further analysis will better elucidate the mechanisms behind these simulation results.

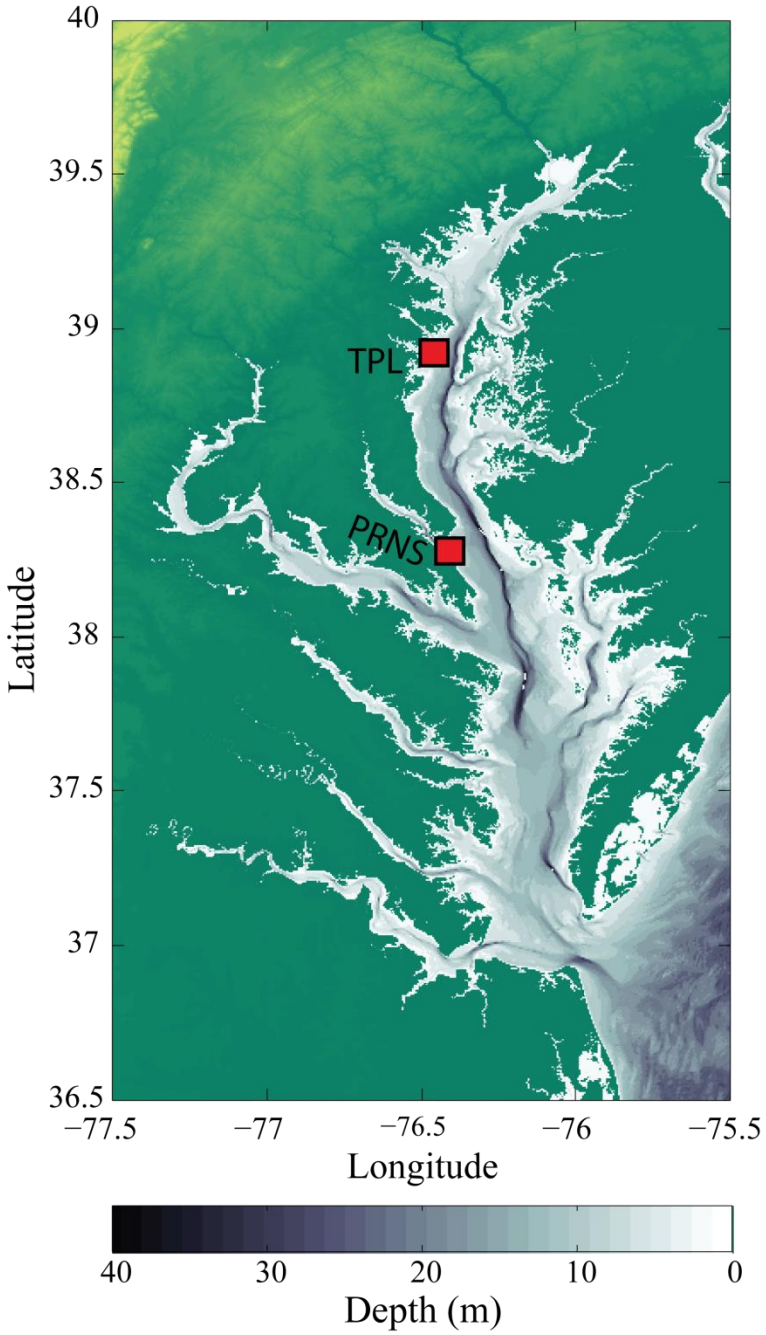

Figure AV.1: Map of Chesapeake Bay with location on wind measurement stations, including the Patuxent River Naval Air Station (PRNS) and Thomas Point Light (TPL).

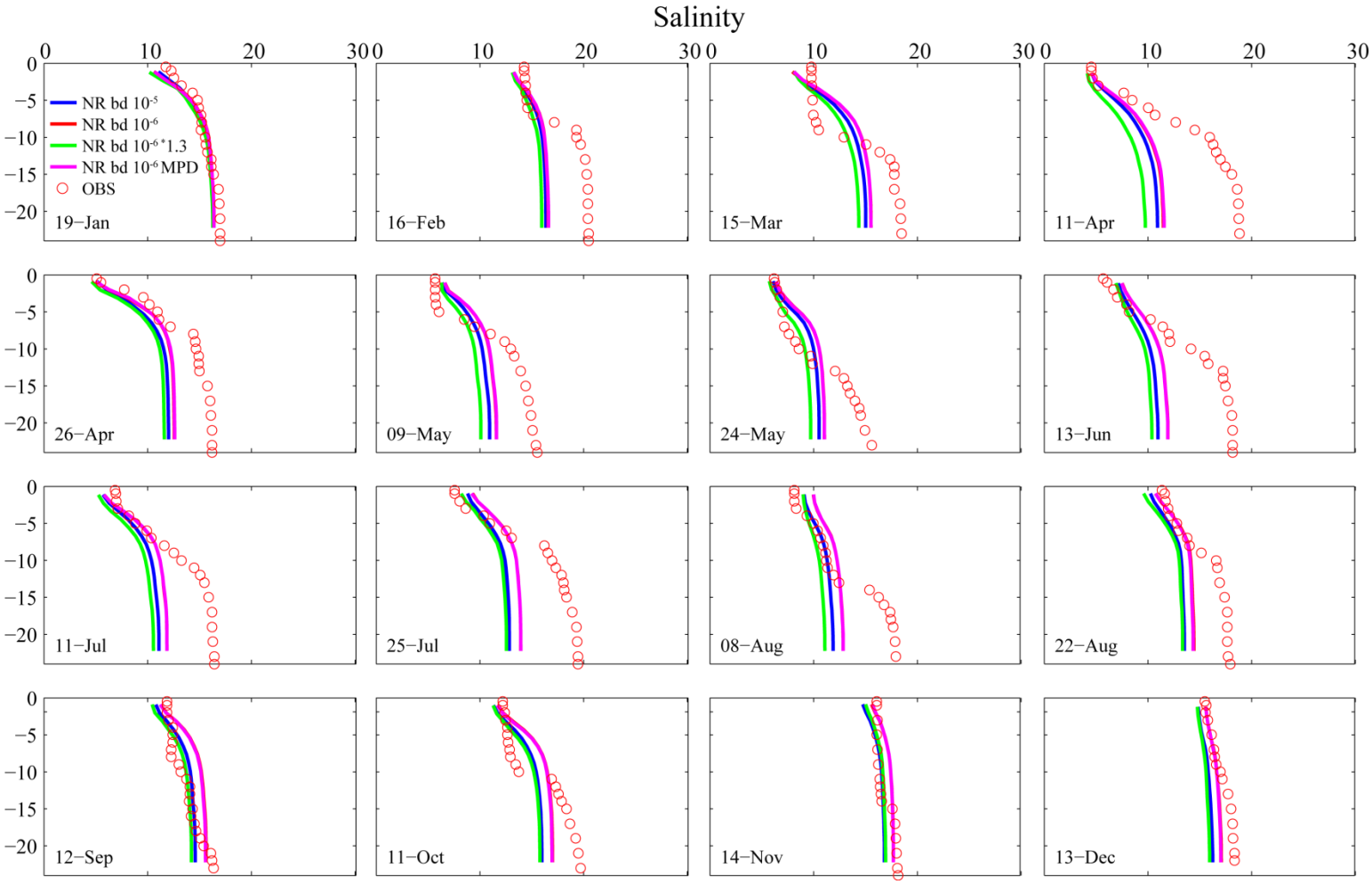

Figure AV.2: Vertical Profiles of salinity for four model simulations using NARR winds (lines) and observed salinity (red circles) at station CB3.3C. bd 10^{-5} and bd 10^{-6} are background diffusivities, *1.3 is NARR winds scaled by 1.3 and MPD denotes MPDATA.

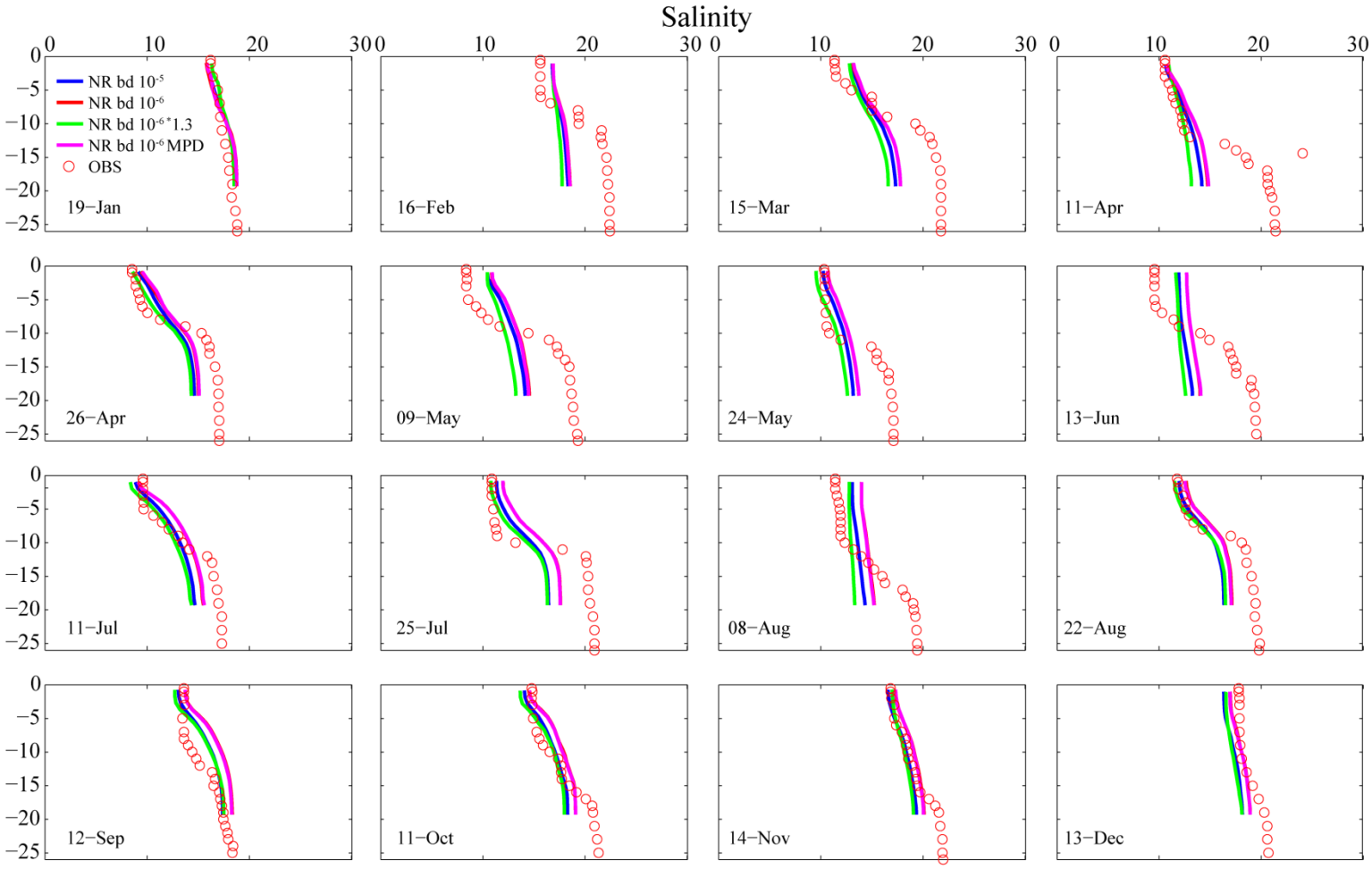

Figure AV.3: Vertical Profiles of salinity for four model simulations using NARR winds (lines) and observed salinity (red circles) at station CB4.3C. bd 10^{-5} and bd 10^{-6} are background diffusivities, *1.3 is NARR winds scaled by 1.3 and MPD denotes MPDATA.

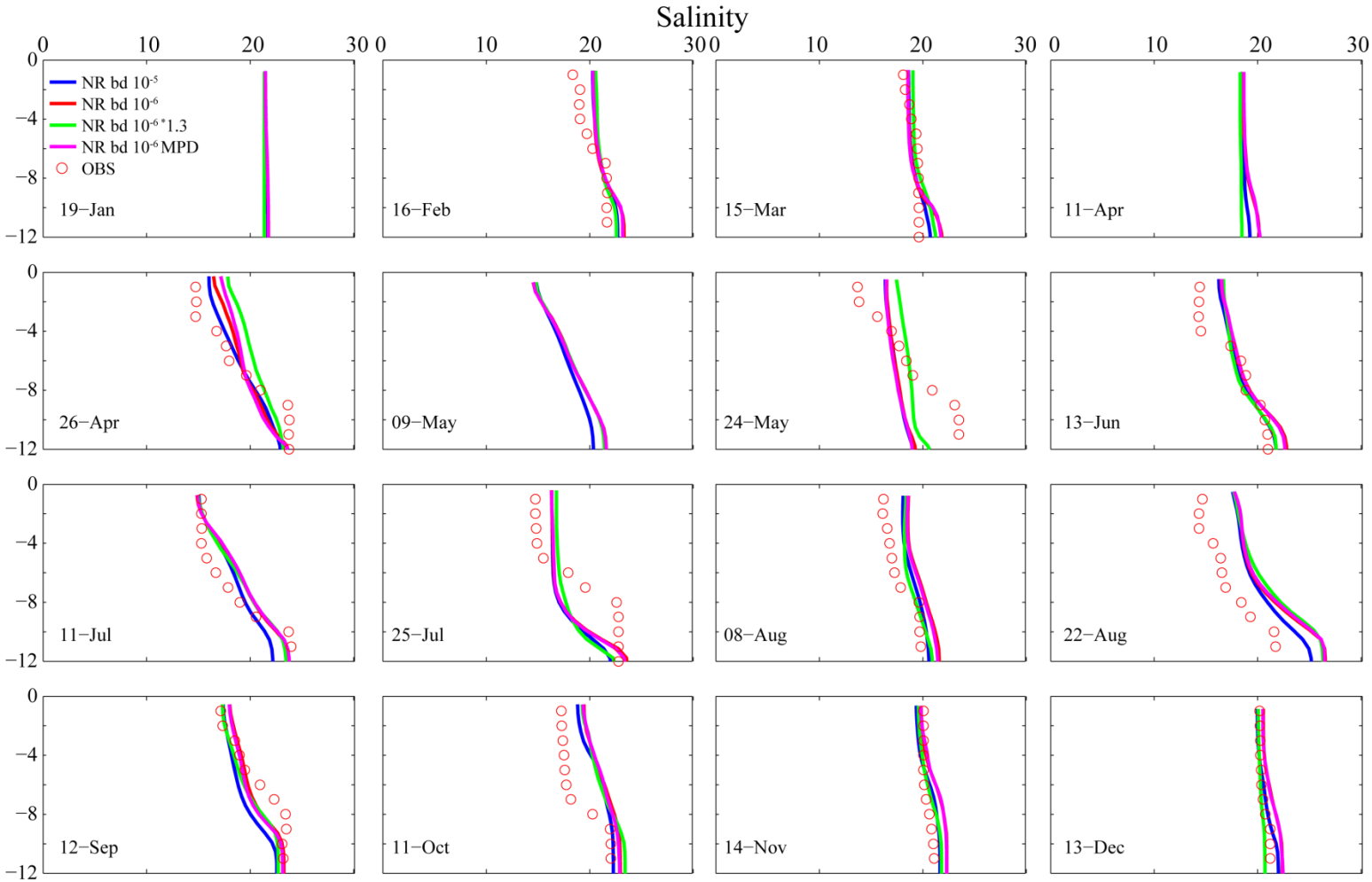

Figure AV.4: Vertical Profiles of salinity for four model simulations using NARR winds (lines) and observed salinity (red circles) at station CB6.1. bd 10^{-5} and bd 10^{-6} are background diffusivities, *1.3 is NARR winds scaled by 1.3 and MPD denotes MPDATA.

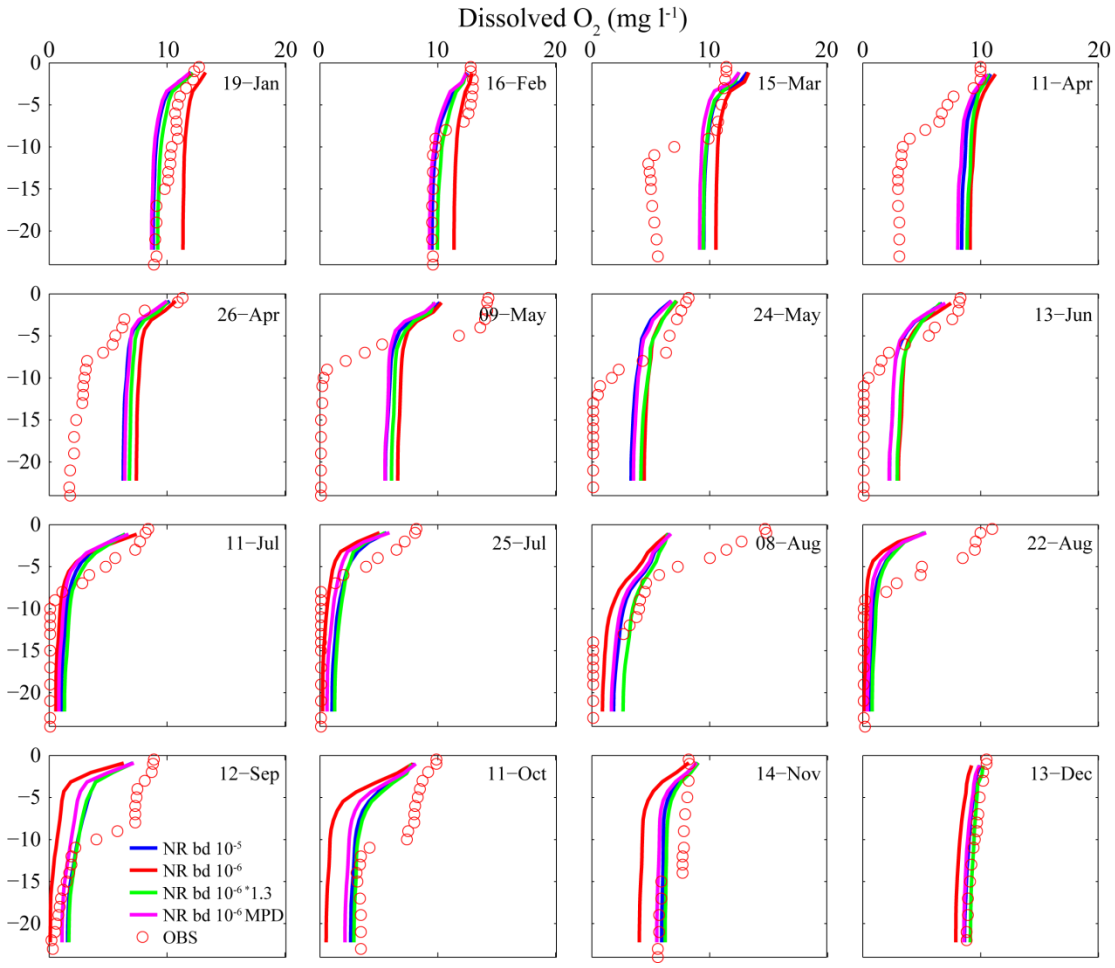

Figure AV.5: Vertical Profiles of dissolved O_2 for four model simulations using NARR winds (lines) and observed salinity (red circles) at station CB3.3C. bd 10^{-5} and bd 10^{-6} are background diffusivities, *1.3 is NARR winds scaled by 1.3 and MPD denotes MPDATA.

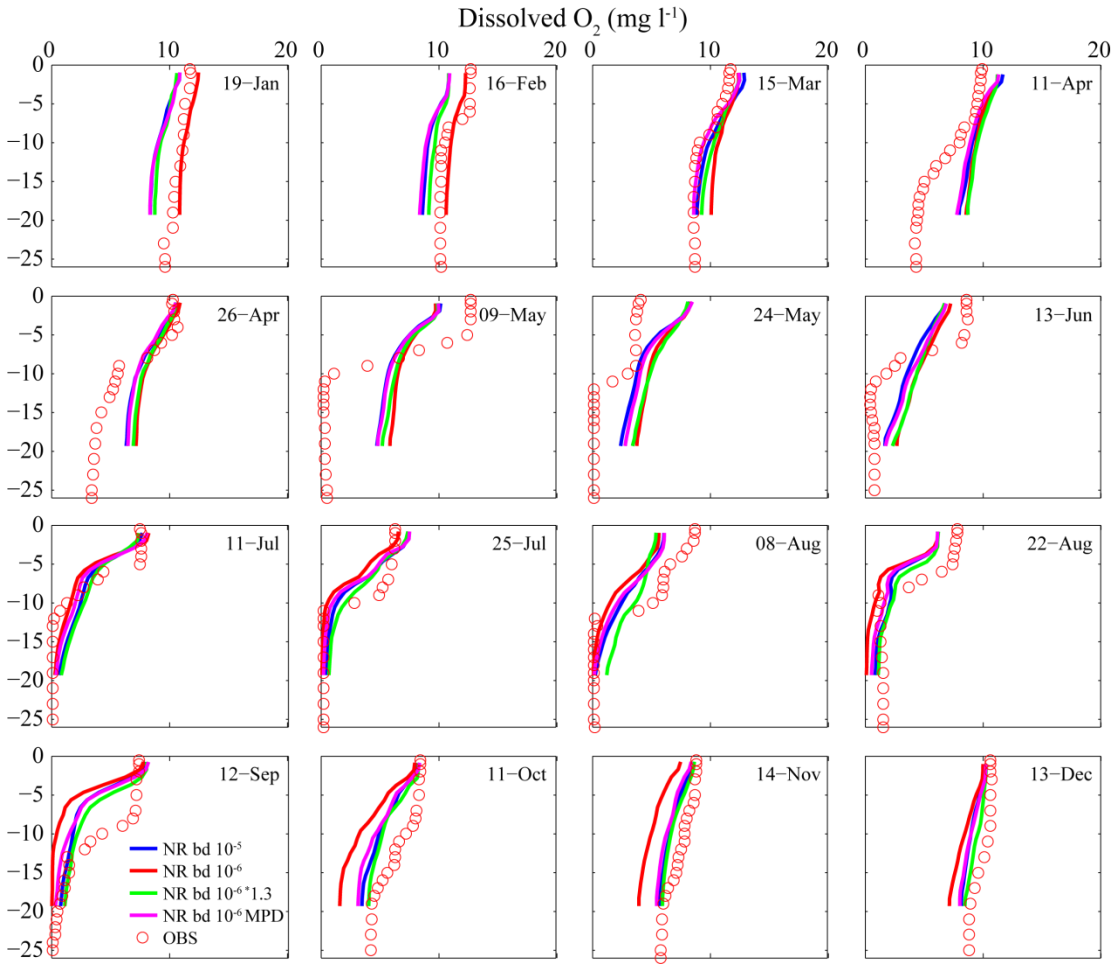

Figure AV.6: Vertical Profiles of dissolved O_2 for four model simulations using NARR winds (lines) and observed salinity (red circles) at station CB4.3C. bd 10^{-5} and bd 10^{-6} are background diffusivities, *1.3 is NARR winds scaled by 1.3 and MPD denotes MPDATA.

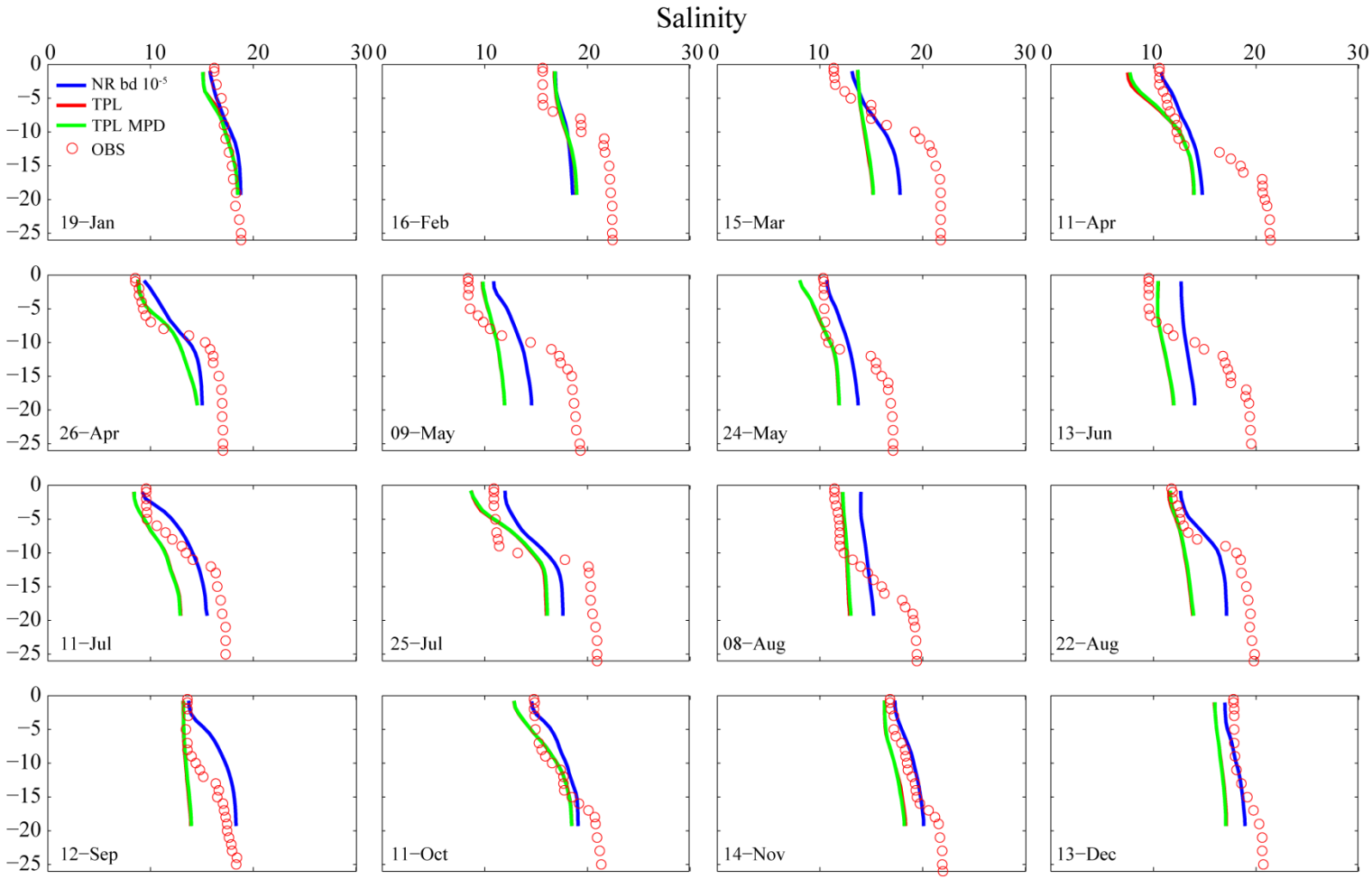

Figure AV.7: Vertical Profiles of salinity for four model simulations using NARR winds with bd 10^{-5} (blue lines), TPL winds (red lines), TPL winds with MPDATA (green lines) and observed salinity (red circles) at station CB4.3C.

APPENDIX VI: A REGIONAL COUPLED HYDRODYNAMIC-BIOGEOCHEMICAL MODEL FOR CHESAPEAKE BAY

High-resolution, coupled hydrodynamic-biogeochemical models are valued for their ability to accurately represent physical and biogeochemical process in coastal ecosystems, especially with increasingly affordable computing power. Less spatially-resolved models (regional scale) are still useful for research needs, as they can be executed quickly (minutes), represent biogeochemistry at the scales where it has been predominantly measured (regionally) and can be used to compute simple and unambiguous budgets of key variables.

Such a model was developed for Chesapeake Bay, using RCA as the biogeochemical model (Chapter 5) and salt- and water-balance model (box model) computations for physical transport (Hagy, 2002; Hagy et al., 2000). The model domain includes 17 boxes (9 surface-layer, 8 bottom-layer; Fig. AVI.1 & 5.1), whose vertical separations is based on mean-pycnocline depths for each region (Hagy, 2002). The model solves a series of linear equations to compute advective and non-advective exchanges between boxes based upon freshwater inputs and salt distributions. Details of the calculation are described elsewhere (Hagy, 2002; Hagy et al., 2000; Testa and Kemp, 2008). The biogeochemical model (RCA) was coupled to the box model transports using the same boundary and initial conditions, external flows and loadings, and sediment initialization as described in Chapter 5. Model simulations were run on a 6-hour time step over the 1986-2006.

The box model represented interannual and regional variations in salinity well, as would be expected for such a model (Fig. AVI.2). The model also represented interannual and regional variations in bottom-water dissolved O_2 (Fig. AVI.3), capturing true

seasonal minima in O_2 (anoxia) in several regions of the Bay. The high-resolution, coupled model failed to capture these minima (Chapter 5). Budget calculations for POC in each box during two seasons, averaged over the 1986-2006 period, suggest the key role of *both* vertical sinking and landward longitudinal transport as mechanisms for POC delivery to bottom waters (Fig. AVI.4). Landward POC inputs in bottom water were highest in lower Bay regions, but muted in upper-Bay regions, while net POC imports (the potential fuel for O_2 depletion) were also greatest in the lower Bay (Fig. AVI.4). This is consistent with the suggestion that landward, bottom-water transport of organic carbon resulting from net surface-layer carbon production in seaward Bay regions is a key aspect of the Bay carbon budget supporting O_2 depletion. Analyses of interannual changes in these transports and the associated O_2 depletion rates will be performed in the future.

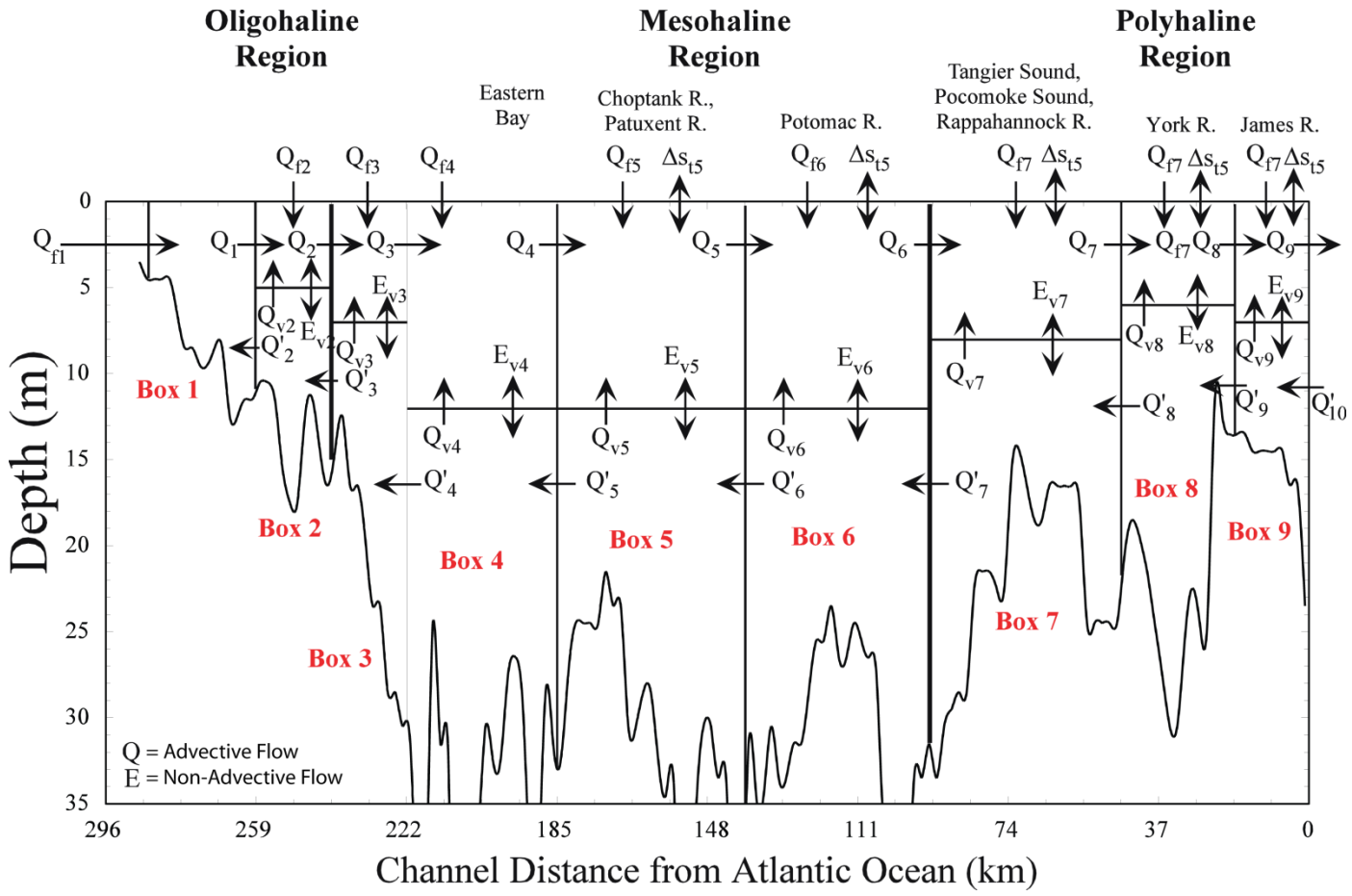

Figure AVI.1: Diagram of salt- and water-balance (box) model for Chesapeake Bay, including relevant freshwater inputs, transport coefficients, and box identifiers. An aerial view of this model is included in Fig. 5.1. Model computations are described elsewhere.

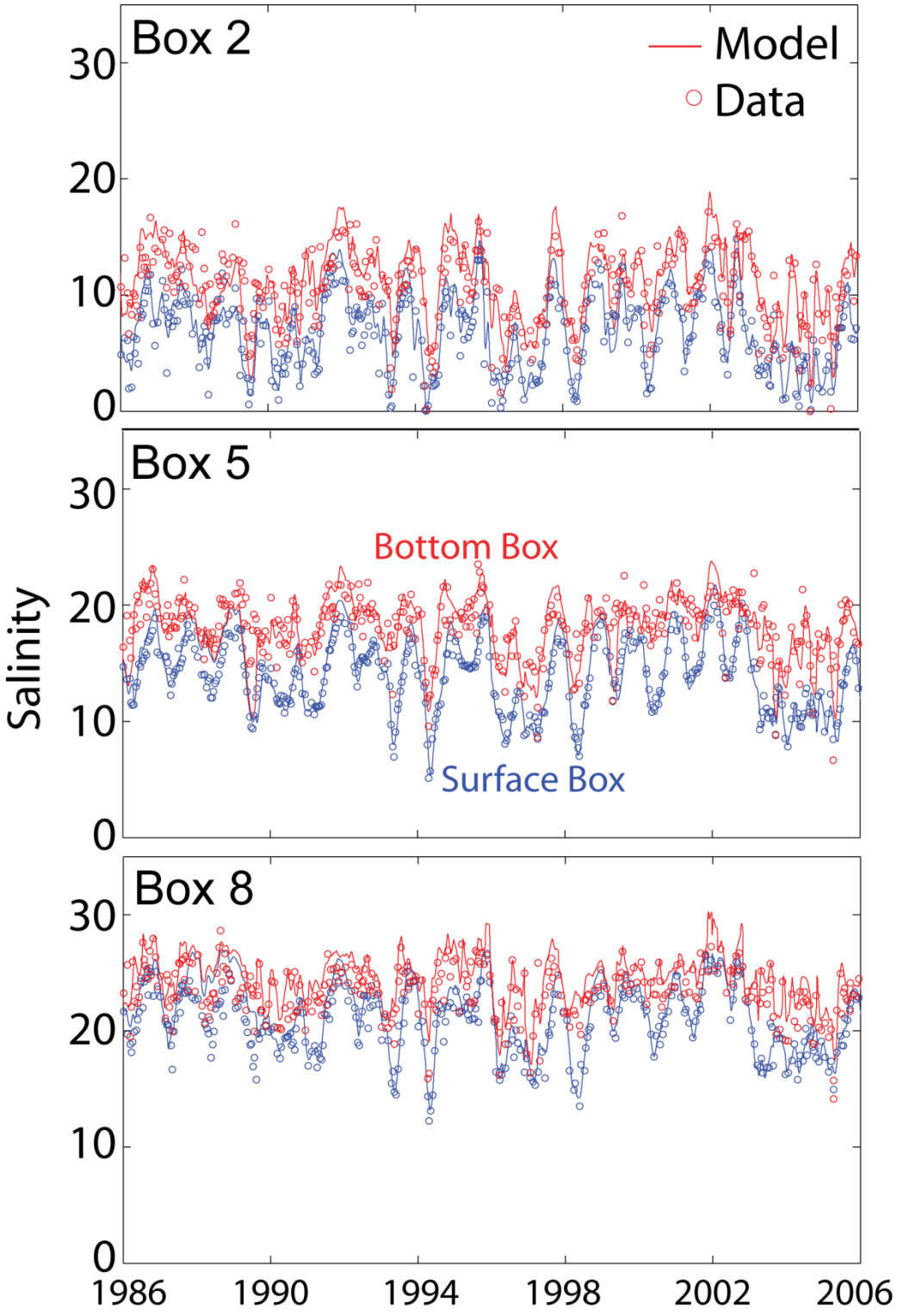

Figure AVI.2: Time-series (1986-2006) of model computed (lines) and observed salinity (circles) in surface- and bottom-layers of three regions of Chesapeake Bay.

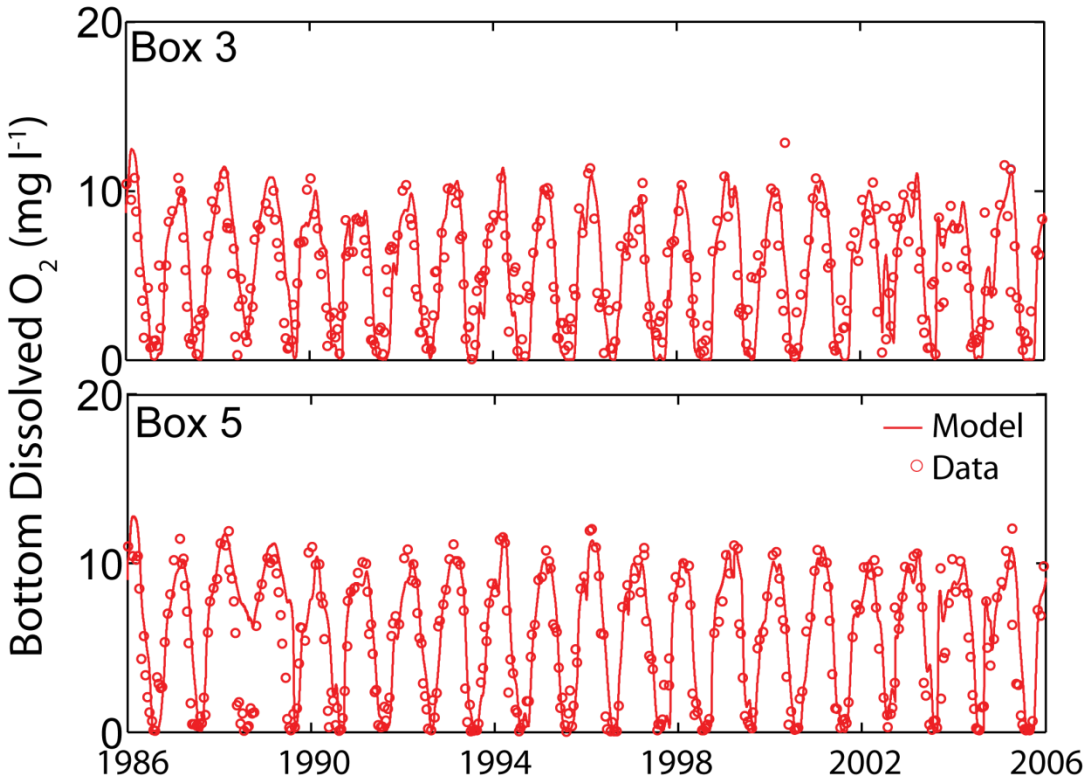

Figure AVI.3: Time-series (1986-2006) of model computed (lines) and observed dissolved O_2 (circles) in the bottom-layer of two regions of Chesapeake Bay.

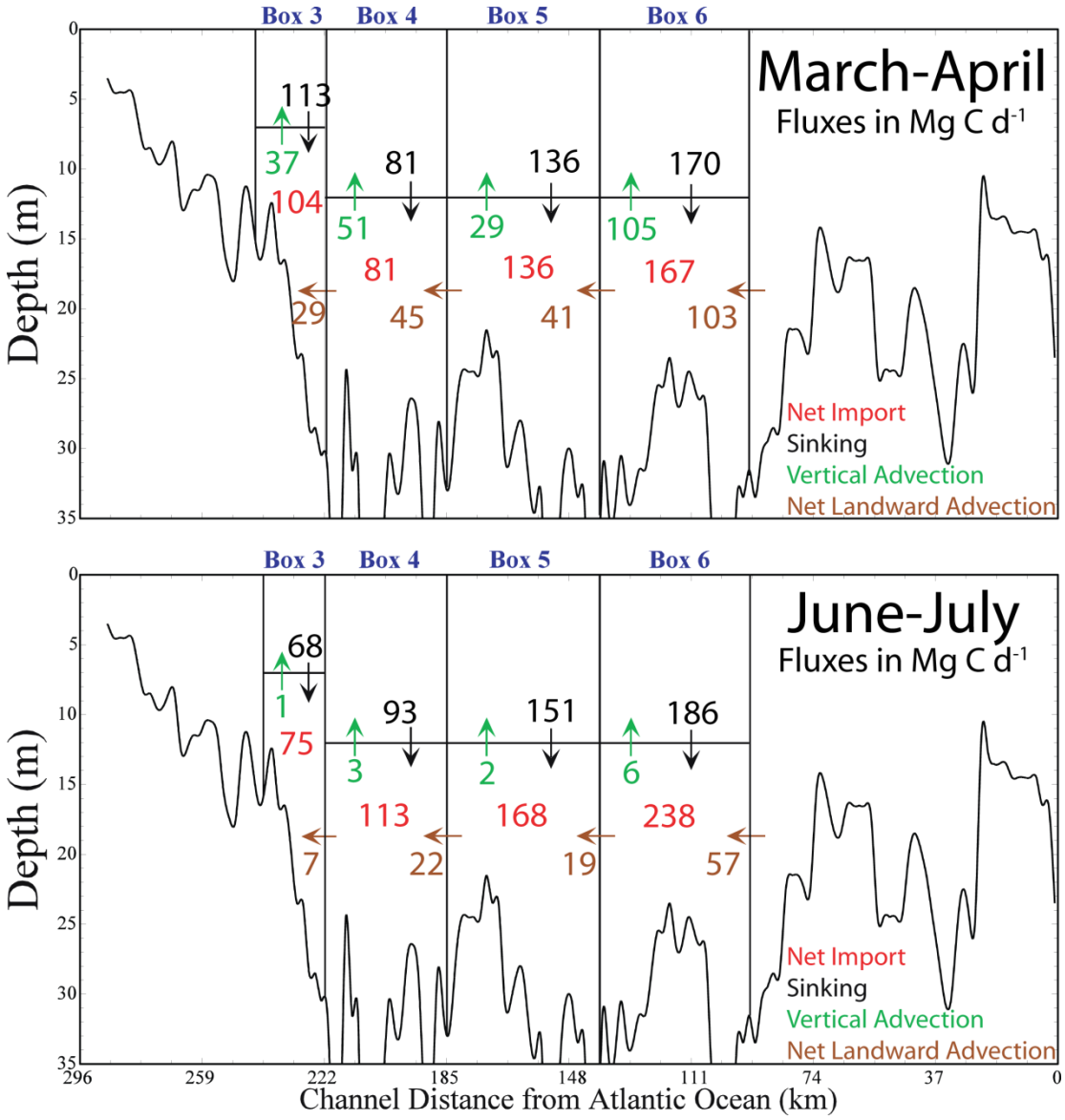

Figure AVI.4: Mean POC budgets for middle-Bay regions as computed from model computations in Chesapeake Bay for two seasons.

REFERENCES

Aller, R.C., 1982. The effects of macrobenthos on chemical properties of marine sediments and overlying water, in: McCall, O.P.L., Tevesz, M.J.S. (Eds.), Animal-Sediment Relations. Plenum Press, New York, pp. 3-52.

An, S., Gardner, W.S., 2002. Dissimilatory nitrate reduction to ammonium (DNRA) as a nitrogen link, versus denitrification as a sink in a shallow estuary (Laguna Madre/Baffin Bay, Texas). Mar. Ecol. Prog. Ser. 237, 41-50.

Andrews, M.J., Rickard, D.G., 1980. Rehabilitation of the inner Thames Estuary. Mar. Pollut. Bull. 11, 327-332.

Arnell, N.W., 1999. The effect of climate change on hydrological regimes in Europe: a continental perspective. Global Environ. Change 9, 5-23.

Baden, S.P., L.O., L., Pihl, L., Rosenberg, R., 1990. Effects of eutrophication on benthic communities including fish: Swedish west coast. Ambio 19, 113-122.

Balzer, W., 1996. Particle mixing processes of Chernobyl fallout in deep Norwegian Sea sediments: Evidence for seasonal effects. Geochim. Cosmochim. Acta 60, 3425-3433.

Banas, N.S., Hickey, B., Newton, J., Ruesink, J., 2007. Tidal exchange, bivalve grazing, and patterns of primary production in Willapa Bay, Washington, USA. Mar. Ecol. Prog. Ser. 34, 123-139.

Bertics, V.J., J.A.Sohm, Treude, T., Chow, C.E.T., Capone, D.C., Fuhrman, J.A., Ziebis, W., 2010. Burrowing deeper into benthic nitrogen cycling: the impact of bioturbation on nitrogen fixation coupled to sulfate reduction. Mar. Ecol. Prog. Ser. 409, 1-15.

Bertics, V.J., Löscher, C.R., Salonen, I., Dale, A.W., Gier, J., Schmitz, R.A., Treude, T., 2013. Occurrence of benthic microbial nitrogen fixation coupled to sulfate reduction in the seasonally hypoxic Eckernförde Bay, Baltic Sea. Biogeosciences 10, 1243-1258.

Bianchi, T.S., DiMarco, S.F., Allison, M.A., Chapman, P., J.H. Cowan, J., Hetland, R.D., Morse, J.W., 2008. Controlling hypoxia on the U.S. Louisiana shelf: beyond the nutrient-centric view. EOS: Transactions of the American Geophysical Union 89, 236-237.

Bicknell, B.R., Imhoff, J.C., Kittle, J.L., Donigian, A.S., Johanson, R.C., 1996. Hydrological Simulation Program - FORTRAN. User's Manual for Release 11. US EPA, Athens, Georgia, p. 100.

Bidle, K.D., Azam, F., 1999. Accelerated dissolution of diatom silica by marine bacterial assemblages. Nature 397, 508-512.

Bienfang, P.K., 1981. Sinking rates of heterogeneous, temperate phytoplankton populations. J. Plankton Res. 3, 235-253.

Bienfang, P.K., Harrison, P.J., Quarmby, L.M., 1982. Sinking rate response to depletion of nitrate, phosphate and silicate in four marine diatoms. Mar. Biol. 67, 295-302.

Billen, G., Garnier, J., Ficht, A., Cun, C., 2001. Modeling the response of water quality in the Seine River estuary to human activity in its watershed over the last 50 years. Estuaries 24, 977-993.

Blackburn, T.H., Blackburn, N.D., Jensen, K., Risgaard-Petersen, N., 1994. Simulation model of the coupling between nitrification and denitrification in a freshwater sediment. Appl. Environ. Microbiol. 60, 3089-3095.

Boesch, D.F., 2002. Challenges and opportunities for science in reducing nutrient over-enrichment of coastal ecosystems. Estuaries 25, 886-900.

Boesch, D.F., Brinsfield, R.B., Magnien, R.E., 2001. Chesapeake Bay eutrophication: scientific understanding, ecosystem resotration, and challenges for agriculture. J. Environ. Qual. 30, 303-320.

Boicourt, W.C., 1992. Influences of circulation processes on dissolved oxygen in the Chesapeake Bay, in: Smith, D.E., Leffler, M., Mackiernan, G. (Eds.), Oxygen Dynamics in the Chesapeake Bay, A Synthesis of Recent Research. Maryland Sea Grant, College Park, Maryland, pp. 7-59.

Boudreau, B.P., 1991. Modelling the sulfide-oxygen reaction and associated pH gradients in porewaters. Geochim. Cosmochim. Acta 55, 145-159.

Boynton, W.R., Bailey, E., 2008. Sediment oxygen and nutrient exchange measurements from Chesapeake Bay, tributary rivers and Maryland coastal bays: Development of a comprehensive database and analysis factors controlling patterns and magnitude of sediment-water exchanges. University of Maryland Center for Environmental Science, Solomons, MD, p. 202.

Boynton, W.R., Garber, J.H., Summers, R., Kemp, W.M., 1995. Inputs, transformations, and transport of nitrogen and phosphorus in Chesapeake Bay and selected tributaries. Estuaries 18, 285-314.

Boynton, W.R., Kemp, W.M., 2000. Influence of river flow and nutrient loads on selected ecosystem processes: A synthesis of Chesapeake Bay data, in: Hobbie, J.E. (Ed.), Estuarine science: A synthetic approach to research and practice. Island Press, Washington DC, pp. 269-298.

Boynton, W.R., Kemp, W.M., 2008. Estuaries, in: Capone, D.G., Bronk, D.A., Mulholland, M.R., Carpenter, E.J. (Eds.), Nitrogen in the marine environment, 2nd ed. Elsevier, Amsterdam, pp. 809-866.

Brady, D.C., Testa, J.M., DiToro, D.M., Boynton, W.R., Kemp, W.M., 2013. Sediment flux modeling: calibration and application for coastal systems. Estuar. Coast. Shelf Sci. 117, 107-124.

Brady, D.C., Testa, J.M., Toro, D.M.D., Boynton, W.R., W.M.Kemp, 2012. Sediment flux modeling: calibration and application for coastal systems. Estuar. Coast. Shelf Sci.

Brandes, J.A., Devol, A.H., 1995. Simultaneous nitrate and oxygen respiration in coastal sediments: Evidence for discrete diagenesis. J. Mar. Res. 53, 771-797.

Breitburg, D.L., 1990. Near-shore hypoxia in the Chesapeake Bay: Patterns and relationships among physical factors. Estuar. Coast. Shelf Sci. 30, 593-609.

Breitburg, D.L., 2002. Effects of hypoxia, and the balance between hypoxia and enrichment, on coastal fishes and fisheries. Estuaries 25, 767-781.

Brosnan, T.M., O'Shea, M.L., 1996. Long-term improvements in water quality due to sewage abatement in the lower Hudson River. Estuaries 19, 890-900.

Brunet, R.D., Garcia-Gill, L.J., 1996. Sulfide-induced dissimilatory nitrate reduction to ammonia in anaerobic freshwater sediments. FEMS Microbiol. Lett. 21, 131-138.

Burdige, D.J., 1991. The kinetics of organic matter mineralization in anoxic marine sediments J. Mar. Res. 49, 727-761.

Burgin, A.J., Hamilton, S.K., 2007. Have we overemphasized the role of denitrification in aquatic ecosystems? A review of nitrate removal pathways. Front. Ecol. Environ. 5, 89-96.

Cai, W.-J., III, G.W.L., Cornwell, J.C., Giblin, A.E., 2010. Carbon cycling and the coupling between proton and electron transfer reactions in aquatic sediments in Lake Champlain. Aquatic Geochemistry 16, 421–446.

Cai, W.-J., Sayles, F.L., 1996. Oxygen penetration depths and fluxes in marine sediments. Mar Chem 52, 123-131.

Caraco, N.F., Cole, J.J., Likens, G.E., 1989. Evidence for sulphate-controlled phosphorus release from sediments of aquatic systems. Nature 341, 316-318.

Carstensen, J., Conley, D.J., Andersen, J.H., Ærtebjerg, G., 2006. Coastal eutrophication and trend reversal: A Danish case study. Limnol. Oceanogr. 51, 398-408.

Casamayor, E.O., García-Cantizano, J., Mas, J., Pedrós-Alió, C., 2001. Primary production in estuarine oxic/anoxic interfaces: contribution of microbial dark CO_2 fixation in the Ebro River Salt Wedge Estuary. Mar. Ecol. Prog. Ser. 215, 49-56.

Cerco, C.F., 1995. Simulation of long-term trends in chesapeake Bay eutrophication. J. Environ. Eng. 121, 298-310.

Cerco, C.F., 2000. Phytoplankton kinetics in the Chesapeake Bay eutrophication model. Water Quality and Ecosystems Modeling 1, 5-49.

Cerco, C.F., Cole, T., 1993. Three-dimensional eutrophication model of Chesapeake Bay. J. Environ. Engr. ASCE 119, 1006-1025.

Cerco, C.F., Meyers, M., 2000. Tributary refinements to Chesapeake Bay model. J. Environ. Eng. 126, 164-174.

Cerco, C.F., Noel, M.R., 2005. Incremental improvements in Chesapeake Bay environmental package. J. Environ. Eng. 131, 745-754.

Cerco, C.F., Noel, M.R., 2007. Can oyster restoration reverse cultural eutrophication in Chesapeake Bay? Estuar. Coast. 30, 331-343.

Cerco, C.F., Seitzinger, S.P., 1997. Measured and modeled effects of benthic algae on eutrophication in Indian River Rehoboth Bay, Delaware. Estuaries 20, 231-248.

Chen, C.-C., Gong, G.-C., Shiah, F.-K., 2007. Hypoxia in the East China Sea: One of the largest coastal low-oxygen areas in the world. Mar. Environ. Res. 64, 399-408.

Chen, S.-N., Sanford, L.P., 2009. Axial wind effects on stratification and longitudinal salt transport in an idealized, partially mixed estuary. J. Phys. Oceanogr. 39, 1905-1920.

Cheng, P., Li, M., Li, Y., 2013. Generation of an estuarine sediment plume by a tropical storm. Journal of Geophysical Research-Oceans, in press.

Cloern, J.E., 2001. Our evolving conceptual model of the coastal eutrophication problem. Mar. Ecol. Prog. Ser. 210, 223-253.

Conley, D.J., Carstensen, J., Ærtebjerg, G., Christensen, P.B., Dalsgaard, T., Hansen, J.L.S., Josefson, A.B., 2007. Long-term changes and impacts of hypoxia in Danish coastal waters. Ecol. Appl. S17, S165-S184.

Conley, D.J., Carstensen, J., Vaquer, R., Duarte, C.M., 2009a. Ecosystem thresholds with hypoxia. Hydrobiologia 629, 21-29.

Conley, D.J., Humborg, C., Rahm, L., Savchuk, O.P., Wulff, F., 2002. Hypoxia in the Baltic Sea and basin-scale changes in phosphorus biogeochemistry. Environ. Sci. Technol. 36, 5315-5320.

Conley, D.J., Paerl, H.W., Howarth, R.W., Boesch, D.F., Seitzinger, S.P., Havens, K.E., Lancelot, C., Likens, G.E., 2009b. Controlling eutrophication: nitrogen and phosphorus. Science 323, 1014-1015.

Conley, D.J., Schelske, C.L., Stoermer, E.F., 1993. Modification of the biogeochemical cycle of silica with eutrophication. Mar. Ecol. Prog. Ser. 101, 179-192.

Cornwell, J.C., Sampou, P.A., 1995. Environmental controls on iron sulfide mineral formation in a coastal plain estuary, in: Vairamurthy, M.A., Schoonen, M.A.A. (Eds.),

Geochemical Transformations of Sedimentary Sulfur. American Chemical Society, Washington D.C., pp. 224-242.

Cowan, J.L., Boynton, W.R., 1996. Sediment-water oxygen and nutrient exchanges along the longitudinal axis of Chesapeake Bay: Seasonal patterns, controlling factors and ecological significance. Estuaries 19, 562-580.

Cowan, J.L., Pennock, J.R., Boynton, W.R., 1996. Seasonal and interannual patterns of sediment-water nutrient and oxygen fluxes in Mobile Bay, Alabama (USA): Regulating factors and ecological significance. Mar. Ecol. Prog. Ser. 141, 229-245.

Cox, T.J.S., Maris, T., Soetaert, K., Conley, D.J., Damme, S.V., Meire, P., Middelburg, J.J., Vos, M., Struyf, E., 2009. A macro-tidal freshwater ecosystem recovering from hypereutrophication: the Schelde case study. Biogeosciences 6, 2935-2948.

Cronin, W.B., Pritchard, D.W., 1975. Additional statistics on the dimensions of Chesapeake Bay and its tributaries: Cross-section widths and segment volumes per meter depth. Chesapeake Bay Institute, The Johns Hopkins University, Baltimore, Maryland, p. 475.

D'Avanzo, C., Kremer, J.N., 1994. Diel oxygen dynamics and anoxic events in an eutrophic estuary of Waquoit Bay, Massachusetts. Estuaries 17, 131-139.

D'Elia, C.F., Sanders, J.G., Boynton, W.R., 1986. Nutrient enrichment studies in a coastal plain estuary: phytoplankton growth in large scale, continuous cultures. Canadian Journal of Fisheries and Aquatic Science 43, 397-406.

Dalsgaard, T., Thamdrup, B., 2002. Factors controlling anaerobic ammonium oxidation with nitrite in marine sediments. Appl. Environ. Microbiol. 6, 3802-3808.

Dame, R.F., Olenin, S., 2005. The comparative roles of suspension feeders in ecosystems, NATO ASI Science Series 4: Earth Environmental Science. Springer-Verlag, Berlin.

Decker, M.B., Breitburg, D.L., Purcell, J.E., 2004. Effects of low dissolved oxygen on zooplankton predation by the ctenophore *Mnemiopsis leidyi*. Mar. Ecol. Prog. Ser. 280, 163-172.

Dhakar, S.P., Burdige, D.J., 1996. Coupled, non-linear, steady state model for early diagenetic processes in pelagic sediments. Am. J. Sci. 296, 296-330.

Di Toro, D.M., 2001. Sediment Flux Modeling. Wiley-Interscience, New York.

Di Toro, D.M., Fitzpatrick, J.J., 1993. Chesapeake Bay Sediment Flux Model. Chesapeake Bay Program Office, U.S. Environmental Protection Agency and U.S. Army Engineer District, Baltimore, Annapolis, Maryland and Baltimore, Maryland, p. 316.

Di Toro, D.M., Matystik, W.F., 1979. Phosphorus recycle and chlorophyll in the Great Lakes. J. Great Lakes Res. 5, 233-245.

Díaz, R.J., 2001. Overview of hypoxia around the world. J. Environ. Qual. 30, 275-281.

Díaz, R.J., Rosenberg, R., 1995. Marine benthic hypoxia: A review of its ecological effects and the behavioural responses of benthic macrofauna. Oceanogr. Mar. Biol. Annu. Rev. 33, 245-303.

Díaz, R.J., Rosenberg, R., 2008. Spreading dead zones and consequences for marine ecosystems. Science 321, 926-929.

Doney, S.C., Lindsay, K., Caldeira, K., Campin, J.-M., Drange, H., Dutay, J.-C., M. Follows, M., Gao, Y., Gnanadesikan, A., Gruber, N., 2004. Evaluating global ocean carbon models: the importance of realistic physics. Global Biogeochem. Cycles 18.

Dong, L.F., Thornton, D.C.O., Nedwell, D.B., Underwood, G.J.C., 2000. Denitrification in sediments of the River Colne estuary, England. Mar. Ecol. Prog. Ser. 203, 109-122.

Duarte, C.M., Conley, D.J., Carstensen, J., Sánchez-Camacho, M., 2009. Return to Neverland: shifting baselines affect eutrophication restoration targets. Estuar. Coast. 32, 29-36.

Durham, W.M., Stocker, R., 2012. Thin phytoplankton layers: characteristics, mechanisms, and consequences. Annual Review of Marine Science 4, 177-207.

Egbert, G.D., Erofeeva, S.Y., 2002. Efficient inverse modeling of barotropic ocean tides. JAtOT 19, 183-204.

Eiola, K., Meier, H.E.M., Almroth, E., 2009. On the dynamics of oxygen, phosphorus and cyanobacteria in the Baltic Sea: A model study. J. Mar. Syst. 75, 163-184.

Emerson, S., Jahnke, R., Heggie, D., 1984. Sediment water exchange in shallow water estuarine sediments. J. Mar. Syst. 42, 709-730.

Enoksson, V., 1993. Nutrient recycling by coastal sediments: Effects of added algal material. Mar. Ecol. Prog. Ser. 92, 245-254.

EPA, 1997. Methods for the determination of chemical substances in marine and estuarine environmental matrices, 2 ed. United States Environmental Protection Agency, Cincinnati, OH, p. 211.

Eyre, B.D., Ferguson, A.J.P., 2009. Denitrification efficiency for defining critical loads of carbon in shallow coastal ecosystems. Hydrobiologia 629, 137-146.

Fairall, C.W., Bradley, E.F., J.E.Hare, Grachev, A.A., Edson, J.B., 2003. Bulk parameterization of air-sea fluxes: Updates and verification for the COARE algorithm. J. Clim. 16, 571-591.

Fanning, K.A., Pilson, M.E.Q., 1974. The diffusion of dissolved silica out of deep-sea sediments. JGR 79, 1293-1297.

Fennel, K., Hu, J., Laurent, A., Marta-Almeida, M., Hetland, R., 2013. Sensitivity of hypoxia predictions for the Northern Gulf of Mexico to sediment oxygen consumption and model nesting. Journal of Geophysical Research: Oceans, 1-14.

Fennel, K., Wilkin, J., Levin, J., Moisan, J., O'Reilly, J., Haidvogel, D., 2006. Nitrogen cycling in the Middle Atlantic Bight: Results from a three-dimensional model and implications for the North Atlantic nitrogen budget. Global Biogeochem. Cycles 20, doi:10.1029/2005GB002456.

Fisher, T.R., Gustafson, A.B., Sellner, K., Lacouture, R., Haas, L.W., Wetzel, R.L., Magnien, R., Everitt, D., Michaels, B., Karrh, R., 1999. Spatial and temporal variation of resource limitation in Chesapeake Bay. Mar. Biol. 133, 763-778.

Fisher, T.R., Peele, E.R., Ammerman, J.W., L.W. Harding, J., 1992. Nutrient limitation of phytoplankton in Chesapeake Bay. Mar. Ecol. Prog. Ser. 82, 51-63.

Flemer, D.A., Mackiernan, G.B., Nehlsen, W., Trippie, V.K., Biggs, R.B., Blaylock, D., Burger, N.H., Davidson, L.C., Haberman, D., Price, K.S., Taft, J.L., 1983. Chesapeake Bay: A profile of environmental change. Us Environmental Protection Agency, Philadelphia, Pennsylvania, p. 200.

Fofonoff, N.P., 1985. Physical properties of seawater: A new salinity scale and equation of state for seawater. JGR 90, 3332-3342.

Froelich, P.N., 1988. Kinetic control of dissolved phosphate in natural rivers and estuaries: A primer on the phosphate buffer mechanism. Limnol. Oceanogr. 33, 649-668.

Froelich, P.N., Bender, M.L., Luedtke, N.A., 1982. The marine phosphorus cycle. Am. J. Sci. 282, 474-511.

Gardner, W.S., McCarthy, M.J., An, S., D., S., Sell, K.S., Brock, D., 2006. Nitrogen fixation and dissimilatory nitrate reduction to ammonium (DNRA) support nitrogen dynamics in Texas estuaries. Limnol. Oceanogr. 51, 558-568.

Gilbert, D., Rabalais, N.N., Diaz, R.J., Zhang, J., 2010. Evidence for greater oxygen decline rates in the coastal ocean than in the open ocean. Biogeosciences 7, 2283-2296.

Glibert, P.M., 1982. Regional studies of daily, seasonal and size fraction variability in ammonium remineralization. Mar. Biol. 70, 209-222.

Goodrich, D.M., Boicourt, W.C., Hamilton, P., Pritchard, D.W., 1987. Wind-induced destratification in Chesapeake Bay. J. Phys. Oceanogr. 17, 2232-2240.

Greene, R.M., Lehrter, J.C., III, J.D.H., 2009. Multiple regression models for hidcasting and forecasting midsummer hypoxia in the Gulf of Mexico. Ecol. Appl.

Gypens, N., .Lancelot, C., Soetaert, K., 2008. Simple parameterisations for describing N and P diagenetic processes: Application in the North Sea. Prog. Oceanogr. 76, 89-110.

Hagy, J.D., 2002. Eutrophication, hypoxia, and trophic transfer efficiency in Chesapeake Bay. University of Maryland, College Park, College Park, Maryland.

Hagy, J.D., Boynton, W.R., Jasinski, D.A., 2005. Modeling phytoplankton deposition to Chesapeake Bay sediments during winter-spring: Interannual variability in relation to river flow. Estuar. Coast. Shelf Sci. 62, 25-40.

Hagy, J.D., Boynton, W.R., Keefe, C.W., Wood, K.V., 2004. Hypoxia in Chesapeake Bay, 1950-2001: Long-term change in relation to nutrient loading and river flow. Estuaries 27, 634-658.

Hagy, J.D., Sanford, L.P., Boynton, W.R., 2000. Estimation of net physical transport and hydraulic residence times for a coastal plain estuary using box models. Estuaries 23, 328-340.

Haidvogel, D.B., Arango, H.G., Hedstrom, K., Beckmann, A., Malanotte-Rizzoli, P., Shchepetkin, A.F., 2000. Model evaluation experiments in the North Atlantic Basin: simulations in nonlinear terrain-following coordinates. DyAtO 32, 239-281.

Harding, L.W., Jr., Mallonee, M.E., Perry, E., 2002. Toward a predictive understanding of primary productivity in a temperate, partially stratified estuary. Estuar. Coast. Shelf Sci. 55, 437-463.

Harding, L.W., Perry, E., 1997. Long-term increase of phytoplankton biomass in Chesapeake Bay, 1950-1994. Mar. Ecol. Prog. Ser. 157, 39-52.

Heip, C.H.R., Goosen, N.K., Herman, P.M.J., Kromkamp, J., Middelburg, J.J., Soetaert, K., 1995. Production and consumption of biological particles in temperate tidal estuaries, in: Ansell, A.D., Gibson, R.N., Barnes, M. (Eds.), Oceanogr. Mar. Biol. Annu. Rev. University College London Press, London, pp. 1-149.

Henriksen, K., Kemp, W.M., 1988. Nitrification in estuarine and coastal marine sediments, in: Blackburn, T.H., Sørensen, J. (Eds.), Nitrogen Cycling in Coastal Marine Environments. John Wiley & Sons, New York, pp. 207-249.

Hetland, R.D., DiMarco, S.F., 2008. How does the character of oxygen demand control the structure of hypoxia on the Texas-Louisiana continental shelf? J. Mar. Syst. 70, 49-62.

Hilton, T.W., Najjar, R.G., Zhong, L., Li, M., 2008. Is there a signal of sea-level rise in Chesapeake Bay salinity. J. Geophys. Res 113, C09002.

Hinkley, D., Schechtman, E., 1987. Conditional bootstrap methods in the mean-shift model. Biometrika 74, 85-93.

Hirsch, R.M., 2012. Flux of nitrogen, phosphorus, and suspended sediment from the Susquehanna River Basin to the Chesapeake Bay during Tropical Storm Lee, September 2011, as an indicator of the effects of reservoir sedimentation on water quality. U.S. Geological Survey, p. 17 p.

Holgate, S.J., Woodworth, P.L., 2004. Evidence for enhanced coastal sea level rise during the 1990s. Geophys. Res. Lett. 31, doi: 10.1029/2004GL019626.

Hooke, R., Jeeves, T.A., 1961. 'Direct search' solution of numerical and statistical problems. Journal of the Association for Computing Machinery (ACM) 8, 212-229.

Huisman, J., Arrayás, M., Ebert, U., Sommeijer, B., 2002. How do sinking phytoplankton species manage to persist? The American Naturalist 159, 245-254.

Ingall, E., Jahnke, R., 1994. Evidence for enhanced phosphorus regeneration from marine sediments overlain by oxygen depleted waters. Geochim. Cosmochim. Acta 58, 2571-2575.

Isleib, R.R., Thuman, A.J., 2011. The Role of estuarine eutrophication models in nutrient criteria development. Proceedings of the Water Environment Federation 2011, 273-298.

Jahnke, R.A., Emerson, S.R., Murray, J.W., 1982. A model of oxygen reduction, denitrification, and organic matter mineralization in marine sediments. Limnol. Oceanogr., 610-623.

Jenkins, M.C., Kemp, W.M., 1984. The coupling of nitrification and denitrification in two estuarine sediments. Limnol. Oceanogr. 29, 609-619.

Jensen, M.H., Lomstein, E., Sorensen, J., 1990. Benthic NH_4^+ and NO_3^- flux following sedimentation of a spring phytoplankton bloom in Aarhus Bight, Denmark. Mar. Ecol. Prog. Ser. 61, 87-96.

Jensen, M.M., Kuypers, M.M.M., Lavik, G., Thamdrup, B., 2008. Rates and regulation of anaerobic ammonium oxidation and denitrification in the Black Sea. Limnol. Oceanogr. 53, 23-36.

Jiang, M.S., Zhou, M., 2008. Massachusetts Bay Eutrophication Model: 2005 Simulation. Massachusetts Water Resources Authority, p. 82.

Jilbert, T., Slomp, C.P., Gustafsson, B.G., Boer, W., 2011. Beyond the Fe-P-redox connection: preferential regeneration of phosphorus from organic matter as a key control on Baltic Sea nutrient cycles. Biogeosciences 8, 1699-1722.

Jones, P.D., 2006. Water quality and fisheries in the Mersey estuary, England: A historical perspective. Mar. Pollut. Bull. 53, 144-154.

Jordan, T.E., Cornwell, J.C., Boynton, W.R., Anderson, J.T., 2008. Changes in phosphorus biogeochemistry along an estuarine salinity gradient: the iron conveyor belt. Limnol. Oceanogr. 53, 172-184.

Jørgensen, B.B., 1977. Bacterial sulfate reduction within reduced microniches of oxidized marine sediments. Mar. Biol. 41, 7-17.

Jørgensen, B.B., Revsbech, N.P., 1985. Diffusive boundary layers and the oxygen uptake of sediments and detritus. Limnol. Oceanogr. 30, 111-122.

Jørgensen, K.S., Sørensen, J., 1988. Two annual maxima of nitrate reduction and denitrification in estuarine sediment (Norsminde Fjord, Denmark). Mar. Ecol. Prog. Ser. 48, 147-154.

Joye, S.B., Hollibaugh, J.T., 1995. Influence of sulfide inhibition of nitrification on nitrogen regeneration in sediments. Science 270, 623-625.

Justíc, D., Rabalais, N.N., Turner, R.E., 2005. Coupling between climate variability and coastal eutrophication: Evidence and outlook for the northern Gulf of Mexico. J. Sea Res. 54, 25-35.

Justíc, D., Turner, R.E., Rabalais, N.N., 2003. Climatic influences on riverine nitrate flux: Implications for coastal marine eutrophication and hypoxia. Estuaries 26, 1-11.

Kana, T.M., Cornwell, J.C., Zhong, L., 2006. Determination of denitrification in the Chesapeake Bay from measurements of N_2 accumulation in bottom water. Estuar. Coast. 29, 222-231.

Kana, T.M., Sullivan, M.B., Cornwell, J.C., Groszkowski, K.M., 1998. Denitrification in estuarine sediments determined by membrane inlet mass spectrometry. Limnol. Oceanogr. 43, 334-339.

Kaushal, S.S., G.E. Likens, Jaworski, N.A., Pace, M.L., Sides, A.M., Seekell, D., Belt, K.T., Secor, D.H., Wingate, R.L., 2010. Rising stream and river temperatures in the United States. Front. Ecol. Environ. 8, 461-466.

Keefe, C.W., 1994. The contribution of inorganic compounds to the particulate organic carbon, nitrogen, and phosphorus in suspended matter and surface sediments of Chesapeake Bay. Estuaries 17, 122-130.

Kemp, W.M., Boynton, W.R., 1992a. Benthic-pelagic interactions: Nutrient and oxygen dynamics, in: Smith, D.E., Leffler, M., Mackiernan, M. (Eds.), Dissolved Oxygen in Chesapeake Bay: A Synthesis of Recent Research. Maryland Sea Grant, College Park, Maryland, pp. 149-221.

Kemp, W.M., Boynton, W.R., 1992b. Benthic-pelagic interactions: Nutrient and oxygen dynamics, in: Smith, D., Leffler, M., Mackiernan, G. (Eds.), Oxygen Dynamics in

Chesapeake Bay: A Synthesis of Research. Maryland Sea Grant College Park, MD, pp. 149-221.

Kemp, W.M., Boynton, W.R., Adolf, J.E., Boesch, D.F., Boicourt, W.C., Brush, G., Cornwell, J.C., Fisher, T.R., Glibert, P.M., Hagy, J.D., Harding, L.W., Houde, E.D., Kimmel, D.G., Miller, W.D., Newell, R.I.E., Roman, M.R., Smith, E.M., Stevenson, J.C., 2005. Eutrophication of Chesapeake Bay: Historical trends and ecological interactions. Mar. Ecol. Prog. Ser. 303, 1-29.

Kemp, W.M., Puskaric, S., Faganeli, J., Smith, E.M., Boynton, W.R., 1999. Pelagic-benthic coupling and nutrient cycling, in: Malone, T.C., Malej, A., L.W. Harding, J., Smodlaka, N., Turner, R.E. (Eds.), Coastal and Estuarine Studies, Ecosystems at the Land-Sea Margin: Drainage Basin to Coastal Sea. American Geophysical Union, Washington, D.C., pp. 295-339.

Kemp, W.M., Sampou, P., Caffrey, J., Mayer, M., Henriksen, K., Boynton, W.R., 1990. Ammonium recycling versus denitrification in Chesapeake Bay sediments. Limnol. Oceanogr. 35, 1545-1563.

Kemp, W.M., Sampou, P.A., Garber, J., Tuttle, J., Boynton, W.R., 1992. Seasonal depletion of oxygen from bottom waters of Chesapeake Bay: Roles of benthic and planktonic respiration and physical exchange processes. Mar. Ecol. Prog. Ser. 85, 137-152.

Kemp, W.M., Smith, E.M., Marvin-DiPasquale, M., Boynton, W.R., 1997. Organic carbon balance and net ecosystem metabolism in Chesapeake Bay. Mar. Ecol. Prog. Ser. 150, 229-248.

Kemp, W.M., Testa, J.M., 2011. Metabolic balance between ecosystem production and consumption, in: Wolansky, E., McLusky, D. (Eds.), Treatise on Estuarine and Coastal Science. Academic Press, Waltham, Massachusetts, pp. 83-118.

Kemp, W.M., Testa, J.M., Conley, D.J., Gilbert, D., Hagy, J.D., 2009. Temporal responses of coastal hypoxia to nutrient loading and physical controls. Biogeosciences 6, 2985-3008.

Kimmel, D.G., Roman, M.R., 2004. Long-term trends in mesozooplankton abundance in Chesapeake Bay, USA: Influence of freshwater input. Mar. Ecol. Prog. Ser. 267, 71-83.

Kimmel, D.K., Newell, R.I.E., 2007. The influence of climate variation on eastern oyster (*Crassostrea virginica*) juvenile abundance in Chesapeake Bay. Limnol. Oceanogr. 52, 959-965.

Krom, M.D., Berner, R.A., 1981. The diagenesis of phosphorus in a nearshore marine sediment. Geochim. Cosmochim. Acta 45, 207-216.

Kronvang, B., Jeppesen, E., Conley, D.J., Søndergaard, M., Larsen, S.E., Ovesen, N.B., Carstensen, J., 2005. Nutrient pressures and ecological responses to nutrient loading reductions in Danish streams, lakes and coastal waters. JHyd 304, 274-288.

Kuo, A.Y., Park, K., Moustafa, M.Z., 1991. Spatial and temporal variabilities of hypoxia in the Rappahannock River, Virginia. Estuaries 14, 113-121.

Langland, M.J., Raffensperger, J.P., Moyer, D.L., Landwehr, J.M., Schwarz, G.E., 2006. Changes in streamflow and water quality in selected nontidal basins in the Chesapeake Bay Watershed, 1985-2004. United States Geological Survey, p. 75.

Laws, E.A., Chalup, M.S., 1990. A microalgal growth model. Limnol. Oceanogr. 35, 597-608.

Lawson, D.S., Hurd, D.C., Pankratz, H.S., 1978. Silica dissolution rates of decomposing phytoplankton assemblages at various temperatures Am. J. Sci. 278, 1373-1393.

Lee, D.Y., Keller., D., Crump, B.C., Hood, R.R., 2012. Community metabolism and energy transfer in the Chesapeake Bay estuarine turbidity maximum. Mar. Ecol. Prog. Ser. 449, 65-82.

Lee, Y., Boynton, W.R., Li, M., Li, Y., 2013. Role of late winter-ppring wind influencing summer hypoxia in Chesapeake Bay. Estuar. Coast., 1-14.

Lee, Y.J., Lwiza, K.M.M., 2008. Factors driving bottom salinity variability in the Chesapeake Bay. Cont. Shelf Res. 28, 1352-1362.

Lehtoranta, J., Ekholm, P., Pitkänen, H., 2009. Coastal eutrophication thresholds: A matter of sediment microbial processes. Ambio 38, 303-308.

Levin, L.A., Ekau, W., Gooday, A.J., Jorissen, F., Middelburg, J.J., Naqvi, S.W.A., Neira, C., Rabalais, N.N., Zhang, J., 2009. Effects of natural and human-induced hypoxia on coastal benthos. Biogeosciences 6, 2063-2098.

Levins, R., 1966. The strategy of model building in population biology. Am. Sci. 54, 421-431.

Li, M., Zhong, L., Boicourt, W.C., 2005. Simulations of Chesapeake Bay estuary: Sensitivity to turbulence mixing parameterizations and comparison with observations. JGR 110, C12004.

Li, M., Zhong, L., Boicourt, W.C., Zhang, S., Zhang, D.-L., 2007. Hurricane-induced destratification and restratification in a partially-mixed estuary. J. Mar. Res. 65, 169-192.

Li, M., Zhong, L., Harding, L.W., 2009. Sensitivity of plankton biomass and productivity to variations in physical forcing and biological parameters in Chesapeake Bay. J. Mar. Res. 67, 667-700.

Li, Y., Li, M., 2011. Effects of winds on stratification and circulation in a partially mixed estuary. JGR 116.

Li, Y., Li, M., Kemp, M.W., 2013. A budget analysis of the physical and biological controls on the seasonal cycle of dissolved oxygen in Chesapeake Bay. JGR *Submitted*.

Lin, J., Xie, L., Pietrafesa, L.J., Ramus, J.S., Paerl, H.W., 2007. Water Quality Gradients across Albemarle-Pamlico Estuarine System: Seasonal Variations and Model Applications. J. Coast. Res. 23, 213-229.

Lin, J., Xu, H., Cudaback, C., Wang, D., 2008. Inter-annual variability of hypoxic conditions in a shallow estuary J. Mar. Syst. 73, 169-184.

Liu, Y., Arhonditsis, G.B., Stow, C.A., Scavia, D., 2011. Predicting the hypoxic volume in Chesapeake Bay with the streeter-phelps model: a bayesian approach. JAWRA 47, 1348-1363.

Liu, Y., Scavia, D., 2010. Analysis of the Chesapeake Bay hypoxia regime shift: insights from two simple mechanistic models. Estuar. Coast. 33, 629-639.

Luff, R., Moll, A., 2004. Seasonal dynamics of the North Sea sediments using a three-dimensional coupled sedimentâ€“water model system. Cont. Shelf Res. 24, 1099-1127.

Mallin, M.A., M. McIver, H. Wells, D. Parsons, and V. Johnson 2005. Reversal of eutrophication following sewage treatment upgrades in the New River estuary, North Carolina. Estuaries 28, 750-760.

Malone, T.C., 1987. Seasonal oxygen depletion and phytoplankton production in Chesapeake Bay: preliminary results of 1985-86 field studies, in: Mackiernan, M. (Ed.), Dissolved Oxygen in Chesapeake Bay. Maryland Sea Grant, College Park, Maryland, pp. 54-60.

Malone, T.C., 1991. River flow, phytoplankton production and oxygen depletion in Chesapeake Bay, in: Pearson, R.V.T.a.T.H. (Ed.), Modern and Ancient Continental Shelf Anoxia. The Geological Society, Londond, pp. 83-93.

Malone, T.C., Conley, D.J., Fisher, T.R., Glibert, P.M., Harding, L.W., Sellner, K.G., 1996. Scales of nutrient-limited phytoplankton productivity in Chesapeake Bay. Estuaries 19, 371-385.

Malone, T.C., Crocker, L.H., Pike, S.E., Wendler, B.W., 1988. Influence of river flow on the dynamics of phytoplankton in a partially stratified estuary. Mar. Ecol. Prog. Ser. 48, 235-249.

Malone, T.C., Kemp, W.M., Ducklow, H.W., Boynton, W.R., Tuttle, J.H., Jonas, R.B., 1986. Lateral variation in the production and fate of phytoplankton in a partially stratified estuary. Mar. Ecol. Prog. Ser. 32, 149-160.

Marchesiello, P., McWilliams, J.C., Shchepetkin, A., 2001. Open boundary conditions for long-term integration of regional oceanic models. Ocean Model. Online 3, 1-20.

Marshall, H.G., Nesius, K.K., 1996. Phytoplankton composition in relation to primary production in Chesapeake Bay. Mar. Biol. 125, 611-617.

Matisoff, G., Wang, X.S., 1998. Solute transport in sediments by freshwater infaunal bioirrigators. Limnol. Oceanogr. 43, 1487-1499.

Mayer, L.M., Gloss, S.P., 1980. Buffering of silica and phosphate in a turbid river. Limnol. Oceanogr. 25, 12-22.

McCarthy, M.J., McNeal, K.S., Morse, J.W., Gardner, W.S., 2008. Bottom-water hypoxia effects on sediment-water interface nitrogen transformations in a seasonally hypoxia, shallow bay (Corpus Christi Bay, TX, USA). Estuar. Coast. 31, 521-531.

McGlathery, K.J., Sundbäck, K., Anderson, I.C., 2007. Eutrophication in shallow coastal bays and lagoons: the role of plants in the coastal filter. Mar. Ecol. Prog. Ser. 348, 1-18.

Mee, L., 2006. Reviving dead zones. Sci. Am. 295, 78-85.

Meier, H.E.M., Andersson, H.C., Eilola, K., Gustafsson, B.G., Kuznetsov, I., Müller-Karulis, B., Neumann, T., Savchuk, O.P., 2011. Hypoxia in future climates: A model ensemble study for the Baltic Sea. Geophys. Res. Lett. 38, L24608, doi:24610.21029/22011GL049929.

Mesinger, F., DiMego, G., Kalnay, E., Mitchell, K., Shafran, P.C., Ebisuzaki, W., Jovic, D., Woollen, J., Rogers, E., Berbery, E.H., 2006. North American regional reanalysis. Bulletin of the American Meteorological Society 87, 343-360.

Middelburg, J.J., Levin, L.A., 2009. Coastal hypoxia and sediment biogeochemistry. Biogeosciences 6, 1273-1293.

Miller, D.C., Geider, R.J., MacIntyre, H.L., 1996. Microphytobenthos: the ecological role of the "secret garden" of unvegetated, shallow-water marine habitats. II. Role in sediment stability and shallow-water food webs. Estuaries 19, 202-212.

Mort, H.P., Slomp, C.P., Gustafsson, B.G., Andersen, T.J., 2010. Phosphorus recycling and burial in Baltic Sea sediments with contrasting redox conditions. Geochim. Cosmochim. Acta 74, 1350-1362.

Murphy, J., Riley, J.P., 1962. A modified single solution method for the determination of phosphate in natural waters. Anal. Chim. Acta 27, 31-36.

Murphy, R.M., Curriero, F.C., Ball, W.P., 2010. Comparison of spatial interpolation methods for water quality evaluation in the Chesapeake Bay. J. Environ. Eng. 136, 160-171.

Murphy, R.R., Kemp, W.M., Ball, W.P., 2011. Long-term trends in Chesapeake Bay seasonal hypoxia, stratification, and nutrient loading. Estuar. Coast. 34, 1293-1309.

Murray, A.G., Parslow, J.S., 1999. Modelling of nutrient impacts in Port Phillip Bay-a semi-enclosed marine Australian ecosystem. Marine and Freshwater Research 50, 597-612.

Najjar, R.G., Pyke, C.R., Adams, M.B., Breitburg, D., Hershner, C., Kemp, M., Howarth, R., Mulholland, M.R., Paolisso, M., Secor, D., 2010. Potential climate-change impacts on the Chesapeake Bay. Estuar. Coast. Shelf Sci. 86, 1-20.

Nestlerode, J.A., Diaz, R.J., 1998. Effects of periodic environmental hypoxia on predation of a tethered polychaete, *Glycera americana*: Implications for trophic dynamics. Mar. Ecol. Prog. Ser. 172, 185-195.

Neumann, T., Fennel, W., Kremp, C., 2002. Experimental simulations with an ecosystem model of the Baltic Sea: a nutrient load reduction experiment. Global Biogeochem. Cycles 16, 7-1 - 7-19.

Newcombe, C.L., Horne, W.A., 1938. Oxygen-poor waters of the Chesapeake Bay. Science 88, 80-81.

Newell, R., Ott, J., 1999. Macrobenthic communities and eutrophication, in: Malone, T.C., Malej, A., Harding, L.W., Smodlaka, N., Turner, R.E. (Eds.), Ecosystems at the Land-Sea Margin: Drainage Basin to Coastal Sea. American Geophysical Union, Washington, D.C., pp. 265-293.

Newell, R.I.E., 1988. Ecological changes in Chesapeake Bay: Are they the result of overharvesting the Eastern oyster (*Crassostrea virginica*)?, in: Lynch, M.P., Krome, E.C. (Eds.), Understanding the Estuary: Advances in Chesapeake Bay Research. Chesapeake Research Consortium Publication 129 (CBP/TRS 24/88), Gloucester Point, Virginia, pp. 536-546.

Newell, R.I.E., Kemp, W.M., Hagy, J.D.I., Cerco, C.F., Testa, J.M., Boynton, W.R., 2007. Top-down control of phytoplankton by oysters in Chesapeake Bay, USA: comment on Pomeroy et al. (2006). Mar. Ecol. Prog. Ser. 341, 293-298

Nixon, S.W., Fulweiler, R.W., Buckley, B.A., Granger, S.L., Nowicki, B.L., Henry, K.M., 2009. The impact of changing climate on phenology, productivity, and benthic-pelagic coupling in Narragansett Bay. Estuar. Coast. Shelf Sci. 82, 1-18.

Nixon, S.W., S.Granger, Buckley, B.A., Lamont, M., Rowell, B., 2004. A one hundred and seventeen year coastal water temperature record from Woods Hole, Massachusetts. Estuaries 27, 397-404.

O'Donnell, J.H., Dam, H.G., W.F. Bohlen, W.F., Fitzgerald, W., Gray, P.S., Houk, A.E., Cohen, D.C., Howard-Strobel, M.M., 2008. Intermittent ventilation in the hypoxic zone of western Long Island Sound during the summer of 2004. JGR 113, 1-13.

Officer, C.B., Biggs, R.B., Taft, J.L., Cronin, E., Tyler, M.A., Boynton, W.R., 1984. Chesapeake Bay anoxia: origin, development and significance. Science 223, 22-27.

Ogi, M., Tachibana, Y., Yamazaki, K., 2003. Impact of the wintertime North Atlantic Oscillation (NAO) on the summertime atmospheric circulation. Geophys. Res. Lett. 30, doi: 10.1029/2003GL017280. .

Oguz, T., Gilbert, D., 2007. Abrupt transitions of the top-down controlled Black Sea pelagic ecosystem during 1960-200: evidence for regime-shifts under strong fishery exploitation and nutrient enrichment modulated by climate-induced variations. Deep-Sea Research I 54, 220-242

Oviatt, C.A., Keller, A.A., Sampou, P.A., Beatty, L.L., 1986. Patterns of productivity during eutrophication: a mesocosm experiment Mar. Ecol. Prog. Ser. 28, 69-80.

Paerl, H.W., Valdes, L.M., Joyner, A.R., Piehler, M.F., 2004. Solving problems resulting from solutions: evolution of a dual nutrient management strategy for the eutrophying Neuse River Estuary, North Carolina. Environ. Sci. Technol. 38, 3068-3073.

Park, K., Kim, C.-K., Schroeder, W.W., 2007. Temporal variability in summertime bottom hypoxia in shallow areas of Mobile Bay, Alabama. Estuar. Coast. 30, 54-65.

Passow, U., 1991. Species-specific sedimentation and sinking velocities of diatoms. Mar. Biol. 108, 449-455.

Patrick, R., 1988. Changes in the chemical and biological characteristics of the upper Delaware River estuary in response to environmental laws, in: Majumdar, S.K., Miller, E.W., Sage, L.E. (Eds.), Ecology and Restoration of the Delaware River Basin. The Philadelphia Academy of Science, Philadelphia, pp. 332-359.

Pelegrí, S.P., Blackburn, H.T., 1995. Effect of bioturbation by *Neris* sp., *Mya arenaria*, and *Cerastoderma* sp. on nitrification and denitrification in estuarine sediments. Opheila 42, 289-299.

Peña, M.A., Katsev, S., Oguz, T., Gilbert, D., 2009. Modeling dissolved oxygen dynamics and coastal hypoxia: a review. Biogeosci. Disc. 6, 9195-9256.

Pettitt, A.N., 1980. A simple cumulative sum type statistic for the change-point problem with zero-one observations. Biometrika 67, 79-84.

Piña-Ochoa, E., Álvarez-Cobelas, M., 2006. Denitrification in aquatic environments: a cross-system analysis. Biogeochemistry 81, 111-130.

Pomeroy, L.R., D'Elia, C.F., Schaffner, L.C., 2006. Limits to top-down control of phytoplankton by oysters in Chesapeake Bay. Mar. Ecol. Prog. Ser. 325, 301-309.

Pond, S., Pickard, G.L., 1983. Introductory dynamical oceanography, 2nd ed. Butterworth-Heinmann, Oxford, UK.

Prins, T.C., Smaal, A.C., Dame, R.F., 1998. A review of the feedbacks between bivalve grazing and ecosystem processes. Aquat. Ecol. 31, 349-359.

Pritchard, D.W., 1967. Observations of circulation in coastal plain estuaries, in: Lauff, G.H. (Ed.), Estuaries. American Association for the Advancement of Science, Washington, D.C., pp. 37-44.

Provoost, P., Braeckman, U., Gansbeke, D.V., Moodley, L., Soetaert, K., Middelburg, J.J., Vanaverbeke, J., 2013. Modelling benthic oxygen consumption and benthic-pelagic coupling at a shallow station in the southern North Sea. Estuar. Coast. Shelf Sci. 120, 1-11.

R Development Core Team, 2009. The R project for statistical computing.

Rabalais, N.N., Gilbert, D., 2009. Distribution and consequences of hypoxia, in: Urban, E., Sundby, B., Malanotte-Rizzoli, P., Melillo, J.M. (Eds.), Watersheds, bays and bounded seas. Island Press, Washington, D.C., pp. 209-226.

Rabalais, N.N., Turner, R.E., 2006. Oxygen depletionin the Gulf of Mexico adjacent to the Mississippi River, in: Neretin, L.N. (Ed.), Past and Present Marine Water Column Anoxia. NATO Science Series: IV-Earth and Environmental Sciences. Kluwer. , Dordrecht, the Netherlands, pp. 225-245.

Rabalais, N.N., Turner, R.E., Díaz, R.J., Justić, D., 2009. Global change and eutrophication of coastal waters. ICES J. Mar. Sci. 66, 1528-1537.

Rabalais, N.N., Turner, R.E., Gupta, B.K.S., Boesch, D.F., Chapman, P., Murrell, M.C., 2007. Hypoxia in the northern Gulf of Mexico: does the science support the plan to reduce, mitigate, and control hypoxia? . Estuar. Coast. 30, 753-772.

Rabouille, C., Gaillard, J.-F., 1991. Towards the EDGE: Early diagenetic global explanation. A model depicting the early diagenesis of organic matter, O_2, NO_3, Mn, and PO_4. Geochim. Cosmochim. Acta 55, 2511-2525.

Rabouille, C., Gaillard, J.F., 1990. The validity of steady-state flux calculations in early diagenesis: a computer simulation of deep-sea silica diagenesis. Deep Sea Research Part A. Oceanographic Research Papers 37, 625-646.

Reed, D.C., Slomp, C.P., Gustafsson, B.G., 2011. Sedimentary phosphorus dynamics and the evolution of bottom-water hypoxia: A coupled benthic–pelagic model of a coastal system. Limnol. Oceanogr. 56, 1075-1092.

Revsbech, N.P., Risgaard-Petersen, N., Schramm, A., Nielsen, L.P., 2006. Nitrogen transformations in stratified aquatic microbial ecosystems. Antonie van Leeuwenhoek Journal of Microbiology 90, 361-375.

Ribeiro, P.J., Diggle, P.J., 2009. geoR: A package for geostatistical analysis using the R software.

Rich, J.J., Dale, O.R., Song, B., Ward, B.B., 2008. Anaerobic ammonium oxidation (Anammox) in Chesapeake Bay sediments. Microb. Ecol. 55, 311-320.

Robbins, J.A., Keilty, T., White, D.S., Edgington, D.N., 1989. Relationships among tubificid abundances, sediment composition, and accumulation rates in Lake Erie. Can. J. Fish. Aquat. Sci. 46, 223-231.

Roman, M.R., Holliday, D.V., Sanford, L.P., 2001. Temproal and spatial patterns of zooplankton in the Chesapeake Bay turbididy maximum. Mar. Ecol. Prog. Ser. 213, 215-227.

Sampou, P., Kemp, W.M., 1994. Factors regulating plankton community respiration in Chesapeake Bay. Mar. Ecol. Prog. Ser. 110, 249-258.

Sanford, L.P., Boicourt, W.C., 1990. Wind-forced salt intrusion into a tributary estuary. JGR 95, 13,357-313,371.

Sanford, L.P., Suttles, S.E., Halka, J.P., 2001. Reconsidering the physics of the Chesapeake Bay estuarine turbidity maximum. Estuaries 24, 655-669.

Savchuk, O.P., Wulff, F., Hille, S., Humborg, C., Pollehne, F., 2008. The Baltic Sea a century ago--a reconstruction from model simulations, verified by observations. J. Mar. Syst. 74, 485-494.

Scavia, D., Kelly, E.L.A., Hagy, J.D., 2006. A simple model for forecasting the effects of nitrogen loads on Chesapeake Bay hypoxia. Estuar. Coast. 29, 674-684.

Scheffer, M., Carpenter, S., Foley, J.A., Folke, C., Walker, B., 2001. Castastrophic shifts in ecosystems. Nature 413, 591-596.

Schink, D.R., Fanning, K.A., Pilson, M.E.Q., 1974. Dissolved silica in the upper pore waters of the Atlantic Ocean floor. JGR 79, 2243-2250.

Schink, D.R., N.L. Guinasso, J., Fanning, K.A., 1975. Processes affecting the concentration of silica at the sediment-water interface of the Atlantic Ocean. JGR 80, 3013-3031.

Scully, M.E., 2010a. The importance of climate variability to wind-driven modulation of hypoxia in Chesapeake Bay. J. Phys. Oceanogr. 40, 1435-1440.

Scully, M.E., 2010b. Wind modulation of dissolved oxygen in Chesapeake Bay. Estuar. Coast. 33, 1164-1175.

Scully, M.E., Friedrichs, C., Brubaker, J., 2005. Control of estuarine stratification and mixing by wind-induced straining of the estuarine density field. Estuaries 28, 321–326.

Seitzinger, S., Nixon, S.W., 1985. Eutrophication and the rate of denitrification and N_2O production in coastal marine sediments. Limnol. Oceanogr. 30, 1332-1339.

Seitzinger, S.P., 1988. Denitrification in freshwater and coastal marine ecosystems: ecological and geochemical significance. Limnol. Oceanogr. 33, 702-724.

Seitzinger, S.P., 1988 Benthic nutrient cycling and oxygen consumption in the Delware estuary, in: Majumdar, S.K., Miller, E.W., Sage, L.E. (Eds.), Ecology and Restoration of the Delware River Basin. The Pennsylvania Academy of Science, Philadelphia, pp. 132-147.

Seitzinger, S.P., Nielsen, L.P., Caffrey, J., Christensen, P.B., 1993. Denitrification measurements in aquatic sediments: a comparison of three methods. Biogeochemistry 23, 147-167.

Seliger, H.H., Boggs, J.A., 1988. Long term pattern of anoxia in Chesapeake Bay, in: Lynch, M., Krome, E.C. (Eds.), Understanding the Estuary: Advances in Chesapeake Bay Research. Chesapeake Research Consortium, Solomons, Maryland, pp. 570-583.

Sellner, K.G., R.V. Lacouture, S.J. Cibil, A. Brindley, and S.G. Brownlee, 1991. Importance of a winter dinoflagellate-microflagellate bloom in the Patuxent River estuary. Estuarine, costal and Shelf Science 32, 27-42.

Sharples, J., Simpson, J.H., Brubaker, J.M., 1994. Observations and modelling of periodic stratification in the Upper York River Estuary, Virginia. Estuar. Coast. Shelf Sci. 38, 301-312.

Shchepetkin, A.F., McWilliams, J.C., 2005. The Regional Oceanic Modeling System: A split-explicit, free-surface, topography-following-coordinate oceanic model. Ocean Model. Online 9, 347-404.

Sigg, L., Stumm, W., 1981. The interaction of anions and weak acids with the hydrous goethite (α-FeOOH) surface. ColSu 2, 101-117.

Skogen, M.D., Moll, A., 2005. Importance of ocean circulation in ecological modeling: An example from the North Sea. J. Mar. Syst. 57, 289-300.

Slomp, C.P., Malschaert, J.F.P., van Raaphorst, W., 1998. The role of adsorption in sediment-water exchange of phosphate in North Sea continental margin sediments. Limnol. Oceanogr. 43, 832-846.

Slomp, C.P., Van Cappellen, P., 2007. The global marine phosphorus cycle: Sensitivity to oceanic circulation. Biogeosciences 4, 155-171.

Smith, E.M., Kemp, W.M., 1995. Seasonal and regional variations in plankton community production and respiration for Chesapeake Bay. Mar. Ecol. Prog. Ser. 116, 217-231.

Smith, E.M., Kemp, W.M., 2001. Size structure and the production/respiration balance in a coastal plankton community. Limnol. Oceanogr. 46, 473-485.

Smith, E.M., Kemp, W.M., 2003. Planktonic and bacterial respiration along an estuarine gradient: responses to carbon and nutrient enrichment. Aquat. Microb. Ecol. 30, 251-261.

Smolarkiewicz, P.K., Margolin, L.G., 1998. MPDATA: a finite-difference solver for geophysical flows. JCoPh 140, 459-480.

Soetaert, K., Herman, P.M.J., 1995. Nitrogen dynamics in the Westerschelde estuary (SW Netherlands) estimated by means of the ecosystem model MOSES. Hydrobiologia 311, 225-246.

Soetaert, K., Middelburg, J.J., 2009. Modeling eutrophication and oligotrophication of shallow-water marine systems: The importance of sediments under stratified and well-mixed conditions. Eutrophication in Coastal Ecosystems, 239-254.

Soetaert, K., Middelburg, J.J., Heip, C., Meire, P., Damme, S.V., Maris, T., 2006. Long-term change in dissolved inorganic nutrients in the heterotrophic Scheldt estuary (Belgium, The Netherlands). Limnol. Oceanogr. 51, 409–423.

Soetaert, K., Middelburg, J.J., Herman, P.M.J., Buis, K., 2000. On the coupling of benthic and pelagic biogeochemical models Earth-Sci. Rev. 51, 173-201.

Sohma, A., Sekiguchi, Y., Kuwae, T., Nakamura, Y., 2008. A benthic-pelagic coupled ecosystem model to estimate the hypoxic estuary including tidal flat--Model description and validation of seasonal/daily dynamics. Ecol. Model. 215, 10-39.

Solorzano, L., 1969. Determination of ammonia in natural waters by the phenolhypochlorite method. Limnol. Oceanogr. 14, 799-801.

Spiteri, C., Slomp., C.P., Charette, M.A., Tuncay, K., Meile, C., 2008. Flow and nutrient dynamics in a subterranean estuary (Waquoit Bay, MA, USA): field data and reactive transport modeling. Geochim. Cosmochim. Acta 72, 3398-3412.

Stæhr, P.A., Testa, J.M., Kemp, W.M., Cole, J.J., Sand-Jensen, K., Smith, S.V., 2012. The metabolism of aquatic ecosystems: history, methods, and applications. Aquat. Sci. 74, 15-29.

Stanley, D.W., Nixon, S.W., 1992. Stratification and bottom-water hypoxia in the Pamlico River estuary. Estuaries 15, 270-281.

Stoecker, D.K., Egloff, D.A., 1987. Predation by *Acartia tonsa* Dana on planktonic ciliates and rotifers. J. Exp. Mar. Biol. Ecol. 110, 53-68.

Stow, C.A., Jolliff, J., McGillicuddy, D.J., Doney, S.C., Allen, J.I., Friedrichs, M.A.M., Rose, K.A., Wallhead, P., 2009a. Skill assessment for coupled biological/physical models of marine systems. J. Mar. Syst. 76, 12-12.

Stow, C.A., Jolliff, J., McGillicuddy, D.J., Doney, S.C., Allen, J.I., Friedrichs, M.A.M., Rose, K.A., Wallheadg, P., 2009b. Skill assessment for coupled biological/physical models of marine systems. Journal of Marine Systems 76, 4-15.

Sundby, B., Gobeil, C., Silverberg, N., Mucci, A., 1992. The phosphorus cycle in coastal marine sediments. Limnol. Oceanogr. 37, 1129-1145.

Taft, J.L., Taylor, W.R., Hartwig, E.O., R.Loftus, 1980. Seasonal oxygen depletion in Chesapeake Bay. Estuaries 3, 242-247.

Taylor, A.H., Stephens, J.A., 1998. The North Atlantic Oscillation and the latitude of the Gulf Stream. Tell 50A, 134-142.

Testa, J.M., Brady, D.C., Toro, D.M.D., Boynton, W.R., Cornwell, J.C., Kemp, W.M., 2013. Sediment flux modeling: Nitrogen, phosphorus and silica cycles. Estuar. Coast. Shelf Sci., in press.

Testa, J.M., Kemp, W.M., 2008. Variability of biogeochemical processes and physical transport in a partially stratified estuary: a box-modeling analysis. Mar. Ecol. Prog. Ser. 356, 63-79.

Testa, J.M., Kemp, W.M., 2011. Oxygen - dynamics and biogeochemical consequences, in: E. Wolansky, McLusky, D.S. (Eds.), Treatise on Estuarine and Coastal Science. Academic Press, Waltham, Massachusetts, pp. 163-199.

Testa, J.M., Kemp, W.M., 2012. Hypoxia-induced shifts in nitrogen and phosphorus cycling in Chesapeake Bay. Limnol. Oceanogr. 57, 835-850.

Testa, J.M., Kemp, W.M., Boynton, W.R., Hagy, J.D., 2008. Long-term changes in water quality and productivity in the Patuxent River estuary: 1985 to 2003. Estuar. Coast. 31, 1021-1037.

Tiedje, J.M., 1987. Ecology of denitrification and dissimilatory nitrate reduction to ammonium, in: Zehnder, A.J.B. (Ed.), Biology of Anaerobic Microorganisms. John Wiley, New York, pp. 179-244.

Tromp, T.K., Cappellen, P.V., Key, R.M., 1995. A global model for the early diagenesis of organic carbon and organic phosphorus in marine sediments. Geochim. Cosmochim. Acta 59, 1259-1284.

Turner, R.E., Rabalais, N.N., Justic, D., 2008. Gulf of Mexico hypoxia: Alternate states and a legacy. Environ. Sci. Technol. 42, 2323-2327.

Turner, R.E., Rabalais, N.N., Justić, D., 2006. Predicting summer hypoxia in the northern Gulf of Mexico: riverine N, P and Si loading. Mar. Pollut. Bull. 52, 139-148.

Turner, R.E., Schroeder, W.W., Jr., W.J.W., 1987. The role of stratification in the deoxygenation of Mobile Bay and adjacent shelf bottom waters. Estuaries 10, 13-19.

Tyler, M.A., Seliger, H.H., 1981. Selection for a red tide organism: Physiological responses to the physical environment. Limnol. Oceanogr. 26, 310-324.

Tyler, R.M., Brady, D.C., Targett, T., 2009. Temporal and spatial dynamics of diel-cycling hypoxia in estuarine tributaries. Estuar. Coast. 32, 123-145.

Upchruch, J.B., Edzwald, J.K., O'Melia, C.R., 1974. Phosphates in sediments of Pamlico estuary. Environ. Sci. Technol. 8, 56-58.

Vahtera, E., Conley, D.J., Gustafsson, B.G., Kuosa, H., Pitkänen, H., Savchuk, O.P., Tamminen, T., Viitasalo, M., Voss, M., Wasmund, N., Wulff, F., 2007. Internal ecosystem feedbacks enhance nitrogen-fixing cyanobacteria blooms and complicate management in the Baltic Sea. Ambio 36, 186-194.

Van Cappellen, P., Berner, R.A., 1988. A mathematical model for the early diagenesis of phosphorus and fluorine in marine sediments; apatite precipitation. Am. J. Sci. 288, 289-333.

Van Cappellen, P., Ingall, E.D., 1994. Benthic phosphorus regeneration, net primary production, and ocean anoxia: A model of the coupled marine biogeochemical cycles of carbon and phosphorus. Paleoceanography 9, 677-692.

Van Cappellen, P., Linqing, Q., 1997a. Biogenic silica dissolution in sediments of the Southern Ocean. I. Solubility. DSR 44, 1109-1128.

Van Cappellen, P., Linqing, Q., 1997b. Biogenic silica dissolution in sediments of the Southern Ocean. II. Kinetics. DSR 44, 1129-1149.

Vanderborght, J.-P., Wollast, R., Billen, G., 1977a. Kinetic-models of diagenesis in disturbed sediments. Part 1. Mass-transfer properties and silica diagenesis. Limnol. Oceanogr. 22 787-793.

Vanderborght, J.-P., Wollast, R., Billen, G., 1977b. Kinetic-models of diagenesis in disturbed sediments. Part 2. Nitrogen diagenesis. Limnol. Oceanogr. 22, 787-793.

Vaquer-Sunyer, R., Duarte, C.M., 2008. Thresholds of hypoxia for marine biodiversity. Proc. Natl. Acad. Sci. U. S. A. 105, 15452-15457.

Warner, J.C., Sherwood, C.R., Arango, H.G., Signell, R.P., 2005. Performance of four turbulence closure models implemented using a generic length scale method. Ocean Model. Online 8, 81-113.

Welsh, B.L., Eller, F.C., 1991. Mechanisms controlling summertime oxygen depletion in western Long Island Sound. Estuaries 14, 265-278.

Welsh, D.T., 2003. It's a dirty job but someone has to do it: The role of marine benthic macrofauna in organic matter turnover and nutrient recycling to the water column. Chem. Ecol. 19, 321-342.

Westrich, J.T., Berner, R.A., 1984. The role of sedimentary organic matter in bacterial sulfate reduction: the G Model tested. Limnol. Oceanogr. 29, 236-249.

White, J.R., Roman, M.R., 1992. Seasonal study of grazing by metazoan zooplankton in the mesohaline Chesapeake Bay. Mar. Ecol. Prog. Ser. 86, 251-261.

Williams, M.R., Fisher, T.R., Boynton, W.R., Cerco, C.F., Kemp, W.M., Eshleman, K.N., Kim, S.-C., Hood, R.R., Fiscus, D.A., Radcliffe, G.R., 2006. An integrated modelling system for management of the Patuxent River estuary and basin, Maryland, USA. Int. J. Remote Sens. 27, 3705-3726.

Wilson, R.E., Swanson, R.L., Crowley, H.A., 2008. Perspectives on long-term variations in hypoxia conditions in western Long Island Sound. JGR 113, doi: 10.1029/2007JC004693.

Wiseman, W.J., Rabalais, N.N., Turner, R.E., Dinnel, S.P., MacNaughton, A., 1997. Seasonal and interannual variability within the Louisiana coastal current: stratification and hypoxia. J. Mar. Syst. 12, 237-248.

Wiseman, W.J.J., Rabalais, N.N., Turner, R.E., Justic, D., 2004. Hypoxia and the physics of the Louisiana coastal current, in: Nihoul, J.C.J., Zavialov, P.O., Micklin, P.P. (Eds.), Dying and Dead Seas, NATO Advanced Research Workshop. NATO ASI Series, Netherlands, Kluwer Academic Publishers., Liè§¥, Belgium, pp. 359-372.

Wong, G.T.F., Grosch, C.E., 1978. A mathematical model for the distribution of dissolved silicon in interstitial waters - an analytical approach. J. Mar. Res. 36, 735-750.

Xu, J., Chao, S.Y., Hood, R.R., Wang, H.V., Boicourt, W.C., 2002. Assimilating high-resolution salinity data into a model of a partially mixed estuary. JGRD *107*, 3074.

Xu, J., Hood, R.R., 2006. Modeling biogeochemical cycles in Chesapeake Bay with a coupled physical-biological model. Estuar. Coast. Shelf Sci. 69, 19-46.

Xu, J., Hood, R.R., Chao, S.-Y., 2005. A simple empirical optical model for simulating light attenuation variability in a partially mixed estuary. Estuaries 28, 572-580.

Xu, J., Long, W., Wiggert, J.D., Lanerolle, L.W., Brown, C.W., Murtugudde, R., Hood, R.R., 2012. Climate forcing and salinity variability in Chesapeake Bay, USA. Estuar. Coast. 35 237-261.

Yamada, S.S., D'Elia, C.F., 1984. Silicic acid regeneration from estuarine sediment cores. Mar. Ecol. Prog. Ser. 18, 113-118.

Zhang, H., Li, S., 2010. Effects of physical and biochemical processes on the dissolved oxygen budget for the Pearl River Estuary during summer. J. Mar. Syst. 79, 65-88.

Zheng, L., Chen, C., Zhang, F.Y., 2004. Development of water quality model in the Satilla River Estuary, Georgia. Ecol. Model. 178, 457-482.

Zillen, L., Conley, D.J., Andren, T., Andren, E., Gjorck, S., 2008. Past occurrences of hypoxia in the Baltic Sea and the role of climate variability, environmental change and human impact. Earth-Sci. Rev. 91, 77-92.

Zimmerman, A.R., Canuel, E.A., 2000. A geochemical record of eutrophication and anoxia in Chesapeake Bay sediments: anthropogenic influence on organic matter composition. Mar. Chem. 69, 117-137.

Zimmerman, A.R., Canuel, E.A., 2001. Bulk organic matter and lipid biomarker composition of Chesapeake Bay surficial sediments as indicators of environmental processes. Estuar. Coast. Shelf Sci. 53, 319-341.